AD_____
(Leave blank)

Award Number: W81XWH-11-2-0031

TITLE: Parallel Human and Animal Models of Blast- and Concussion-Induced Tinnitus and Related Traumatic Brain Injury (TBI)

PRINCIPAL INVESTIGATOR: Jinsheng Zhang, Ph.D.

CONTRACTING ORGANIZATION:

Wayne State University, Detroit, MI 48201

REPORT DATE: January 2013

TYPE OF REPORT: Annual Report

PREPARED FOR: U.S. Army Medical Research and Materiel Command
Fort Detrick, Maryland 21702-5012

REPORT DOCUMENTATION PAGE

Form Approved
OMB No. 0704-0188

1. REPORT DATE *(DD-MM-YYYY)*	**2. REPORT TYPE**	**3. DATES COVERED** *(From - To)*
January 2013	Annual Report	1January2012-31December2012

4. TITLE AND SUBTITLE

Parallel Human and Animal Models of Blast- and Concussion-Induced Tinnitus and Related Traumatic Brain Injury (TBI)

5a. CONTRACT NUMBER

5b. GRANT NUMBER
W81XWH-11-2-0031

5c. PROGRAM ELEMENT NUMBER

6. AUTHOR(S): Jinsheng Zhang, PhD; Anthony Cacace, PhD; E. Mark Haacke, PhD; Bruce Berkowitz, PhD; Jiani Hu, PhD; Randall Benson, MD; Pamela VandeVord, PhD; John Woodard,PhD.

5d. PROJECT NUMBER

5e. TASK NUMBER

5f. WORK UNIT NUMBER

7. PERFORMING ORGANIZATION NAME(S) AND ADDRESS(ES)

Wayne State University Detroit, MI

8. PERFORMING ORGANIZATION REPORT NUMBER

9. SPONSORING / MONITORING AGENCY NAME(S) AND ADDRESS(ES)

US Army Medical Research Acquisition Act
U.S. Army Medical Research and Materiel Command
Fort Detrick, MD 21702-5012

10. SPONSOR/MONITOR'S ACRONYM(S)

11. SPONSOR/MONITOR'S REPORT NUMBER(S)

12. DISTRIBUTION / AVAILABILITY STATEMENT

Approved for public release; distribution unlimited

13. SUPPLEMENTARY NOTES

14. ABSTRACT

In the second year, we continued our work concerning blast- or concussion-induced traumatic brain injury (TBI) that is often associated with tinnitus. In animal studies, we conducted behavioral testing of tinnitus, anxiety and spatial cognition, MRI-DTI and MEMRI imaging, and electrophysiology in the dorsal cochlear nucleus (DCN), inferior colliculus (IC) and auditory cortex (AC), and histological assays. We found that blast-induced tinnitus was accompanied with high anxiety and hyperactivity in the basolateral nuclei of the amygdala, and hypoactivity in the ipsilateral anterior cingulate cortex, along with variable changes in broadband noise-induced responses in the AC, IC and DCN. Blast also caused significant axonal injuries in auditory white matter tracts and enhanced astroglial activity. In addition, we found that concussion induced acute tinnitus and auditory detection deficits, along with axonal injury in the brainstem. In human studies, we conducted audiological, psychophysical, electroacoustic, and neuroimaging studies. Patients with blast-induced tinnitus showed symmetrical hearing thresholds and abnormal DPOAEs, normal middle ear power reflectance, but with increased fractional anisotropy (FA) of DTI data particularly in the corpus callosum and corona radiata and normal SWI in most patients. Patients with concussions had unpredictable hearing loss with large variability and asymmetric power reflectance values. While patients with blast + concussion-induced had less hearing loss than those with blast or concussion alone, tinnitus loudness was greatest for patients with blast + concussion, least for blast alone, with concussion alone having intermediate loudness.

15. SUBJECT TERMS

Blast, Tinnitus, Traumatic Brain Injury

16. SECURITY CLASSIFICATION OF:			**17. LIMITATION OF ABSTRACT**	**18. NUMBER OF PAGES**	**19a. NAME OF RESPONSIBLE PERSON**
					USAMRMC
a. REPORT U	**b. ABSTRACT** U	**c. THIS PAGE** U	UU	63	**19b. TELEPHONE NUMBER** *(include area code)*

Table of Contents

INTRODUCTION:

Blast- or concussion-induced traumatic brain injury (TBI) is often associated with tinnitus which is a perception of bothersome sound in the absence of external stimulation. The goal of this project is to determine that blast- and concussion-induced tinnitus results from a cascade of plastic changes in auditory brain structures. The scope of the research effort will cover investigations using both animal and human models. During the second year, we focused on both blast- and concussion-induced tinnitus, hearing loss and related TBI. Specifically, we put forth a strong effort in analyzing the large volume of data we collected from our blast experiments, including anatomical, electrophysiological, and neurobiochemical changes in the brain, as well as behavioral changes, and have incorporated these findings into manuscripts. Specifically, in animal studies, we conducted behavioral testing of tinnitus, anxiety and spatial cognition, MEMRI neuroimaging, and simultaneous electrophysiological recordings in the left dorsal cochlear nucleus (DCN), right inferior colliculus (IC) and right auditory cortex (AC), and histological assays of TBI. We found that single and repetitive blasts induced tinnitus at multiple frequencies along with significant hearing threshold shift. The duration of tinnitus became longer lasting with repeated blast exposure at higher intensities. Neuroimaging showed that blast induced tinnitus is accompanied with high anxiety and hyperactivity in the basolateral nuclei of amygdala, and hypoactivity in the ipsilateral anterior cingulate cortex. Electrophysiologically, we found blast-induced significant changes in responses to broadband noise (BBN) stimulation in the AC, IC and DC depending on the post-blast recovery times. Histologically, blast induced significant axonal injuries and in auditory white mater tracts and enhanced astroglial activity. In concussion studies, we found that concussion induced acute tinnitus and auditory detection deficits, along with axonal injury particularly in the reticuformation.

In human studies, we have recruited 28 qualified human subjects with blast-, concussion- and both blast-and concussion-induced tinnitus. Among the subjects recruited, 17 were blasted, 6 concussed and 5 with both blast concussions. Based on our established protocols, we conducted tests using audiometric, neuropsychological, psychoacoustic, questionnaire, and magnetic resonance imaging measures. The audiometric studies included audiograms, word recognition studies in quiet and noise conditions, loudness measures, middle-ear power reflectance, DPOAE, tinnitus handicap questionnaire data. The neuroimaging tests included standard MRI, DTI and SWI and MRS in resting state. Our studies demonstrated that patients with blast-induced tinnitus showed symmetrical hearing thresholds, normal DPOAE which is consistent with outer hair cell conditions, but with increased fractional anisotropy (FA) particularly in the corpus callosum and corona radiata, normal SWI except for a few patients. Our results also showed that patients with concussions have more significant HL with excessive variability (mixed and sensorineural) with asymmetric power reflectance values (200-2000 Hz) and a differential pattern for left and right ears. While patients with both blast and concussion-induced tinnitus had less hearing loss than blast or concussion categories, tinnitus loudness was greatest for blast and concussion patients and least for blast alone, with concussion having intermediate loudness values. Below are detailed descriptions our animal and human studies over the past year, which are organized chronologically.

BODY OF REPORT:

ANIMAL STUDIES:

1. Blast-induced tinnitus and hearing loss

Blast was conducted using a custom-designed shock tube located at WSU (ORA, Inc.). Following anesthesia (IP injection of ketamine and xylazine mixture), each animal was placed in supportive apparatus with a locking mechanism. The blast was delivered at approximately 14 and 22 PSI, which generated a noise of 10 ms duration at ~194 dB SPL. Auditory brainstem responses (ABRs) were tested to examine the hearing threshold of each rat. Rats were then tested with gap-detection (GAP) and prepulse inhibition (PPI) paradigms to obtain stable baseline behavioral results of tinnitus and central hearing detection.

a) ABR data

ABR thresholds:

Click and tone-burst ABRs were performed to test the hearing condition. Figure 1 shows that blast exposure caused a significant hearing threshold shift in the exposed (left) ear, which was not protected by an earplug. However, hearing thresholds recovered to pre-blast levels by one-month post blast and remained unchanged by three months post-blast. This supports our previously published results (Mao et al., 2011).

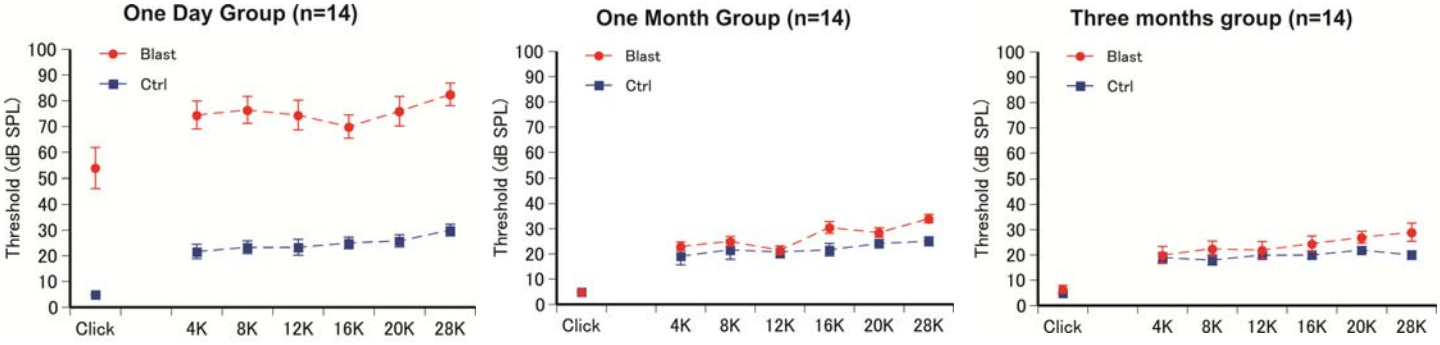

Fig. 1. ABR hearing threshold shifts. Thresholds are elevated one day post-blast but return to normal within a month and remain normal through three months.

Amplitude of P1-N1 waves:

Before the blast exposure, the amplitudes of P1-N1 waveforms of all three groups were not significantly different at frequency of 28 kHz during tone burst test of ABR ($p > 0.05$). At the time of the MRI scanning (35 days after the blast), the amplitudes of the P1-N1 waveforms of the rats in the control group were significantly higher compared to that of the rats in the blasted groups with or without tinnitus ($p < 0.001$). Compared to the amplitudes of the P1-N1 waveforms of the baseline data, the blasted rats with tinnitus showed decreased amplitudes in the higher sound level regions (>55 dB SPL), yet the blasted rats without tinnitus showed decreased amplitudes of the P1-N1 waveform in sound level of 45-50 dB SPL (Figure 6).

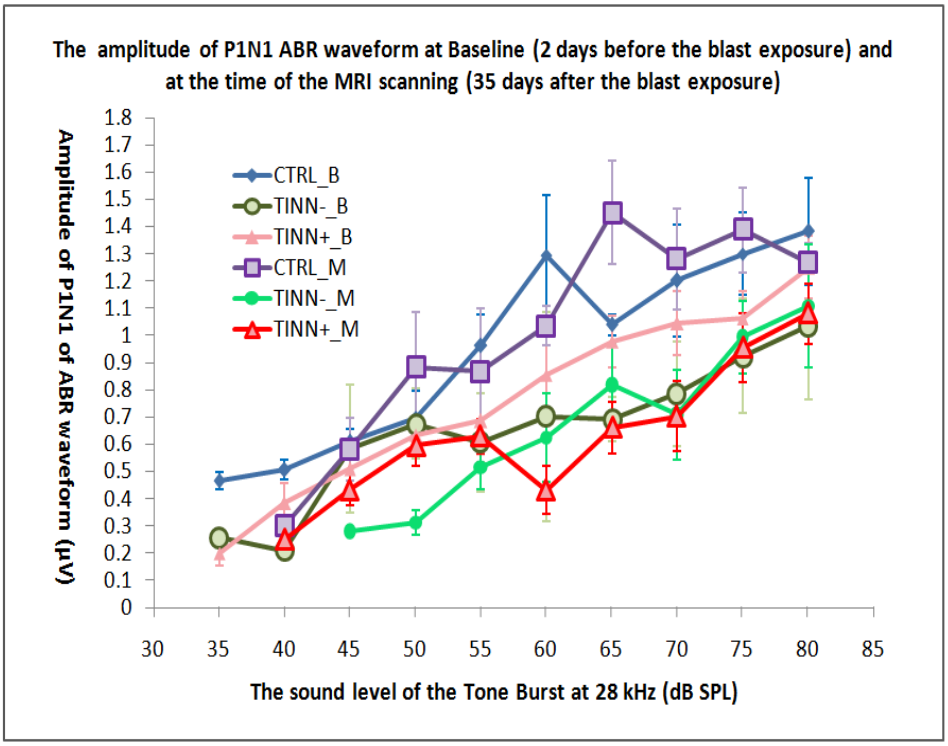

Figure showing the ABR Amplitude of P1-N1 waveforms of the rats in the control group, tinnitus (-) group and the tinnitus (-) group before and 35 days after the blast exposure. 35 days after the exposure, at the time of MRI scanning, the amplitudes of P1-N1 waveforms decreased in the blasted groups; compared to that of the rats in the control group, these changes were statistically significant ($p<0.001$).

b) Behavior data (gap detection and prepulse inhibition)

For GAP detection procedure, each rat was given a constant 60 dB SPL background noise consisting of 6-8, 10-12, 14-16, 18-20, or 26-28 kHz, or broadband noise. During the background noise, rats were either presented with a 115 dB, 50 ms white noise startle (Startle Only condition), or were presented with the startle preceded by a 40 ms silent gap in the background noise (GAP condition). For PPI, background noise was absent. Rats were either presented with the startle stimulus (Startle Only condition), or were presented with the startle stimulus preceded by a 40 ms narrow-band noise at 60 dB SPL. The noise was centered at the same frequencies as background noise in the GAP paradigm. Following blast treatment, GAP, PPI and were collected to monitor the progression of tinnitus and hearing loss. Below are the summary of the blast-induced effects on behavioral evidence of tinnitus at different time points:

1. One day after blast exposure, GAP and PPI ratios results were significantly higher compared to control rats at all frequency bands except for broadband noise (BBN), demonstrating significant tinnitus and central auditory detection deficits (Fig. 2a).
2. One month after blast, GAP ratio results showed that all blasted animals except for one (not included) had tinnitus at 14-16 and 26-28 kHz compared to the controls, supporting our previous findings. PPI data showed no change (Fig. 2b).
3. Three months after blast, 5 rats showed low (6-8 kHz) and high-frequency (26- 28 kHz) tinnitus while the other 4 rats demonstrated tinnitus recovery (not shown). PPI data was not affected (Fig. 2c).

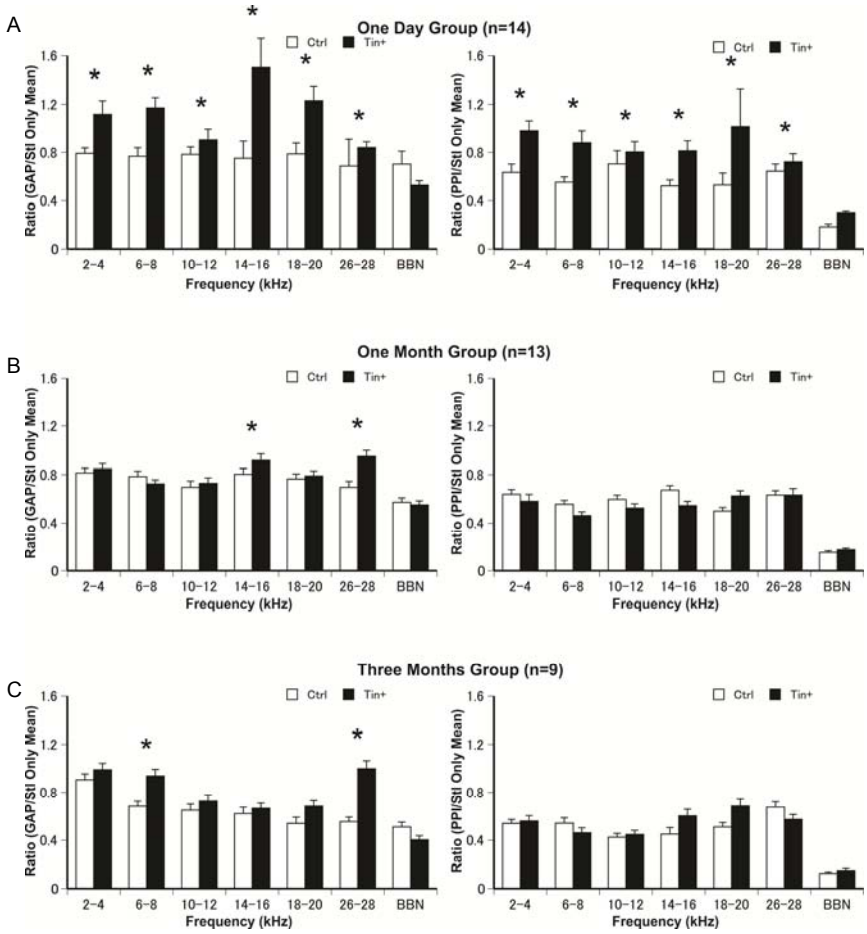

Fig. 2. At one day post-blast, rats show significant evidence of tinnitus (Gap) and auditory detection deficits (PPI) across multiple frequencies (Fig.2a). By one month post-blast, auditory deficits recover whereas tinnitus remains in most rats at 14-16 and 26-28 kHz (Fig.2b). Low-frequency tinnitus emerges while high-frequency tinnitus remains at 3 months post-blast in 5 out of 9 rats (Fig.2c).

2. Manganese-enhanced MRI (MEMRI) imaging

The intensity of the Mn^{2+} enhanced magnetic resonance signals are used to represent excitatory synaptic activities. Prior to MRI imaging, anesthesia was induced through inhalation with a mixture of air and isoflurane. Each animal was placed in a prone position and restrained on a cradle with a custom-built palate holder. The holder was equipped with an adjustable nose cone. All scans were performed on 7T Bruker USR magnet (Ultra Shielded Refrigerated, bore size 30 cm). In data analyses, for each scanning, 2 MPRAGE and PDGE image sets were created with Siemens software. Images then were processed with ImageJ and Rgui (2.12.1 version) to reduce intensity field bias. The resulting images were then analyzed with MRIcro. The region of interest (ROI) was drawn and compared in both coronal and sagittal views. The intensity of ROI was obtained with MRIcro. The signal intensity ratios of brain structures over that of surrounding muscles was measured and analyzed. At the time of MEMRI scanning, certain animals developed chronic tinnitus, and they are referred to “tinnitus positive group” or “chronic tinnitus group”. Other animals recovered from tinnitus. They are referred to “tinnitus negative group” or “transient tinnitus group”.

Our latest MEMRI data analysis showed that, compared to rats in the control group, rats in the blasted group with or without tinnitus demonstrated higher level of anxiety. MEMRI data demonstrated that rats with tinnitus at the time of the scanning exhibited hyperactivity in the contralateral basolateral nuclei of amygdala (AMG), and hypoactivity in the ipsilateral anterior cingulate cortex (ACC) (see Table below).

These changes may have contributed to psychological sequalea of blast-induced tinnitus, TBI and the posttraumatic anxiety disorders, aka. PTSD.

Table. Normalized intensity ratio of regions of interest. C: control group (n=4); B+A: blast group with high level of anxiety (n=7); T-: blasted rats without tinnitus (n=5); T+: blasted rats with tinnitus. Values with statistical significance are in bold letters.

Normalized Intensity Ratio		Amygdaloid Complex						ACC		Nucleus Accumbens				Hippocampus	
		AMG_S		AMG_D		AMG_C				Shell		Core			
		L	R	L	R	L	R	L	R	L	R	L	R	L	R
C	Mean	142	144	148	145	149	150	**108**	112	140	146	142	143	134	123
	SEV	4	3.8	4.6	3.1	2.4	3.7	**1.5**	1.1	5.7	4.8	6.2	5.9	6.6	7.8
T (-)	Mean	143	149	147	**143**	141	151	106	107	143	145	145	149	142	133
	SEV	5	5.3	5	**4.7**	5	4.4	1.2	2	5.5	5.1	6.6	6.5	9.9	7.3
	p (T- vs. C)	*1*	*1*	*1*	*1*	*0.37*	*1*	*0.51*	*0.15*	*1*	*1*	*1*	*1*	*1*	*0.97*
	p (T- vs. T+)	*1*	*1*	*1*	***0.04***	*1*	*1*	*0.49*	*1*	*1*	*0.68*	*1*	*1*	*1*	*1*
T (+)	Mean	144	150	151	**155**	146	152	**103**	108	146	152	149	154	134	138
	SEV	1.9	2.2	2.7	**2.4**	2.4	2.2	**1.1**	0.9	2.2	2.2	5.2	3.9	6.2	3.9
	p (T+ vs. C)	*1*	*0.97*	*1*	*0.18*	*1*	*1*	***0.02***	*0.31*	*1*	*0.85*	*1*	*0.48*	*1*	*0.29*
	p (T+ vs. T-)	*1*	*1*	*1*	***0.04***	*1*	*1*	*0.49*	*1*	*1*	*0.68*	*1*	*1*	*1*	*1*

3. Electrophysiology

Electrophysiological recordings were performed to obtain stimulus-driven responses from the left DCN, right IC and AC. The acoustic stimulus was broadband noise of 50 ms duration, delivered at 74 dB SPL to the left ear. Electrophysiological recordings were simultaneously performed in the left dorsal cochlear nucleus (DCN) with a 32 channel electrode array, right inferior colliculus (IC) with a 32 channel array and right auditory cortex (AC) with a 16 channel array. During data analysis, neural spikes from snipped data were acquired according to the following parameters: each sound sweep lasted 5 s, bin width = 1ms, 60 sweeps, 1s pre-sound onset as baseline, 4s after sound onset. Comparisons were made with baseline/pre-stimulation spike counts from the snipped data. Only the channels that had differentiable frequency tuning curves were analyzed. In the AC, the responses had three phases. The first peak was relate to sound onset with a peak latency of 50 ms; the second peak sound evoked response with a peak latency of 100 ms; the third one was steady-state response that appeared after the second peak and started from 200 ms, with 200 ms time window. Electrophysiology data were processed using custom-developed MatLab software.

Data*:* We found that the blast-induced responses were reduced in response to broadband noise (BBN) stimulation (Fig. 3). In the AC, a lower level BBN stimulation of blast-rats induced a smaller neural response at all three post-blast recovery times, but a higher level BBN stimulation induced the same level of responses compared to age-matched control rats except for the one-month post-blast exposure group. In the IC, there were no differences in BBN-induced responses between blasted rats and non-blasted control rats at one day after blast exposure group. However, the BBN-induced responses in blasted rats were significantly smaller than controls at both one- and three-month post-blast time points. In the DCN, blast exposure caused both immediate and long-lasting effect on BBN-induced responses at one day, one month and three month post-blast exposure time points. Compared to the control group, blast exposure at the three post-blast recovery times significantly decreased BBN-induced responses. These results indicate that blast shock wave can cause complex changes in the auditory system.

One Day group

75 dB

85 dB

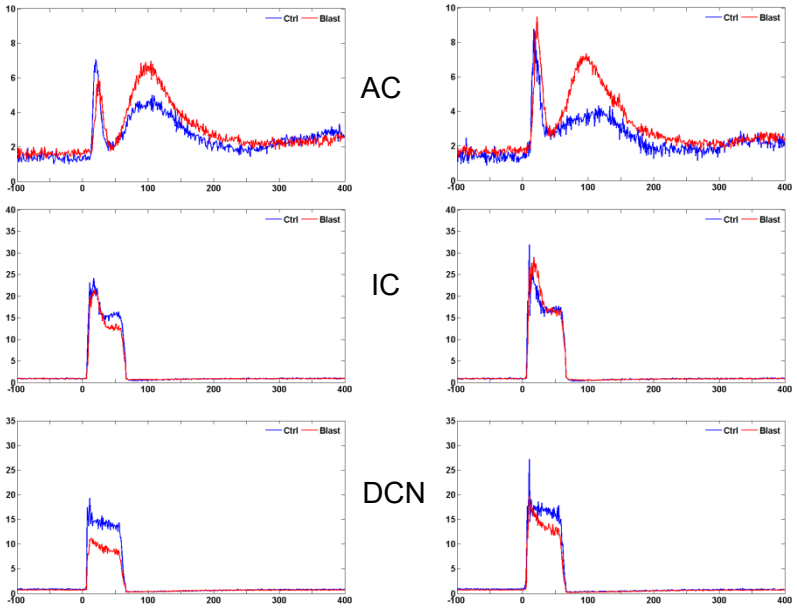

One Month group

75 dB

85 dB

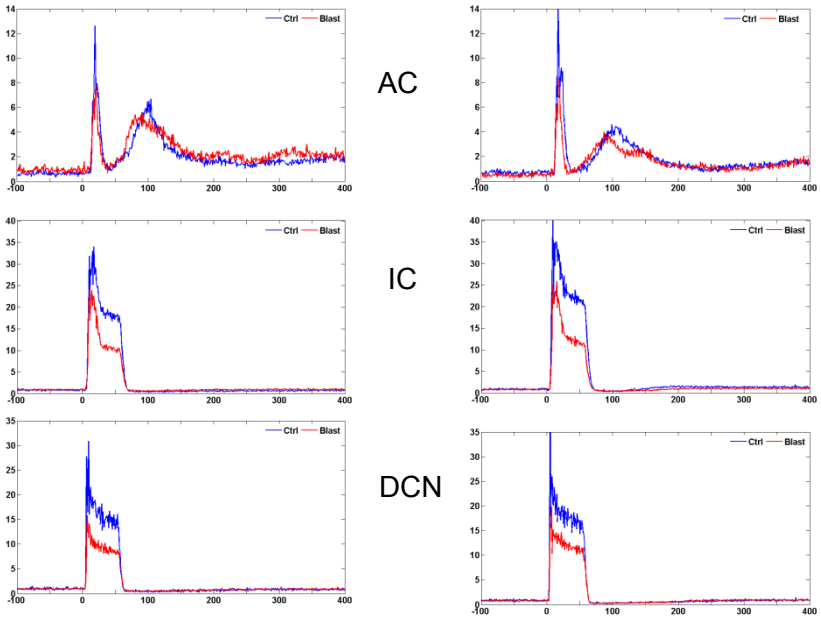

Three months group

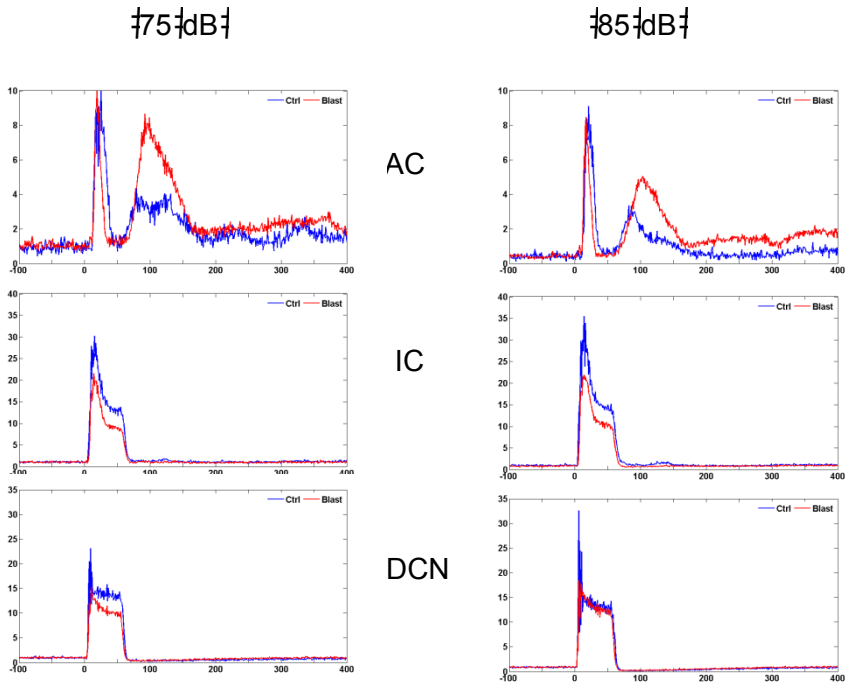

Fig. 3. Blast induced changes in stimulus-driven responses from the DCN, IC and AC.

4. Histology

a) Completion of validation of neurophysiology recording array positioning: As part of efforts to validate the positioning of neurophysiological recording arrays in dorsal cochlear nucleus (DCN), inferior colliculus (IC) and auditory cortex (AC), a sectioning procedure has been established. A total of 28 brains were processed as part of this procedure. Electrode arrays with their tips dipped in a fluorescent dye were positioned in DCN, IC and AC at the time of neurophysiology recordings. At the conclusion of their survival period (1, 30 and 90 days) and neurophysiology recordings, brains from blast exposed and sham rats were harvested and 50 µm thick frozen sections encompassing the regions of DCN, IC and AC were collected in 1X PBS filled multi-well plates. DCN sections were collected between bregma -10.68 and -11.76. For IC, sections between -7.80 and -9.24 from bregma were collected. For AC, sections between -4.08 and -6.84 from bregma were collected based on rat stereotaxic atlas [4].

Shown below are beginning and ending section co-ordinates for DCN analysis

Shown below are beginning and ending section co-ordinates for IC analysis

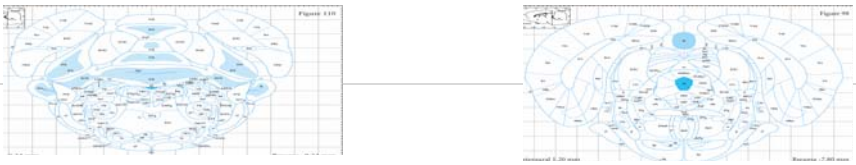

Shown below are beginning and ending section co-ordinates for AC analysis

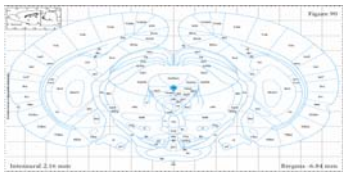

For the next step, each section was observed (4x) under a microscope and the tracks left by positioning of recording array were validated by taking a digital image. The brain sections were stored again in 1X PBS for subsequent staining procedures to observe axonal injury and inflammatory changes. With the establishment of this methodology, we were able to validate the placement of the electrode arrays (arrow head) in DCN (Figure 4a), IC (Figure 4b) and AC (Figure 4c). This validation offers credence to the neurophysiogy data recorded from these locations.

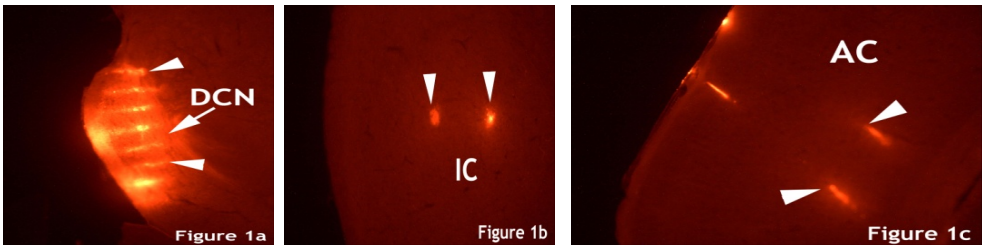

Fig. 4. Histological data showing the tracks of the implanted electrodes for electrophysiological recordings.

b) Blast overpressure induced axonal injury changes in auditory white matter tracts

We hypothesize that blast induced tinnitus may also be related to axonal injury (AI) changes in various white matter (WM) tracts of auditory pathway. Therefore, as part of our understanding on the pathomechanisms of blast induced tinnitus, representative brainstem sections (n=5 sections/location/rat) with DCN and IC and sections of AC were subjected to a silver impregnation staining technique described previously [1]. This staining technique was previously used to demonstrate the extent of diffuse axonal injury (DAI) following traumatic brain injury in rats [3]. It was also shown that blast overpressure induces DAI in cerebellar WM tracts as shown by amino cupric silver staining [2]. However, studies related to such changes in the auditory pathway are non-existent. As part of this effort we were able to establish a silver impregnation procedure that reliably revealed axons in various regions of DCN, IC and AC sections.

Data: Our results indicate the utility of this staining technique in exposing axons undergoing degenerative changes in the form of terminal retraction balls (arrow heads) and axons with swollen regions (arrow) in sections from some rats (Figure 5).

In sham sections, axons with uniform caliber could be seen coursing through the region (Figure 5A). In the DCN, degenerating axons could be seen in various regions of the section stained. The one day survival section shows axonal swellings (arrows) in a region between DCN and ganglion of the spinal nerve 5 (Figure 5B). In this section of IC at 1 month after exposure (Figure 5C), we saw degenerating axons in the form swellings (arrow) and retraction balls and debris (arrow heads Figure 5C). In this section encompassing AC, swollen axons (arrows) and axons with vacuoles and retraction balls (arrow heads) could be observed in thalamic region besides others (Figure 5D).

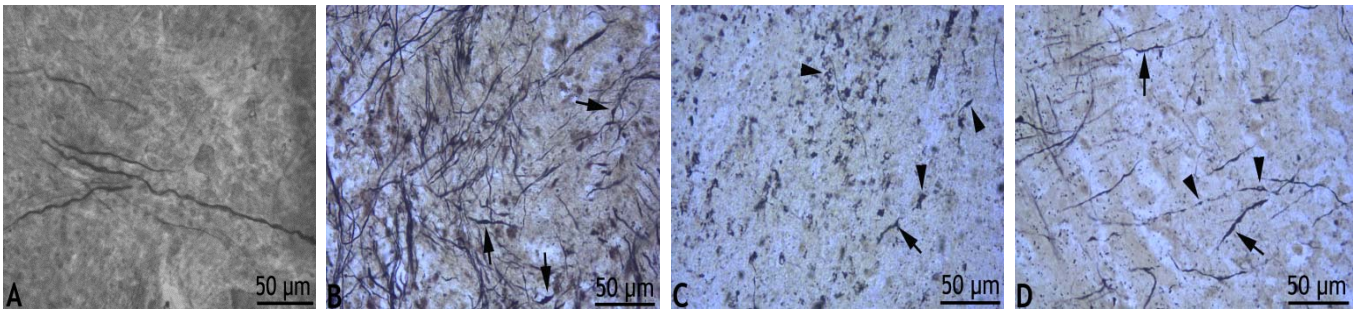

Fig. 5. Images showing the extent of degenerating axons.

c) Blast overpressure and reactive astrocytosis: We hypothesized that blast overpressure leads to inflammatory changes in brain as evidenced by astroglial reactivity in areas of auditory pathway. This astroglial reactivity was assessed in representative brainstem sections (n=5 sections/location) encompassing DCN, IC and AC subjected to overnight incubation in anti glial fibrillary acidic protein (GFAP, mouse anti GFAP cocktail, NE1015, EMD chemicals, Gibbstown, NJ) antibody and processed by avidin biotin peroxidase method.

Data: Observation of sections from sham, 1 day, 1 month and 3 month post blast revealed the presence of astrocytes in all the brain regions. However, quantification on the extent astrocyte presence was limited to the DCN (figure 6), IC (figure 7) and AC (figure 8) considering their predominant involvement in auditory functions. Quantification of the extent of reactive astrocytosis revealed that sections from blast overpressure exposure expressed a significantly higher number of astrocytes ($p=<0.05$) compared to sections from sham exposure (figure 9). Furthermore, the extent of astrocytosis was significantly higher in blast exposure sections harvested after 1 month compared to sham ($p=0.027482$). The number of astrocytes although were high at 1 day and 3 months after exposure they were not significantly different from sham and no other changes were observed (figure 7).

In the DCN, although considerably high astrocytic proliferation was observed at 1 day, 1 month and 3 months post blast, it was not significant compared to levels in sham (Figure 10A). In IC, the extent of astrocytic proliferation was markedly high at 1 month period after exposure (Figure 10B). In AC, the extent of astrocytic proliferation was significantly high at 1 month period after exposure that stayed elevated even 3months after exposure (Figure 10C).

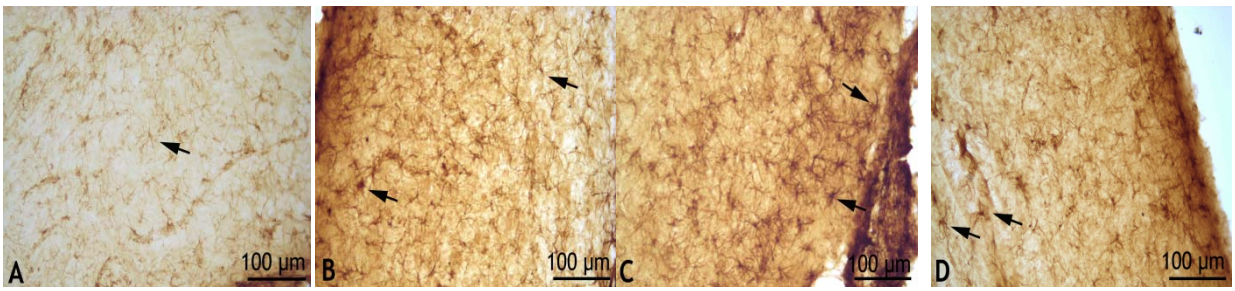

Fig. 6. Astrocytic reaction in brain section encompassing DCN. Figure 6A shows GFAP reactive astrocytes in sham sections. Figure 6B shows astrocytic reaction 1day after blast overpressure

exposure. Figure 6C shows astrocytes in DCN 1 month after exposure. Figure 6D shows GFAP reactivity in region of AC after 3 months.

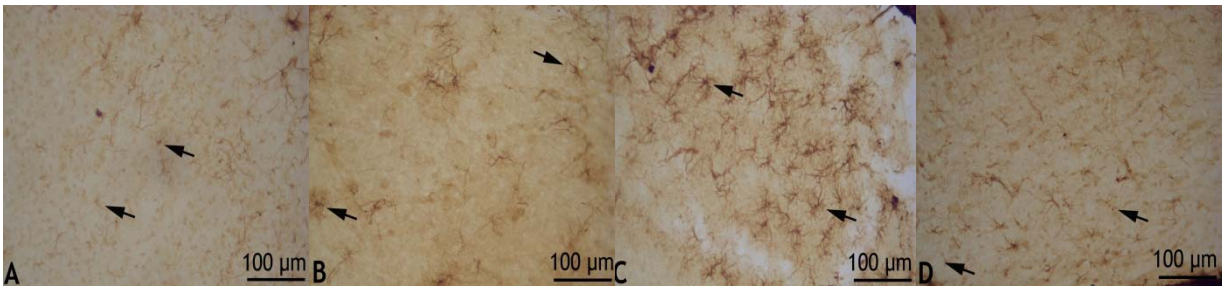

Figure 7. Astrocytic reaction in brain section encompassing IC. Figure 7A shows GFAP reactive astrocytes in sham sections. Figure 7B shows astrocytic reaction 1 day after blast overpressure exposure. Figure 7C shows astrocytes in IC 1 month after exposure. Figure 7D shows GFAP reactivity in region of AC after 3 months.

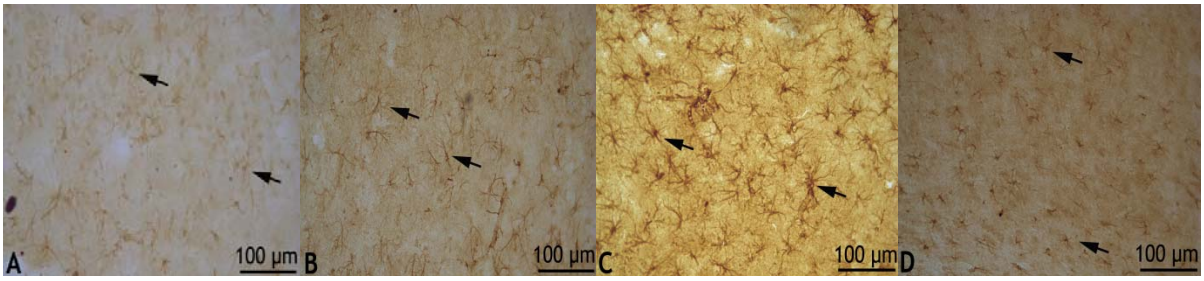

Fig. 8. Astrocytic reaction in brain section encompassing AC. Figure 8A shows GFAP reactive astrocytes in sham sections. Figure 8B shows astrocytic reaction 1day after blast overpressure exposure. Figure 8C shows astrocytes in AC 1 month after exposure. Figure 8D shows GFAP reactivity in the region of AC after 3 months.

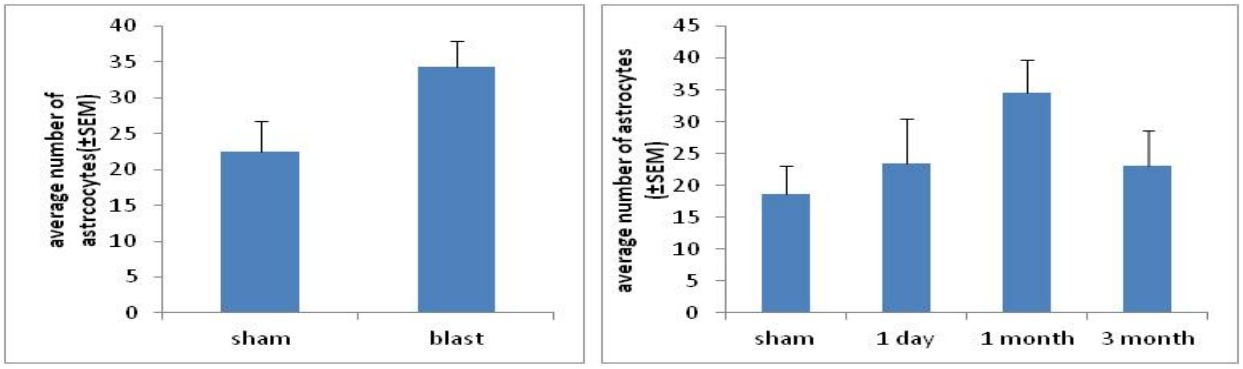

Fig. 9 Extent of astrocytic proliferation in blast and sham exposed rats. Astrocytic proliferation was significantly higher 1 month after overpressure exposure.

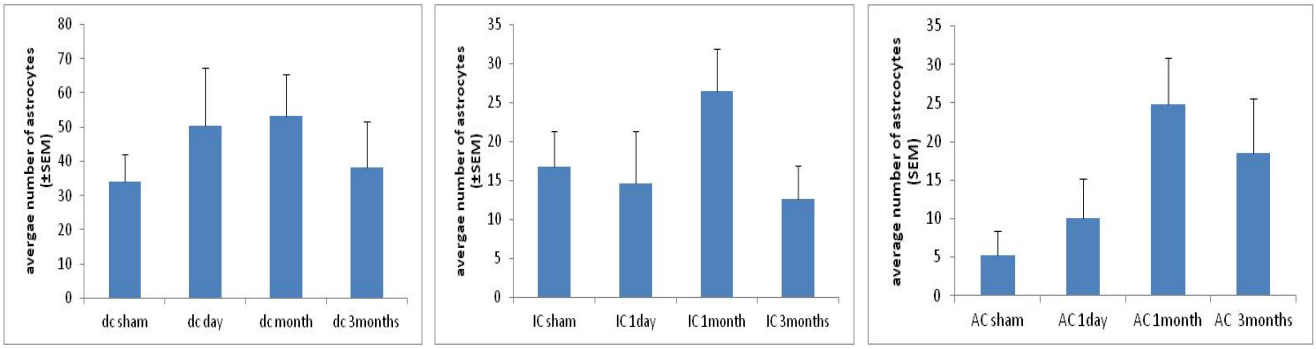

Fig. 10. Extent of astrocytic proliferation in brain sections encompassing regions of DCN, IC and AC. In DCN, although considerably high astrocytic proliferation was observed at 1 day, 1 month and 3 months post blast, it was not significant compared to levels in sham (Figure 10A). In IC, the extent of astrocytic proliferation was markedly high at 1 month period after exposure (Figure 10B). In AC, the extent of astrocytic proliferation was significantly high at 1 month period after exposure that stayed elevated even 3months after exposure (Figure 10C).

5. Concussion-induced tinnitus and hearing loss.

Rats were subjected to a single traumatic brain injury (TBI) insult using the Marmarou impact acceleration (IA) injury model. No skin incision was made in these rats unlike the traditional Marmarou model that involves exposing the skull through a longitudinal skin incision exposing the periosteum to affix a steel disc (10 mm diameter; 3 mm thickness) at the middle between bregma and lambdoid sutures. Rats were anesthetized (4% Isoflurane +0.6L/min oxygen) for 4 minutes in an induction chamber and then were positioned in a prone position on a foam bed contained in Plexiglas box. Then, 450 g cylindrical brass weight (18mm diameter) was dropped directly onto the scalp. The impact location would correspond approximately to a location between bregma and lambdoid sutures. Sham rats were subjected to anesthesia alone but not injured. Rats were subjected to 1) mild TBI by dropping the impactor from a height of 1.0m, 2) moderate TBI by dropping the impactor from a height of 1.5 m, and 3) severe TBI by dropping the impactor from a height of 1.8 m and 2.0 m respectively. Immediately after the impact, rats were removed to avoid a second impact and monitored for latency to surface right considered as an indirect indicator of loss of consciousness.

Rats were tested for tinnitus using gap-detection procedure and for auditory detection and hearing using prepulse inhibition and ABR procedures, respectively. Mild TBI (1.0 m height impactor weight drop) was initially investigated, but was not further explored due to lack of sustained anatomical, physiological, and behavioral impairment.

a) ABR data. Immediately following concussion (Post-Conc. Day 0-1), there were no significant hearing threshold shifts among the weight-drop groups in either ear (Fig11 a and b).

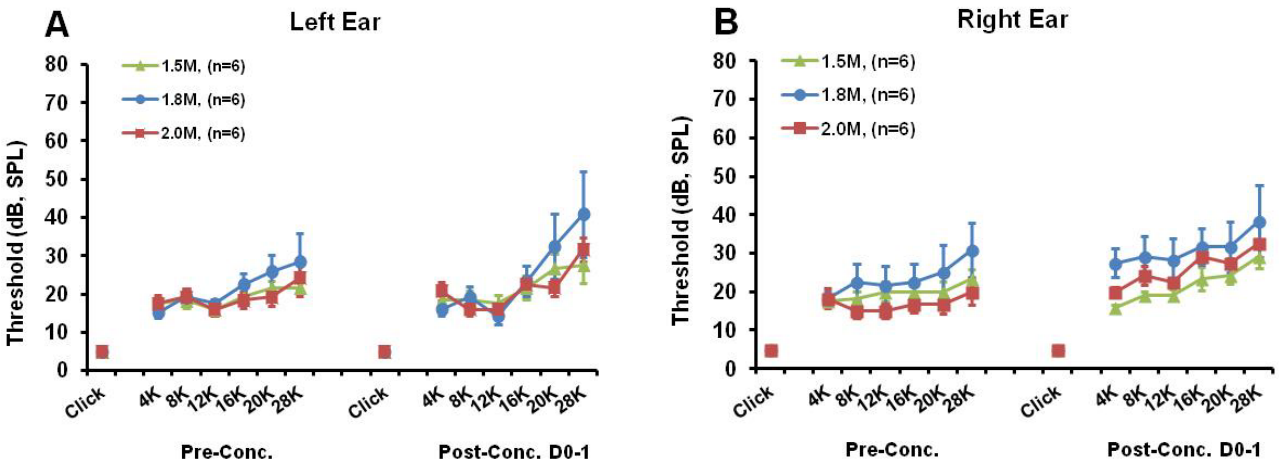

Figure 11. ABR data showing no significant threshold elevations.

b) Behavior results. Immediately following trauma (Post-Day 0), all concussed groups showed significantly elevated gap detection ratio values across the majority of frequency bands, in comparison to baseline (Pre) gap detection values (Fig 12a-f). PPI ratio values are similarly increased. These data suggest that while concussion exposure may have induced tinnitus, deficits in central auditory detection were also induced and may play a role in the apparent tinnitus behavior. At one week post-concussion, the majority of gap-detection and PPI values had returned to baseline levels, and by two weeks post-concussion, gap-detection and PPI values had completely recovered to baseline levels. Taken together, these data indicate that concussion may induce immediate tinnitus and auditory detection deficits, however this impairment mostly disappears within one week. Additionally, using 2.0 m height for impact acceleration does not seem to cause significantly greater behavioral impairments than using the 1.5 m height. We are currently subjecting rats to repeated impact acceleration to see if longer lasting behavioral impairments can be obtained.

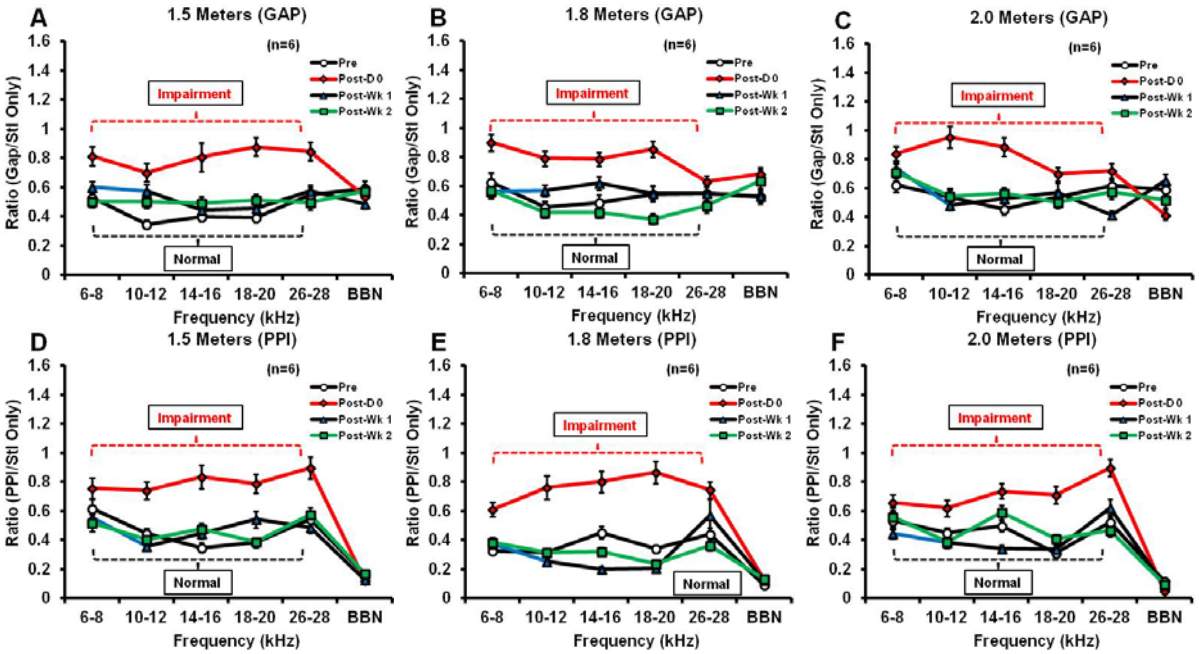

Figure 12. Gap-detection and PPI behavioral data showing tinnitus and auditory detection impairments, respectively, immediately following concussion, which mostly recovers by 1 week and completely recovers by 2 weeks.

6. Concussion histopathology.

Histopathology has been performed on 2 rats exposed to 1.0 m, 1.5 m, and 1.8 m impactor weight drop height. Rats were sacrificed two weeks after TBI for histological observations of axonal injury.

Data. No skull fractures, respiratory depression or seizures were observed in any of the rats. 40 µm thick sections of brainstem were subjected to beta amyloid precursor protein (βAPP) immunocytochemistry. βAPP reactivity is a reliable marker of axonal injury. Rats subjected to severe TBI (1.8 m) exhibited prolonged duration to surface right compared to rats from other groups (Fig. 13a). Rats subjected to TBI from 1.8 m showed axonal injury in regions of brainstem (Fig. 13b) predominantly in the reticular formation and pyramidal tracts. No apparent axonal injury was evident in rats exposed to the 1.0 m impactor weight drop height (Fig. 13c).

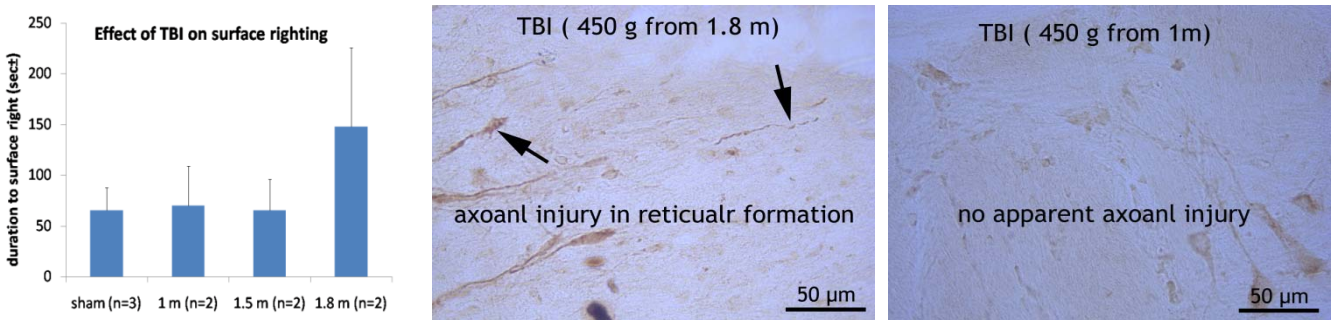

Fig. 13: Image showing surface righting duration in rats subjected to varying severities of TBI (Fig. 13a). Rats subjected to TBI from 1.8 m (Fig. 13b) showed prominent axonal injury while those exposed to 1.0 m (Fig. 13c) did not.

HUMAN STUDIES

In the second year, we were able to recruit 28 qualified human subjects with blast-, concussion- and both blast-and concussion-induced tinnitus. Among the subjects recruited, 17 were blasted, 6 concussed and 5 with both blast concussions. Based on our established protocols, we conducted tests using audiometric, neuropsychological, psychoacoustic, questionnaire, and magnetic resonance imaging measures. The audiometric studies included audiograms, word recognition studies in quiet and noise conditions, loudness measures, middle-ear power reflectance, DPOAE, tinnitus handicap questionnaire data. The neuroimaging tests included standard MRI, DTI and SWI and MRS in resting state. Our studies demonstrated that patients with blast-induced tinnitus showed symmetrical hearing thresholds, normal DPOAE which is consistent with outer hair cell conditions, but with increased fractional anisotropy (FA) particularly in the corpus callosum and corona radiadata, normal SWI except for a few patients. Our results also showed that patients with concussions have more significant HL with excessive variability (mixed and sensorineural) with asymmetric power reflectance values (200-2000 Hz) and a differential pattern for left and right ears. While patients with both blast and concussion-induced tinnitus had less hearing loss than blast or concussion categories, tinnitus loudness was greatest for blast and concussion patients and least for blast alone, with concussion having

intermediate loudness values. Below are detailed descriptions our human studies over the past year, which are organized chronologically.

April, 2012
Behavioral and imaging studies
Anthony T. Cacace, Ph.D.

As noted in our previous report, auditory based protocols that have been established to assess for blast-induced, concussion-induced, and blast + concussion induced tinnitus and they are working smoothly and without problems. Recruitment through the VA Medical Center in Ann Arbor Michigan continues to be slow, although this should pick up for two reasons: 1) a new satellite clinical has just been opened in Toledo, Ohio (about a 1 hour drive to Detroit) is now operational and seeing patients, and 2) the Polytrauma group at the VA Medical Center in Ann Arbor will help to recruit subjects both from their database and as new subjects are enrolled at their facility.

We continue receiving referrals through Dr. Randall Benson, a neurologist that is collaborating on this project and we have reached out to others at the Rehabilitation Institute of Detroit, and other facilities that have special interest in mild traumatic brain injury, including tinnitus. Furthermore, recruitment efforts through advertisements in both local Detroit area newspapers and through the Wayne State University campus-wide intranet is in place and should be activated shortly.

Below, two participants are reviewed in this progress report. The first, (Participant A) is a 68 year old male with blast-induced tinnitus secondary to a munitions round from a tank accidently exploding when the he was standing beside the vehicle without any type of ear protection being worn. Since the insult, he had developed mild to profound sensorineural hearing loss bilaterally and constant tinnitus. He did not report hearing loss or tinnitus prior to the time of the blast, and has always worked as a grocer in a small lake town in Michigan.

The second participant (Participant B) is a 57 year old male with tinnitus secondary to a motor vehicle accident, where he was rear ended and suffered a severe concussion. Following the accident, he was knocked out for more than 20 minutes and had post concussion syndrome, and saw stars. Since the motor vehicle accident, he has had chronic tinnitus. Hearing loss appears consistent with his age.

Participant A.
Automatic Neuropsychological Assessment Metric (ANAM):

	Average or below	Below Average	Clearly below
Simple reaction time		**X**	
Processing speed:		**X**	
Code substitution (learning)			**X**
Code substitution (delayed memory)			**X**
Math processing (working memory)	**X**		
Match-to-sample (spatial memory)	**X**		

Iowa Tinnitus Handicap Questionnaire

Total	Mild-moderately depressed
Social Emotional Behavioral	Mildly depressed
Tinnitus and Hearing	Moderately depressed

Audiometric Data and psychoacoustic data

TinnitusLoudness Level: 68 dB SPL
Base on Magnitude Estimation

Audiogram:
Left ear: Borderline normal hearing sensitivity 0.25-1.0 kHz, mild to profound sensorineural hearing loss 1.5-8.0 kHz.
Right ear: Borderline normal hearing sensitivity 0.25-1.0 kHz, moderate to profound sensorineural hearing loss 1.5-8.0 kHz.

Distortion Product Otoacoustic emissions (DPOAEs):
Left ear: Present DPOAEs 0.842 kHz – 1.831 kHz, absent 2.0-7.996 kHz.
Right ear: Present DPOAEs 0.842 kHz – 1.831 kHz, absent 2.0-7.996 kHz.
Middle ear Power Reflectance:
Left ear: Normal; but lower reflectance seen in the 0.2-0.3 kHz region.
Right ear: Normal

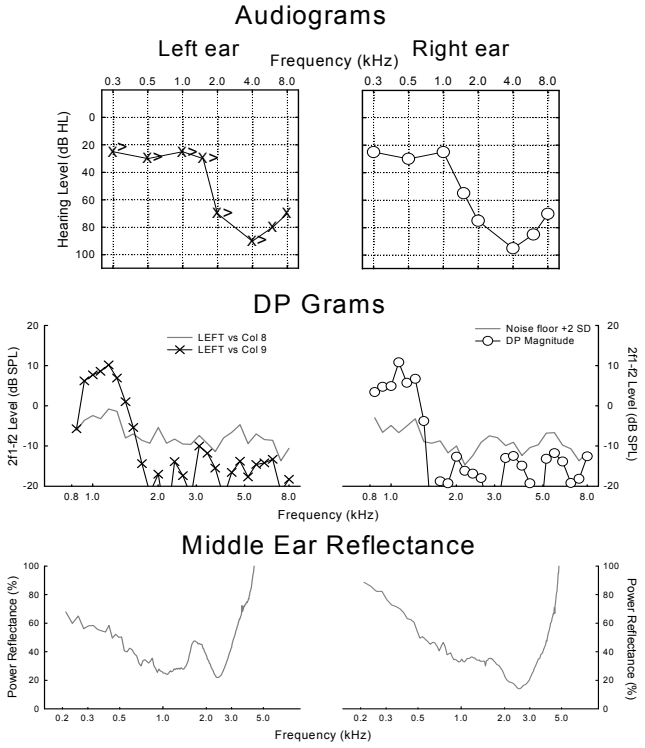

Figure 1. *Audiometric Data from participant A: Top) audiograms for left and right ears; middle) distortion product otoacoustic emission data for left and right ear; bottom) middle ear power reflectance data for left and right ears.*

Participant B.
Automatic Neuropsychological Assessment Metric (ANAM):

	Average or below	Below Average	Clearly below
Simple reaction time			**X**
Processing speed:			**X**
Code substitution (learning)			**X**
Code substitution (delayed memory)	**X**		
Math processing (working memory)			**X**
Match-to-sample (spatial memory)			**X**

Iowa Tinnitus Handicap Questionnaire

Total	In progress
Social Emotional Behavioral	In progress
Tinnitus and Hearing	In progress

Audiometric Data and psychoacoustic data

Tinnitus Loudness Level: 52 dB SPL
Base on Magnitude Estimation

Audiogram:
Left ear: Mild to moderately severe sensorineural hearing loss, 0.25-8.0 kHz.
Right ear: Borderline normal to moderately severe sensorineural hearing loss, 0.25-8.0 kHz.

Distortion Product Otoacoustic emissions (DPOAEs):
Left ear: Present DPOAEs 0.842 kHz –2.185, absent 2.380-7.996 kHz.
Right ear: Present DPOAEs 0.842 kHz –2.380, absent 2.600-7.996 kHz.
Middle ear Power Reflectance:
Left ear: Normal
Right ear: Normal

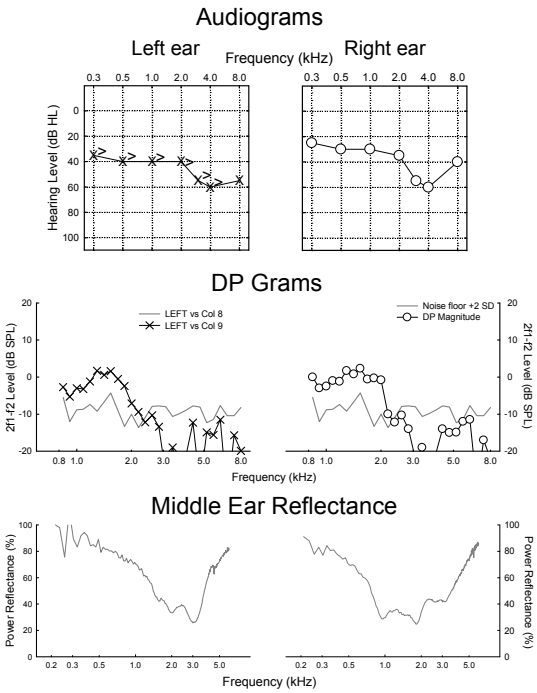

Figure 2. *Audiometric Data from participant B: Top) audiograms for left and right ears; middle) distortion product otoacoustic emission data for left and right ear; bottom) middle ear power reflectance data for left and right ears.*

Magnetic Resonance Imaging Data

MRI data is only available for Participant A; Participant B was tested on 04/09/2012, and data analysis is not completely analyzed. Technical parameters for the standard high resolution MRI sequences (MPRAGE), susceptibility weighted imaging (SWI, and diffusion tensor imaging (DTI) are shown below in the table.

Sequence Name	TR	T E	Flip Angle	Bandwidth	Matrix	Spacing	Thickness	Spacing
Localizer	8.6	4	20	320	512*512	0.5*0.5	7	8.4
T1 Flash Sagittal	443	2.54	90	330	256*256	1*1	3	3.75
MPR Coronal	1600	4.28	8	180	384*384	0.67*0.67	1.34	-
SWI	30	6.97	15	465	512*384	0.5*0.5	2	-
DTI	7400	106	90	1395	128*128	2*2	3	3

With respect to the DTI aresults, the graph below shows global fractional anisotropy (FA) data vs. age for a group of i*ndividuals having hearing loss alone (in blue) and subject with hearing loss and tinnitus.* Hearing loss alone is the relevant control group in this comparison. In this context, global white matter FA values for this individual with

Voxels	Z-MAX	Z-MAX X (vox)	Z-MAX Y (vox)	Z-MAX Z (vox)	side	JHU White matter Labels
668	10.2	117	118	103	L	SCR
135	6.6	101	86	83	-	Splenium
128	8.04	113	96	120	L	SLF
117	9.65	63	151	90	R	ACR
81	5.5	114	115	88	L	ACR

blast-induced tends to be in the upper normal range when compared to the subjects having hearing loss with no tinnitus.

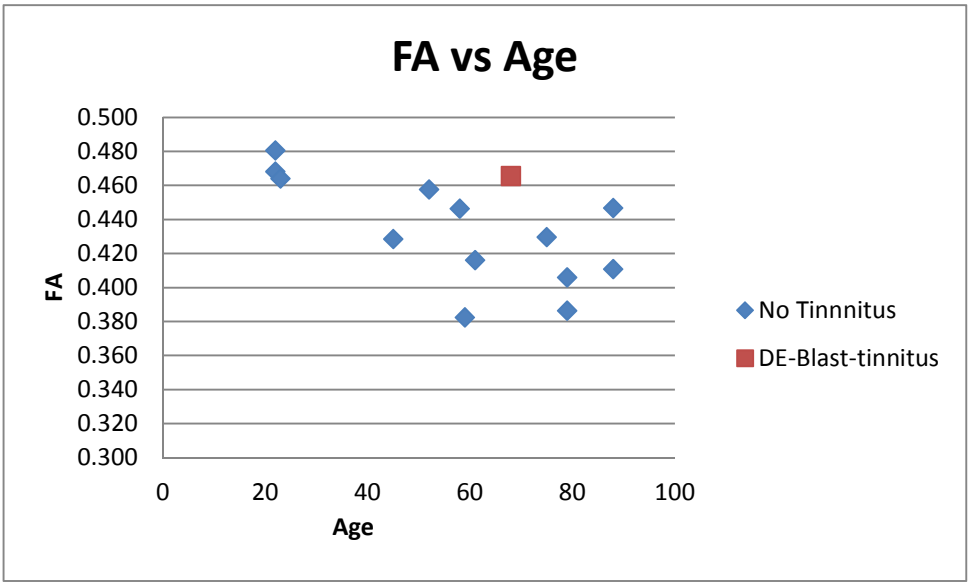

Using track based spatial statistics, while there were locations **of <u>lower</u>** FA in the superior and anterior corona radiata on the left side, superior longitudinal faciculus on the left side, and the anterior carona radiate on the right side (table shown below).

<u>Table showing the regions with lower FA:</u>

**SCR – Superior Corona Radiata; SLF- Superior Longitudinal Fasiculus; ACR Anterior Corona Radiata. *SCR – Superior Corona Radiata; SLF- Superior Longitudinal Fasiculus; ACR- Anterior Corona Radiata, ATR-Anterior Thalamic Radiation.*

However, the new and most important findings were areas of **<u>increased FA</u>** primarily on the left side of the brain. (see figure below).

The colored areas on the left side of the axial brain images are noteworthy since they show regions that are +3 standard deviations above the mean FA of the group that have hearing loss but no tinnitus. Thus, high FA values in the participant with blast-induced tinnitus are abnormal and may represent areas of increased myelination, decreased axonal diameter, and possible increased packing density.

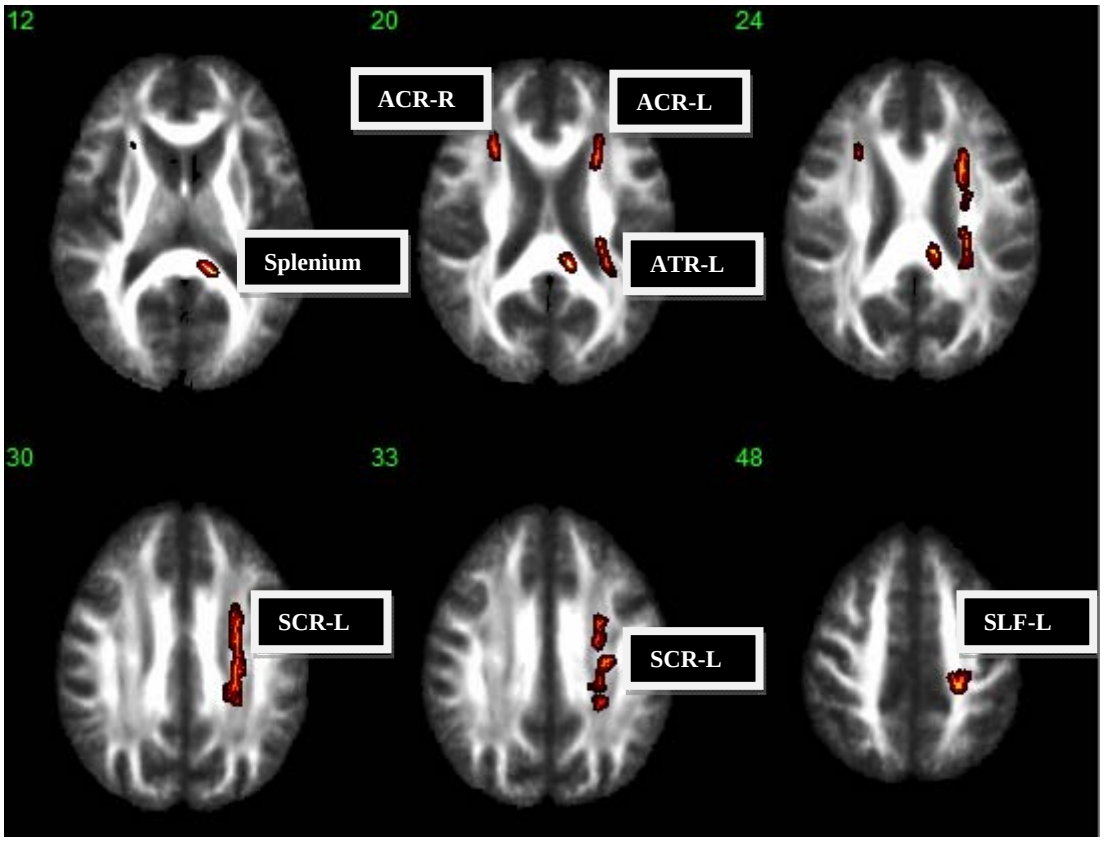

<u>Figure showing the regions with increased FA.</u>

<u>Susceptibility Weighted Imaging (SWI)</u>.
The SWI data were quantified for iron content in each selected structure CN: Caudate Nucleus; GP: Globus Pallidus; PUT: Putamen; PT: Pulvinar Thalamus;RN: Red Nucleus; SN: Substantia Nigra; THA: Thalamus. In general, iron content in the deep grey matter for this subject was considered normal, but four out of seven regions were found to have iron content lying close to the 95% confidence interval on the iron vs age plots seen below.

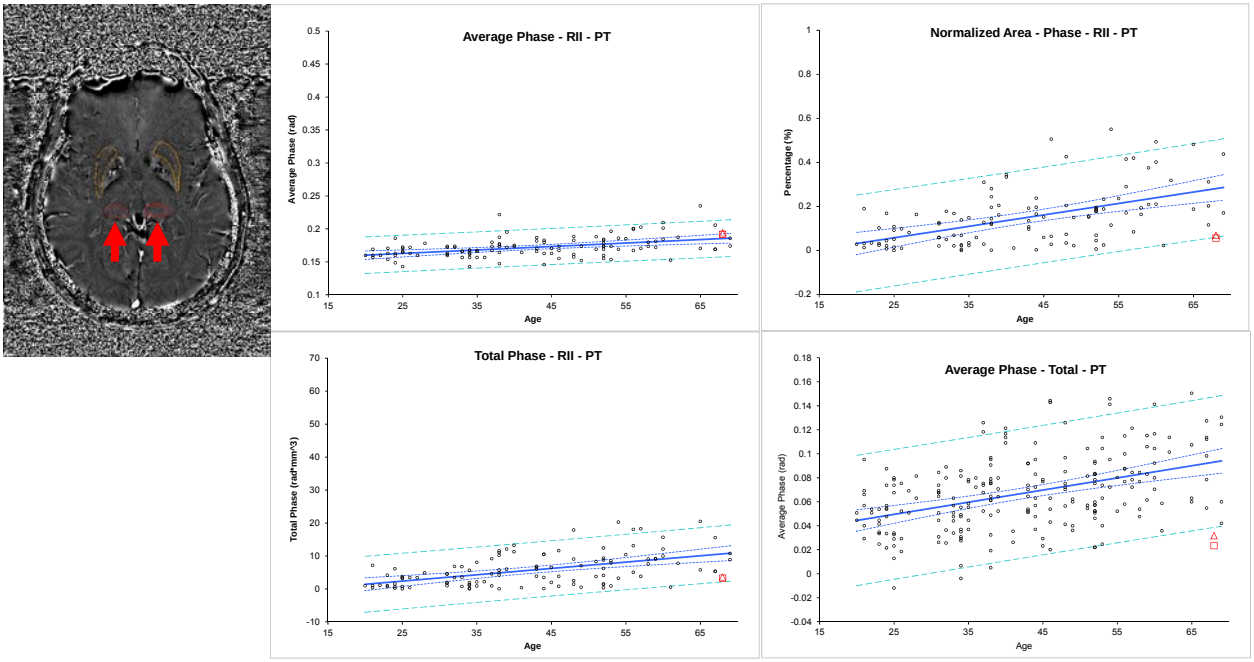

In summary, the individual with blast induced tinnitus had abnormal imaging findings of increased FA primarily focused in while matter on the left side of the brain using DTI. These are new and potentially important findings that will require further data to substantiate.

Blast + concussion. Trends in this category (n = 1) cannot be observed due to limited data. However, borderline normal to moderate sensorineural hearing loss is observed.

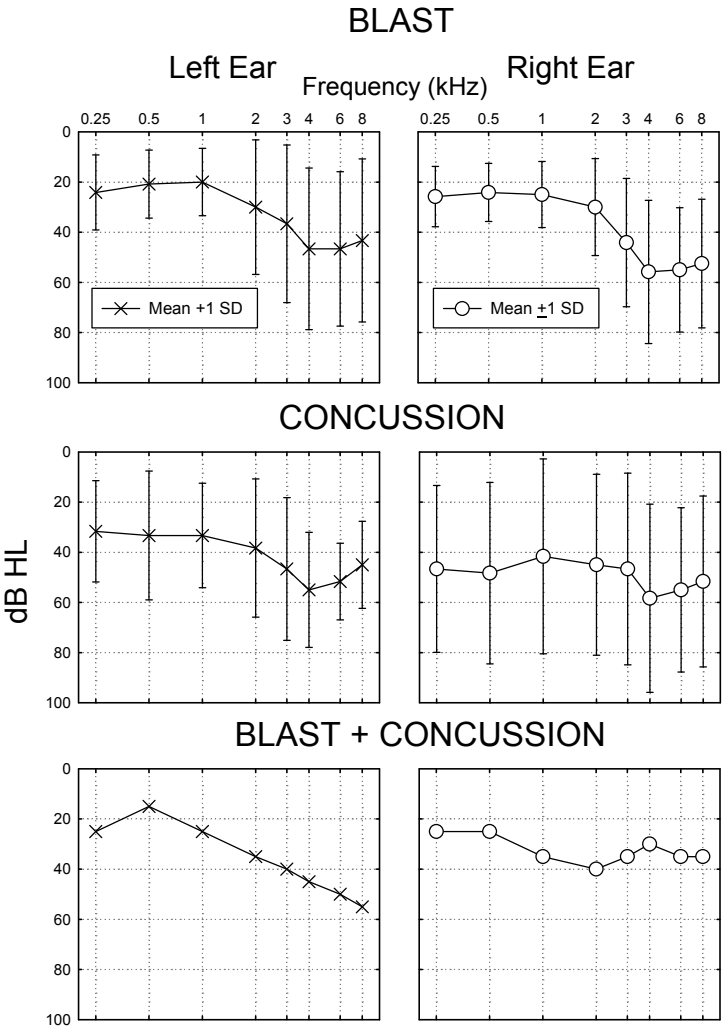

***Figure 2**. Summary audiometric data as a function of category (blast, concussion, and blast + concussion) and ear.*

Middle ear power reflectance.

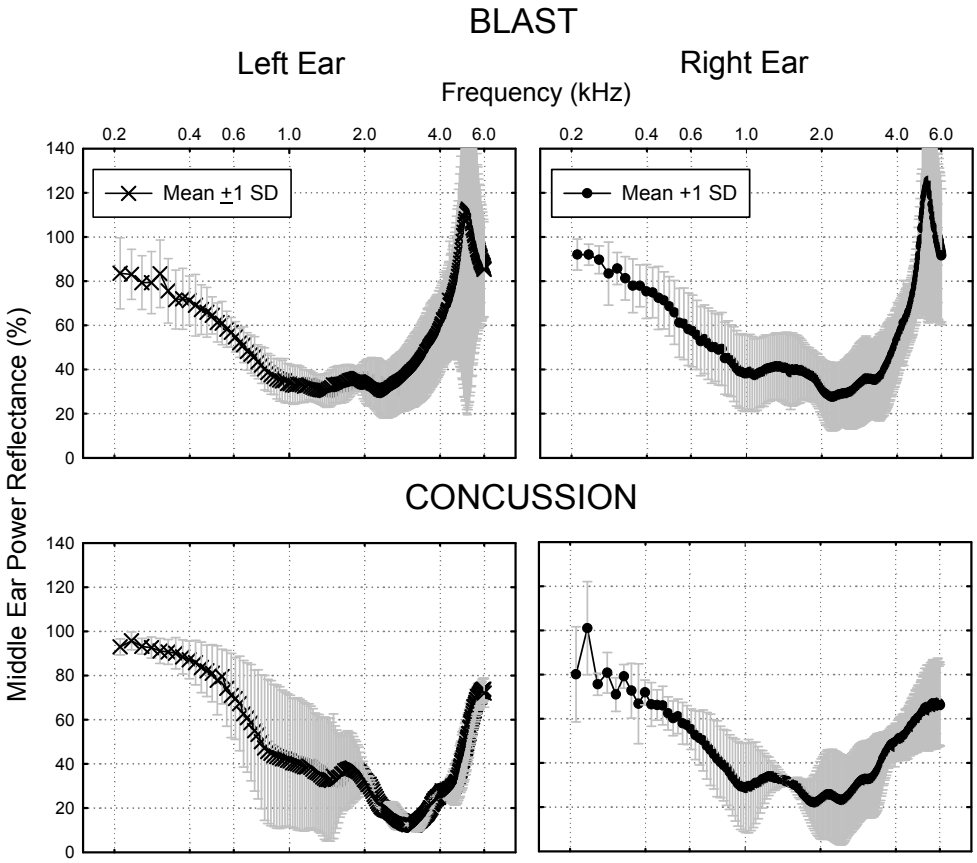

Figure 3. *Middle ear power reflectance for blast and concussion categories.*

Distortion Product Otoacoustic Emissions.

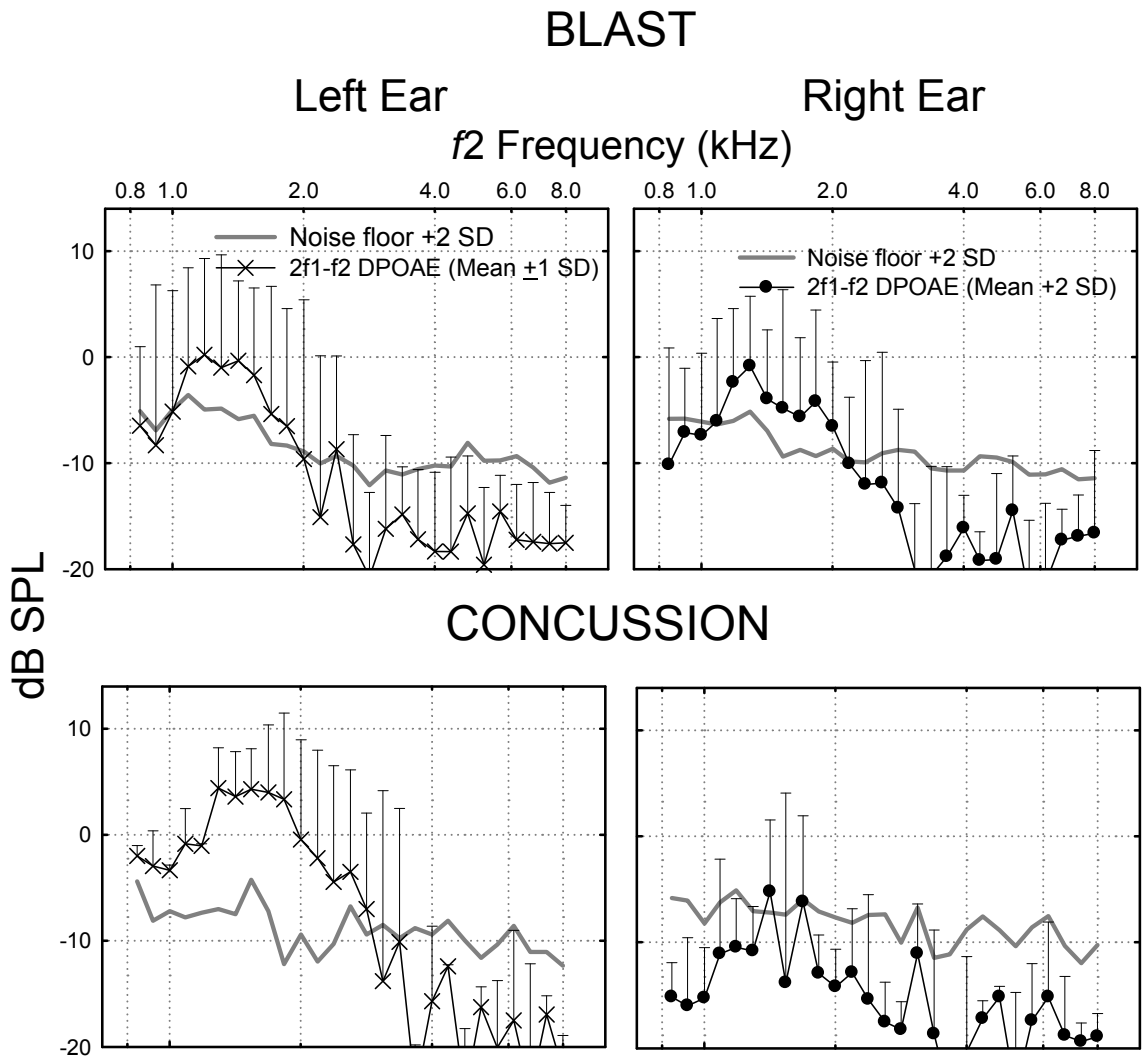

Figure 4. Distortion production otoacoustic emissions for blast and concussion categories for left and right ears.

Word recognition performance.
Monosyllabic word recognition performance was measured in quiet and in the presence of background noise for each ear at an input level at eight 75 or 80 dB HL. The Words-in-Noise (WIN) Test varies the speech-to-babble ration from 24 to 0 dB, at seven levels, and in 4-dB steps in order to generate a psychometric function. The 50% point of the psychometric function is determined and a single value expressed as a signal-to-noise or speech-to-babble (SBR) ratio is reported. Performance ranges from normal: -2.0-6.0, mild: 6.8-10.0, moderate: 10.8-14.8, severe: 15.6-19.6, to profound: 20.4-25.2.
Speech in Quiet:
Blast: Near 100% performance is observed bilaterally.
Concussion: Because of increased degree of peripheral hearing loss in this category, mild to moderately depressed performance is observed bilaterally (> for right ear) for reasons previously described (Figure 4).
Speech in Noise:
Blast: Normal performance to mildly depressed scores.
Concussion: Normal to moderately depressed scores (Figure 5). The WIN test seems to better segregate categories.

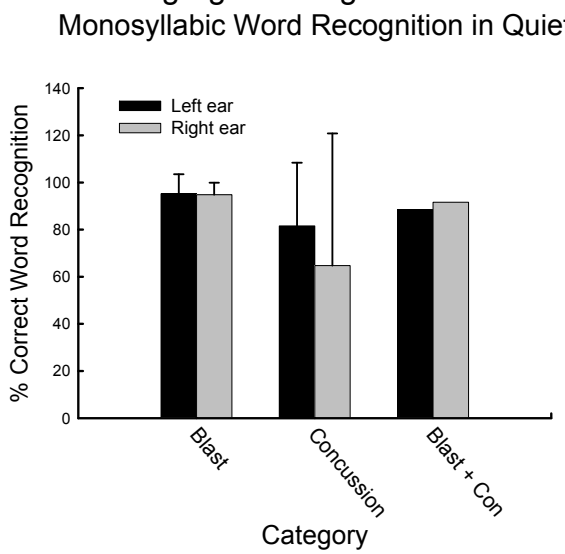

Figure 5*. Word recognition performance in quiet as a function of category and ear.*

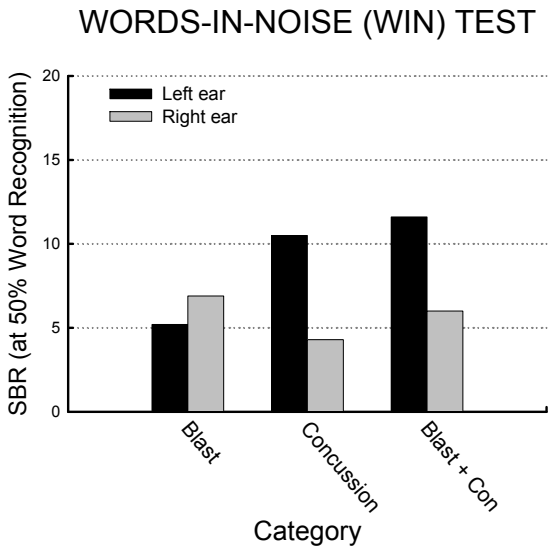

Figure 6*. WIN Test performance as a function of category and ear*.

Tinnitus Loudness.

Loudness level measures were derived from a magnitude estimation (ME) function for a 1.0 kHz tone. Once obtained, participants estimated tinnitus loudness by provided a numerical estimate. The ME function was bisected at this value and the loudness level in dB was obtained.

Blast. Moderate tinnitus loudness levels were observed.

Concussion. Moderate-to-moderately severe tinnitus loudness levels were observed.

Tinnitus loudness increased in severity among the various carigories (Figure 6).

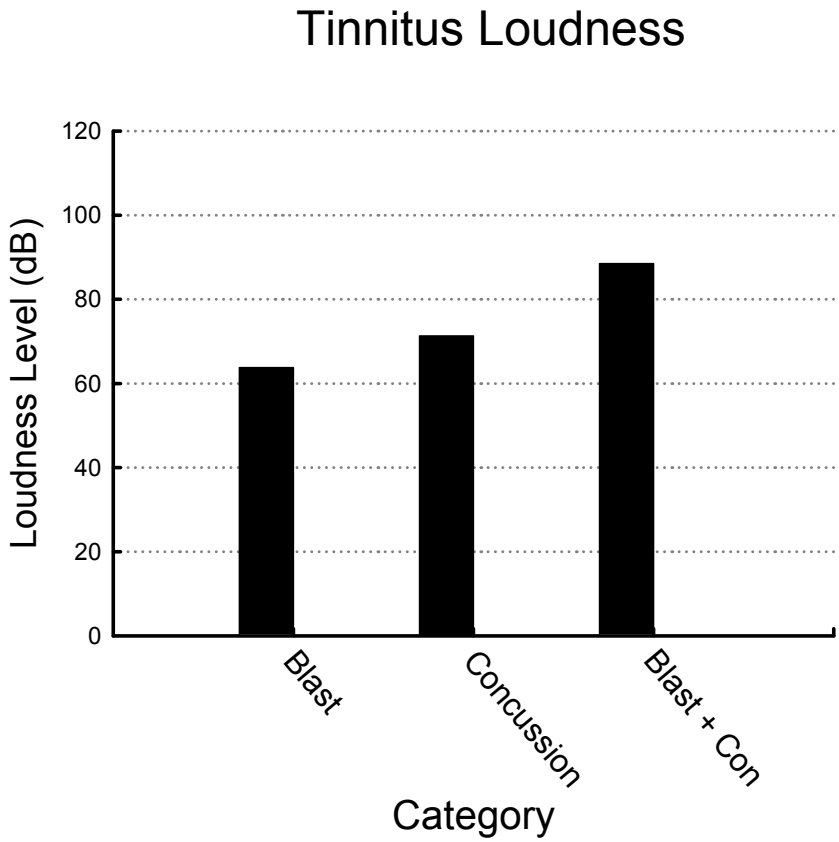

Figure 7*. Tinnitus loudness levels as a function of category.*

Tinnitus Handicap Questionnaire (THQ).
The THQ is a reliable measure of tinnitus distress, broken into 3 factors or subscales. Factor 1: social, emotional, and behavioral issues; Factor 2: issues related to tinnitus and hearing; factor 3: Total composite score across factors or subscales (Figure 7).
Blast. Moderately depressed performance across all factors.
Concussion. Moderately depressed performance across all factors.

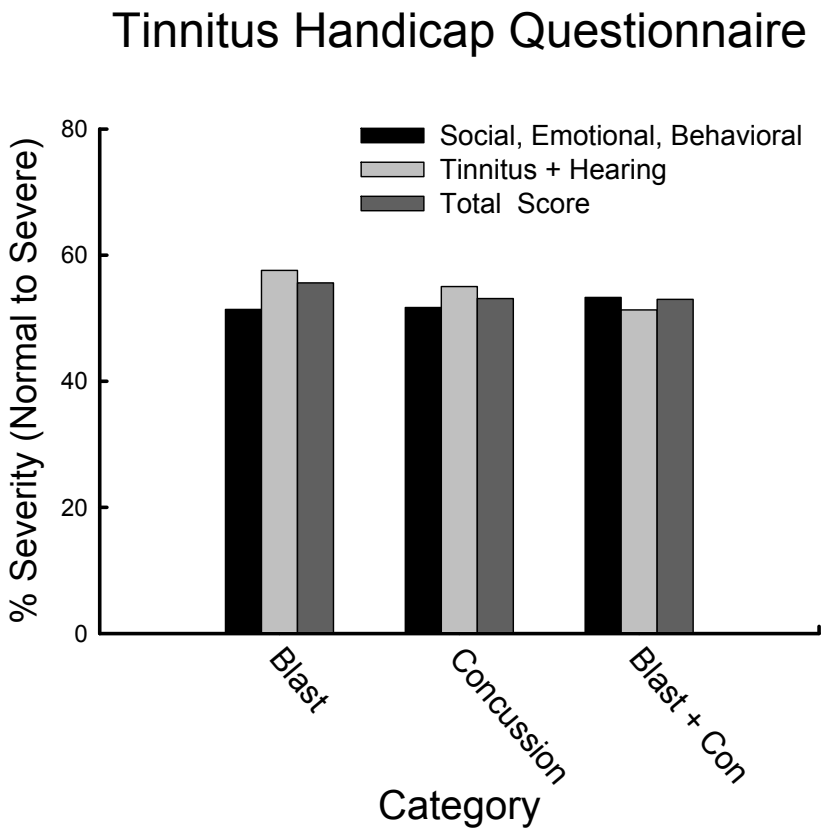

***Figure 8**. Tinnitus Handicap Questionnaire as a function of individual factors or subscales.*

Neuropsychological Assessment.

As of 9 July 2012, we have tested 7 participants who have experienced a blast injury, 3 participants who have experienced a concussive injury, and one participant who has experienced both blast and concussive injuries. The relatively small cell sizes preclude statistical analysis at this point, but we anticipate that our group sizes will increase over the coming months. At that point, preliminary statistical analyses can be performed. Using the computerized neuropsychological testing program, ANAM, there are a number of variables that can be investigated. The principal dependent variables are 1) Mean (and Median) Reaction Time to Correct Responses; 2) Percent Correct (Accuracy); 3) Standard Deviation of Reaction Times to Correct Responses (SDRTC; to investigate patterns of intra-individual variability); and 4) Throughput (number of correct responses per minute, which combines speed and accuracy into a single measure). Cognitive measures from ANAM include 1) Simple Reaction Time (SRT), repeated twice to evaluate for fatigability; 2) Procedural (Choice) Reaction Time (PRO); 3) Mathematical Processing (MTH); 4) Matching-to-Sample (Working Memory; MTS); 5) Code Substitution (Processing Speed; CDS); and 6) Code Substitution Delayed (delayed incidental recall; CDD). Mood data and Traumatic Brain Injury (TBI) symptom data are currently being aggregated.

Below, we present a table of means and standard deviations for relevant variables in this aspect of the study. Interpretation of patterns of these means and standard deviations is somewhat speculative, given the small cell sizes. With that caveat in mind, the mean age of the groups is relatively comparable. Reaction times to correct responses suggest a trend toward slowed reaction times in the concussion group, and there also appears to be considerably more inter-individual variability (greater standard deviations) for the concussion group relative to the blast group). Accuracy across most measures was at 80% or greater, with the exception of Code Substitution Delayed. The relatively low performance across groups suggests difficulty with incidental learning. Accuracy for SRT 1 and SRT 2 are omitted because the accuracy is 100% for all individuals by default. Throughput indexes (number of correct responses per minute) suggest greater cognitive efficiency in the blast group relative to the concussion group. This disparity was greatest for Simple Reaction Time and Mathematical Processing. However, throughput appeared to increase for the concussed group during the second administration of Simple Reaction Time, compared to the first administration. This pattern suggests somewhat less fatigability for the concussed group relative to the blast group. Finally, inspection of the standard deviation of reaction times for correct responses suggests considerable intra-individual variability among concussed participants relative to the blast participants. This pattern of performance may underlie the concussed group's reduced cognitive efficiency.

		Blast (n=7)		Blast+Concussion (n=1)		Concussion(n=3)	
	Variable	mean	sd	mean	sd	mean	sd
	Age	58.29	13.5	62	NA	55.33	7.64
SRT 1	MeanRTCorrect	284.93	60.36	264.51	NA	463.51	196.79
SRT 2	MeanRTCorrect	315.79	131.02	267.79	NA	491.58	410.93
PRO	MeanRTCorrect	686.04	77.7	626.52	NA	763.93	253.59
MTS	MeanRTCorrect	2309.71	679.99	2416	NA	2852.2	1678.41
MTH	MeanRTCorrect	2695.7	740.13	3514.75	NA	3914.75	1278.89
CDS	MeanRTCorrect	1703.19	380.47	1918.85	NA	2016.37	221.45
CDD	MeanRTCorrect	1984.26	1010.56	1498.72	NA	2243.1	427.91
PRO	Accuracy	96.43	4.58	96.88	NA	98.96	1.8
MTS	Accuracy	85.71	10.18	65	NA	83.33	10.41
MTH	Accuracy	92.14	9.51	80	NA	95	8.66
CDS	Accuracy	96.82	2.62	100	NA	95.37	3.49
CDD	Accuracy	62.7	12.72	50	NA	68.52	8.93
SRT 1	Throughput	217.45	38.28	226.83	NA	150.84	77.06
SRT 2	Throughput	210.98	62.22	224.05	NA	179.3	104.21
PRO	Throughput	84.88	11.68	93.1	NA	82.34	25.69
MTS	Throughput	24.43	9.61	17.07	NA	20.14	9.76
MTH	Throughput	21.69	6.75	12.39	NA	15.77	7.7
CDS	Throughput	35.49	7.9	31.27	NA	28.71	2.94
CDD	Throughput	19.45	9.56	17.86	NA	16.87	2.14
SRT 1	SDRTCorrect	85.34	42.48	81.65	NA	506.85	670.38
SRT 2	SDRTCorrect	225.44	161.47	125.64	NA	338.44	417.35
PRO	SDRTCorrect	225.23	117.89	163.88	NA	377.18	284.17
MTS	SDRTCorrect	662.98	273.91	979.91	NA	1405.98	920.08
MTH	SDRTCorrect	808.47	259.92	1204.89	NA	1220.09	526.3
CDS	SDRTCorrect	477.38	140.61	504.62	NA	723.93	170.54
CDD	SDRTCorrect	739	401.35	460.31	NA	1468.08	465.3

Magnetic Resonance Imaging Data (Blast results only).

Goal: To process and analyze Magnetic Resonance images acquired to better understand the neurobiology of tinnitus and its relationship to white matter connectivity in the brain using Diffusion Tensor Imaging (DTI) besides with Susceptibility Weighted Imaging (SWI) to measure iron in seven different structures located in the deep grey matter.

A. Methods and Data Processing: There are 7 subjects with blast-induced tinnitus and 13 subjects without tinnitus considered to be normative control data to carry out preliminary statistical analysis.

C. DTI Results:

2.1 Global results (FA vs Age) :

The following graphs illustrate the FA values plotted against age for a group of people having hearing loss alone (in blue) and subject with hearing loss and Tinnitus in different colors.

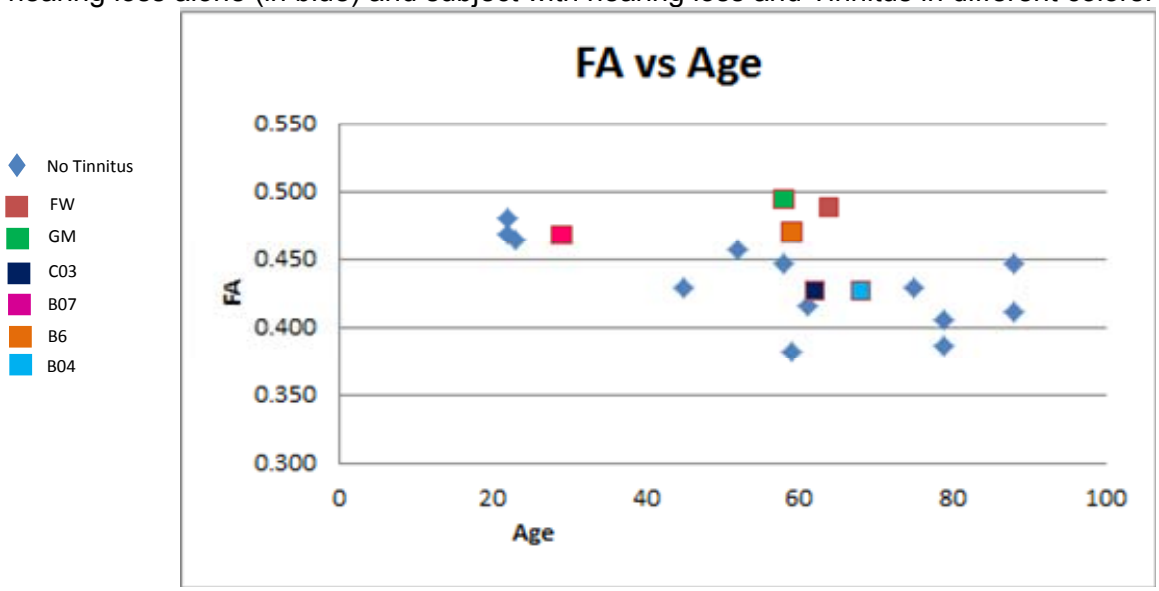

Discussion

Global WM FA values for all the subjects with Tinnitus and hearing loss, tends to be within the range when compared to the subjects having hearing loss with no Tinnitus. This result indicates that there is no difference in the white matter FA globally.

2.2 TBSS group wise results:

Table showing the regions with decreased/increased FA:

	DECREASED FA			INCREASED FA		
CASE ID	SLICE NO.	REGION NAME	RIGHT/LEFT	SLICE NO.	REGION NAME	RIGHT/LEFT
GROUP	65	CBT	LEFT	65	IFO/ILF/UNC	RIGHT
	119	SCR	RIGHT	70	GCC	LEFT
				78	PLIC	RIGHT
				90	PCR	LEFT
				95	ACR	RIGHT
				99	SCR	LEFT

				104	BCC	RIGHT
				129	SPCR	RIGHT

**SCR – Superior Corona Radiata; SLF- Superior Longitudinal Fasiculus; SPCR- Superior Posterior Corona Radiata, ACR- Anterior Corona Radiata, IFO - Inferior Fronto-Occipital Fasciculus; ILF – Inferior Longitudinal Fasciculus; UNC – Uncinate Fasciculus; PLIC – Posterior Limb of Internal Capsule; PCR – Posterior Corona Radiata.*

Figure showing the regions with decreased/increased FA:

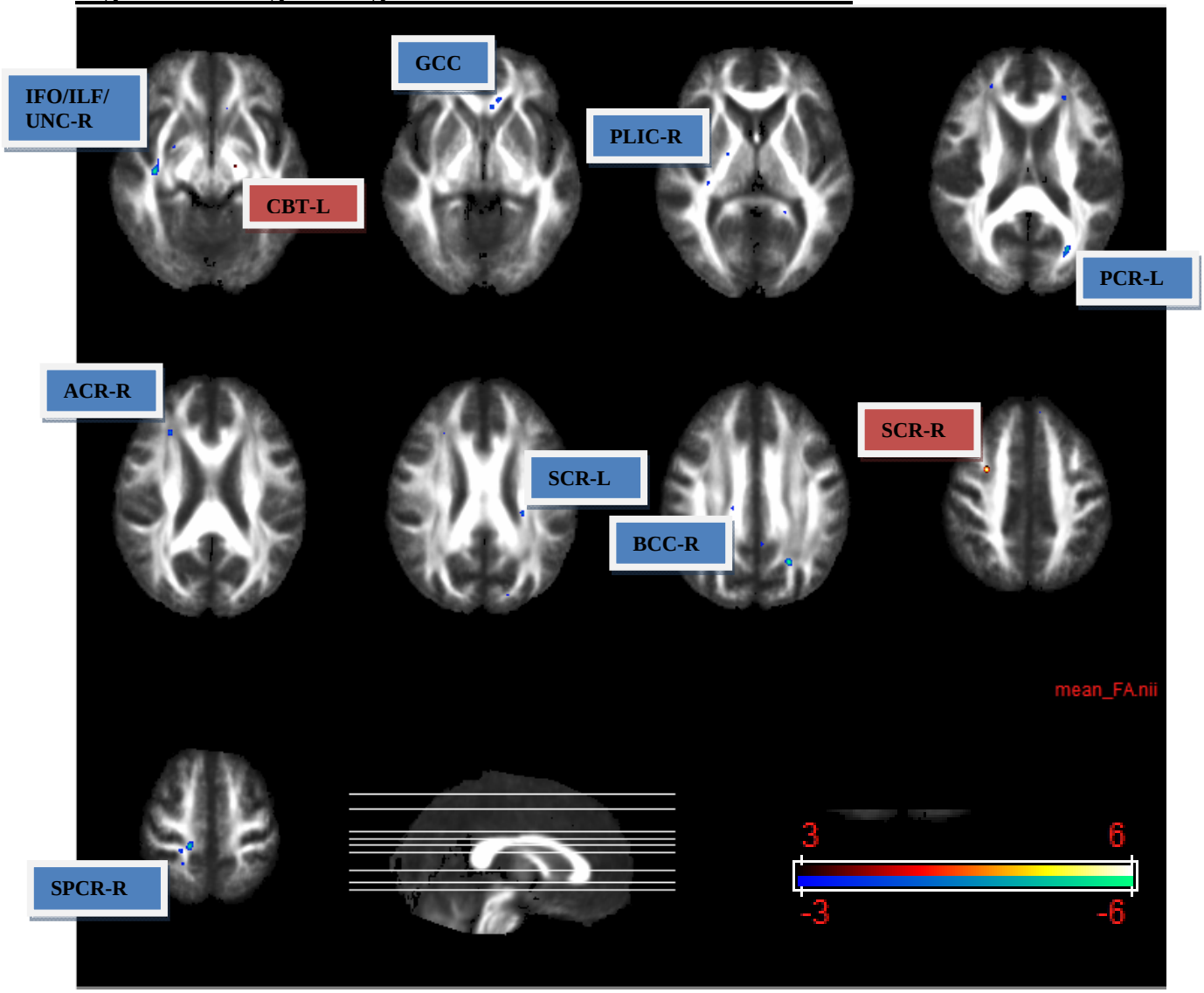

Discussion

The overlays in blue indicate the regions that are 3 standard deviations above the mean FA and red/yellow overlays indicate the regions below the mean FA of the group that have hearing loss but no Tinnitus. For display purposes overlays are filtered to show a cluster size of 5 or more and hereby smoothed by filter size of FWHM [3 3 3].

D. SWI results:

Hemorrhage is seen in one subject.
Red nucleus and substantia nigra show high iron content in two subjects.
Thalamus shows high iron content in two subjects and low iron content in one subject.
high iron content in the right globus pallidus for TR-AI, RII-TI, RII-NA and in the left globus pallidus for TR-AI, RII-TI, RII-AI and RII-NA, B04 case shows low iron content in the right globus pallidus for TR-AI and the remaining subjects are in normal range.

October 2012

Since the last report, we have added seven additional cases (3 blast; 4 concussions). In fact, there would have been more individuals studied however, our MRI technician returned to China for 1 month and this reduced our data collection rate. We plan to resume testing when he returns in ~2 weeks.

The topics covered here were inspired by the need to understand how blast and concussion injuries can affect middle and inner ear function. Most importantly, we assess their role in hearing sensitivity and their role in triggering tinnitus activity in the nervous system. The psychophysical dimensions demonstrate how loudness and responses to questionnaires affect the individual. The imaging data provide the central nervous system correlates of these overall effects.

Audiometric data are summarized in the graphs below.

Blast. Trends in this category (n = 12) show relatively symmetric pure tone hearing sensitivity, bilaterally. The average results show normal thresholds from 0.25-1.0 kHz with mild-to-moderate sensorineural hearing loss, 2.0-8.0 kHz, bilaterally. In this sample, there is more variability and greater hearing loss in the higher frequency range (2.0-8.0 kHz).

Concussion. Trends in this category (n = 6) show greater hearing loss than in the blast group with more variability throughout the entire frequency range. The average pure tone loss is in the mild-to-moderately severe range.

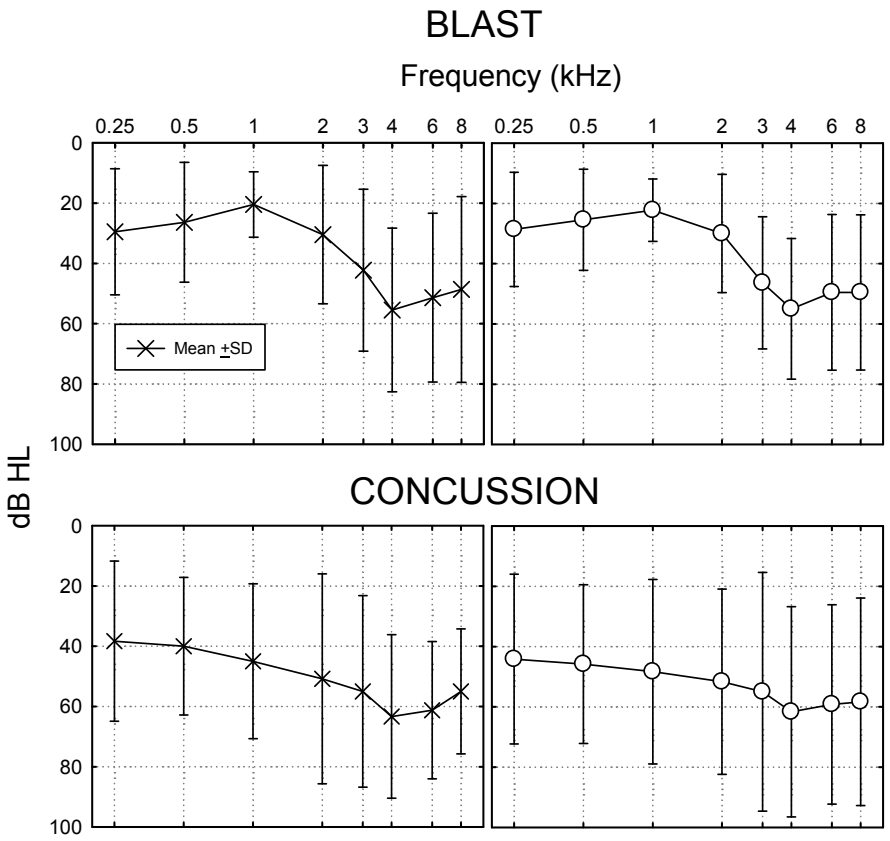

Middle ear power reflectance.
Middle ear power reflectance measures continue to show two general trends for the blast and concussion group.
Blast. This category shows trends of increased variability in the mid-to-higher frequency range, 2.0-6.0 kHz, bilaterally, which is more prominent for the right ear.
Concussion. This category shows more variability in the mid-frequency range (0.4-2.0 kHz), with higher frequencies being more preserved. These data are shown in Figure2.

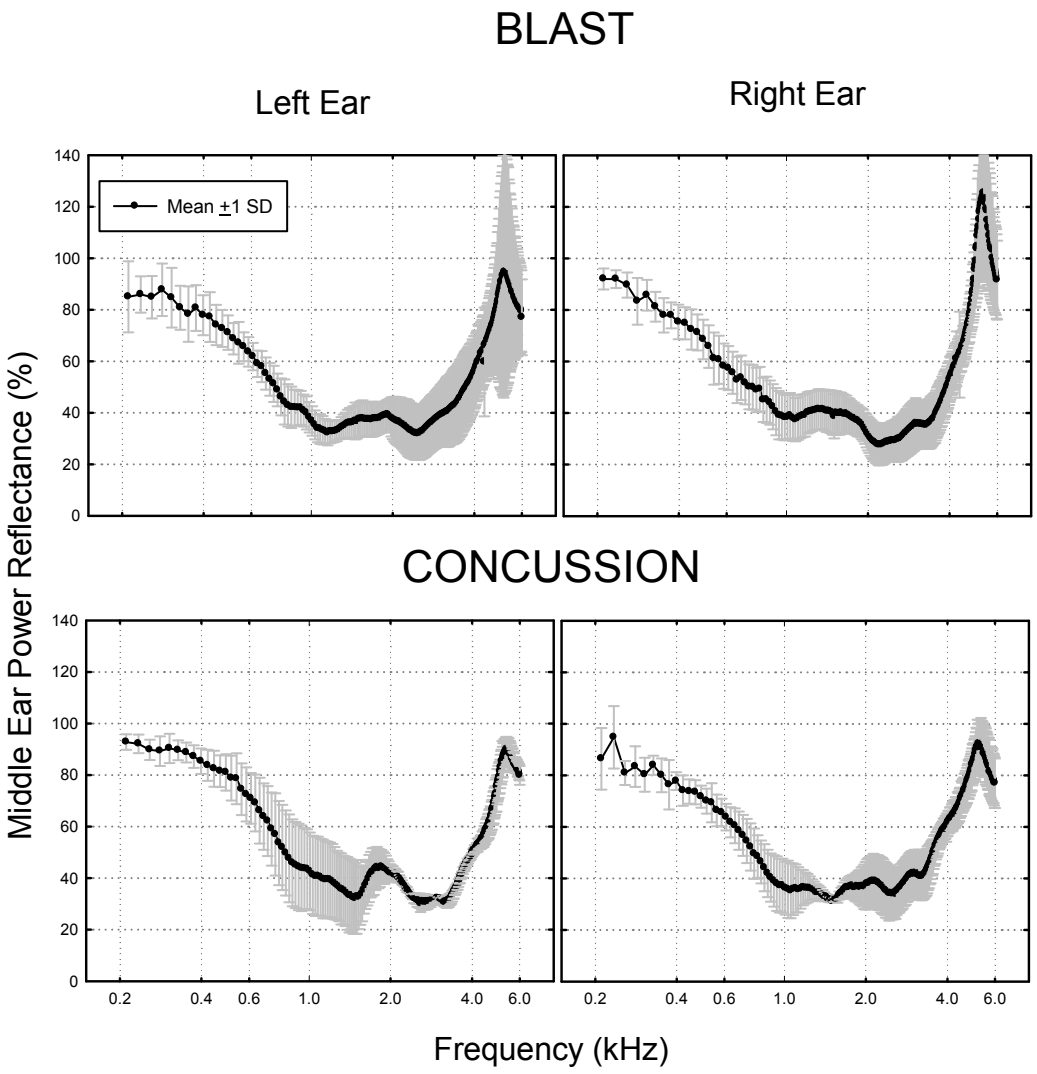

***Figure 10**. Middle ear power reflectance for blast and concussion categories.*

Distortion Product Otoacoustic Emissions.
Blast. Trends observed in this category are consistent with degree, configuration and type of hearing loss via preserved DPOAEs below 2.0 kHz (i.e., responses being above the noise floor); responses were absent above this frequency range (i.e., responses were below the noise floor). These data reflect intact outer hair cell (OHC) function within the inner ear and dysfunctional/damaged OHC function above 2.0 kHz, where responses are absent (below the noise floor).

Concussion. Preserved responses (~<2.0 kHz) and absent responses above this frequency were observed for the left ear with the general absence of responses for the right ear is consistent with the degree and type of hearing loss.

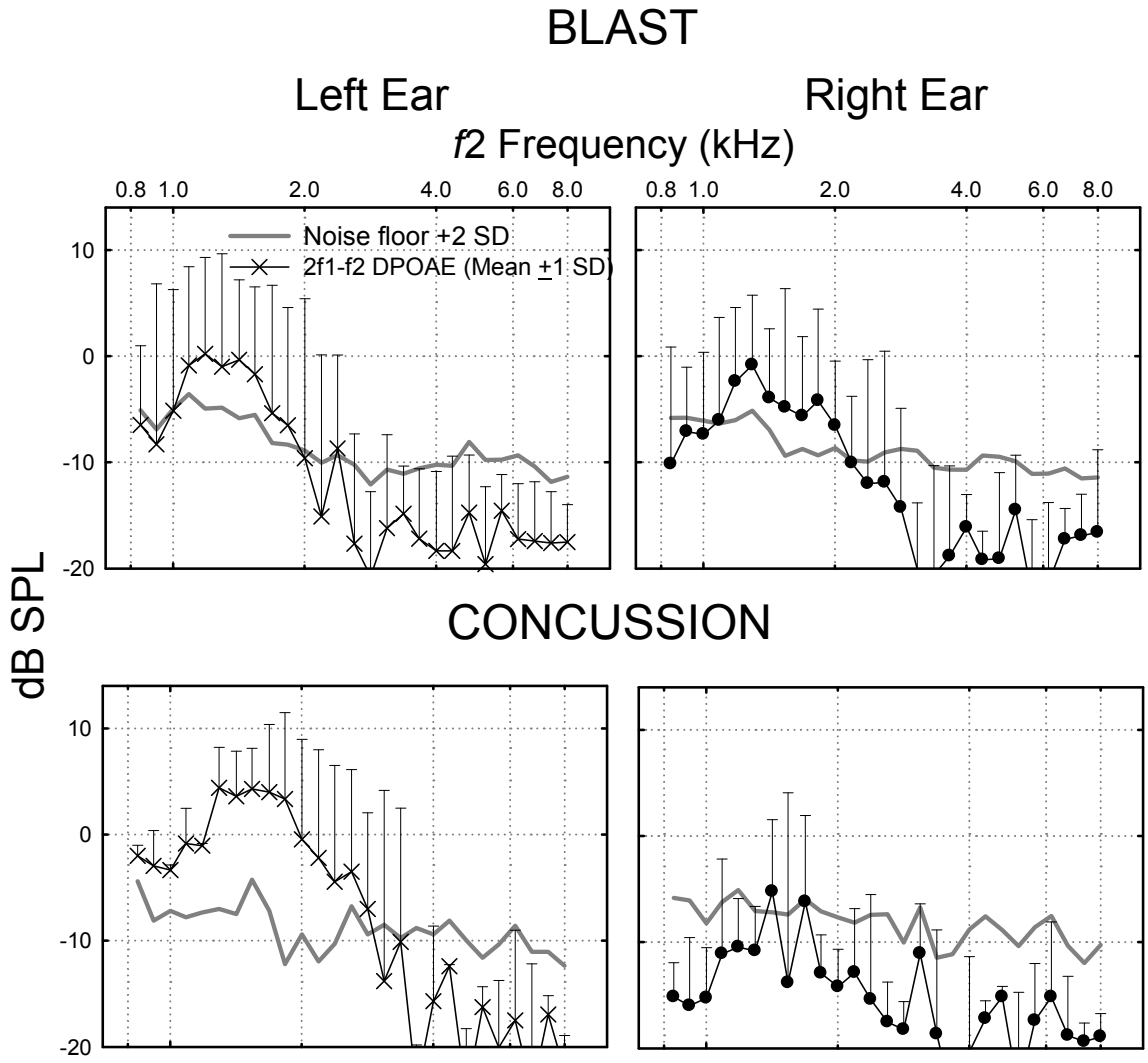

Figure 11. Distortion production otoacoustic emissions for blast and concussion categories for left and right ears. Thick gray line represents the noise floor +2 SD. DPOAEs for the left ear are shown as X's; the right ear is shown as filled circles.

Word recognition performance.
Monosyllabic word recognition performance was measured in quiet and in the presence of background noise for each ear at an input level of 75 or 80 dB HL. The Words-in-Noise (WIN) Test varies the speech-to-babble ratio from 24 to 0 dB, at seven levels, and in 4-dB steps in order to generate a psychometric function. The 50% point of the psychometric function is determined and a single value and a single signal-to-noise or speech-to-babble (SBR) ratio is derived. Performance ranges from normal: -2.0-6.0, mild: 6.8-10.0, moderate: 10.8-14.8, severe: 15.6-19.6, to profound: 20.4-25.2.
Speech in Quiet:
Blast: Normal or near normal performance is observed bilaterally.
Concussion: Because of increased degree of peripheral hearing loss in this category, mild to moderately depressed performance is observed bilaterally (greater for right vs. left ear).
Speech in Noise:
Blast: Normal performance to mildly depressed scores was observed.
Concussion: Normal to moderately depressed scores was observed. The WIN test seems to better segregate categories. As we increase our sample size, we should be able to establish these relations more accurately.
Tinnitus Loudness
Tinnitus loudness level measures were derived from a magnitude estimation (ME) function for a 1.0 kHz tone. Once the ME is obtained, participants estimated the loudness of their tinnitus by provided a numerical estimate. The ME function is then bisected at this value and the loudness level in dB is obtained.
Blast. Moderate tinnitus loudness levels were observed, remaining consistent near 60 dB (average values).
Concussion. Moderate-to-moderately severe tinnitus loudness levels were observed and continue to be slightly higher than in the blast-exposed individuals (~64 dB; average values).
Tinnitus Handicap Questionnaire (THQ).
The THQ is a reliable measure of tinnitus distress, broken into 3 factors or subscales. Factor 1: social, emotional, and behavioral issues; Factor 2: tinnitus and hearing-related issues; factor 3: total composite score across factors or subscales.
Blast. Consistent with the previous report, moderately depressed performance was observed across all factors.
Concussion. Consistent with the previous report, moderately depressed performance was observed across all factors.

Neuropsychology

To date, we have tested 10 participants who have experienced a blast injury, 5 participants who have experienced a concussive injury, and 3 participants who have experienced both blast and concussive injuries. The relatively small cell sizes preclude extensive statistical analysis, although the 10 blast injury and 5 concussed participants were compared using independent groups t-tests. There was a trend for concussed participants to show slower reaction times and reduced throughput (number of correct responses per minute) during the Mathematical Processing subtest. No other cognitive or mood differences were observed.

Using the computerized neuropsychological assessment metric (ANAM), there are a number of variables that can be investigated. The principal dependent variables are: 1) Mean (and Median) Reaction Time to Correct Responses; 2) Percent Correct (Accuracy); 3) Standard Deviation of Reaction Times to Correct Responses (SDRTC; to investigate patterns of intra-individual variability); and 4) Throughput (number of correct responses per minute, which combines speed and accuracy into a single measure). Cognitive measures obtained from ANAM include: 1) Simple Reaction Time (SRT), repeated twice to evaluate for fatigability; 2) Procedural (Choice) Reaction Time (PRO); 3) Mathematical Processing (MTH); 4) Matching-to-Sample (Working Memory; MTS); 5) Code Substitution (Processing Speed; CDS); and 6) Code Substitution Delayed (delayed incidental recall; CDD). During this period, data from the Mood Scale were analyzed. Traumatic Brain Injury (TBI) symptom data is still being aggregated.

Below, we present a table of means and standard deviations for relevant variables in this aspect of the study. Interpretation of patterns of these means and standard deviations is still somewhat speculative, given the small cell sizes. The mean age of the groups remains quite comparable. The pattern of mean reaction times to correct responses generally suggest a trend toward slowed reaction times in the concussion group, and there also still appears to be considerably more inter-individual variability (greater standard deviations) for the concussion group relative to the blast group. None of these group differences were statistically significant, however. Accuracy across most measures was again at 80% or greater, with the exception of Code Substitution Delayed. The relatively low performance across groups suggests difficulty with incidental learning. Accuracy for SRT 1 and SRT 2 are omitted because the accuracy is 100% for all individuals by default. The pattern of means for throughput indexes (number of correct responses per minute) continues to suggest greater cognitive efficiency in the blast group relative to the concussion group. However, throughput still increases for the concussed group during the second administration of Simple Reaction Time, compared to the first administration. This pattern suggests somewhat less fatigability for the concussed group relative to the blast group. Finally, inspection of the standard deviation of reaction times for correct responses suggests considerable intra-individual variability among concussed participants relative to the blast participants. This pattern of performance may underlie the concussed group's tendency toward reduced cognitive efficiency.

The right-most column in the table below indicates the p value for the independent groups *t*-test contrasting the blast group with the concussion group.

	Blast (n=10)	Concussion (n=5)	Blast+Concussion (n=3)

	Variable	mean	sd	mean	sd	mean	sd	*t*-test p
	Age	59.2	12.7	60.8	12.5	63.0	1.0	0.82
SRT 1	MeanRTCorrect	279.7	50.4	386.7	174.7	292.9	39.6	0.24
SRT 2	MeanRTCorrect	304.9	109.4	399.9	316.5	278.4	23.7	0.55
PRO	MeanRTCorrect	660.0	80.2	727.6	190.1	645.2	31.8	0.48
MTS	MeanRTCorrect	2194.1	602.0	2304.1	1404.5	2148.9	274.4	0.87
MTH	MeanRTCorrect	2509.7	691.3	3550.4	1034.2	2687.0	728.4	0.09
CDS	MeanRTCorrect	1661.1	364.4	1787.2	359.8	1633.9	426.5	0.54
CDD	MeanRTCorrect	1943.1	904.9	1885.8	655.4	1471.0	421.7	0.89
PRO	Accuracy	97.2	4.0	97.5	2.6	96.9	3.1	0.86
MTS	Accuracy	88.0	9.8	87.0	10.4	80.0	13.2	0.86
MTH	Accuracy	93.5	8.2	89.0	12.4	81.7	12.6	0.49
CDS	Accuracy	97.5	2.4	94.7	3.6	96.8	3.5	0.17
CDD	Accuracy	66.4	14.3	66.1	16.4	64.8	14.0	0.97
SRT 1	Throughput	219.6	31.9	179.1	67.2	207.2	26.2	0.26
SRT 2	Throughput	212.7	52.3	199.1	78.6	216.5	17.6	0.74
PRO	Throughput	89.0	12.3	83.7	18.9	90.3	7.2	0.59
MTS	Throughput	25.8	8.4	26.8	11.9	22.3	4.9	0.87
MTH	Throughput	23.7	6.8	15.8	5.6	18.8	6.5	0.04
CDS	Throughput	36.7	8.2	32.9	7.0	37.4	10.3	0.37
CDD	Throughput	21.9	11.4	19.5	4.3	25.6	11.4	0.58
SRT 1	SDRTCorrect	75.6	39.4	326.7	534.4	91.4	18.6	0.35
SRT 2	SDRTCorrect	177.1	153.3	238.7	325.3	92.3	28.9	0.70
PRO	SDRTCorrect	205.5	102.5	299.1	237.3	145.4	16.5	0.43
MTS	SDRTCorrect	712.7	241.0	1054.7	824.4	1015.5	212.4	0.41
MTH	SDRTCorrect	744.0	238.1	1029.6	459.4	817.8	340.8	0.25
CDS	SDRTCorrect	470.4	124.4	603.5	222.6	496.3	105.6	0.27
CDD	SDRTCorrect	783.1	449.2	1138.8	625.1	445.0	134.5	0.30
SRT 1	Median RT Correct	264.8	57.0	319.0	160.8	273.3	54.8	0.50
SRT 2	Median RT Correct	267.9	103.9	317.9	196.5	254.8	32.3	0.61
PRO	Median RT Correct	618.1	82.3	651.9	97.0	620.7	39.7	0.52
MTS	Median RT Correct	2049.6	616.0	1953.8	1070.4	1899.8	310.6	0.86
MTH	Median RT Correct	2374.1	674.4	3309.9	967.8	2583.0	766.1	0.10
CDS	Median RT Correct	1562.4	335.6	1674.8	365.2	1515.2	438.4	0.58
CDD	Median RT Correct	1741.8	807.0	1449.4	467.5	1394.0	381.1	0.39
Mood	Vigor	3.4	1.6	3.6	1.8	3.1	0.9	0.85
	Restlessness	1.1	1.1	1.1	1.5	1.9	2.3	0.95
	Depression	1.1	1.4	1.7	1.9	1.7	1.6	0.53
	Anger	0.7	0.8	1.1	1.7	1.5	1.4	0.66
	Fatigue	1.2	1.1	1.8	1.8	1.7	1.9	0.57
	Anxiety	1.0	0.9	1.2	1.3	1.8	2.0	0.81
	Happiness	3.9	1.5	3.5	1.5	3.1	0.8	0.65

Magnetic Resonance Imaging (MRI)

This area of investigation is of critical importance to understanding the neural substrate contributing to the tinnitus perception. We include standard high resolution MRI,

diffusion tensor imaging (DTI), susceptibility-weighted imaging (SWI), and magnetic resonance spectroscopy (MRS). The MRS data will be reported in the next quarterly report.

A. Methods and Data Processing: There are 17 subjects with blast and concussion induced Tinnitus and 13 subjects without Tinnitus and the data appears to be following the protocols very well. These 13 subjects without tinnitus are considered to be normative control data, which allow for statistical analysis. (Note: one participant with tinnitus and severe hyperacusis was extremely bothered by the MRI related scanner noise and was unable to perform the battery of tests.

DTI processing: DTIStudio is used to generate different components (maps) of DTI data i.e. Eigen maps, apparent diffusion coefficient (ADC), fractional anisotropy (FA) and Trace. B0 images are brain extracted and used as a mask to remove the skull area and non-brain matter on each of these maps. FA maps are spatially normalized to a standard space and then segmented into three different classes: grey matter (GM), white matter (WM), and cerebrospinal fluid (CSF).

Global Analysis: Briefly, the WM maps are thresholded and a mask is created and applied onto the linearly spatially normalized FA map to extract the mean FA of those white-matter voxels. Mean FA for each subject with tinnitus is plotted against the subject's age along with a group of subjects without tinnitus that are scanned with the same parameters. In similar fashion, the remaining components are also transformed into the same space and a global mean is extracted for the same voxels as that of the FA and plotted against respective ages. This plot examines white matter integrity vs. age.

Voxel Based Analysis: The FA image is non-linearly registered to a standard template in ICBM_MNI space using an in house built FA template (n=13). Z score statistic approach is used to ascertain which WM regions are 3 standard deviations above or below the mean FA values.

Tract Based Spatial Statistics (TBSS): This is a statistical method of comparing voxels on any WM track across two or more groups All FA images in two groups are registered to a standard FA template and transformed into a standard space. Subsequently, a mean FA image is created. A search algorithm then creates an average skeleton template used in the individual data analysis. Then a voxel-wise permutational analysis is carried out between the skeletons of two groups and a 2-tailed t-test statistic is performed to extract the voxels that fall below or above a certain threshold. These voxels are converted to a *p*-value based on the threshold set by the t-stat value and the cluster size.

SWI processing: Susceptibility Weighted Imaging (SWI) is a non-invasive MR imaging method that uses phase and magnitude components of the SWI data to quantify iron content within selected brain regions, identity potential blood products or abnormal signal in the parenchyma of the brain.

Lesion load: Usually the lesions appear dark in the phase data implicating the presence of iron. The lesion load is quantified by drawing the region of interest (ROI) around the lesion and multiplying the number of pixels in the given ROI by the in plane resolution and the slice thickness so the resulting value will be expressed in mm^3.

SWI Minimum Intensity Projection (mIP): This provides information about the continuity of the venous structure in the brain. This helps to delineate actual veins from pathologic blood products from microhemorrhages (brain bleeds).

Iron quantification in the deep grey matter structures: SWI provides the ability to quantify the iron present in various deep grey matter structures and how this pchanges with age. Thus, iron is quantified in SWI phase images in the following regions: caudate Nucleus (CN), globus pallidus (GP), putamen (PUT), thalamus (THA), pulvinar thalamus (PT), red nucleus (RN), and substantia nigra (SN).

Each of these seven regions is drawn on both hemispheres of the brain following well established guidelines in identifying these specific structures. Furthermore, a two region approach in quantifying the iron is used to visualize and localize the regions with high iron content. All the seven regions are divided into Region 1 (RI- Region with iron content below threshold value) and Region 2 (RII- Region with iron content above the threshold value). The threshold values are established from a group of 20 healthy normal controls.
The following parameters are extracted to quantify the iron content from individual participants:
Average iron of the total region (TR-AI)

- Total iron of the high iron content region (RII-TI)
- Average iron of region II (RII-AI)
- Normalized region II area (RII-NA)

Susceptibility Weighted Image Mapping (SWIM): SWI images are further post processed using an inverse procedure to generate susceptibility maps of the veins. With sufficient resolution major veins in the brain could be visualized with this approach thus creating the venograms of the brain and also be used as a tool for quantifying oxygen saturation levels in these vessels. Future applications of this method might be helpful in serving the quantitative means to distinguish oxygen saturation abnormalities in SWI data and also in measuring iron in the tissues.
The technical parameters used in this analysis are noted below.

Sequence Name	TR	T E	Flip Angle	Bandwidth	Matrix	Spacing	Thickness
Localizer	8.6	4	20	320	512*512	0.5*0.5	7
T1 Flash Sagittal	443	2.54	90	330	256*256	1*1	3
MPR Coronal	1600	4.28	8	180	384*384	0.67*0.67	1.34
SWI	30	6.97	15	465	512*384	0.5*0.5	2
DTI	7400	106	90	1395	128*128	2*2	3

DTI Results:

Global results (FA vs Age):

The following table illustrates increased or decreased FA values for a group of individuals with hearing loss alone versus individuals with hearing loss and tinnitus.

TBSS: Group-wise results:

	DECREASED FA			INCREASED FA		
CASE ID	**SLICE NO.**	**REGION NAME**	**RIGHT/LEFT**	**SLICE NO.**	**REGION NAME**	**RIGHT/LEFT**
GROUP	48	UNC	RIGHT	49	Cg	RIGHT
	52	CST	LEFT	63	IFO/ILF/UNC	RIGHT
	61	CST	RIGHT	70	IFO/ILF	RIGHT
	65	CBT	LEFT	70	PLIC	RIGHT
	70		RIGHT	78	PCR	LEFT
	77	PLIC	RIGHT/LEFT	86	Genu	RIGHT
	83	SLF	RIGHT	88	PCR	LEFT
	98	SFO	LEFT	92	Genu	
	118	SCR	RIGHT	107	VOF	RIGHT/LEFT
	122		RIGHT	116	SCR	LEFT
	133		RIGHT	131	SPCR	RIGHT

Table showing the regions with decreased/increased FA:

**Cg-Cingulum;SCR – Superior Corona Radiata; SLF- Superior Longitudinal Fasiculus; SPCR- Superior Posterior Corona Radiata, ACR- Anterior Corona Radiata, IFO - Inferior Fronto-Occipital Fasciculus; ILF – Inferior Longitudinal Fasciculus; UNC – Uncinate Fasciculus; PLIC – Posterior Limb of Internal Capsule; PCR – Posterior Corona Radiata. VOF-Vertical Occipital Fasciculus.*

Global WM FA values for all the subjects with tinnitus and hearing loss tends to be within the range when compared to the subjects having hearing loss with no tinnitus. This result indicates that there is no difference in the white matter FA from a global point of view.

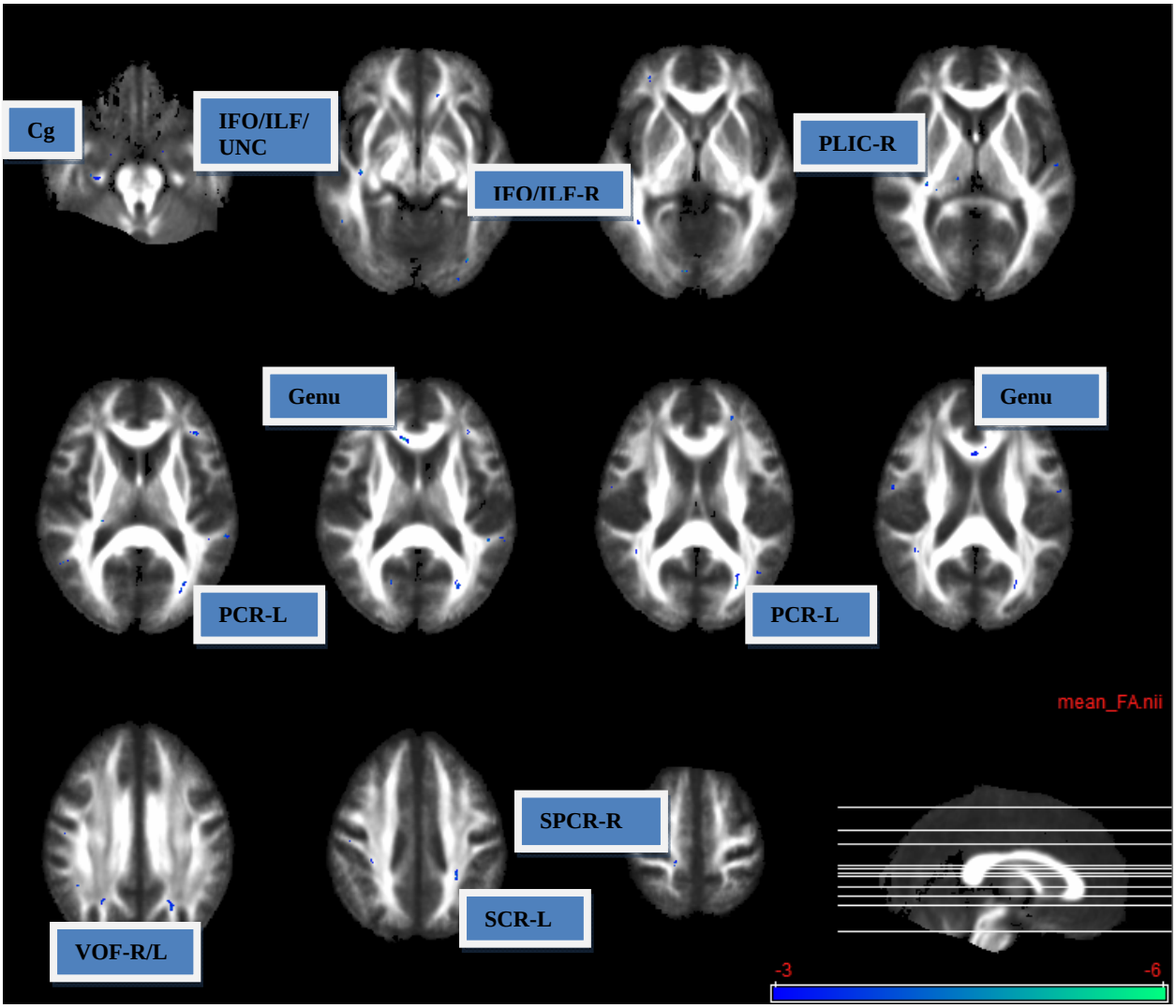

Figure showing the regions with increased FA:

The overlays in blue indicate the regions that are 3 standard deviations above the mean FA and red/yellow overlays indicate the regions below the mean FA of the group that have hearing loss but no Tinnitus. For display purposes overlays are filtered to show a cluster size of 10 or more.

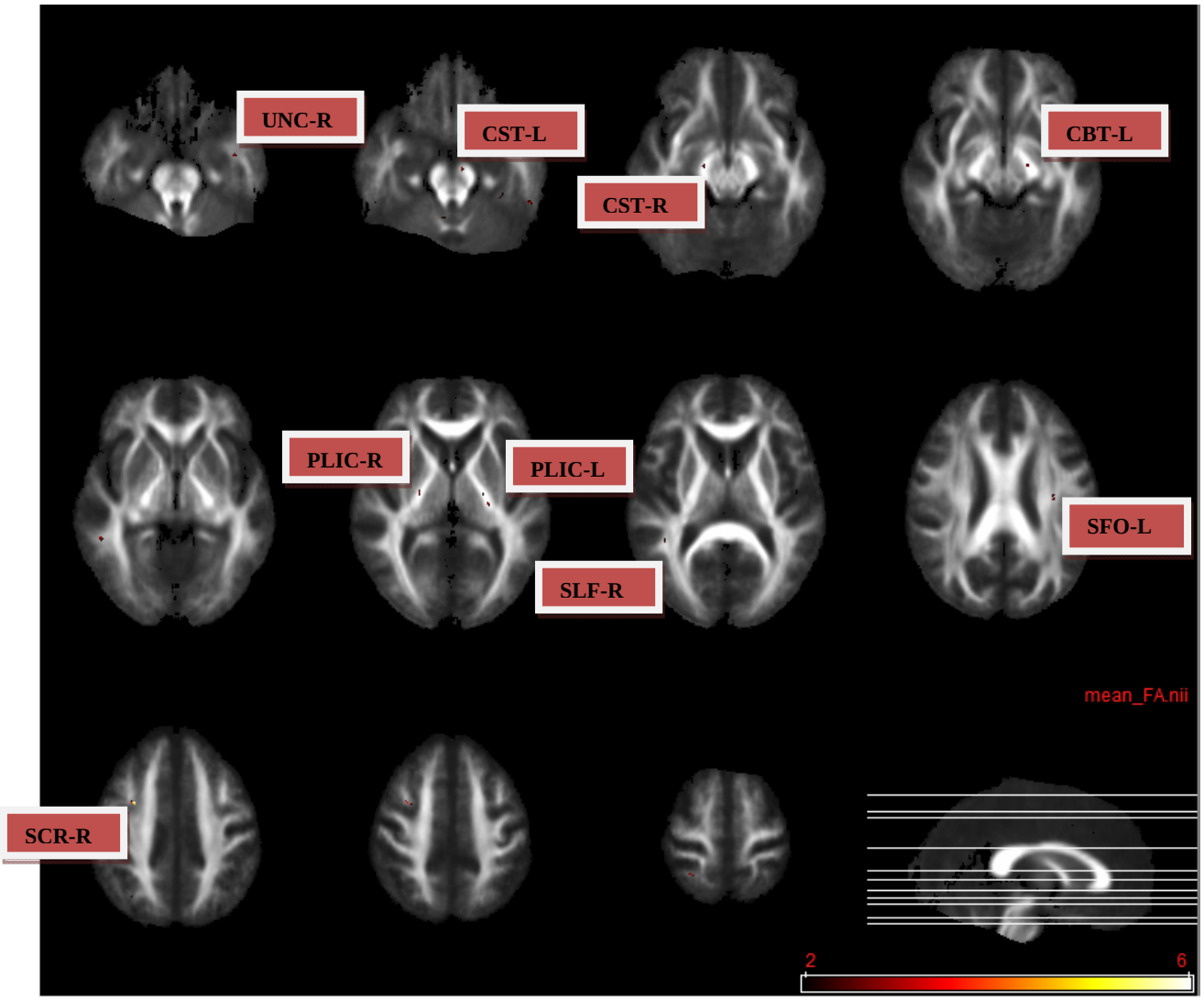

Figure showing the regions with decreased FA:

The overlays in red/yellow indicate the regions that are 2 standard deviations below the mean FA of the group that have hearing loss but no tinnitus. For display purposes, overlays are filtered to show a cluster size of 5 or more.

Iron Quantification of the Deep Gray matter

Abnormal iron content was found in each selected structure CN: caudate nucleus; GP: globus pallidus; PUT: putamen; PT: pulvinar thalamus; RN: red nucleus; SN: substantia nigra; THA: thalamus.

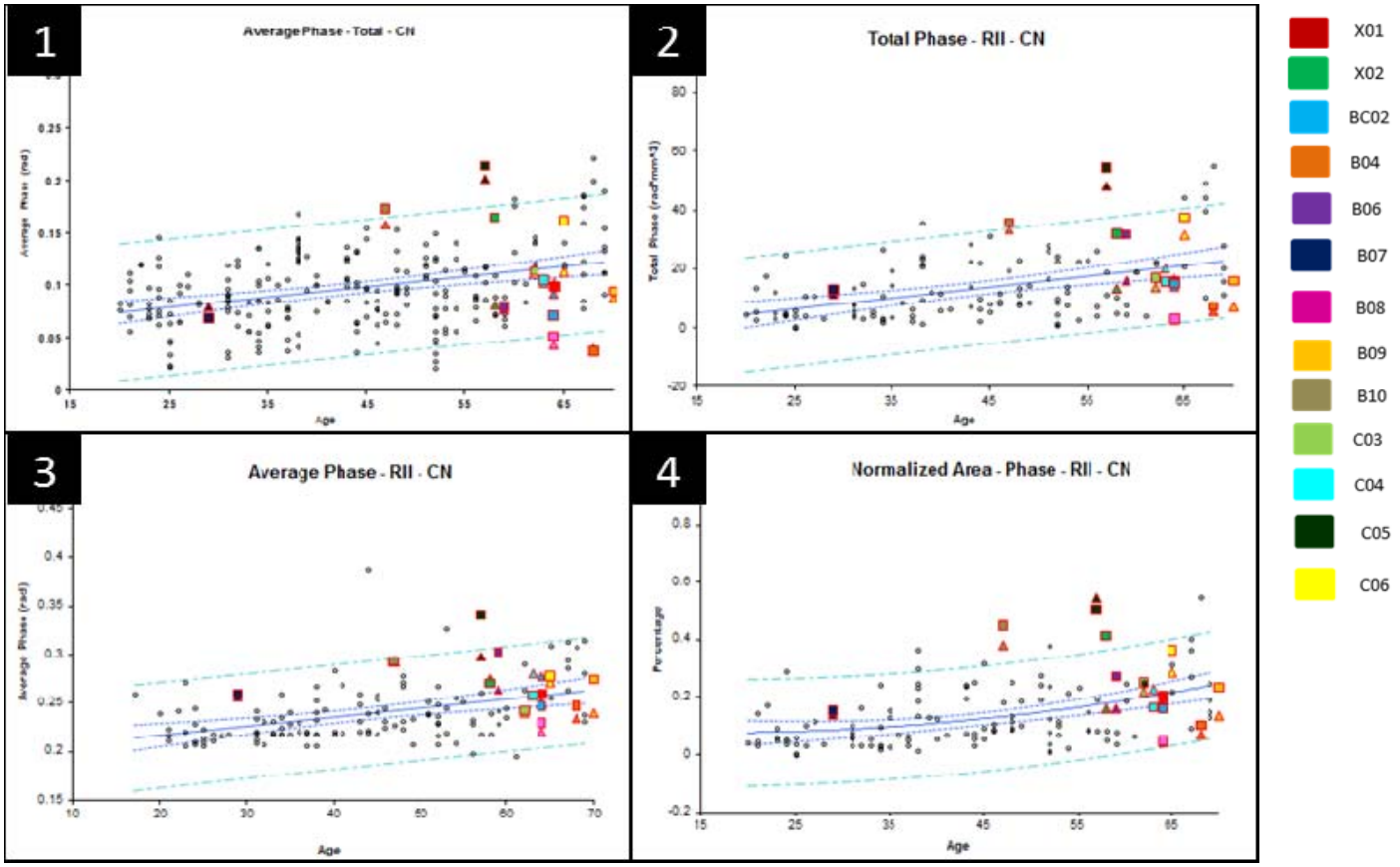

Figure Legend. A: SWI phase image, B: magnitude image; red arrows points to caudate nu d tri In nu l- TI nu rig h ca to

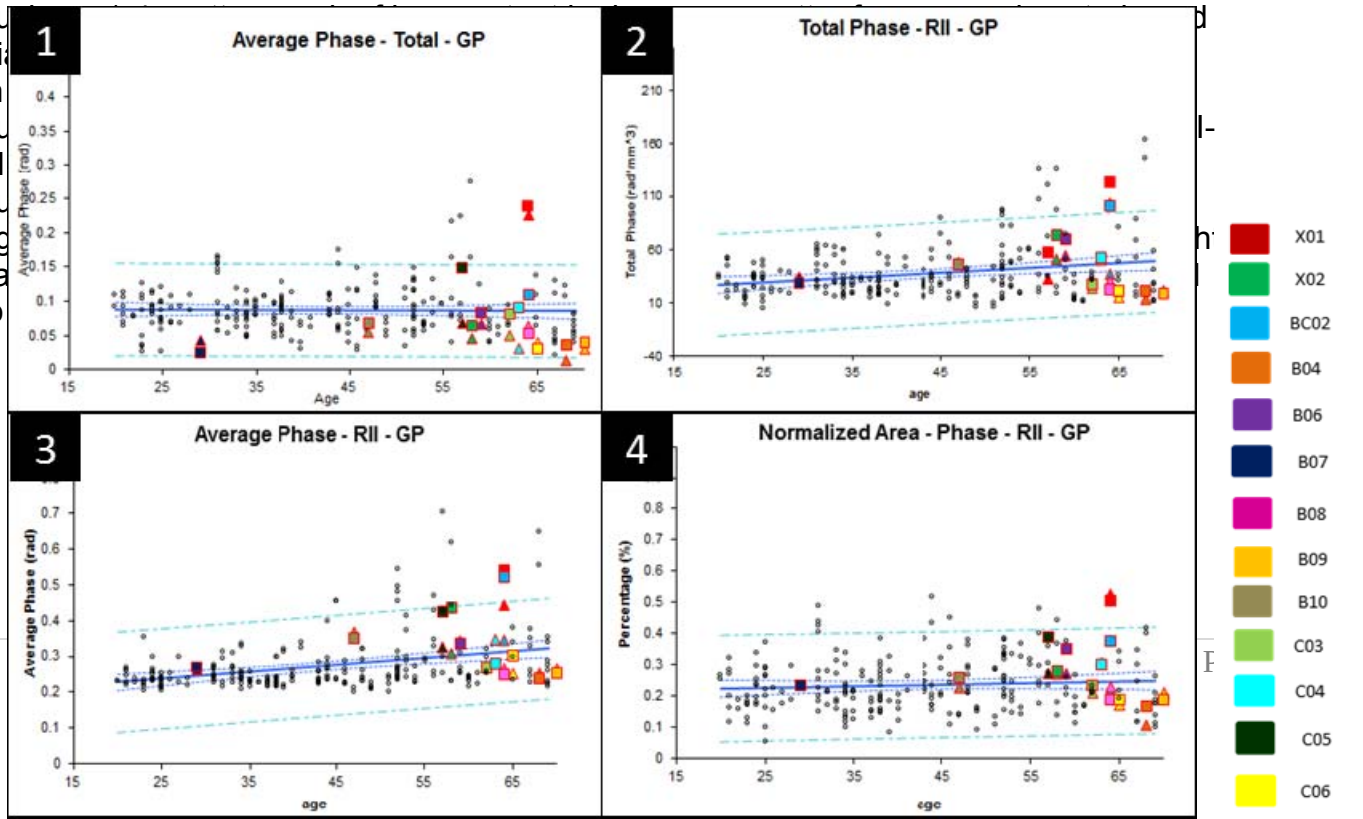

Figure Legend: 1-4: scatter graph of iron content in deep grey matter from normal controls, red triangle (right) and rectangular (left) are iron content.

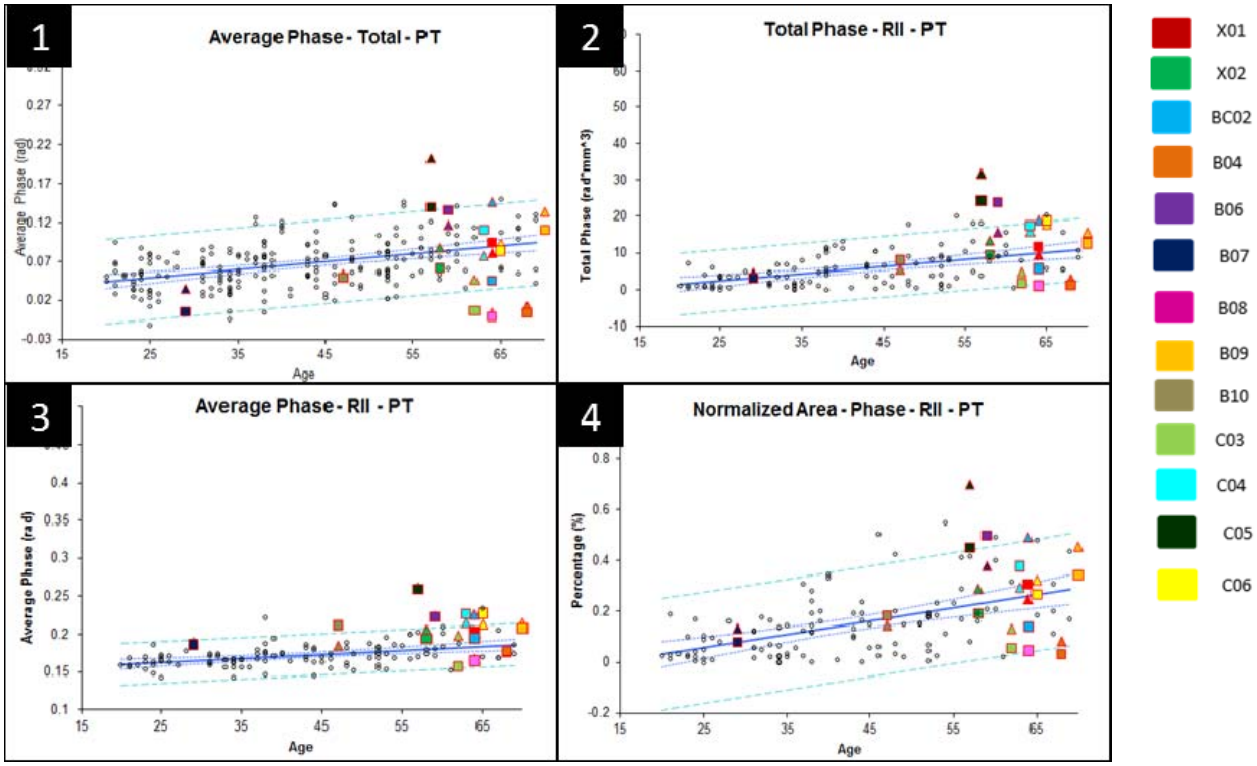

Figure Legend: 1-4: scatter graph of iron content in deep grey matter from normal controls, red triangle (right) and rectangular (left) are iron content.

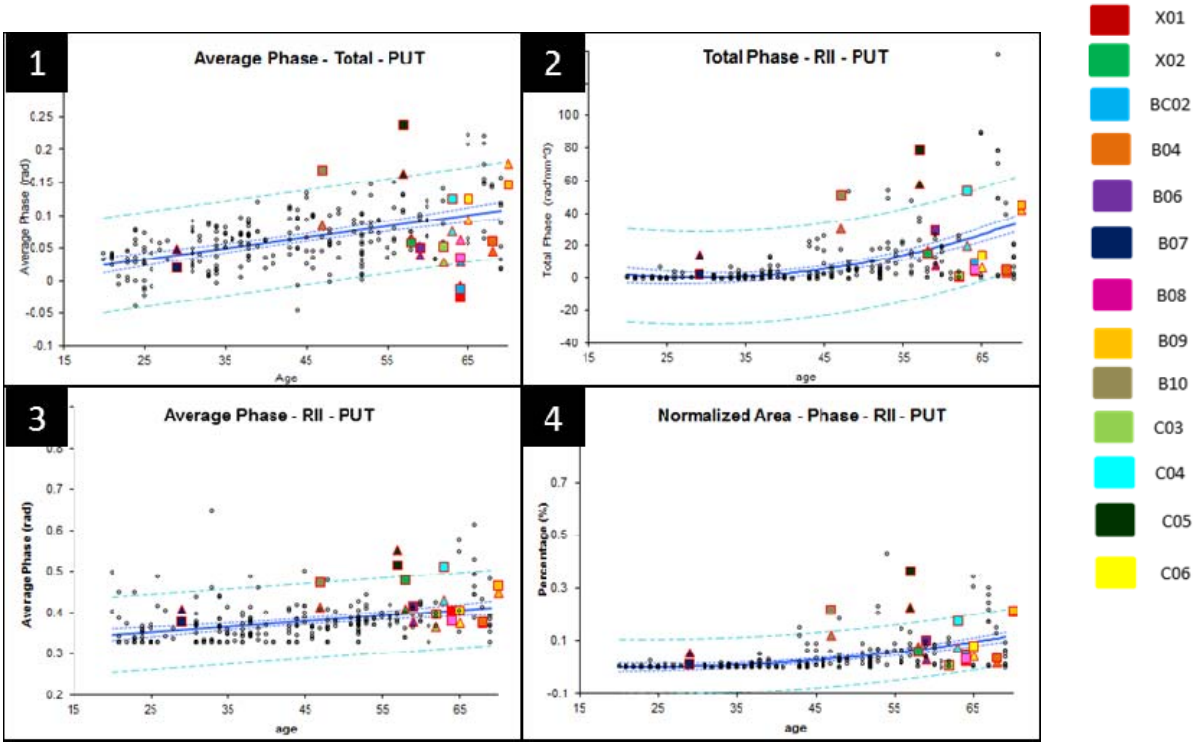

Figure Legend: 1-4: scatter graph of iron content in deep grey matter from normal controls, red triangle (right) and rectangular (left) are iron content.

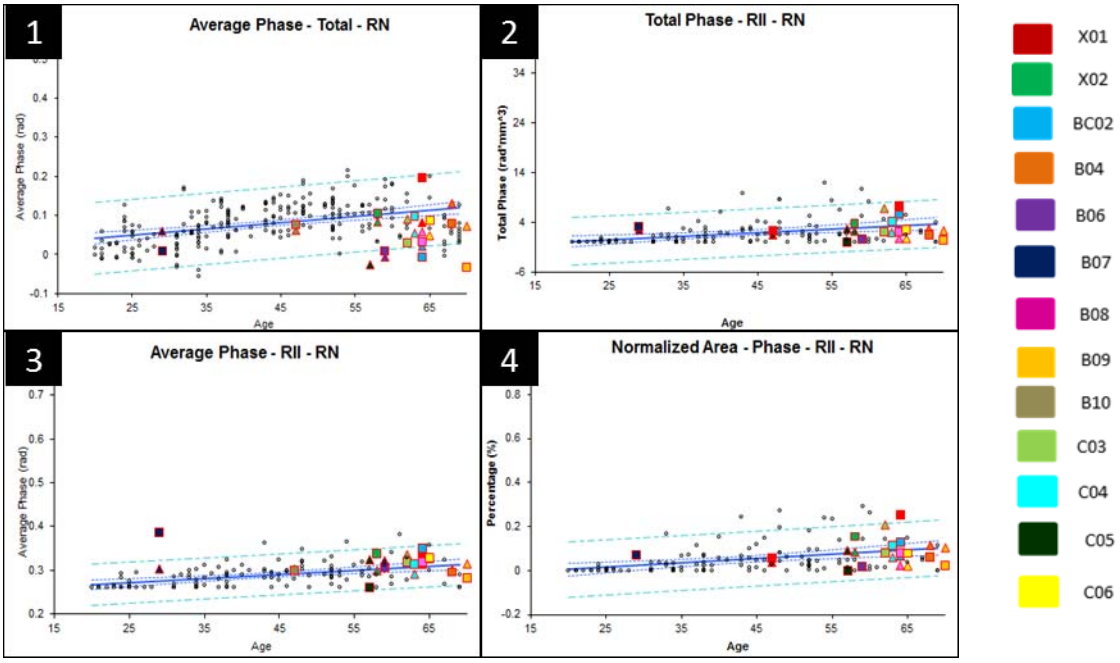

Figure Legend: 1-4: scatter graph of iron content in deep grey matter from normal controls, red triangle (right) and rectangular (left) are iron content.

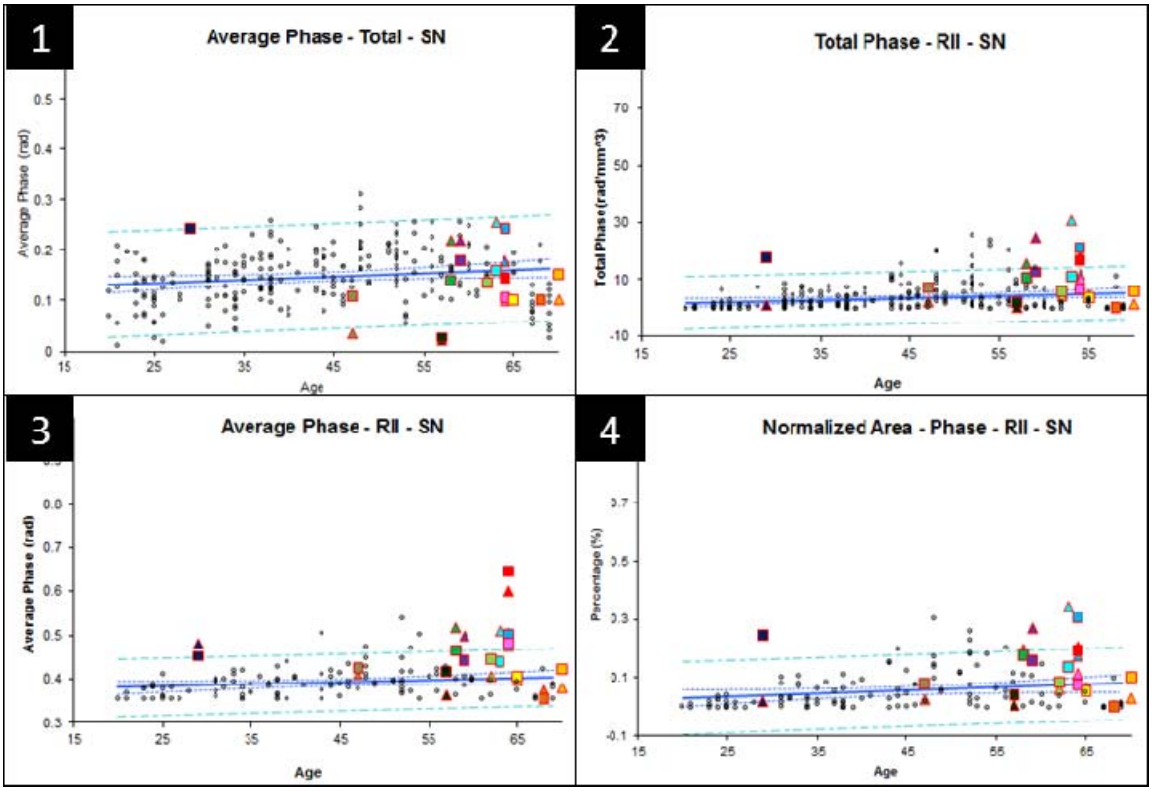

Figure Legend: 1-4: scatter graph of iron content in deep grey matter from normal

Figure

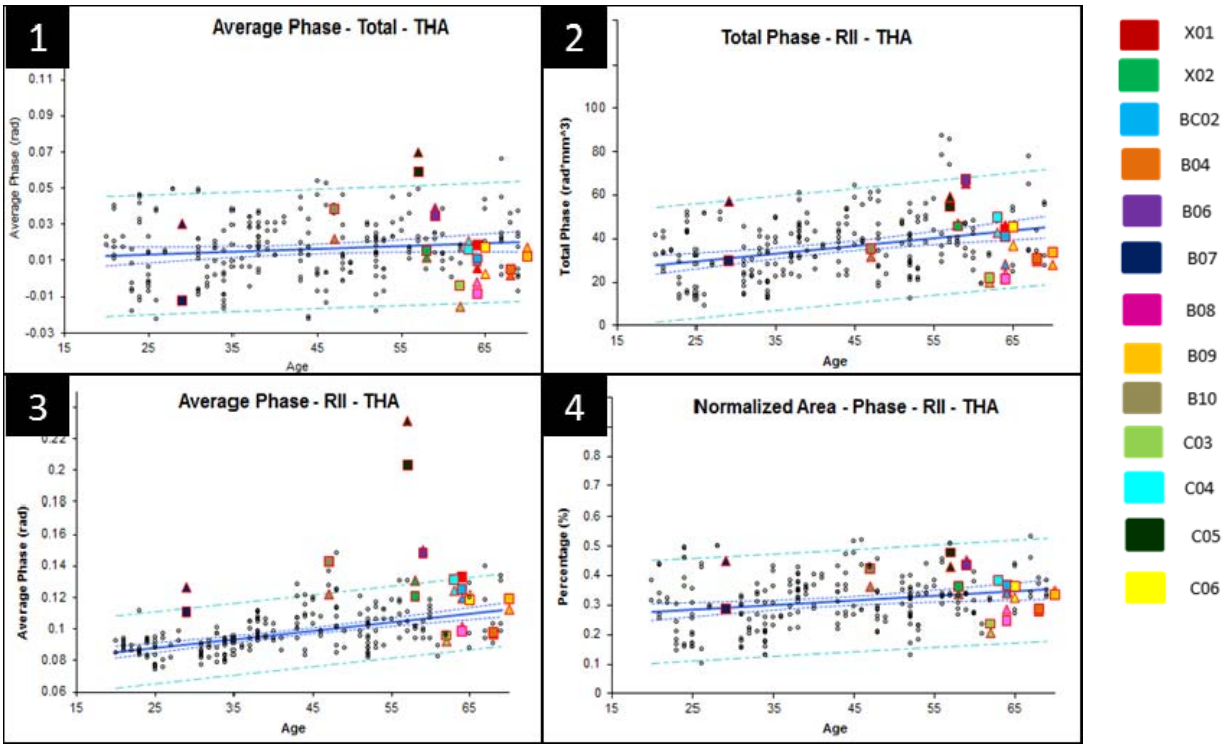

Legend: 1-4 scatter graph of iron content in deep grey matter from normal controls, red triangle (right) and rectangular (left) are iron content.

Conclusion:

As per the DTI findings, the anterior corona radiata (n = 4; two in right and two in left hemisphere), superior corona radiata (n = 3), two in left and one in right hemisphere), superior longitudinal fasciculus (n = 2; two in left hemisphere) shows *increased* FA values.

SWI shows one subject with blood in the left superior portion of the brain. In terms of the iron content, five regions show high iron content in both the sides of the brain. Four regions in the brain show lower iron content in both the sides of the brain. A detailed description of the regions having higher or lower iron content is illustrated in the table.

	X01		X02		BC2		B04		B06		B07	
	Right	Left	Right	Left	Right	Left	Right	Left	Right	Left	Right	Left
CN	N	N	N	↑	N	N	↓	↓	N	N	N	N
GP	↑	↑	N	N	↑	↑	↓	N	N	N	N	N
PT	N	N	N	N	↑	N	↓	↓	↑	↑	N	N
PUT	↓	↓	N	N	N	↓	N	N	N	N	N	N
RN	N	↑	N	N	N	↓	N	N	↓	N	N	↑
SN	↑	↑	↑	N	N	↑	N	N	↑	N	↑	↑
TH	N	N	N	N	N	N	N	N	↑	↑	↑	N

	B08		B09		B10		C03		C04		C05		C06	
	Right	Left	Right	Left	Right	Left	Right	Left	Right	Left	Right	Left	Right	Left
CN	↓	N	N	N	↑	↑	N	N	N	N	↑	↑	N	N
GP	N	N	N	N	N	N	N	N	N	N	N	N	N	N
PT	↓	↓	N	N	N	↑	N	↓	↑	↑	↑	↑	N	↑
PUT	N	N	N	N	N	↑	N	N	N	↑	↑	↑	N	N
RN	N	N	N	↓	N	N	N	N	N	N	↓	N	N	N
SN	↑	↑	N	N	↓	N	N	N	↑	N	↓	↓	N	N
TH	N	N	N	N	N	↑	↓	N	N	N	↑	↑	N	N

N indicates normal iron content.

January 31, 2013

In humans, blast-induced tinnitus, concussion-induced tinnitus, and tinnitus induced by blast + concussion are complex entities that are not clearly understood. To date, the largest sample we have accumulated is from the group where tinnitus is induced primarily from exposure to blasts. Therefore, we will focus primarily on blast-induced tinnitus in this report, since there is considerable variability in the concussion group and blast + concussion with small sample sizes. Nevertheless, the format of this report contains three general areas where trends are developing in: **1)** audiologic**, 2)** neuroimaging, **3)** and neuropsychological assessments. The audiologic data presented below is based on: **a)** pure tone audiometry, monosyllabic word recognition performance in quiet and monosyllabic word recognition performance in the presence of background noise, characterized as a speech-to-babble ratio (SBR), a psychophysical tinnitus loudness metric based on a magnitude estimation procedure; **b)** electroacoustic data (middle ear power reflectance and distortion product otoacoustic emissions, DPOAEs), and **c)** responses to a standardized Tinnitus Handicap Questionnaire (THQ) which captures responses to: social, emotional, and behavioral issues (SEB), issues pertaining to tinnitus and hearing (T&H), and a total score (T), which represents a combination of all sub-scores.

The pure tone audiometric data shown below (Figure 1) are representative of those participants with tinnitus exposed to blasts (n = 15), blast + concussion (n = 7), and concussion alone (n = 6).

Blast Left Ear

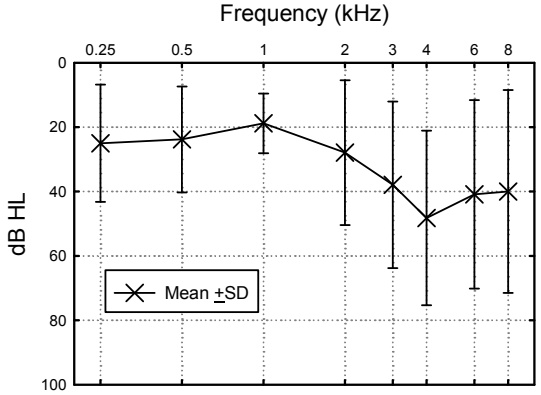

Blast Right Ear

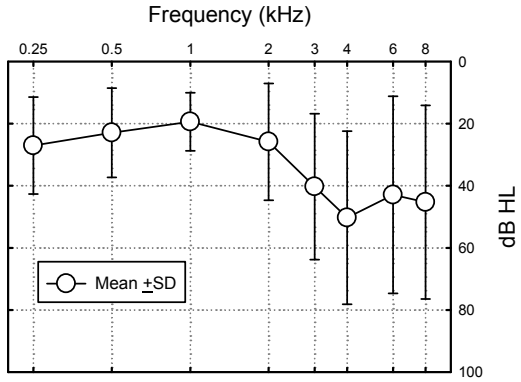

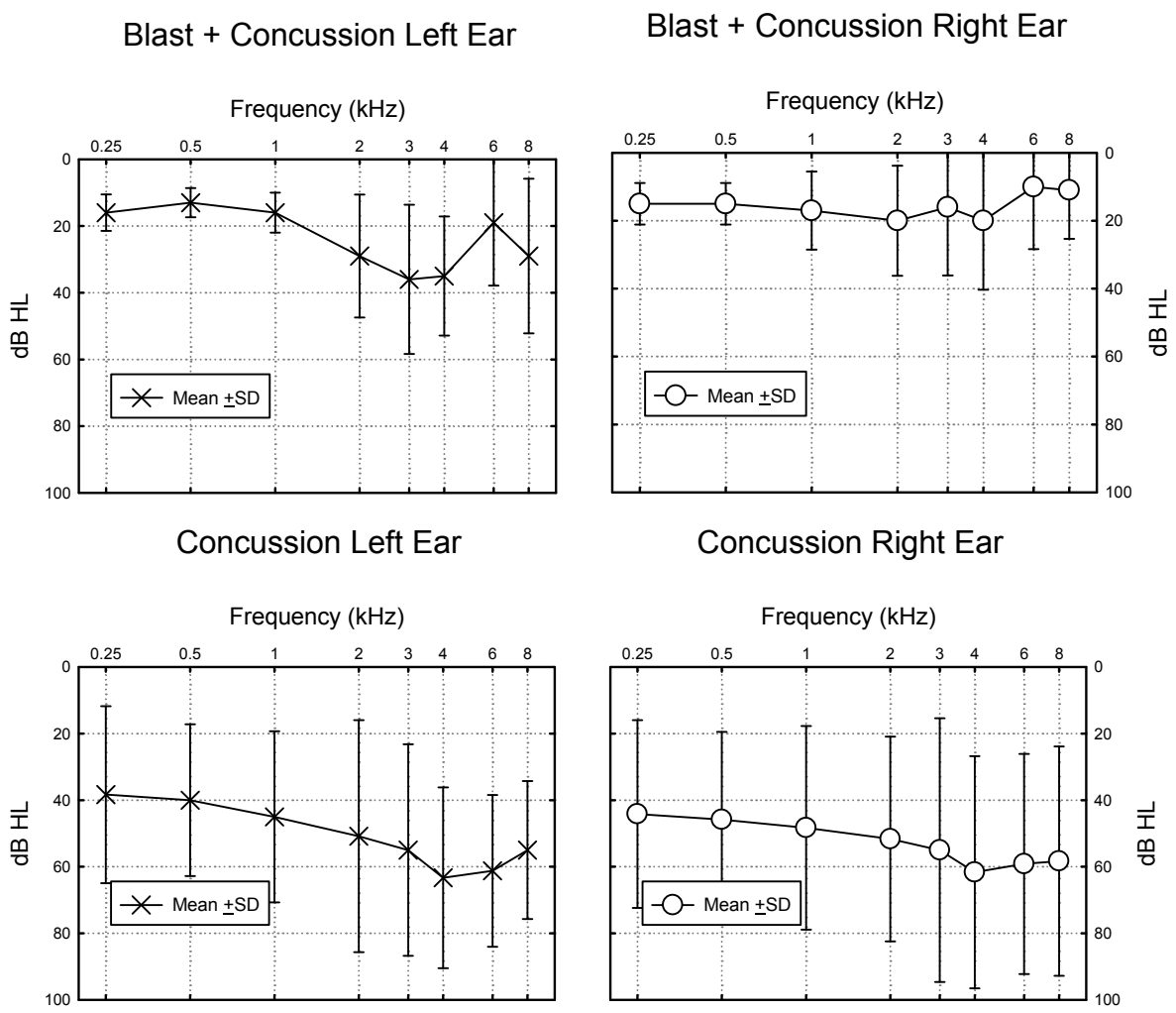

Figure 12*. Pure tone audiometric data for the left ear and right ears.* ***Top blast:*** *On average, they show borderline normal hearing sensitivity ≤1.0 kHz, with middle to moderate loss 2.0-8.0 kHz. The losses are relatively symmetric. The error bars show the variability and indicate a range of greater hearing loss in the higher frequency range.* ***Middle Blast + concussion:*** *these data are asymmetric with borderline normal hearing0.25-2 kHz and 8.0 kHz, with mild hearing loss in the 3.0-4.0 kHz range (left ear); normal hearing in the right ear.* ***Concussion:****Moderate to moderately severe hearing loss bilaterally, 0.25-8.0 kHz.*

Because of the relatively small sample sizes in the blast + concussion and concussion groups alone, the remaining audiometric and questionnaire-based data is focused primarily on the blast-induced tinnitus. For the blast-induced tinnitus group word recognition in quiet was considered excellent bilaterally (left ear mean: 95.8%, SD: 7.6%; right ear mean: 94.6%, SD: 7.6%). However, word recognition in noise derived from the speech-to-babble ratio (SBR) of the Words-in-Noise test was mild-to-moderately depressed bilaterally (left ear mean SBR: 7.6, SD: 4.2; right ear mean SBR: 8.2, SD: 4.1). The mean loudness level of the tinnitus was 68.8 dB (SD: 14.8 dB) and the THQ scores for the three scales (SEB mean: 51.9, SD: 23.6), T&H (mean: 54.1, SD: 22.7); and T scores (51.1, SD: 20.0) were moderately depressed, indicating that the combination of these factors were having a moderate impact on the individual's perception of handicap with respect to tinnitus. As part of our initial assessment, we also evaluated correlations among these variables. Not surprising, we found modest and strong correlation between left and right audiometric data ($r = 0.84$, $p<0.05$), SBR for left and right ears ($r = 0.67$, $p<0.05$), monosyllabic word recognition of left and right ears ($r = 0.53$, $p<0.05$), and

THQ SEB subscale and total score (r = 0.90, p<0.05) and THQ T&H subscale and total score (r = 0.70, p<0.05). Most notably, the tinnitus loudness metric was not significantly correlated with any of these audiometric or questionnaire-based variables (p>0.05).

Middle ear power reflectance data plots are shown in the figures below for the blast-induced tinnitus group. These results were symmetric bilaterally and considered normal.

Figure 13.*Middle ear power reflectance measures for left and right ears.*

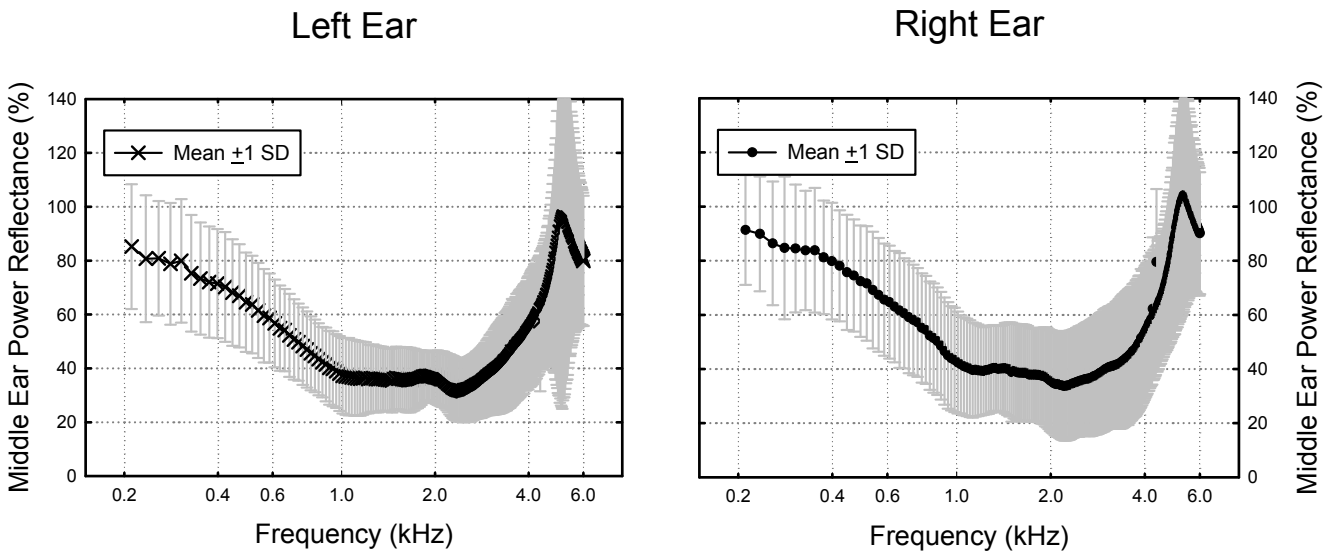

Distortion product otoacoustic emission data plots are shown below for the blast-induced tinnitus group. These data plots are clearly abnormal and follow the general pattern of the audiograms.

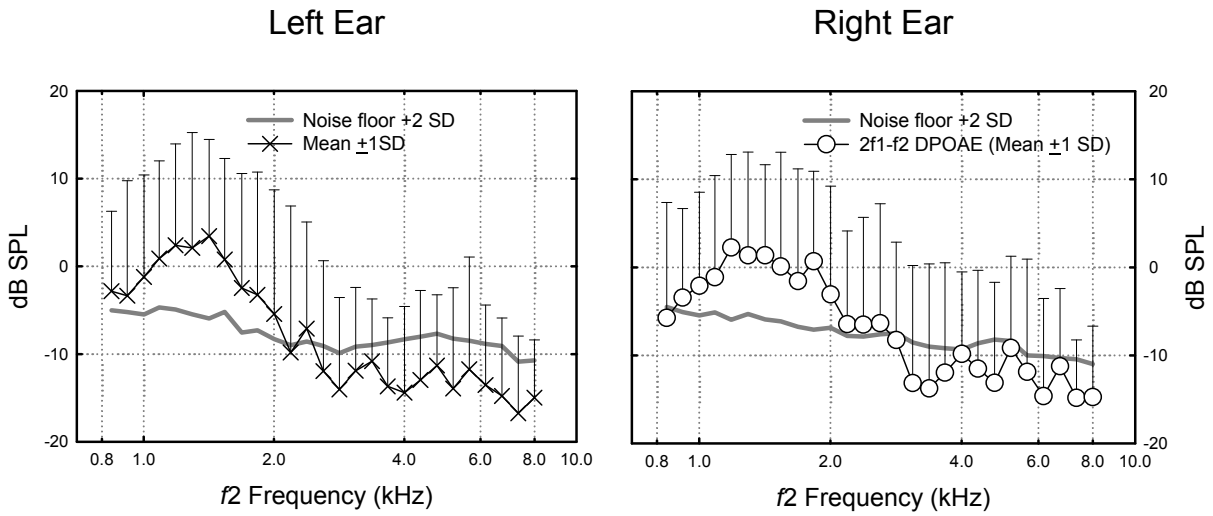

Figure 14. *Distortion product otoacoustic emissions for left and right ears. On average, DPOAE responses are present and above the noise floor below ~2400 Hz and but are absent and fall below the noise floor above this frequency range. This is consistent with the average moderate hearing loss noted in the audiometric data (Figure 1), they are consistent with outer hair cell dysfunction within the inner ear. The fact that middle ear power reflectance data are unimpaired provides further support for a cochlear site-of-lesion in this group.*

Neuroimaging Data

Again, because of the small sample sizes in the blast + concussion and concussion alone groups, and to limitations in statistical analysis, we focus here on the blast-induced tinnitus group. In this context, our current strategy is unchanged from previous reports in that we are capturing: high resolution magnetic resonance imaging (MRI) scans, evaluating its relationship to white matter connectivity in the brain using diffusion tensor imaging (DTI), capturing susceptibility weighted imaging (SWI) data was a way to evaluate the vascular system and assess for micro bleeds, and also to measure iron in seven different brain structures located in the deep grey matter. We are also assessing metabolites through the use of magnetic resonance spectroscopy (MRS) and resting state data. Herein, we focus on the MRI, DTI and SWI data in the blast exposed sample.

Methods and Data Processing: Fourteen participants with blast induced Tinnitus (mean age 52 ± 16 years) and thirteen subjects (mean age 58 ± 24 years) without Tinnitus participated in this study. One individual could not be imaged due to severe hyperacusis. When statistical comparisons were made with respect to the blast induced tinnitus group, subjects with noise induced hearing loss *without* tinnitus were used as controls. The technical parameters that are used for the above mentioned scans are listed below in the MR Imaging protocol section.

MR Imaging protocol

Localizer, T1 Flash sagittal, Mpr_coronal, SWI, DTI, and Spectroscopy

Technical Parameters of Sequences Included

Sequence Name	TR	T E	Flip Angle	Bandwidth	Matrix	Spacing	Thickness
Localizer	8.6	4	20	320	512*512	0.5*0.5	7
T1 Flash Sagittal	443	2.54	90	330	256*256	1*1	3
MPR Coronal	1600	4.28	8	180	384*384	0.67*0.67	1.34
SWI	41	20.75	15	391	512*384	0.5*0.5	2
DTI	7400	106	90	1395	128*128	2*2	3

DTI processing: DTIStudio is used to generate different components (maps) of DTI i.e. Eigen maps, apparent diffusion doefficient (ADC), fractional anisotropy (FA) and traces. B0 images are brain extracted and used as a mask to remove the skull area and non-brain matter on each of these maps. FA maps are spatially normalized to a standard space and then segmented into: grey matter (GM), white matter (WM), and cerebrospinal fluid (CSF).

Global Analysis: The WM maps were "thresholded" to *exclude* nonwhite matter voxels and a mask is created and applied onto the linearly spatially normalized FA map to extract the mean FA of those voxels that are considered to be white matter voxels. Mean FA for each subject with blast-induced tinnitus is plotted against the subject's age along with a group of subjects without tinnitus that are scanned with the same parameters. In similar fashion, the remaining components are also transformed into the same space and a global mean is extracted for the same voxels as that of the FA and plotted against respective ages. This plot provides a general trend on the relationship between white matter integrity and age.

Tract based spatial statistics (TBSS): This is a statistical method of comparing voxels to improve the sensitivity, objectivity and interpretability of analysis of multi-subject diffusion imaging studies. All native FA images in two groups are registered nonlinearly to a standard FA template and are transformed into a standard space. Subsequently, a mean FA image is created from these set of nonlinearly transformed images. A voxel wise permutation-inference analysis is carried out between the skeletons of two groups and a non-parametric two tailed *t*-statistic is performed to extract the voxels that fall above or below a certain threshold. These voxels are converted to a p value, based on the threshold set by the *t*-statistic value and the cluster size.

SWI processing: Susceptibility Weighted Imaging uses phase and magnitude components of the MR data to quantify iron content with the basal ganglia and thalamus, and identity potential blood products or abnormal signal in the parenchyma of the brain. With the Siemens Verio scanner, veins appear white in the images shown in subsequent sections.

Lesion load: Usually the lesions appear dark in the phase data indicating the presence of iron. The lesion load is quantified by drawing the region of interest (ROI) around the lesion and multiplying the number of pixels in the given ROI by the in plane resolution and the slice thickness so the resulting value could be expressed in mm^3.

SWI minimum intensity projection (mIP): This gives the information about the venous structure in the brain and by doing the mIP we get to know the continuity of the vessel like where it extends from and where it ends. This will be very helpful in getting a clear perspective of being discerning enough to distinguish between a vein and a bleed.

Iron quantification in the deep grey matter structures: SWI demonstrates the ability to quantify the iron present in various deep grey matter structures. It has been widely studied now how iron build up with ageing. This gives the ability to study is there a role of iron in the underlying pathology of any diseased brain compared to the normal brains in a certain age.

Iron is quantified in SWI Phase images in the following seven regions:

- Caudate Nucleus (CN)
- Globus Pallidus (GP)
- Putamen (PUT)
- Thalamus (THA)
- Pulvinar Thalamus (PT)
- Red Nucleus (RN)
- Substantia Nigra (SN)

Each of these seven regions is drawn on both the hemispheres of the brain following well established guidelines in identifying the structures. Furthermore a two region approach in quantifying the iron is used to visualize and localize the regions with high iron content. All the seven regions are divided into Region 1 (RI- Region with iron content below threshold value) and Region 2 (RII- Region with iron content above the threshold value). The threshold values are established from a group of 20 healthy normal controls developed at the Imaging Research Center at Wayne State University by Dr. E. Mark Haacke.

The following parameters from an in house processing tool are extracted to quantify the iron content of the individual participant.

- Average iron of the total region (TR-AI)
- Total iron of the high iron content region (RII-TI)
- Average iron of region II (RII-AI)
- Normalized region II area (RII-NA)

Results

DTI

Global results (FA vs Age) :

The following graphs illustrate the FA values plotted against age for a group of individuals having hearing loss but no tinnitus (plotted in red) and subjects with blast-induced Tinnitus (plotted in blue). Vertical error bars indicate two standard deviations.

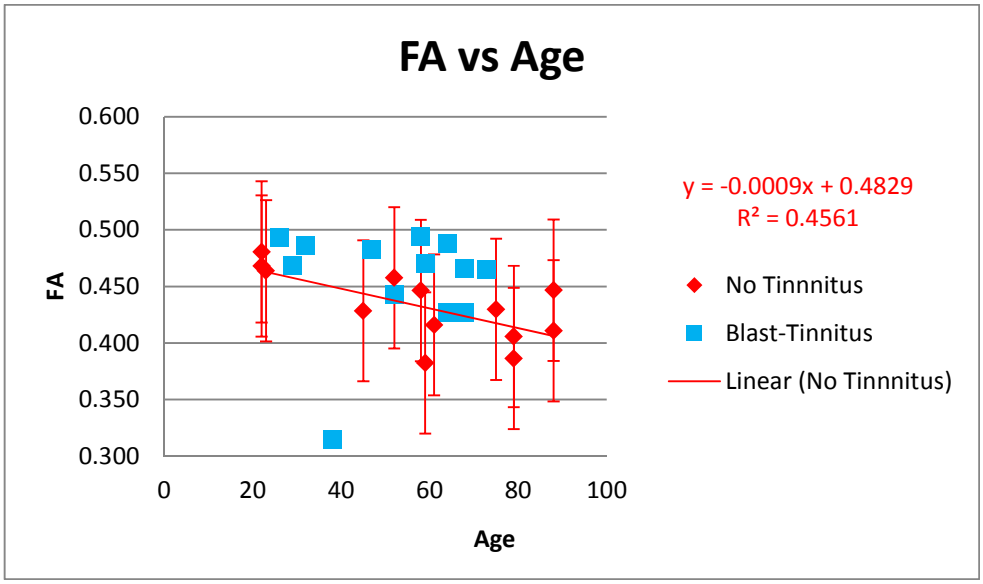

Figure 15. *FA vs. age for blast-induced tinnitus and control group.*

Global WM FA values for all the subjects with blast induced tinnitus except B12, tends to be within the range when compared to the subjects having hearing loss with no tinnitus. There tends to be a slight increase in white matter FA globally in the blast-induced tinnitus group which is strongly supported by the shift in the global FA histograms to the right (higher FA values) which is shown in the next section.

Global FA histograms

The following graphs illustrate the FA histograms for a group of people having hearing loss but no tinnitus (in red) and subjects with blast-induced tinnitus (in blue). Horizontal error bars indicate two standard deviations.

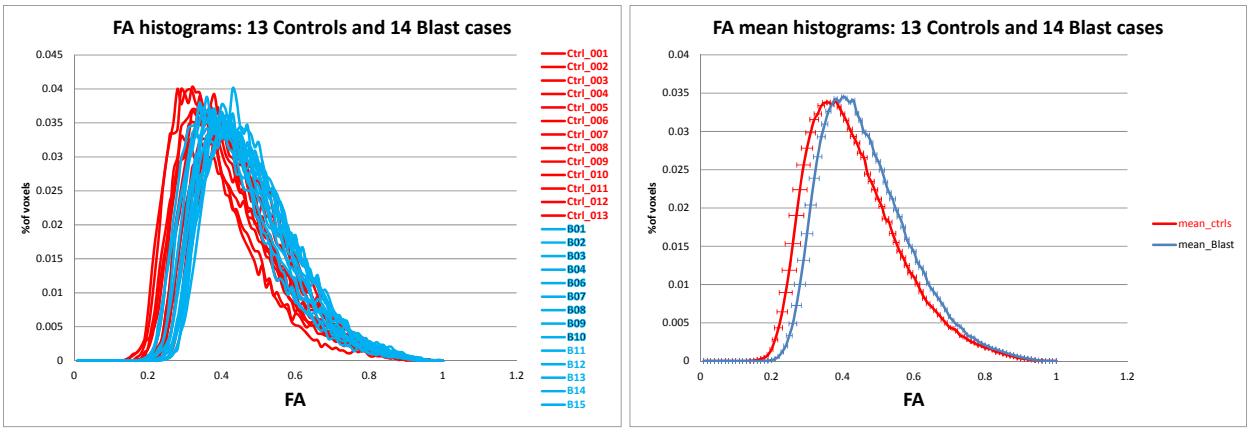

Figure 16. *Top). Histograms of control and blast-induced tinnitus. Bottom). Mean data collapsed across control and blast-induced tinnitus subjects.*

Discussion

Global WM FA values for all the subjects with blast induced tinnitus tend to be slightly higher when compared to the subjects having hearing loss with no tinnitus. This is strongly supported by the shift in the global FA histograms to the right (i.e., higher FA values).

c) TBSS group wise results:

The following figures illustrate the regions showing increased FA ($p<0.05$) for the blast induced tinnitus group when compared to the subjects without tinnitus.

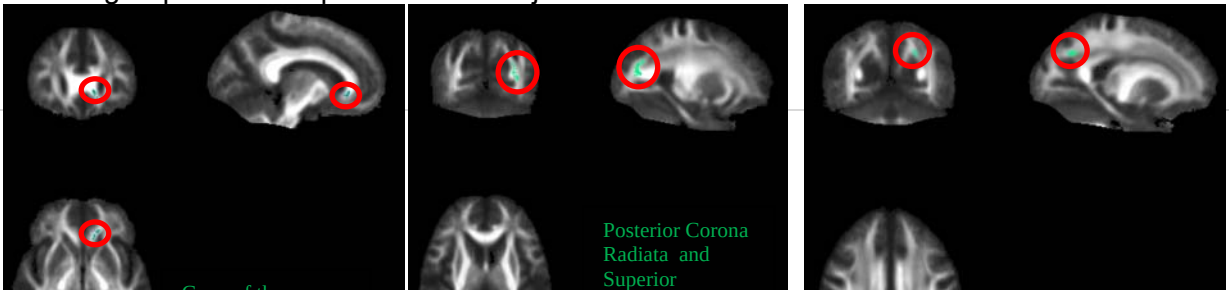

The overlays in light green indicate the regions that are 3 standard deviations above the mean FA of the group that have no tinnitus. For illustration purposes, overlays are indicated with circles in all the three views. Genu of the corpus callom (50 voxels), posterior corona radiate and superior longitudinal fasciculus (176 voxels) and the superior corona radiate (127 voxels), all showing FA values.

TBSS: Individual results

The following figures illustrate the mean FA values for the regions that show significantly increased FA ($p<0.05$) for the blast induced tinnitus group when compared to the subjects without tinnitus. The error bars in the plot show 2 standard deviations of the group that had no tinnitus.

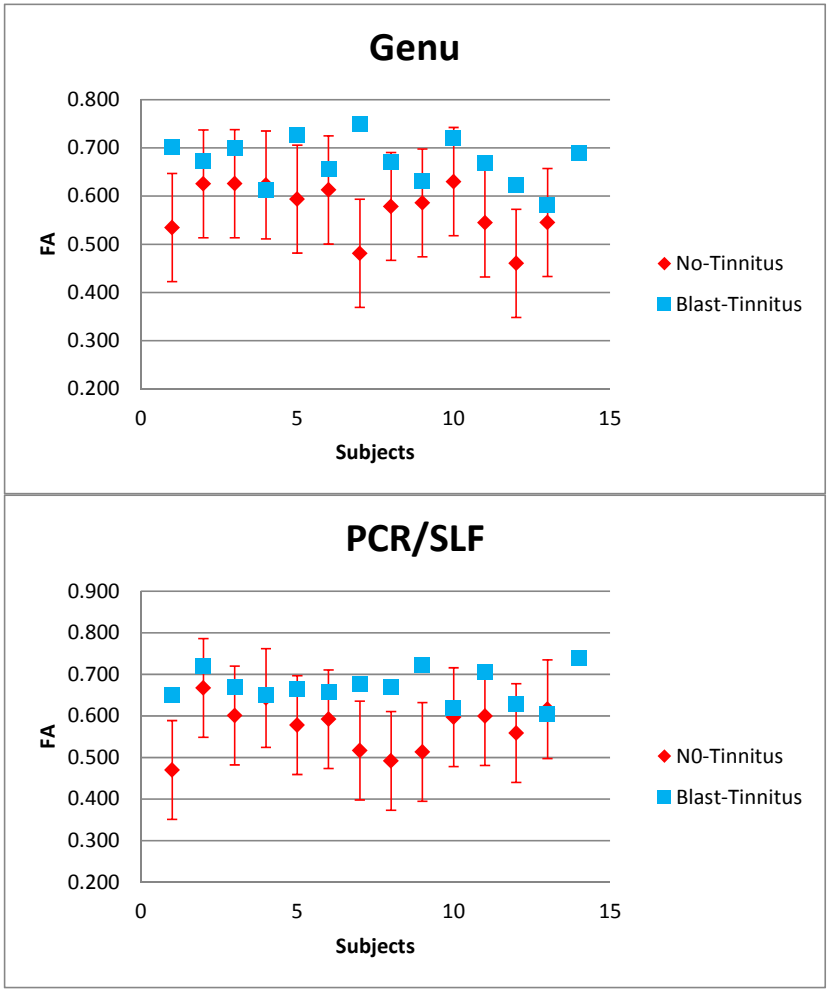

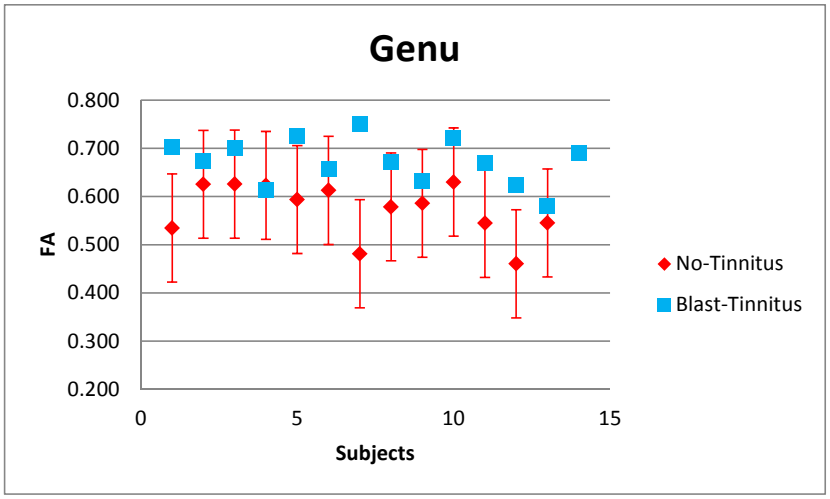

Figure 17. Scatter plots (top, middle, and bottom) of FA values for blast-induced tinnitus and control group.

SWI results:
In general, the majority of subjects with blast-induced showed normal SWI results. However, five subjects have showed abnormal phase behavior bilaterally in at least 3 of the structures out of the selected 7 structures. We will pay close attention to these interesting results as we collect more data, to determine if a trend or subgroups emerge. Nevertheless, a detailed description of the regions having higher or lower iron content are indicated in the table below.

	B01		B02		B03		B04		B06		B07		B08	
	Right	Left	Right	Left	Right	Left	Right	Left	Right	Left	Right	Left	Right	Left
CN	N	N	N	N	N	↑	↓	↓	N	N	N	N	↓	N
GP	N	N	↑	↑	N	N	↓	N	N	N	N	N	N	N
PT	N	N	N	N	N	N	N	N	N	N	N	↑	↓	↓
PUT	N	N	↓	↓	N	N	N	N	N	N	N	N	N	N
RN	N	N	N	↑	N	N	N	N	N	N	↑	↑	N	N
SN	N	N	↑	↑	N	N	N	N	N	N	↑	↑	↑	↑
TH	N	N	N	N	N	N	N	N	↑	↑	↓	↓	N	N

	B09		B10		B11		B12		B13		B14		B15	
	Right	Left	Right	Left	Right	Left	Right	Left	Right	Left	Right	Left	Right	Left
CN	N	N	↑	↑	N	N	N	N	N	N	N	N	↑	↑
GP	N	N	N	N	N	N	N	↑	N	N	N	N	N	N
PT	N	N	↑	↑	N	N	↑	↑	↑	N	N	N	↑	↑
PUT	N	N	↑	↑	N	N	N	N	N	N	N	N	N	N
RN	N	↓	N	N	N	N	↑	↑	N	N	N	N	↓	↓
SN	N	N	N	N	N	N	↑	↑	N	N	↑	N	N	N
TH	N	N	↑	↑	N	↑	↑	↑	↑	↑	N	N	↑	↑

N indicates normal iron content. Blue up arrows indicate increased iron content and red down arrows indicate low iron content.

Neuropsychological Data
We have tested 15 participants who have experienced a blast injury, 6 participants who have experienced a concussive injury, and 7 participants who have experienced both blast + concussive injuries.
Using the computerized neuropsychological testing program (ANAM), there are a number of variables that can be investigated. The principal dependent variables are 1) Mean (and Median) Reaction Time to Correct Responses; 2) Percent Correct (Accuracy); 3) Standard Deviation of Reaction Times to Correct Responses (SDRTC; to investigate patterns of intra-individual variability); and 4) Throughput (number of correct responses per minute, which combines speed and accuracy into a single measure).
Cognitive measures from ANAM include 1) Simple Reaction Time (SRT), repeated twice to evaluate for fatigability; 2) Procedural (Choice) Reaction Time (PRO); 3) Mathematical Processing (MTH); 4) Matching-to-Sample (Working Memory; MTS); 5) Code Substitution (Processing Speed; CDS); and 6) Code Substitution Delayed (delayed incidental recall; CDD).
During this period, data from the Mood Scale were analyzed. Traumatic Brain Injury (TBI) symptom data are still being aggregated.

Although none of the results were statistically significant, there were a number of emerging trends. The Blast + Concussion group shows a trend toward being younger than the other groups. There was also a trend for concussed participants to show slower mean reaction times and reduced throughput (number of correct responses per minute) during the Mathematical Processing and first administration of Simple Reaction Time subtests. Trends toward increased intra-individual variability on the first administration of Simple Reaction Time, as well as on Code Substitution and Matching-to-Sample were also observed. No other cognitive or mood differences were observed.

Below, we present a table of means and standard deviations for relevant variables in this aspect of the study. Interpretation of patterns of the means and standard deviations is still somewhat speculative, given the small cell sizes. The right-most column in the table below indicates the p value for the one-way between groups analysis of variance (ANOVA) contrasting the three groups. Below the table, vertical bar graphs are also presented.

		Blast (n = 15)		Concussion (n=6)		Blast+Concussion (n=7)		
	Variable	Mean	SD	Mean	SD	Mean	SD	p-value
	Age	52.5	15.3	61.2	11.2	41.3	16.4	0.07
SRT 1	MeanRTCorrect	286.0	51.1	368.2	162.6	258.9	44.4	0.07
SRT 2	MeanRTCorrect	295.5	92.3	377.0	288.7	254.2	36.3	0.33
MTS	MeanRTCorrect	1994.7	577.3	2231.4	1268.7	1740.5	524.3	0.52
MTH	MeanRTCorrect	2623.8	711.3	3316.0	1088.7	2474.8	500.1	0.12
CDS	MeanRTCorrect	1450.5	432.2	1680.0	415.4	1298.3	436.6	0.3
CDD	MeanRTCorrect	1684.2	829.4	1744.2	681.2	1416.5	438.2	0.66
MTS	Accuracy	17.8	1.7	17.3	1.9	18.0	2.4	0.81
MTH	Accuracy	18.5	1.5	18.0	2.3	17.7	2.1	0.65
CDD	Accuracy	26.7	5.9	24.5	5.5	27.4	6.6	0.66
SRT 1	Throughput	215.3	33.6	185.5	62.1	237.3	37.8	0.1
SRT 2	Throughput	215.6	45.8	204.0	71.3	240.2	33.8	0.4
MTS	Throughput	28.4	8.4	26.8	10.7	33.2	11.2	0.45
MTH	Throughput	22.7	7.3	17.4	6.3	22.4	5.7	0.27
CDS	Throughput	44.1	13.5	35.6	9.2	48.6	14.3	0.21
CDD	Throughput	28.4	14.7	22.7	8.8	34.9	18.7	0.35
SRT 1	SDRTCorrect	85.4	46.8	291.1	485.9	72.1	29.6	0.14
SRT 2	SDRTCorrect	154.8	128.9	211.2	298.6	83.6	42.4	0.39
MTS	SDRTCorrect	687.1	226.5	1086.2	741.4	668.2	310.2	0.11
MTH	SDRTCorrect	860.9	334.0	951.9	452.8	787.4	195.7	0.68
CDS	SDRTCorrect	397.7	148.3	567.4	217.9	415.4	158.5	0.12
CDD	SDRTCorrect	685.1	410.8	999.5	654.9	575.3	290.6	0.23
SRT 1	Median RT Correct	266.7	55.8	306.6	147.0	243.0	44.6	0.38
SRT 2	Median RT Correct	262.2	88.5	307.3	177.6	231.7	30.7	0.44
MTS	Median RT Correct	1859.3	585.7	1888.0	970.9	1538.6	433.8	0.52
MTH	Median RT Correct	2439.9	701.4	3096.6	1011.1	2423.9	532.2	0.17
CDS	Median RT Correct	1366.9	400.5	1567.0	420.0	1197.5	409.6	0.28
CDD	Median RT Correct	1503.3	742.4	1371.8	459.3	1261.9	363.7	0.69

Mood	Vigor	3.4	1.6	3.6	1.8	3.1	0.9	0.44
	Restlessness	1.1	1.1	1.1	1.5	1.9	2.3	0.46
	Depression	1.1	1.4	1.7	1.9	1.7	1.6	0.2
	Anger	0.7	0.8	1.1	1.7	1.5	1.4	0.64
	Fatigue	1.2	1.1	1.8	1.8	1.7	1.9	0.4
	Anxiety	1.0	0.9	1.2	1.3	1.8	2.0	0.24
	Happiness	3.9	1.5	3.5	1.5	3.1	0.8	0.57

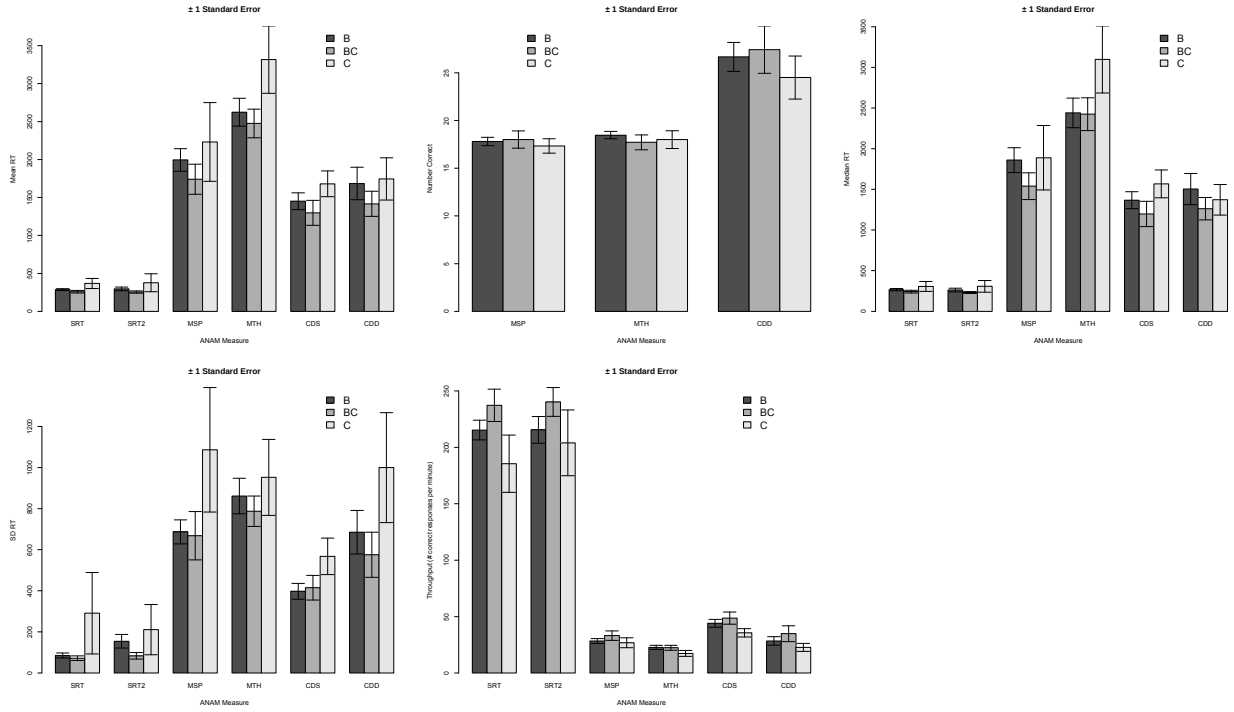

Figure 7 . A. *Mean reaction time (correct responses) for ANAM subtests;* ***B.*** *Number correct for ANAM subtests;* ***C.*** *Median reaction time (correct responses) for ANAM subtests;* ***D:*** *Standard deviation of reaction times for correct responses across ANAM subtests;* ***E.*** *Throughput for ANAM subtests (number correct responses per minute) Note:* ***B*** *= blast,* ***BC*** *= blast+concussion,* ***C*** *= concussion. Cognitive measures from ANAM include: 1) simple reaction time (SRT), repeated twice to evaluate fatigability; 2) mathematical processing (MTH); 3) matching-to-sample (working memory; MTS); 4) code substitution (processing speed, CDS); and 5) code substitution delayed (delayed incidental recall, CDD).*

KEY RESEARCH ACCOMPLISHMENTS:

Animal Studies:

- Prepared four manuscripts which we plan to submit.

- Formally analyzed our blast data, confirming that blast induced significant evidence of tinnitus at multiple frequency bands at 1 day after blast exposure, which migrated to high frequency bands at 1 months post-blast and low- and high-frequency bands at 3 months after blast. We also confirmed that blast-induced hearing loss may recover one month after blast exposure.
- Blast reduced responsivity to BBN sound stimulation in auditory structures.
- Completed our analysis and confirmed that blast induced axonal injury changes in white matter tracts and astroglial activation.
- Concussion causes immediate tinnitus and auditory detection deficits, which mostly recover within one week. Hearing loss is not induced
- Concussion causes significant axonal injury in the brainstem at 1.8 m height or higher.

Human Studies:

- Tinnitus was present following traumatic brain injury from a motor vehicle accident.
- Hearing loss was present bilaterally (right > left ear); however, the loss in the right ear was long standing from mumps at age 6 years and was unrelated to the accident.
- DPAOEs are consistent with an inner ear/outer hair cell lesion. However, in this case, the trigger for the tinnitus was probably related to the brain injury and not the peripheral hearing loss.
- Abnormal DTI and SWI data are of particular interest in this regard. It will be of particular interest to see if this trend continues.

REPORTABLE OUTCOMES:

Animal Studies:

Articles:

Jessica Ouyang, Edward Pace, Laura Lepczyk, Wei Zhang, and Jinsheng Zhang (To be submitted) Blast induced tinnitus and its related "invisible wounds" in limbic structures: a combined behavioral and MEMRI study.

Laura Lepczyk, Edward Pace, Jessica Ouyang and Jinsheng Zhang (To be submitted) Blast-Induced Tinnitus and Its Related Traumatic Brain Injury in auditory Centers: A Combined Behavior and Manganese-Enhanced MRI Study

Kallakuri Srinivas, Huichao Lu, Luo Hao, Edward Pace, Xueguo Zhang, Cavanaugh John M and Zhang Jinsheng (To be submitted). Blast overpressure induces long lasting astroglial up-regulation and diffuse axonal injury.

Hao Luo, Xueguo Zhang, Edward Pace and Jinsheng Zhang (in completion) Blast-Induced Tinnitus and Spontaneous Firing Changes in Auditory Centers of Rats

Abstracts (Podium and poster):

Zhang, J.S. (2012). Invited Speaker, "*What Have We Learned from Brain Stimulation in Tinnitus Suppression.*" 16th annual conference of International Association of Physician in Audiology (IAPA), Oct 19th-21st, 2012, Beijing, China.

Luo, L., Zhang, X, Kallakuri, S., and Zhang, J.S. (2013) Blast-Induced Tinnitus and Changesin Spontaneous Firing Rates along the Auditory Axis in Rats, Assoc. Res. Otolaryngol.

Jinsheng Zhang, Xueguo Zhang, Jessica Ouyang, Edward Pace, Hao Luo, Laura Lepczyk, Gulrez Mahmood, Zhigang Mei, Srinivasu Kallakuri, and Huichao Lu, E. Mark Haacke, and Pamela VandeVord (2012) Mechanisms and Treatment Strategies of Blast-Induced Tinnitus and Its Related TBI. *Military Health*

System Research Symposium (MHSRS), Harbor Beach Marriott, Ft Lauderdale, Florida, 13-16 August 2012.

Human Studies
Articles:

Randall R. Benson, Ramtilak Gattu, Anthony T. Cacace (acceptance pending revision). Left hemisphere fractional anisotropy increase in noise-induced tinnitus: A diffusion tensor imaging (DTI) study of white matter tracts in the brain. Hearing Research.

Mahoney M, McFarlan D, Capenter M, Rizvi S, Cacace A. (submitted) Reliability of broadband middle-ear power-reflectance in younger and older adults: Application of Generalizability Theory. The American J. Audiology.

CONCLUSION:

Animal studies:

Blast induction causes immediate hearing loss and widespread tinnitus, the former of which recovers one month post-blast and latter whereas the latter shifts to high-frequency tinnitus at one month followed by low and high-frequency tinnitus at 3 months post-blast. Responsivity to BBN sound stimulation is reduced in the DCN, IC and AC at one-day, one-month, and three-months post-blast. Axonal injury and astroglial activation is induced by blast at multiple time points in the DCN, IC, and AC. Concussion can induced immediate tinnitus and auditory detection deficits, however this mostly recovers within one week and completely recovers within two weeks. Hearing thresholds are significantly affected. In spite of this, evidence of axonal injury is apparent in brain processed from rats exposed to 1.8 m impact accelerator drop height.

Human studies:

With continued increase in the number of our subject recruitments, we are geared towards completing the proposed experiments. Results from this year showed that patients with blast-induced tinnitus showed symmetrical hearing thresholds and normal DPOAE, but with increased fractional anisotropy (FA) particularly in the corpus callosum and corona radiata and normal SWI in most patients. Patients with concussions had unpredictable hearing loss with large variability and asymmetric power reflectance values. While patients with both blast and concussion-induced tinnitus had less hearing loss than blast or concussion alone, tinnitus loudness was greatest for patients with both blast and concussion and least for blast alone, with concussion alone having intermediate loudness values.

REFERENCES:
References:

[1] F. Gallyas, J.R. Wolff, H. Bottcher, L. Zaborszky, A reliable method for demonstrating axonal degeneration shortly after axotomy, Stain Technol 55 (1980) 291-297.

[2] R.H. Garman, L.W. Jenkins, R.C. Switzer Iii, R.A. Bauman, L.C. Tong, P.V. Swauger, S. Parks, D.V. Ritzel, C.E. Dixon, R. Clark, H. Bayir, V. Kagan, E. Jackson, P.M. Kochanek, Blast exposure in rats with body shielding is characterized by diffuse axonal injury, Journal of neurotrauma (2011).

[3] S. Kallakuri, J.M. Cavanaugh, A.C. Ozaktay, T. Takebayashi, The effect of varying impact energy on diffuse axonal injury in the rat brain: a preliminary study, Exp Brain Res 148 (2003) 419-424.

[4] G. Paxinos, C. Watson, The rat brain in stereotaxic coordinates, Academic Press, New York, 2007.

[5] Mao, J., Pace, E., Pierozynski, P., Bobak, L., Kou, Z. F., VandeVord, P., Shen, Y.M., Haacke, M., Zhang, X.G., Zhang, J.S. (2011) Blast-induced tinnitus and hearing loss in rats: Behavioral and imaging assays. *J. Neurotrauma,* 2011 Nov 22 [Epub ahead of print].

APPENDICES:

Jessica Ouyang, Edward Pace, Laura Lepczyk, Wei Zhang, and Jinsheng Zhang (To be submitted) Blast induced tinnitus and its related "invisible wounds" in limbic structures: a combined behavioral and MEMRI study.

Laura Lepczyk, Edward Pace, Jessica Ouyang and Jinsheng Zhang (To be submitted) Blast-Induced Tinnitus and Its Related Traumatic Brain Injury in auditory Centers: A Combined Behavior and Manganese-Enhanced MRI Study

Kallakuri Srinivas, Huichao Lu, Luo Hao, Edward Pace, Xueguo Zhang, Cavanaugh John M and Zhang Jinsheng (To be submitted). Blast overpressure induces long lasting astroglial up-regulation and diffuse axonal injury.

Blast induced tinnitus and its related "invisible wounds": a combined behavioral and manganese-enhanced magnetic resonance imaging (MEMRI) study of limbic structures

Jessica Ouyang[(a)(c)], Edward Pace[(a)], Laura Lepczyk[(a)], Wei Zhang[(a)], and Jinsheng Zhang[(a)(b)]

(a) Department of Otolaryngology-Head and Neck Surgery, Wayne State University School of Medicine, 4201 Saint Antoine, Detroit, Michigan 48201
(b) Department of Communication Sciences & Disorders, Wayne State University College of Liberal Arts & Sciences, 60 Farnsworth St., Detroit, Michigan 48202
(c) Department of Physiology, Wayne State University School of Medicine, 550 E Canfield Road, Detroit, Michigan 48201

Running head: Blast-induced tinnitus
Number of figures: 6
Tables: 3

Candidate journals:
Experimental Neurology

**Correspondence:* Dr. Jinsheng Zhang, Otolaryngology-Head and Neck Surgery, 5E-UHC, Wayne State University School of Medicine, 4201 Saint Antoine, Detroit, Michigan 48201, USA; Phone: (313) 577 0066; Fax: (313) 577 6318; E-mail: jinzhang@med.wayne.edu.

Abbreviations:
ACC: anterior cingulate cortex
AMG: amygdala
DCN: dorsal cochlear nucleus
DTI: diffusion tensor imaging
IC: inferior colliculus
MEMRI: manganese-enhanced magnetic resonance imaging
MGB: medial geniculate body
NA: nucleus accumbens
NMDA: *N*-methyl-D-aspartate
NIR: Normalized Intensity Ratio
PTSD: post traumatic stress disorder
SUD: subjective unit of distress
TBI: traumatic brain injury
vmPFC: ventral medial prefrontal cortex

Abstract:

Tinnitus and hearing loss are common auditory-related co-morbidities of blast trauma. Tinnitus along with other cognitive problems, such as anxiety, memory loss, emotional disturbances and depression, are often observed following a traumatic blast event. We set out to develop a rodent model to address the cognitive status (memory) and the psychological state (anxiety) that are associated with blast induced tinnitus. In this study, 16 adult rats were randomly divided into blast and control groups. The left ears of the rats in the blast group were exposed to blast shock wave at 14 psi. Blast-induced tinnitus was evaluated using gap detection acoustic startle reflex paradigm and prepulse inhibition (PPI) paradigm. The level of anxiety and the spatial memory were evaluated with the elevated plus maze and the Morris water maze, respectively. Using MEMRI, a functional imagining tool that depicts neuronal activity, we investigated blast-induced neuronal changes in several limbic structures.

Compared to rats in the control group, rats in the blasted group with or without tinnitus demonstrated higher level of anxiety. MEMRI data demonstrated that rats with tinnitus at the time of the scanning exhibited hyperactivity in the contralateral basolateral nuclei of amygdala (AMG), and hypoactivity in the ipsilateral anterior cingulate cortex (ACC). These changes may have contributed to psychological sequalea of blast-induced tinnitus, TBI and the posttraumatic anxiety disorders, aka. PTSD.

Keywords: Blast-induced tinnitus, PTSD, anxiety, blast-induced TBI, limbic structures

Introduction:

Blast injuries account for over 80% of the combat-related injuries. Blast-induced TBI and PTSD are the "signature injuries" of Global War on Terrorism, with prevalence as high as 16% and 14%, respectively (Cernak and Noble-Haeusslein, 2010). Blast-induced tinnitus is the most common sequalea of blast injuries, and it is listed as the number one diagnosis for service-connected disability claims. Tinnitus, referred as "ringing in the ear" in layman's terms, is scientifically defined as sound perception without an external acoustic event. Combined with overpressure, blast exposures can be extremely pathogenic to the auditory system. Of all the military personnel who have been exposed to blast injuries, 70% reported symptom of tinnitus within 72 hours of the exposure, and 43% reported suffering persistent tinnitus one month after. The annual cost to compensate veterans for tinnitus in the U.S. is nearly $2 billion per year (ATA, 2012). PTSD, an anxiety disorder following an exposure to a traumatic event, is characterized by symptoms of intrusion, hyperarousal, numbing, and/or avoidance of traumatic triggers. Along with depression, PTSD is strongly associated with blast-induced tinnitus. Thirty-four percent of veterans with tinnitus carry diagnose of PTSD concurrently (Fagelson, 2007). Tinnitus is often intensified by the sounds that trigger "flash-

backs"; and service members who carry both tinnitus and PTSD diagnoses have reported that their symptoms of PTSD were more intense and frequent than that of veterans with PTSD only (Hinton et al., 2006). In order to develop reliable treatments for blast-induce tinnitus and its related neurological disorders, a need to investigate the underlying mechanisms is rendered. To develop efficacious treatments, it is of vital importance to reveal the causal relationship if any between blast-induced tinnitus and PTSD.

The concepts of limbic system has been evolving and unfolding as more scientific eyes were gazed upon it. It is widely accepted that the limbic system encompasses the AMG, the hippocampus, the ACC, the nucleus accumbens (NA), and the ventral medial prefrontal cortex (vmPFC) (Roxo et al., 2011). Evidence from both human and animal studies has indicated the involvement of limbic structures in the ideology of tinnitus (Goble et al., 2009; Landgrebe et al., 2009; Lockwood et al., 1998; Mirz et al., 2000) and PTSD (Karl et al., 2006). Neuronal hyperactivity in the AMG, the hippocampus, and the NAs, as well as neuronal hypoactivity in the ACC of subjects with chronic tinnitus (De Ridder et al., 2006; Landgrebe et al., 2009; Leaver et al., 2011; Plewnia et al., 2007; Schecklmann et al., 2011; Shulman et al., 1995; Vanneste et al., 2011). Ample data have supported that the AMG plays a pivotal role in the mechanism of PTSD (Liberzon et al., 1999; Pissiota et al., 2002; Rauch et al., 2006). Hyperactivity in the AMG is associated with PTSD, and is positively correlated with the severity of the symptoms (Pissiota et al., 2002). Adjacent to the ACC, the vmPFC, which includes ventral medial gyrus, is also indicated in PTSD. Neuronal hypoactivity in the rostral ACC has been linked to PTSD, and is negatively correlated to the severity of the symptoms (Bremner et al., 1999). The function of the hippocampus is altered in the patients with PTSD; however, the direction of the change depends on the tasks. In virtual water maze and emotional word retrieval studies, which test for spatial and semantic memory, subjects with PTSD showed hypoactivity in the hippocampus (Astur et al., 2006; Bremner et al., 2003). In addition, in encoding face-occupation association and script-driven imagery studies, which tests for episodic memory, subjects with PTSD showed hyperactivity in the hippocampus (Osuch et al., 2008; Werner et al., 2009).

Thus far investigations of the underlying mechanisms of blast-induced tinnitus are very limited. In a recent paper, we reported that blast at 14 psi induced early onset tinnitus and hearing impairment, which was associated with significant axonal damage to certain auditory brain regions such as medial genicula bodies and inferior colliculi 2 weeks after the exposure as revealed by diffusion tensor imaging (DTI) (Mao et al., 2012). Using DTI imaging, the single 14 psi blast did not induce significant micro-structural changes in the corpus callosum, indicating that the direct impact onto the brain parenchyma may not be evident at this time point with this level of single blast exposure (Mao et al., 2012). However, it is still not clear whether the DTI is sensitive to show all changes as a result of blast exposure. This prompts studies using different methodologies.

Mn^{2+} is a paramagnetic contrast agent that can significantly reduce both T_1 and T_2. After systematically administered, Mn^{2+} enters brain through the blood

brain barrier (BBB) at low dose and through choroid plexuses at higher dose (Murphy et al., 1991). Once entering the neuron through synapses, Mn^{2+} is transported anterogradely down axons and released into synaptic cleft with glutamine. The neuronal clearance for Mn^{2+} takes weeks. The intensity of the Mn^{2+} enhanced MR signals thus represents accumulated synaptic activities since the administration of manganese chloride. MEMRI is hemodynamic-independent. It has been used to probe the functions of central nervous system (Silva and Bock, 2008) and to study tinnitus (Brozoski et al., 2007; Holt et al., 2010). Utilizing a 7 Tesla MRI scanner, the neuronal activity of visual cortex has been analyzed in layer-specific detail with this technique (Bissig and Berkowitz, 2009). The present study used MEMRI technique to explore the changes in the limbic structures associated with blast induced tinnitus.

We hypothesize that blast-induced tinnitus, hearing impairment, and PTSD are associated with mild TBI as a result from neural plasticity in the brain. Specifically, we hypothesize that the induced hyperactivity occurs in the AMG, hippocampus, and NA as well as hypoactivity in the ACC for rats that exhibit anxiety and tinnitus. To test these hypotheses, we set out to investigate the neuronal changes in these structures using manganese enhanced magnetic resonance imaging (MEMRI) in a rat model.

Materials and Methods:

Animal subjects

Twenty-four Sprague-Dawley rats (male, 60-70 days old) were purchased from Harlan Laboratories. All rats were kept on a 12/12h day/light cycle and were cared for in a federally approved animal vivarium. Rats that did not demonstrate normal startle behavior responses after 2 weeks of gap detection (GAP) and pre-pulse inhibition (PPI) behavioral training, rat that died, and rats that did not uptake manganese into brain parenchyma, were excluded from the experiments. Of the 16 rats that finished the protocol that consisted of a series of experiments, 4 rats were in the control group and 12 rats were in the experimental group.

After rats were acclimated, a baseline auditory brainstem response (ABR) was conducted while tri-weekly (3 times/week) GAP/PPI paradigms recordings were performed on all rats. Four weeks after arrival, rats in experimental group were exposed to blast, and ABR was repeated for these rats within 24 hours after the blast. Biweekly (twice/week) GAP/PPI paradigms recordings were performed for all rats after the blast. All rats underwent tests in elevated plus maze and Morris water maze 4-5 weeks after the blast and one day before the MEMRI scanning. Of 12 rats in the experimental group, 7 rats exhibited tinnitus at the time of the scanning.

All experimental protocols were in accordance with the guidelines of the Institutional Animal Care and Use Committee (IACUC) at Wayne State University.

Auditory Brainstem Responses (ABR):

ABR thresholds and the amplitude of ABR P1N1 waveforms were evaluated at the baseline, and within 24 h before MEMRI. Each rat was anesthetized by administering 2% isoflurane/air mixture via a nose cone for the procedure. To test the threshold of the left ear, a set of three platinum coated tungsten electrodes were subcutaneously at the vertex, below the left pinna, and contralateral temporal muscle to serve as active, return, and ground electrodes, respectively. To test the threshold of right ear, the active, return, and ground electrodes were inserted at the vertex, below the right pinna, and contralateral temporal muscle, respectively. Click and tone bursts of 10 ms duration at 8 kHz, 12 kHz, 16 kHz, 20 kHz, and 28 kHz (0.1 ms rise/fall time) were delivered to the ear canal from an electrostatic speaker at intensity level from 80 dB to 5 dB SPL in increment of 5 dB SPL in descending order. The stimuli were generated by RX6 Multifunction Processor and SigGenRP software (TDT system 3). Calibration was achieved using SigCalRP® software. ABR signals were amplified; they were band-filtered from 0.3 to 3 kHz and notch-filtered at 60 Hz; and they were averaged 300 times as well.

Behavioral testing: before and after blast exposure

Gap/PPI behavioral paradigm, a currently widely used behavior tool was used to screen for tinnitus in rats (Turner et al., 2006; Zhang et al., 2011), using a behavioral testing system (Kinder Scientific, Poway, CA). During the testing, the rat along with a custom-made conditioning restrainer in which the rat stayed was placed in a behavior chamber for gap detection and PPI testing. The testing was conducted 3 times a week (2-3 days between each testing) for 4 weeks before blast and twice a week (3-4 days between each testing) after exposure. Each time the testing took 1 day and was considered 1 testing session. The first 6 testing sessions were for conditioning training, and the data obtained from these first 6 sessions were excluded from baseline analysis. In the soundproof testing chamber, the startle force (N) of the rat was detected with a piezoelectric transducer attached under the platform. Peak-to-baseline startle responses were monitored and recorded in real time using startle monitor software (Kinder Scientific). Prior to each testing session, calibration was performed. A Newton impulse calibrator was used to calibrate the piezoelectric transducer, and a sound pressure level meter was used to calibrate the speaker inside the chamber.

In the gap detection procedure, each rat was tested in the chamber with a continuous background noise of 60 dB SPL at various frequency bands. The width of the frequency band was 2 kHz, and frequencies were 8-10 kHz, 12-14 kHz, 16-18 kHz, 20-22 kHz, 26-28 kHz, and 2-30 kHz broadband. At each frequency, 2 sections of 8 trials each were recorded. The first 8 trials were referred to startle trials, in which a noise burst of 115 dB SPL with duration of 50-msec was delivered by an in-chamber speaker to induce a startle response from the rat. The startle response was recorded as the forces that the rat exerted on the platform. The second 8 trials were referred to gap trials, in which an absence of background noise with duration of 40-msec (a noise gap) was introduced 50-msecs before the startle noise burst. This gap acted as a “warning” of incoming startling noise burse. With

training, a rat with normal hearing would inhibit startle responses upon hearing the gap, whereas a rat with tinnitus would startle because the tinnitus fully or partially "filled" the gap. The ratio of average forces recorded during gap trials divided by the average forces recorded during startle trials at each frequency band was used to indicate the degree of inhibition at that frequency band. Inhibition was defined as the gap/startle ratio ≤ 0.8 (Turner et al., 2006).

Using gap detection paradigm alone cannot differentiate tinnitus from hearing loss because a rat with hearing loss would not be able to hear the noise gap and consequently would startle. To further differentiate tinnitus from hearing loss, we introduced PPI paradigm. In a PPI paradigm, there was no background noise. To replace the noise gap in gap paradigm as a "warning" of incoming startle burst, a prepulse noise of 60 dB SPL was used in PPI paradigm. The ratio of average forces recorded during PPI trials divided by the average forces recorded during startle trials at each frequency band was used to indicate the degree of inhibition at that frequency band. Inhibition was defined as the PPI/startle ratio ≤ 0.8. If the rat has hearing loss, the rat would not be able to hear the prepulse noise and consequently would startle. If the rat had normal hearing or tinnitus, it would recognize the warning prepulse noise and would show inhibition (Fitch et al., 2008).

One of biggest challenges of gap/PPI behavioral experiment was that rats could not consistently exhibit stable behavioral manifestations in that rat's physical condition and/or emotional condition might affect its startle responses. To minimize the impacts of these factors, the rats were handled by the same personnel, and extreme values were excluded. The mean of forces and standard deviation (SD) of each 8-trial session was calculated. The values of forces that were above or below 2 SDs from the mean force were deleted. Three out of four gap/PPI sessions were selected to composite group average. Each session contained both gap detection and PPI paradigm data collected on the same day for that session. For the gap/PPI sessions that were excluded, the exclusion criteria were, that startle forces were less than 1 N throughout the session during startle trials at all frequency bands, and/or that the rat startled throughout the session during PPI trials at all frequency bands.

Blast exposure

A single blast exposure for the experimental group was conducted using a shock tube located in the Department of Biomedical Engineering at Wayne State University (ORA, Inc). To avoid excessive trauma to the rat, the rat was placed on a mesh platform 198 inches downstream from the bursting membrane and 44 inches upstream from the open end of driven cylinder (Leonardi et al., 2011). After the rat was anesthetized with ketamine/xylazine (0.1ml/kg with concentration of 100/20 mg/ml) intraperitoneal injection, the right ear of the rat was plugged with a Mack's ® earplug, sealed with mineral oil, and sutured closed at the pinna with one stitch. The animal was then wrapped in protective garment and secured on a holder in the driven cylinder. A Mylar membrane was placed between the driver cylinder and driven cylinder. The sudden increase of pressure in the driver cylinder burst the

membrane, which generates a shock wave in the driven cylinder, similar to that of a free-field blast wave (Leonardi et al., 2011). The simulated blast was delivered at 14 PSI (96.5kPa) above atmospheric pressure, which generated an explosive sound at the level of 194 dB SPL. The positive phase duration was 2 msec. After the exposure, each rat was carefully monitored until it regained consciousness and restored normal movement.

Elevated plus maze (EPM)

Two days before the MEMRI scanning, rats' anxiety-like behaviors were measured with an elevated plus maze (Tracoustics Inc., Austin, TX). The lighting in the testing room was adjusted to a dim setting. The intensity of the light in the room, measured by a light meter, was 1.5 lux around open arms and 0.09 lux in closed arms, respectively. Prior to testing, rats were handled once a day for five days to minimize the anxiety of being transferred from the cage onto the maze. Each rat received handling for exact 2 min each time by the same person who would handle the rats on the day of testing. On the day of testing, rats were transported to the testing room and acclimated in the dim light for 4 hours before testing. During testing, each rat was placed in the center of the maze facing north, and their behaviors were recorded with a digital camcorder mounted on the ceiling above the EPM. Each rat was allowed to be on the maze for 5 min. Following the test, the rat was returned to its cage and the maze was cleaned with 70% alcohol. Two people rated the videos independently. The scores of the two raters were averaged for each measure. Anxiety-like behaviors were determined by calculating the percentage of the time the rat stayed in the open arm over the period of 5 min and by the percentage of the number of entries the rat made to the open arms over all the entries. An entry was defined as setting all four paws in an arm (Perrine et al., 2006).

Morris water maze (MWM)

At least 24 hours after the EPM testing, all rats were tested for spatial learning and memory using a one-day Morris water maze protocol (Frick et al., 2000; Kraemer et al., 1996). A circular fiberglass pool (183 cm in diameter), which was filled with commercially made opaque acrylic, non-toxic paint/water mixture, was used in this protocol. The pool was divided into 4 designated quadrants. A hidden platform (11 cm in diameter) was placed in the middle of such quadrant one inch below the water surface (Morris, 1984). Visual cues were painted on the walls. The room where the experiment took place is 3 m by 3 m in size and free from other distractions. After each swimming, the rat was dried with dry towels immediately, and the swimming was interspersed with rest period. The trajectories of the rats were recorded using a digital camcorder mounted on the ceiling above the water tank. Rats were tracked by Ethovision software (Noldus Information Technology, Inc) installed in a computer workstation.

(1) Spatial task acquisition:

Rats were trained to use extramaze cues to find the hidden platform. The submerged platform (hidden) was placed in southeast quadrant (Zone 4) of the

tank. The sequences of four start positions (N, S, E, and W) differed from block to block. In this task, each rat swam total of 12 trials, which were organized into 3 blocks of 4 trials each. Each rat was placed into the pool facing the pool wall. If a rat failed to locate the hidden platform within 60 seconds, it was taken from the water and placed on the platform for approximately 10 seconds. After the rat finished one trial, the next trial started immediately until all 4 trials were finished for the block. All rats rested in their cages for 30 minutes between 2 blocks. Swim time (s), swim speed (cm/s), and swim path-length (cm) were recorded to represent spatial learning.

(2) Probe trial:

One probe trial followed the spatial task acquisition 30 minutes later. During this trial, the platform was removed. Rats swam for 60 seconds before they were removed from the pool. The percentage of the time the rat spent in Zone 4 where the platform used to be and the number of entry the rat made to the Zone 4 were measured to reflect spatial memory.

This compressed protocol has been validated as a sufficient tool to assess spatial reference memory and spatial learning elsewhere (Frick et al., 2000; Kraemer et al., 1996). Compared to the traditional MWM protocols that last 5 or more days, this protocol is more cognitively challenging yet less physically intense. For rats that had been exposed to blast shock wave injury, this protocol was well tolerated and adequately effective.

MEMRI

Five weeks after the blast exposure, all rats were scanned with a 7.0 T Siemens ClinScan MRI scanner (Siemens Medical Solutions USA, Inc. Malvern, PA). Alert rats were injected with Manganese chloride solution ($MnCl2{\cdot}4H2O$, 0.1 M) intraperitoneally. The dosage was 67 mg per kilogram weight. Rats were then placed in a sound-proof room for 8 hours before scanning. Accumulating uptake of manganese for 8 hours is adequate for functional imaging, and utilization of anesthesia during scanning does not affect manganese uptake (Bissig and Berkowitz, 2009; Silva et al., 2004). Before MRI scanning, rats were induced with 4% isoflurane/air mixture in an induction chamber. Anesthesia was maintained with 2% isoflurane/air mixture via a commercially made MRI compatible nose cone. During scanning, the rat was placed on a heated re-circulating water pad to maintain core body temperature. A whole-body transmit-only coil and a 4-element Burker mouse-brain receive-only surface coil were used for scanning. The coils were placed to the rat's head, and the proper placement was verified by a testing scan. Individual images were acquired with 2 sets of MPRAGE (TR: 2500 ms, TE: 3 ms, TI: 1500 ms) and PDGE (TR: 1000 ms, TE: 3 ms) sequences with flip angle of 3 and total scanning time of 23 min. The field of view was 25 by 25 section of space (192 pixels by 192 pixels, or 130 μm by 130 μm). The thickness of the slice was 260 μm. At the end of the scan, the rat was monitored until regaining consciousness on a heated pad. They were then returned to their home cages.

Images were processed with R (v2.12.1, http://www.r-project.org) scripts developed by Mr. D. Bissig (Ref). The addition of two sets of MPRAGE images

was divided by the addition of two sets of PDGE images to mitigate the intensity field bias (Van de Moortele et al., 2009). The corrected images were used for analysis. Regions of interest (ROIs) were manually drawn using MRIcro v.1.40 with gingerly referencing to the Paxinos and Watson (4th Edition; 1998) rat brain atlas (Table 1). Average signal intensity of ROIs was obtained with MRIcro. ROI signal intensities (SI) were normalized with that of adjacent muscle (normalized ROI SI = ROI SI/muscle SI). Muscle normalization was utilized to mitigate inter-individual differences in peripheral MnCl2 uptake due to the liver sequestration. The following structures were included for analysis: amygdala (AMG), ACC, NA, and hippocampus. Two people analyzed the images independently, using the same criteria. All image sets were randomized and coded so that the people who analyzed the image were blinded with regard to the identity of the image sets.

Table 1. Selection of ROIs and reference figures according to the rat brain atlas by Paxinos and Watson (4th Edition; 1998).

Structures		ROIs	Reference figure# from the Paxinos and Watson (4th Edition; 1998) rat brain atlas
AMG	AMG_S (including PMCo and AHiAL)	One 3D ball (radius 260μm)	Figure 35
	AMG_D (Including BMP, BLA, BLP, LaVM, and LaVL)	One 3D ball (radius 260μm)	Figure 33
	AMG_C (including CeM, CeL, and CeC)	One 3D ball (radius 260μm)	Figure 30
ACC	ACC (including Cg1 and Cg2)	One 3D ball (radius 260μm)	Figure 18
NA	Shell (Acb_S)	One 3D ball (radius 260μm)	Figure 14
	Core (Acb_C)	One 3D ball (radius 260μm)	Figure 14
Hippocampus (including only CA1)		4 lines on each of 3 consecutive images	Figure 42, 43 and 44

(1) Normalized Intensity Ratios (NIR) of AMG, ACC, and NA:

The AMG was divided into three subdivisions: the centromedial nuclei (AMG_C), the superficial or cortical-like nuclei (AMG_S), and deep or basolateral nuclei complex (AMG_D). Spherical 3D ROIs were used to characterize AMG, ACC, and NA (radius: 260 μm). The ROIs were drawn in the way that they were placed at the rostrocaudal center of each anatomical region in the coronal profile, excluding a buffer (≥1 voxel wide, depending on the ROI) at borders with neighboring brain regions. Appropriate ROI placement was confirmed in parasagittal and transverse profiles (Figure 1). The resulting intensity ratios were then multiplied by 100 to yield NIRs.

Figure 1. Illustration of the selection of ROIs for AMG, ACC, and NA.

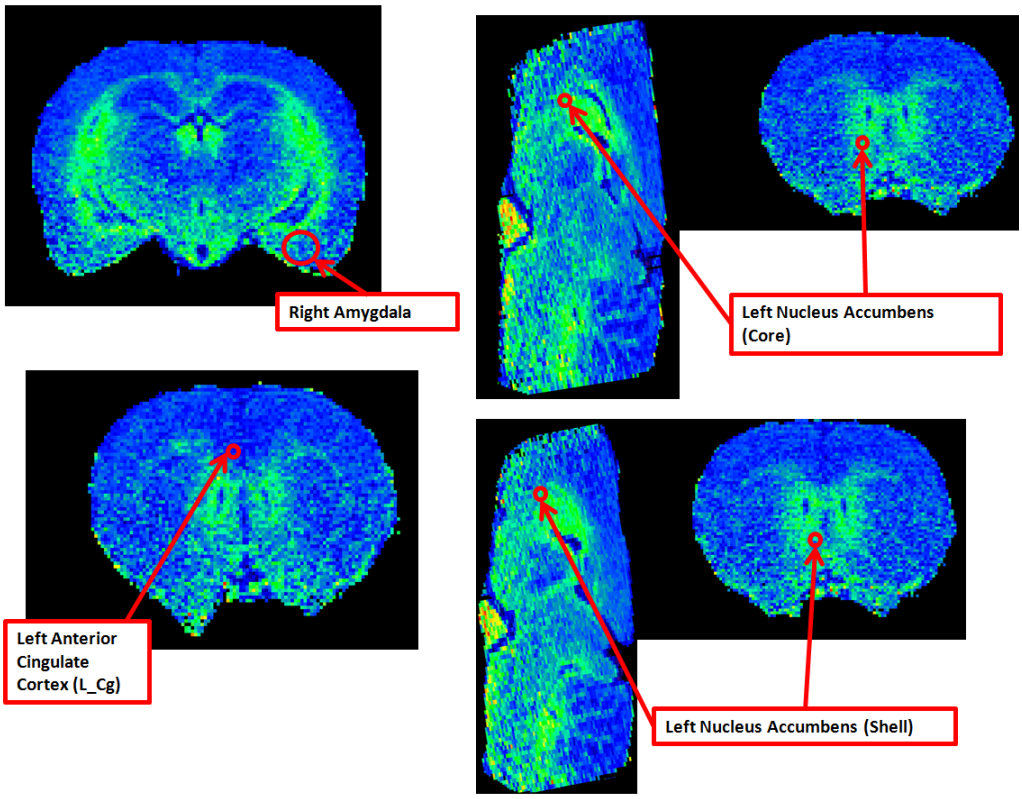

(2) NIR of hippocampus:

Intensity of hippocampus was obtained with ImageJ. Three consecutive slices were used on both sides. The first slice immediately followed the slice where the dentate gyrus became evident. Four lines were drawn on each side perpendicular to the curvature of forceps major corpus callosum. Intensity of combined CA1 and CA2 was determined by the peak gray value in the gray value linear plot (Figure 2). All 12 peak values on one side of hemisphere were averaged and multiplied by 1000 to yield the NIR.

Figure 2. Illustration of obtaining intensity of CA1/CA2 from the peak gray linear plot.

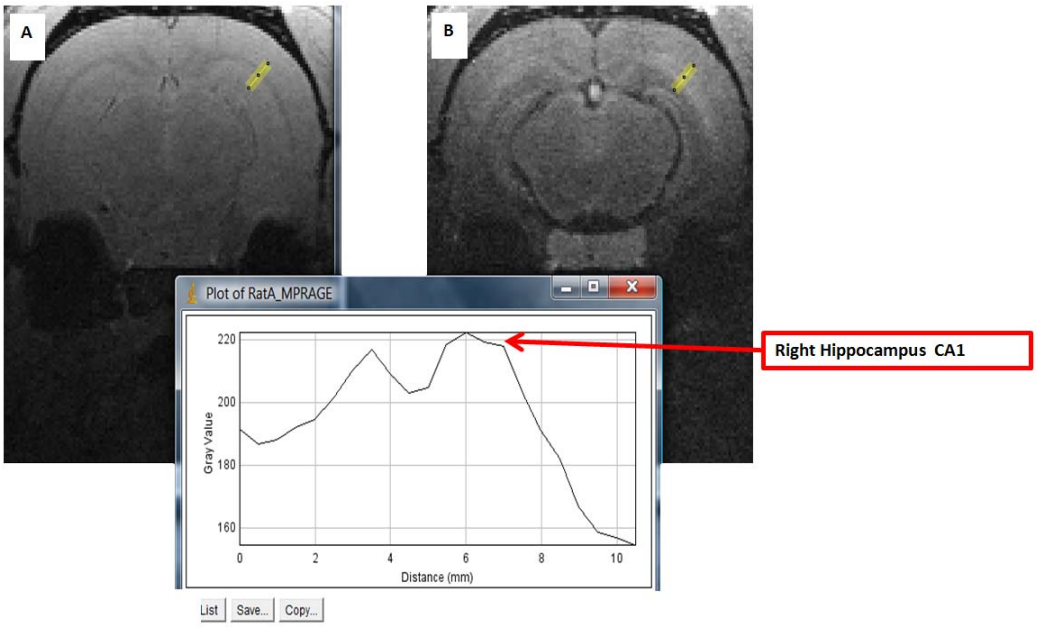

Statistical analysis

One-way ANOVA was performed, and the post-hoc Bonferroni method was used to adjust α value to compare data among three groups: the control group, the blasted group with tinnitus, and the blasted group without tinnitus. $P<0.05$ was considered statistically significant. When two people rated video or images independently, a Pearson comparison test was done to assess inter-rater reliability.

Results:

Both ABR and behavioral data indicated that all 16 rats showed normal hearing at the baseline. At the time of MRI scanning (35 days after the blast), five rats in the blasted group did not show behavioral evidences of tinnitus. They were grouped into the "tinnitus (-) group" (n=5). On the other hand, seven blasted rats exhibited robust behavioral evidence of tinnitus at 26-28 kHz at the time of MRI scanning, and they were grouped into the "tinnitus (+) group (n=7). At the time of scanning, ABR thresholds of the blasted rats have returned to the pre-blast baseline level. No significant differences in the ABR thresholds among 3 groups were found at the time of MRI scanning ($p>0.05$), however, compared to that of rats in the control group, the amplitudes of P1N1 waveforms in tone burst ABR at 28 kHz of the rats in blasted groups with or without tinnitus were significantly lower ($p< 0.001$). Compared to the rats in the control group, rats in the tinnitus (+) group spent less time in the open arms and made less entries to the open arms on the elevated plus maze ($p<0.05$). In the second block of the MWM, compared to the rats in the control group, the velocity of the rats in the tinnitus (+) group was slower ($p<0.05$). Compared to the rats in control group, the rats in the tinnitus (+) group had lower Manganese uptake in the ipsilateral ACC and higher manganese uptake

in contralateral basolateral AMG ($p<0.05$).

Behavior testing of tinnitus and hearing impairment

At baseline, all groups showed inhibition at all frequencies in the gap detection tests and the PPI paradigm tests (gap/startle ratio ≤ 0.8 & PPI/startle ratio ≤ 0.8), confirming the detection of normal hearing. Among three groups, the gap/startle ratios and PPI/startle ratios of the blasted rats with or without tinnitus were not higher than that of the rats in the control group, and the gap/startle ratios and the PPI/startle ratios of the rats in the tinnitus (+) group were not higher than that of the rats in the tinnitus (-) group (Figure 3).

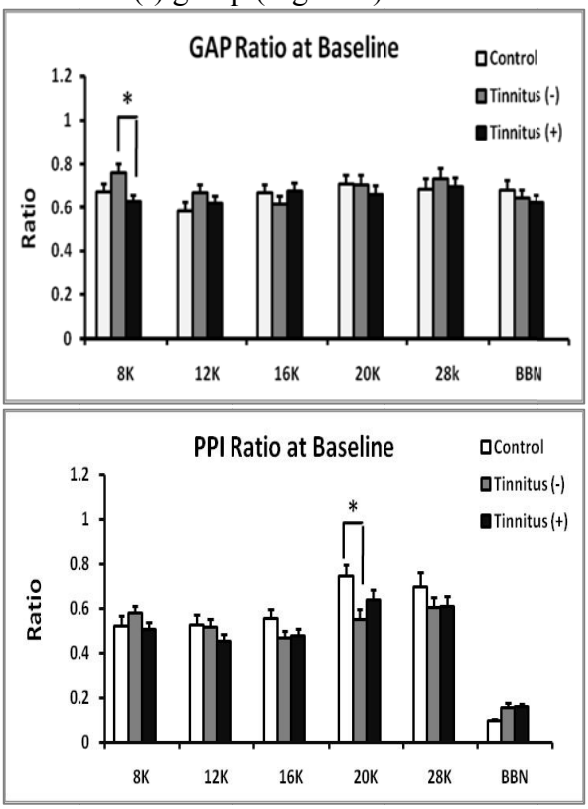

Figure 3. Baseline data showing group average ratio values of gap and PPI data at different frequency bands. At all frequencies, the gap/startle ratios and PPI/startle ratios of rats in the tinnitus (+) group (n=7) were not higher than that of the rats in the control group (n=4) and in the tinnitus (-) group (n=5).

At the time of MRI scanning, the group average of the gap/startle ratios of the rats in the tinnitus (+) group was higher than 0.8 at frequency bands of 8-10 kHz, 20-22 kHz, and 26-28 kHz. The group average gap/startle ratios of the rats in the control group and in the tinnitus (-) group remained below 0.8 at all frequency bands. Additionally, at all frequency bands, all groups exhibited inhibition in PPI paradigm tests (group average PPI/startle ratio ≤ 0.8). Compared to that of the rats in the control group, the group average gap/startle ratios of the rats in the tinnitus (+) group were higher at all frequency bands ($p<0.05$); additionally, the group average gap/startle ratios of the rats in the tinnitus (+) group were higher than that

of the rats in the tinnitus (-) groups at frequency bands of 8-10 kHz, 20-22 kHz and 26-28 kHz ($p<0.05$). There was no significant difference between the group average of gap/startle ratios of the rats in the control group and in the tinnitus (-) group at all frequency bands ($p>0.05$). These results indicated that rats in the tinnitus (+) group exhibited behavioral manifestations of tinnitus (Figure 4).

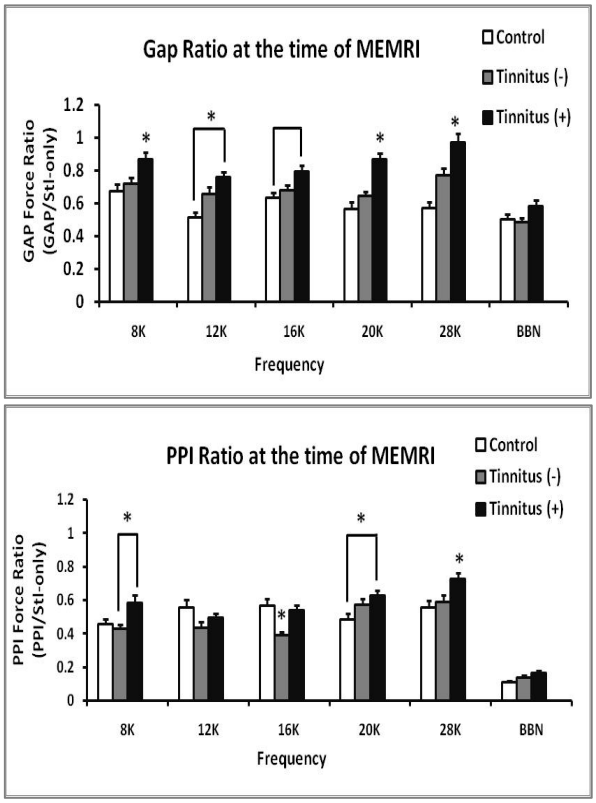

Figure 4. 35 days post-blast data showing group average gad/startle ratios (top panel) and PPI/startle ratios (bottom panel) at different frequency bands. At the time of scanning (35 days after the blast), group average gap/startle ratios of the rats in the tinnitus$^{(+)}$ group was more than 0.8 and higher than that of control group and/or tinnitus$^{(-)}$ group at most of frequency bands ($p<0.05$); additionally, the group average of PPI/startle ratios of all three groups remained below 0.8.

ABR data

(1) ABR threshold

Overall, 1 month after blast exposure, the thresholds of click and tone burst tests at all frequency bands were not higher than the baseline for both ears of all 3 groups (Figure 5). At the baseline, thresholds of tone burst at 8-10 kHz through 26-28 kHz were lower than 45 dB SPL for both ears of all groups, and there was no difference among groups and between two ears ($p>0.05$).

At the time of the scanning, for control group, the average tone burst threshold of left ears at 8kHz was lower than baseline ($p<0.05$); for tinnitus$^{(-)}$ group, one month after blast, the average tone burst threshold of right ears at 20 kHz and average click threshold of left ears were lower than the baseline ($p<0.05$);

and for tinnitus$^{(+)}$ group, one month after the blast, the average tone burst thresholds of left ears at 8 kHz, 12 kHz, of right ears at 8 kHz through 28 kHz were lower than baseline ($p<0.05$). Among groups, the thresholds of tone burst at 8 kHz and 20 kHz in the left ears of tinnitus$^{(-)}$ group were lower than that of control group ($p<0.05$).

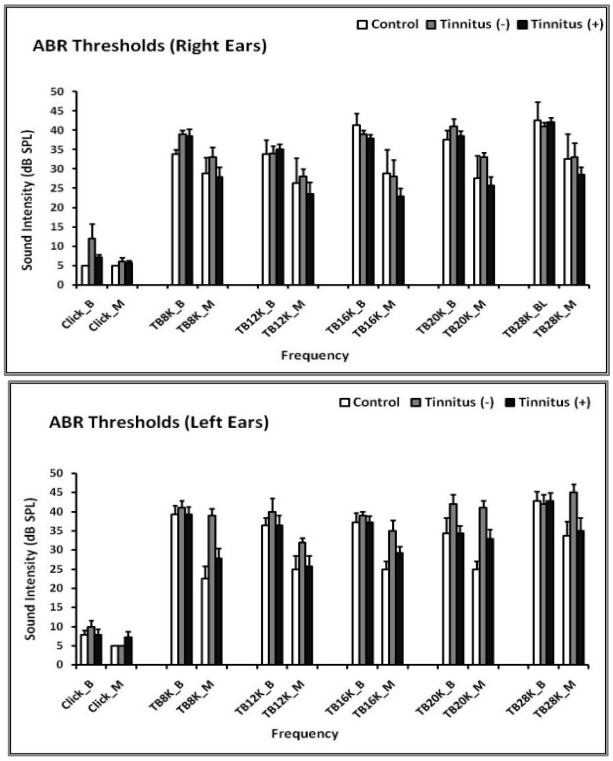

Figure 5. ABR thresholds before and after unilateral blast exposure to the left ear. Note that the ABR thresholds of both ears were under 45 dB SPL and that there was no significant difference in ABR thresholds between before and 35 days after blast exposure.

(2) Amplitude of P1N1 waveform

Before the blast exposure, the amplitudes of P1N1 waveforms of all three groups were not significantly different at frequency of 28 kHz during tone burst test of ABR ($p > 0.05$). At the time of the MRI scanning (35 days after the blast), the amplitudes of the P1N1 waveforms of the rats in the control group were significantly higher compared to that of the rats in the blasted groups with or without tinnitus ($p < 0.001$). Compared to the amplitudes of the P1N1 waveforms of the baseline data, the blasted rats with tinnitus showed decreased amplitudes in the higher sound level regions (>55 dB SPL), yet the blasted rats without tinnitus showed decreased amplitudes of the P1N1 waveform in sound level of 45-50 dB SPL (Figure 6).

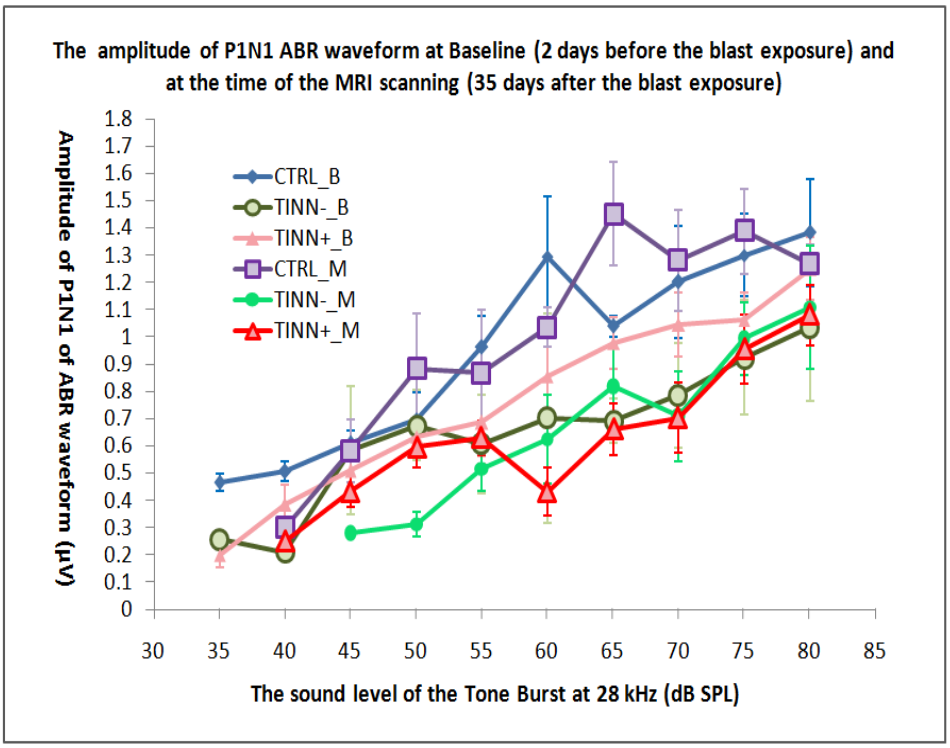

Figure 6. The ABR Amplitude of P1N1 waveforms of the rats in the control group, tinnitus (-) group and the tinnitus (-) group before and 35 days after the blast exposure. 35 days after the exposure, at the time of MRI scanning, the amplitudes of P1N1 waveforms decreased in the blasted groups; compared to that of the rats in the control group, these changes were statistically significant ($p<0.001$).

Elevated plus maze

Rats in the control group made average of 40% entries to the open arms and spent average of 100 seconds (33.6%) on the open arms. Tinnitus$^{(-)}$ group made average of 11% entries to the open arms and spent average of 20 seconds (6.6%) on the open arms. Tinnitus$^{(+)}$ group made 18% entries to the open arms and spent average of 13 seconds (4.2%) on the open arms. Among three groups, rats in control group spent more time on the open arms than both blasted groups did ($p<0.05$); rats in the control group also made significantly more entries to the open arms than rats in the tinnitus$^{(+)}$ group did ($p<0.05$).

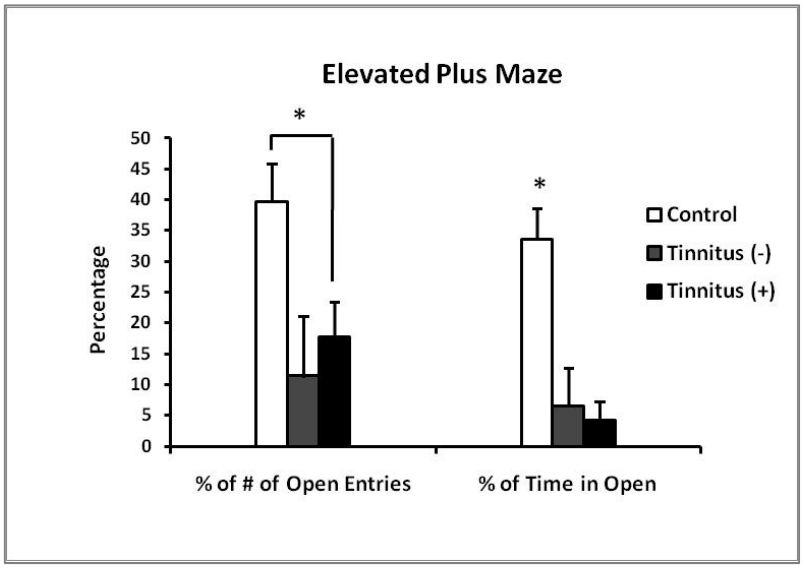

Figure 7. Numbers of entries (in percentage) made to the open arms and time spent on the open arms. Rats in the control group spent more than 30% of time on the open arms and made more than 40% of entries to the open arms, indicating normal level of anxiety. Rats in both blasted groups spent significantly less time in the open arms ($p<0.05$); and rats in tinnitus$^{(+)}$ group made significantly less entries to the open arms compared to the control group.

Morris water maze

(1) Spatial task acquisition: The first three blocks were spatial task acquisition trials, which consisted of four trials for each block. For block 1,2, and 3, the average time rats in control group swam before they escaped to the platform were 45.6, 27.5 and 20.0 seconds, respectively; the average escape latencies of all blasted rats were 46.7, 26.8 and 18.1 seconds, respectively; the average time for rats in tinnitus(-) group to reach the platform were 50.6, 21.7 and 13.1 seconds; and the average time for tinnitus(+) rats to escape the pool were 43.9, 30.4 and 21.7 seconds. The control rats swam an average distance of 11.8, 7.8 and 5.7 m at a speed of 26.7, 30.7 and 29.2 cm/sec, respectively for these three blocks. Rats in blasted group swam an average distance of 12.8m, 7.3 m, and 4.8 m at the speed of 27.2 cm/sec, 27.6 cm/sec, and 27.0 cm/sec, respectively; tinnitus(-) rats swam an average distance of 14.1 m, 5.9 m, and 3.5 m at the speed of 27.7 cm/sec, 28.0 cm/sec, and 26.0 cm/sec, respectively; and tinnitus$^{(-)}$ rats swam an average distance of 12.0 m, 8.3 m, and 5.7 m at the speed of 26.8 cm/sec, 27.4 cm/sec, and 27.8 cm/sec, respectively. Velocity of the control group was significantly slowing in the second block compared to the blasted animals, especially tinnitus$^{(+)}$ rats ($p<0.05$). Savings in the pathlength between the first block and second block has been used as an indicator for short-term or intermediate-term memory. The average saving of pathlength for control group, tinnitus(-) group, and tinnitus$^{(+)}$ group were 4.0 m, 8.2 m, and 3.7 m, respectively. The tinnitus$^{(-)}$ group saved marked more distance to reach the platform in the second block; however, the differences from control group and tinnitus$^{(+)}$ group were not statistically significant ($p=0.25$, *and* 0.10,

respectively).

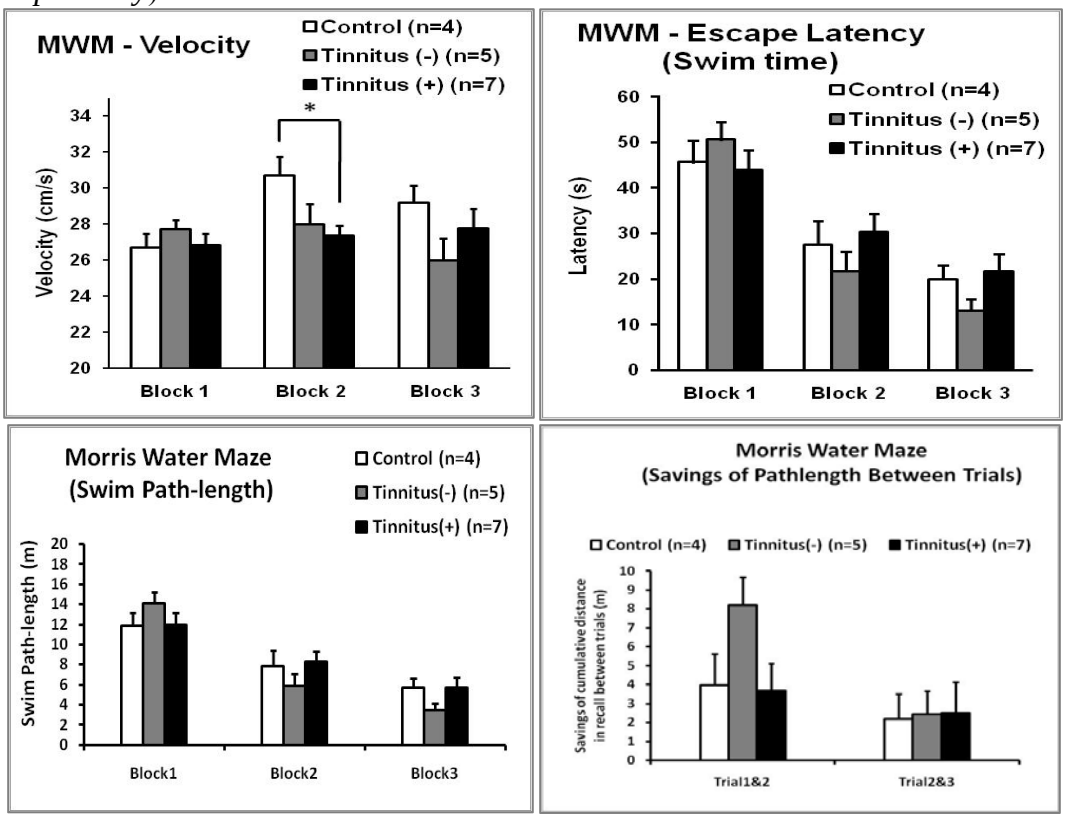

Figure 8. Morris Water Maze—Spatial Task Acquisition: Velocity, Escape Latency, Swim Path-length, and Savings of Path-length between trials. A. The average velocity of control rats was higher than tinnitus$^{(+)}$ rats ($p<0.05$). B and C. There was no difference in escape latency swim path-length among 3 groups ($p>0.05$). D. Compared to control and tinnitus$^{(+)}$ rats, tinnitus$^{(-)}$ rats tended to save pathlength between the first and the second block on average, although the difference was not statistically significant ($p=0.25$, 0.10; respectively).

Table 2. Morris water maze - Spatial task acquisition. Group average values of escape latency, velocity, pathlength of three blocks, and the savings in the pathlength between blocks.

		Escape Latency (second)			Velocity (cm/second)			Pathlength (PL) (m)			Savings in PL (m)	
Morris Water Spatial task acquisition		Block1 (T1)	Block2 (T2)	Block3 (T3)	Block1 (V1)	Block2 (V2)	Block3 (V3)	Block1 (D1)	Block2 (D2)	Block3 (D3)	D1-D2	D3-D2
Control (C)	Mean	45.6	27.5	20	26.7	**30.7**	29.2	11.8	7.8	5.7	4	2.1
	SD	5.2	5.8	3.5	0.8	1.1	1	1.3	1.6	1	1.6	1.4
All blasted (B)	Mean	46.7	26.8	18.1	27.2	**27.6**	27	12.8	7.3	4.8	5.5	2.5
	SD	3	2.9	2.5	0.4	0.6	0.8	0.8	0.8	0.7	1.1	1.1
	p (C vs. B)	*0.86*	*0.91*	*0.67*	*0.61*	***0.02***	*0.1*	*0.52*	*0.76*	*0.46*	*0.43*	*0.85*
Tinnitus$^{(-)}$ (T-)	Mean	50.6	21.7	13.1	27.7	28	26	14.1	5.9	3.5	8.2	2.4
	SD	3.8	4.2	2.4	0.5	1.1	1.2	1.1	1.2	0.7	1.5	1.2
	p (C vs. T-)	*1*	*1*	*0.63*	*1*	*0.16*	*0.23*	*0.71*	*0.94*	*0.41*	*0.25*	*1*
	p (T- vs. T+)	*0.82*	*0.47*	*0.22*	*1*	*1*	*0.76*	*0.59*	*0.48*	*0.24*	*0.1*	*1*
Tinnitus$^{(+)}$ (T+)	Mean	43.9	30.4	21.7	26.8	**27.4**	27.8	12	8.3	5.7	3.7	2.6
	SD	4.3	3.9	3.8	0.6	0.5	1.1	1.2	1	1	1.5	1.6
	p (C vs. T+)	*1*	*1*	*1*	*1*	***0.04***	*1*	*1*	*1*	*1*	*1*	*1*
	p (T+ vs. T-)	*0.82*	*0.47*	*0.22*	*1*	*1*	*0.76*	*0.59*	*0.48*	*0.24*	*0.1*	*1*

(2) Probe trial acquisition: Rats made average 8-9 entries to the zone where the platform used to be and spent average 20-23 sec in that zone. There was no difference among groups in terms of numbers of entry and time spent in that zone.

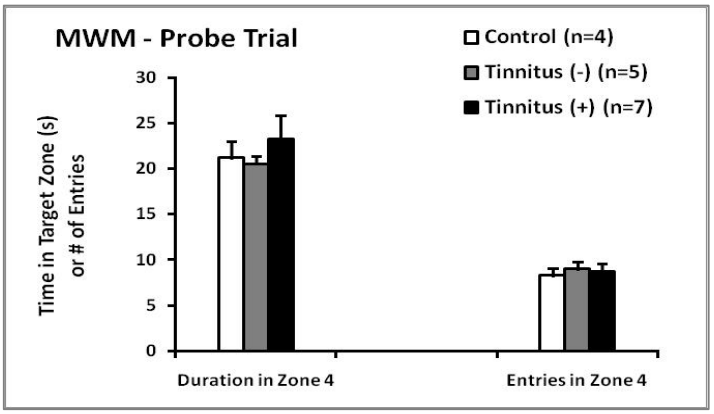

Figure 9. Morris Water Maze—Probe Trial Acquisition: Duration in platform zone and Entries in platform zone. The differences of average time spent in the zone where the platform used to be and average entries to that zone among groups were not significant ($p>0.05$).

MEMRI

From injection to scanning, time of manganese uptake for control group, tinnitus$^{(-)}$ group and tinnitus$^{(+)}$ were 650.8 ± 7.1, 639.2 ± 11.2 and 639.9 ± 6.5 min, respectively. There was no significant difference in time needed for manganese uptake among groups ($p>0.05$). Table 3 listed the normalized intensity ratio for the

regions of interest. Compared to tinnitus$^{(-)}$ rats, tinnitus$^{(+)}$ rats demonstrated higher manganese uptake in the right (contralateral to blast-exposed left ear) basolateral nuclei of the amygdala (*p=0.04*), but lower manganese uptake in the left (ipsilateral) ACC (p=0.02). In addition, we observed that blast exposure tended to have less manganese uptake in the contralateral ACC, although the differences were not statistically significant (p=0.15 for tinnitus$^{(-)}$ group and p=0.31 for tinnitus$^{(+)}$ group). A trend of higher manganese uptake in the contralateral hippocampus was also observed in tinnitus$^{(+)}$ group compared to the control group (*p=0.29*).

Table 3. Normalized intensity ratio of regions of interest. C: control group (n=4); B+A: blast group with high level of anxiety (n=7); T-: blasted rats without tinnitus (n=5); T+: blasted rats with tinnitus. Values with statistical significance are in bold letters.

Normalized Intensity Ratio		Amygdaloid Complex						ACC		Nucleus Accumbens				Hippocampus	
		AMG_S		AMG_D		AMG_C				Shell		Core			
		L	R	L	R	L	R	L	R	L	R	L	R	L	R
C	Mean	142	144	148	145	149	150	**108**	112	140	146	142	143	134	123
	SEV	4	3.8	4.6	3.1	2.4	3.7	**1.5**	1.1	5.7	4.8	6.2	5.9	6.6	7.8
T (-)	Mean	143	149	147	**143**	141	151	106	107	143	145	145	149	142	133
	SEV	5	5.3	5	**4.7**	5	4.4	1.2	2	5.5	5.1	6.6	6.5	9.9	7.3
	p (T- vs. C)	*1*	*1*	*1*	*1*	*0.37*	*1*	*0.51*	*0.15*	*1*	*1*	*1*	*1*	*1*	*0.97*
	p (T- vs. T+)	*1*	*1*	*1*	***0.04***	*1*	*1*	*0.49*	*1*	*1*	*0.68*	*1*	*1*	*1*	*1*
T (+)	Mean	144	150	151	**155**	146	152	**103**	108	146	152	149	154	134	138
	SEV	1.9	2.2	2.7	**2.4**	2.4	2.2	**1.1**	0.9	2.2	2.2	5.2	3.9	6.2	3.9
	p (T+ vs. C)	*1*	*0.97*	*1*	*0.18*	*1*	*1*	***0.02***	*0.31*	*1*	*0.85*	*1*	*0.48*	*1*	*0.29*
	p (T+ vs. T-)	*1*	*1*	*1*	***0.04***	*1*	*1*	*0.49*	*1*	*1*	*0.68*	*1*	*1*	*1*	*1*

Discussion:

Summary of major findings

Blast-induced tinnitus is unique in that plastic changes induced by tinnitus intertwine with those induced by TBI and traumatic emotional stress. To understand the dynamics of this interaction, we used a unilateral ingle blast exposure rat model and performed elevated plus maze, Morris water maze and MEMRI to investigate psychological and cognitive consequences of blast-induced tinnitus and its related injury. Our major findings are that blasted-induced tinnitus is strongly associated with blast-induced PTSD as revealed by EPM data, that the mechanisms underlying the psychological manifestation of blast-induced tinnitus may be attributable to hyperactivity in the basolateral amygdala, hypoactivity in the anterior cingulate cortex, and AMG-ACC uncoupling. The no significant effects of blast-induced tinnitus on neural activity in the hippocampus could be due to interaction of tinnitus and PTSD.

Involvement of the amygdala, ACC, and AMG/ACC coupling

Our findings in the elevated plus maze experiment indicated that regardless of manifestations of tinnitus, blasted rats exhibited high anxiety level compared to control rats ($p<0.05$). In addition, we found that tinnitus$^{(+)}$ rats had a lower manganese accumulation in the ipsilateral ACC ($p=0.02$) and a trend of higher manganese accumulation in the contralateral basolateral AMG ($p=0.18$) than control rats, and that tinnitus(-) rats had a lower manganese uptake in the contralateral basolateral AMG ($p=0.04$). These findings indicate that manifestation of blast-induced tinnitus along with blast-induced PTSD may be related to dysfunction of the ACC. The findings resonate with the current understanding of the neural mechanisms of tinnitus and PTSD based on available human functional imaging and animal studies.

Indeed, hyperactivity in the AMG has been associated with tinnitus caused by noise exposure and salicylates (Lockwood et al., 1998; Mahlke and Wallhausser-Franke, 2004; Zhang et al., 2003). Findings from PET-guided repetitive transcranial magnetic stimulation (rTMS) study also showed that the efficacy of the treatment correlated with the tinnitus-associated ACC activation, inferring that ACC may play an essential regulatory role in coping with tinnitus (Plewnia et al., 2007). In addition, clinical trials that targeted limbic structures showed promising results. For example, when a GABA agonist (amobarbital) was unilaterally injected into anterior choroidal artery which supplies amygdalohippocampal region, tinnitus on the contralateral side was suppressed (De Ridder et al., 2006). Evidence also showed reduced gray matter volume and decreased resting neuronal activity in the ACC of patients with PTSD from both civilian and combat veteran population (Nardo et al., 2010; Woodward et al., 2009). Increased activity in the amygdala was indicated and decreased functional connectivity between the ACC and amygdala as well as the contralateral medial frontal cortex was associated with PTSD (Fonzo et al., 2010).

Involvement of the NA and hippocampus

The NA has been implicated in the neural mechanism of tinnitus. For example, a recent fMRI study with voxel-based morphometry (VBM) has demonstrated hyperactivity in the NA when the sounds with their frequencies that matched with patient's tinnitus were played for patient. (Leaver et al., 2011). A trend that the tinnitus$^{(+)}$ group showed higher manganese uptake in contralateral NA than the control group was observed in the current study, but the difference was not statistically significant ($p=0.48$). One of possible explanations for this insignificant finding is that the plasticity of NA in the implications of tinnitus and/or PTSD is GABA receptors mediated; Manganese accumulation mainly reflects the NMDA receptors mediated synaptic plasticity. Another possible explanation is that NA may involve in plasticity of both tinnitus and PTSD, and that such plastic changes mitigate each other.

Studies have demonstrated that functions of NA, which was involved in addiction, behavioral error proofing, and coping, were dopaminergic and regulated by GABA receptors mediated processes (Doherty and Gratton, 2007; Munte et al.,

2007; Russo et al., 2010). In addition, cognitive behavioral therapy was efficacious treatment for tinnitus and PTSD; and coping as well as behavioral error proofing are important aspects of cognitive behavioral therapy (Hoare et al., 2011; Salloum and Overstreet, 2012). Further investigations of NA involvement in the mechanism of blast induced tinnitus and co-existing PTSD, employing investigating tools other than MEMRI will be a next logical step.

The hippocampus receives inputs indirectly from the auditory system and consists of entorhinal cortex, dentate gyrus (DG), *Cornu ammonis* (CA) 1 region, CA3 region and subiculus. Auditory inputs and hippocampal outputs are relayed into and from the hippocampus through the temporal association area, perirhinal cortex, as well as parahippocampal cortex. It has been established that the storage of memory depends on the hippocampus (Mizuno and Giese, 2005). The surprising result from the current study was that though there was a trend that manganese accumulation in the CA1 region of the hippocampus was higher in blasted animals than in control animals, this difference was not statistically significant ($p>0.05$). This contradicts with the findings in neuroimaging studies of patients with PTSD or tinnitus. However, previous animal studies with rat models have shown that acoustic trauma induced tinnitus did not impair spatial memory (Zheng et al., 2011). Results from Morris water maze in the current study showed that blast-induced tinnitus did not affect spatial memory, which was similar to what was observed with acoustic trauma induced tinnitus. Such results are possibly due to the fact that encoding episodic memory may not require the participation of spatial memory functions, though encoding spatial memory may not be feasible without episodic representation to form a spatial environment map (Eichenbaum, 1999). Moreover, current study is the first study to investigate the limbic structures in blast-induced tinnitus rat model, utilizing both behavioral tests and 7T MEMRI. The intensity of manganese accumulation in the hippocampus was extracted from the CA1 region only due to the technical limitations. It is possible that functions of CA1 region, which include intermediate-term memory, temporal pattern association, and temporal pattern completion, are not strongly associated with the mechanism of blast induced tinnitus.

Hypotheses underlying blast-induced tinnitus and related PTSD

Based on the data collected, it is tempting to propose the following hypotheses that could help delineate the limbic mechanisms of blast induced tinnitus and related PTSD (Fig. 6). Traumatic injuries inflicted by blast exposure include but not limited to perforation of the tympanic membrane, shear injury of the middle ear, axonal injury, and hypoperfusion to the brain (Bass et al., 2012; Darley and Kellman, 2010; Garth, 1994). The effects of blast on astrogliosis, neurogenesis, parenchyma inflammation, and cerebral metabolic disturbances further impact pathogenesis of blast induced tinnitus and related PTSD (Cernak and Noble-Haeusslein, 2010; Kovesdi et al., 2011; Kwon et al., 2011).

Following blast induced peripheral auditory deafferentation, hyperactive plastic changes are observed in DCN, IC, MGB, and AC to generate “phantom” perception (Zhang et al., 2011). Basolateral nucleus of the AMG receive auditory

inputs from AC, then projects to central nucleus of AMG, NA, and PFC (Sah et al., 2003). Hyperactive plastic changes in the AC may lead to hyperactivity in the AMG, NA and PFC. It has been indicated that ACC exerts regulatory effects on AMG (Bissiere et al., 2008; Hahn et al., 2011). Using MEMRI, we demonstrated that NMDA mediated hyperactivity in the contralateral basolateral AMG and hypoactivity of ipsilateral ACC are associated with blast induced tinnitus and co-existing anxiety. The fact that only rats with both high anxiety level and tinnitus exhibited these plastic changes implies that stress and anxiety may be the risk factors for chronic tinnitus yet AMG-ACC uncoupling is likely a tinnitus specific phenomenon. The roles of the hippocampus, vmPFC, and NA in the pathogenesis of blast induced tinnitus and co-existing PTSD remain yet to be elucidated. It is authors' humble opinion that further investigations into involvements of limbic structures in the blast induced tinnitus and co-existing PTSD call for an animal model that better represent blast induced PTSD and other method to probe GABA mediated neuronal functions in limbic structures.

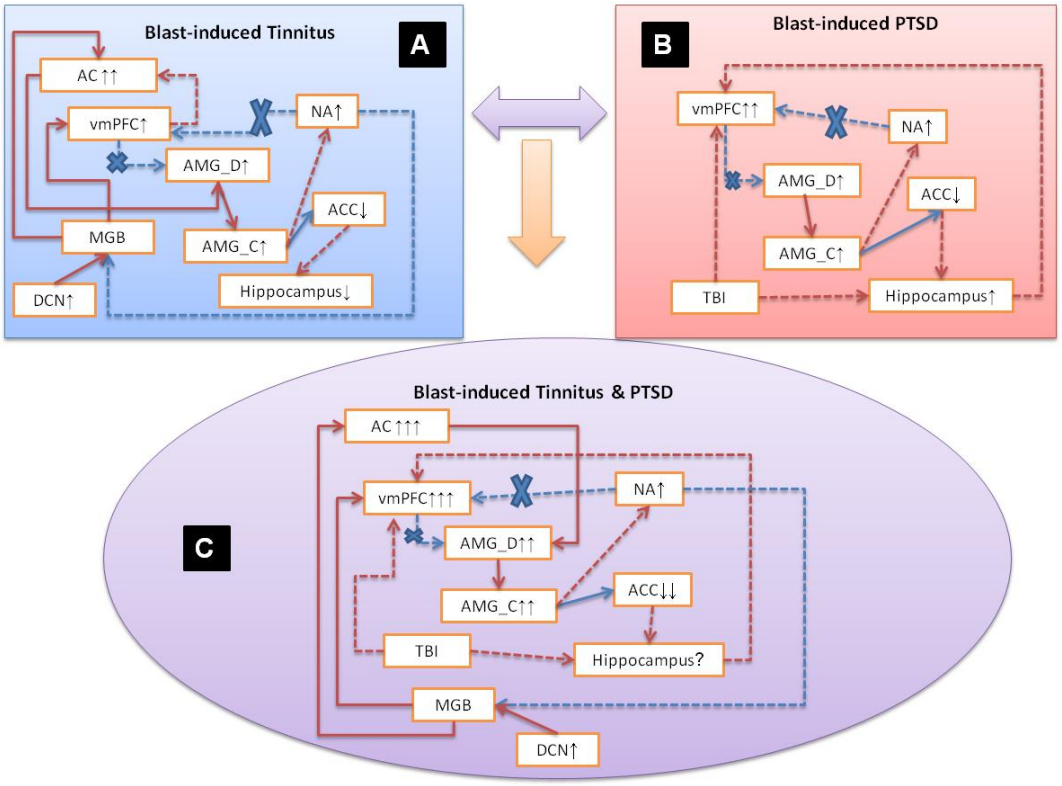

Figure 10. Hypotheses of blast-induced tinnitus and PTSD. A: Blast-induced auditory deafferentation that triggers hyperactivity in the DCN and AC, which in turn causes hyperactivity in the AMG and hypoactivity in ACC. The AMG exerts inhibitory effects on the NA. ACC may play a role in regulates AMG. B: TBI-induced plastic changes in limbic structures. Blast induced TBI affects astrogliosis, neurogenesis, metabolism and inflammation of limbic structures. These changes may be the neuronal substrate of PTSD. C. Blast-induced tinnitus and PTSD are associated with hyperactivity in the AMG

hypoactivity in the ACC. Red lines and arrows indicate stimulation; blue lines and arrows indicate inhibition; and dotted lines indicate mechanisms were not studied but possible links may exist.

Conclusion:

In conclusion, we demonstrated that (1) compared to rats in the control group, rats in the experimental groups, including both tinnitus(+) and tinnitus(-) groups, spent significant less time in the open arms on elevated plus maze, which indicates significant higher level of anxiety; that (2) compared to rats in the control group, rats in the tinnitus(+) groups exhibited NMDA mediated neuronal hyperactivity in the contralateral basolateral nucleus of AMG; that (3) compared to rats in the control group, rats in the tinnitus(+) groups exhibited neuronal hypoactivity in the ipsilateral ACC; and that (4) the spatial memory and learning was not affected with current level of blast shock wave exposure.

Results of the current study support the notions that plastic changes in the limbic structures, specifically AMG/ACC uncoupling, may have contributed to the psychological sequalea of blast induced tinnitus, TBI and PTSD.

Acknowledgements:

This work was supported by a grant from the Department of Defense (grant award #W81XWH-11-2-0031) to J.S. Zhang and a grant from AANA Foundation to J. Ouyang. The authors wish to thank Dr. Berkowitz for granting us access to 7T MRI scanner, to thank Dr. Bissig for training us of MEMRI techniques, to thank Dr. Perrine for giving us access to the elevated plus maze, to thank Dr. VandeVord for giving us access to the Morris water maze facility, and to thank Mr. Gulrez Mahmood for his assistance during MEMRI.

Author Disclosure Statement

No conflicting financial interests exist.

References:

Astur, R.S., St Germain, S.A., Tolin, D., Ford, J., Russell, D., Stevens, M., 2006. Hippocampus function predicts severity of post-traumatic stress disorder. Cyberpsychology & behavior : the impact of the Internet, multimedia and virtual reality on behavior and society. 9**,** 234-40.

ATA, 2012. Facts About the Military, Veterans and Tinnitus. Vol., ed.^eds. American Tinnitus Association.

Bass, C.R., Panzer, M.B., Rafaels, K.A., Wood, G., Shridharani, J., Capehart, B., 2012. Brain injuries from blast. Annals of biomedical engineering. 40**,** 185-202.

Bissiere, S., Plachta, N., Hoyer, D., McAllister, K.H., Olpe, H.R., Grace, A.A., Cryan, J.F., 2008. The rostral anterior cingulate cortex modulates the efficiency of amygdala-dependent fear learning. Biological psychiatry. 63**,** 821-31.

Bissig, D., Berkowitz, B.A., 2009. Manganese-enhanced MRI of layer-specific activity in the visual cortex from awake and free-moving rats. NeuroImage. 44**,** 627-35.

Bremner, J.D., Staib, L.H., Kaloupek, D., Southwick, S.M., Soufer, R., Charney, D.S., 1999. Neural correlates of exposure to traumatic pictures and sound in Vietnam combat veterans with and without posttraumatic stress disorder: a positron emission tomography study. Biological psychiatry. 45**,** 806-16.

Bremner, J.D., Vythilingam, M., Vermetten, E., Southwick, S.M., McGlashan, T., Staib, L.H., Soufer, R., Charney, D.S., 2003. Neural correlates of declarative memory for emotionally valenced words in women with posttraumatic stress disorder related to early childhood sexual abuse. Biological psychiatry. 53**,** 879-89.

Brozoski, T.J., Ciobanu, L., Bauer, C.A., 2007. Central neural activity in rats with tinnitus evaluated with manganese-enhanced magnetic resonance imaging (MEMRI). Hear.Res. 228**,** 168-179.

Cernak, I., Noble-Haeusslein, L.J., 2010. Traumatic brain injury: an overview of pathobiology with emphasis on military populations. Journal of cerebral blood flow and metabolism : official journal of the International Society of Cerebral Blood Flow and Metabolism. 30**,** 255-66.

Darley, D.S., Kellman, R.M., 2010. Otologic considerations of blast injury. Disaster medicine and public health preparedness. 4**,** 145-52.

De Ridder, D., Fransen, H., Francois, O., Sunaert, S., Kovacs, S., Van De Heyning, P., 2006. Amygdalohippocampal involvement in tinnitus and auditory memory. Acta oto-laryngologica. Supplementum. 50-3.

Doherty, M., Gratton, A., 2007. Differential involvement of ventral tegmental GABA(A) and GABA(B) receptors in the regulation of the nucleus accumbens dopamine response to stress. Brain research. 1150**,** 62-8.

Eichenbaum, H., 1999. The hippocampus and mechanisms of declarative memory. Behavioural brain research. 103**,** 123-33.

Fagelson, M.A., 2007. The association between tinnitus and posttraumatic stress disorder. Am.J.Audiol. 16**,** 107-117.

Fitch, R.H., Threlkeld, S.W., McClure, M.M., Peiffer, A.M., 2008. Use of a modified prepulse inhibition paradigm to assess complex auditory discrimination in rodents. Brain research bulletin. 76**,** 1-7.

Fonzo, G.A., Simmons, A.N., Thorp, S.R., Norman, S.B., Paulus, M.P., Stein, M.B., 2010. Exaggerated and disconnected insular-amygdalar blood oxygenation level-dependent response to threat-related emotional faces in women with intimate-partner violence posttraumatic stress disorder. Biological psychiatry. 68**,** 433-41.

Frick, K.M., Stillner, E.T., Berger-Sweeney, J., 2000. Mice are not little rats: species differences in a one-day water maze task. Neuroreport. 11**,** 3461-5.

Garth, R.J., 1994. Blast injury of the auditory system: a review of the mechanisms and pathology. The Journal of laryngology and otology. 108**,** 925-9.

Goble, T.J., Moller, A.R., Thompson, L.T., 2009. Acute high-intensity sound exposure alters responses of place cells in hippocampus. Hear Res. 253**,** 52-9.

Hahn, A., Stein, P., Windischberger, C., Weissenbacher, A., Spindelegger, C., Moser, E., Kasper, S., Lanzenberger, R., 2011. Reduced resting-state functional connectivity

between amygdala and orbitofrontal cortex in social anxiety disorder. NeuroImage. 56**,** 881-9.

Hinton, D.E., Chhean, D., Pich, V., Hofmann, S.G., Barlow, D.H., 2006. Tinnitus among Cambodian refugees: relationship to PTSD severity. Journal of traumatic stress. 19**,** 541-6.

Hoare, D.J., Kowalkowski, V.L., Kang, S., Hall, D.A., 2011. Systematic review and meta-analyses of randomized controlled trials examining tinnitus management. The Laryngoscope. 121**,** 1555-64.

Holt, A.G., Bissig, D., Mirza, N., Rajah, G., Berkowitz, B., 2010. Evidence of key tinnitus-related brain regions documented by a unique combination of manganese-enhanced MRI and acoustic startle reflex testing. PloS one. 5**,** e14260.

Karl, A., Schaefer, M., Malta, L.S., Dorfel, D., Rohleder, N., Werner, A., 2006. A meta-analysis of structural brain abnormalities in PTSD. Neuroscience and biobehavioral reviews. 30**,** 1004-31.

Kovesdi, E., Gyorgy, A.B., Kwon, S.K., Wingo, D.L., Kamnaksh, A., Long, J.B., Kasper, C.E., Agoston, D.V., 2011. The effect of enriched environment on the outcome of traumatic brain injury; a behavioral, proteomics, and histological study. Frontiers in neuroscience. 5**,** 42.

Kraemer, P.J., Brown, R.W., Baldwin, S.A., Scheff, S.W., 1996. Validation of a single-day Morris Water Maze procedure used to assess cognitive deficits associated with brain damage. Brain research bulletin. 39**,** 17-22.

Kwon, S.K., Kovesdi, E., Gyorgy, A.B., Wingo, D., Kamnaksh, A., Walker, J., Long, J.B., Agoston, D.V., 2011. Stress and traumatic brain injury: a behavioral, proteomics, and histological study. Frontiers in neurology. 2**,** 12.

Landgrebe, M., Langguth, B., Rosengarth, K., Braun, S., Koch, A., Kleinjung, T., May, A., De, R.D., Hajak, G., 2009. Structural brain changes in tinnitus: grey matter decrease in auditory and non-auditory brain areas. Neuroimage. 46**,** 213-218.

Leaver, A.M., Renier, L., Chevillet, M.A., Morgan, S., Kim, H.J., Rauschecker, J.P., 2011. Dysregulation of limbic and auditory networks in tinnitus. Neuron. 69**,** 33-43.

Leonardi, A.D., Bir, C.A., Ritzel, D.V., VandeVord, P.J., 2011. Intracranial pressure increases during exposure to a shock wave. Journal of neurotrauma. 28**,** 85-94.

Liberzon, I., Taylor, S.F., Amdur, R., Jung, T.D., Chamberlain, K.R., Minoshima, S., Koeppe, R.A., Fig, L.M., 1999. Brain activation in PTSD in response to trauma-related stimuli. Biological psychiatry. 45**,** 817-26.

Lockwood, A.H., Salvi, R.J., Coad, M.L., Towsley, M.L., Wack, D.S., Murphy, B.W., 1998. The functional neuroanatomy of tinnitus: evidence for limbic system links and neural plasticity. Neurology. 50**,** 114-120.

Mahlke, C., Wallhausser-Franke, E., 2004. Evidence for tinnitus-related plasticity in the auditory and limbic system, demonstrated by arg3.1 and c-fos immunocytochemistry. Hear.Res. 195**,** 17-34.

Mao, J.C., Pace, E., Pierozynski, P., Kou, Z., Shen, Y., VandeVord, P., Haacke, E.M., Zhang, X., Zhang, J., 2012. Blast-induced tinnitus and hearing loss in rats: behavioral and imaging assays. Journal of neurotrauma. 29**,** 430-44.

Mirz, F., Gjedde, A., Ishizu, K., Pedersen, C.B., 2000. Cortical networks subserving the perception of tinnitus--a PET study. Acta oto-laryngologica. Supplementum. 543**,** 241-3.

Mizuno, K., Giese, K.P., 2005. Hippocampus-dependent memory formation: do memory type-specific mechanisms exist? Journal of pharmacological sciences. 98**,** 191-7.

Morris, R., 1984. Developments of a water-maze procedure for studying spatial learning in the rat. Journal of neuroscience methods. 11**,** 47-60.

Munte, T.F., Heldmann, M., Hinrichs, H., Marco-Pallares, J., Kramer, U.M., Sturm, V., Heinze, H.J., 2007. Nucleus Accumbens is Involved in Human Action Monitoring: Evidence from Invasive Electrophysiological Recordings. Frontiers in human neuroscience. 1**,** 11.

Murphy, V.A., Wadhwani, K.C., Smith, Q.R., Rapoport, S.I., 1991. Saturable transport of manganese(II) across the rat blood-brain barrier. Journal of neurochemistry. 57**,** 948-54.

Nardo, D., Hogberg, G., Looi, J.C., Larsson, S., Hallstrom, T., Pagani, M., 2010. Gray matter density in limbic and paralimbic cortices is associated with trauma load and EMDR outcome in PTSD patients. Journal of psychiatric research. 44**,** 477-85.

Osuch, E.A., Willis, M.W., Bluhm, R., Ursano, R.J., Drevets, W.C., 2008. Neurophysiological responses to traumatic reminders in the acute aftermath of serious motor vehicle collisions using [15O]-H2O positron emission tomography. Biological psychiatry. 64**,** 327-35.

Perrine, S.A., Hoshaw, B.A., Unterwald, E.M., 2006. Delta opioid receptor ligands modulate anxiety-like behaviors in the rat. British journal of pharmacology. 147**,** 864-72.

Pissiota, A., Frans, O., Fernandez, M., von Knorring, L., Fischer, H., Fredrikson, M., 2002. Neurofunctional correlates of posttraumatic stress disorder: a PET symptom provocation study. European archives of psychiatry and clinical neuroscience. 252**,** 68-75.

Plewnia, C., Reimold, M., Najib, A., Reischl, G., Plontke, S.K., Gerloff, C., 2007. Moderate therapeutic efficacy of positron emission tomography-navigated repetitive transcranial magnetic stimulation for chronic tinnitus: a randomised, controlled pilot study. J.Neurol.Neurosurg.Psychiatry. 78**,** 152-156.

Rauch, S.L., Shin, L.M., Phelps, E.A., 2006. Neurocircuitry models of posttraumatic stress disorder and extinction: human neuroimaging research--past, present, and future. Biological psychiatry. 60**,** 376-82.

Roxo, M.R., Franceschini, P.R., Zubaran, C., Kleber, F.D., Sander, J.W., 2011. The limbic system conception and its historical evolution. TheScientificWorldJournal. 11**,** 2428-41.

Russo, S.J., Dietz, D.M., Dumitriu, D., Morrison, J.H., Malenka, R.C., Nestler, E.J., 2010. The addicted synapse: mechanisms of synaptic and structural plasticity in nucleus accumbens. Trends in neurosciences. 33**,** 267-76.

Sah, P., Faber, E.S., Lopez De Armentia, M., Power, J., 2003. The amygdaloid complex: anatomy and physiology. Physiological reviews. 83**,** 803-34.

Salloum, A., Overstreet, S., 2012. Grief and trauma intervention for children after disaster: exploring coping skills versus trauma narration. Behaviour research and therapy. 50**,** 169-79.

Schecklmann, M., Landgrebe, M., Poeppl, T.B., Kreuzer, P., Manner, P., Marienhagen, J., Wack, D.S., Kleinjung, T., Hajak, G., Langguth, B., 2011. Neural correlates of tinnitus duration and Distress: A positron emission tomography study. Hum Brain Mapp.

Shulman, A., Strashun, A.M., Afriyie, M., Aronson, F., Abel, W., Goldstein, B., 1995. SPECT Imaging of Brain and Tinnitus-Neurotologic/Neurologic Implications. Int.Tinnitus.J. 1**,** 13-29.

Silva, A.C., Lee, J.H., Aoki, I., Koretsky, A.P., 2004. Manganese-enhanced magnetic resonance imaging (MEMRI): methodological and practical considerations. NMR in biomedicine. 17**,** 532-43.

Silva, A.C., Bock, N.A., 2008. Manganese-enhanced MRI: an exceptional tool in translational neuroimaging. Schizophrenia bulletin. 34**,** 595-604.

Turner, J.G., Brozoski, T.J., Bauer, C.A., Parrish, J.L., Myers, K., Hughes, L.F., Caspary, D.M., 2006. Gap detection deficits in rats with tinnitus: a potential novel screening tool. Behavioral neuroscience. 120**,** 188-95.

Van de Moortele, P.F., Auerbach, E.J., Olman, C., Yacoub, E., Ugurbil, K., Moeller, S., 2009. T1 weighted brain images at 7 Tesla unbiased for Proton Density, T2* contrast and RF coil receive B1 sensitivity with simultaneous vessel visualization. NeuroImage. 46**,** 432-46.

Vanneste, S., Van de Heyning, P., De Ridder, D., 2011. Contralateral parahippocampal gamma-band activity determines noise-like tinnitus laterality: a region of interest analysis. Neuroscience. 199**,** 481-90.

Werner, N.S., Meindl, T., Engel, R.R., Rosner, R., Riedel, M., Reiser, M., Fast, K., 2009. Hippocampal function during associative learning in patients with posttraumatic stress disorder. Journal of psychiatric research. 43**,** 309-18.

Woodward, S.H., Kaloupek, D.G., Grande, L.J., Stegman, W.K., Kutter, C.J., Leskin, L., Prestel, R., Schaer, M., Reiss, A.L., Eliez, S., 2009. Hippocampal volume and declarative memory function in combat-related PTSD. Journal of the International Neuropsychological Society : JINS. 15**,** 830-9.

Zhang, J., Zhang, Y., Zhang, X., 2011. Auditory cortex electrical stimulation suppresses tinnitus in rats. J Assoc Res Otolaryngol. 12**,** 185-201.

Zhang, J.S., Kaltenbach, J.A., Wang, J., Kim, S.A., 2003. Fos-like immunoreactivity in auditory and nonauditory brain structures of hamsters previously exposed to intense sound. Exp Brain Res 153**,** 655-660.

Zheng, Y., Hamilton, E., Begum, S., Smith, P.F., Darlington, C.L., 2011. The effects of acoustic trauma that can cause tinnitus on spatial performance in rats. Neuroscience. 186**,** 48-56.

Blast-Induced Tinnitus and its related TBI in auditory structures: A MEMRI Study

Laura Lepczyk[(a)] , Jessica Ouyang[(a)], Edward Pace[(a)], Jinsheng Zhang[(a)(b)]

(a) Department of Otolaryngology and Head and Neck surgery, Wayne State University School of Medicine
(b) Department of Communication Sciences & Disorders, Wayne State University College of Liberal Arts and Sciences

Abstract

Blast-induced traumatic brain injury (TBI) is associated with tinnitus in military and civilian populations. Accumulative evidence suggests that noise-induced tinnitus can develop as a result of peripheral insult to the auditory system that causes hyperactivity and plastic changes at the central level. The underlying mechanisms of blast-induced tinnitus and its related TBI are an underexplored but crucial area of research for tinnitus treatment and prevention. In this study, we used manganese-enhanced MRI (MEMRI) to study neural activity in auditory structures of rats that were behaviorally tested for tinnitus following blast exposure (10ms, 14 psi). We evaluated hearing thresholds using ABR, tested for tinnitus using the gap detection acoustic startle reflex paradigm, and performed MEMRI scanning to determine neural activity changes in auditory structures. Five weeks after one single blast, MEMRI scanning was performed. At the time of scanning, all the animals had normal hearing thresholds and 7 of the 12 blasted animals displayed robust behavioral evidence of tinnitus (tinnitus$^{(+)}$). The remaining 5 blasted animals were termed tinnitus$^{(-)}$. MEMRI data showed tinnitus and/or blast-related differences in manganese accumulation in the dorsal cochlear nucleus (DCN), ventral cochlear nucleus (VCN), central nucleus of the inferior colliculus (CIC), external cortex of the inferior colliculus (ECIC), dorsal cortex of the inferior colliculus (DCIC), and medial geniculate body (MGB). The data suggest that tinnitus may be caused by acoustic overexposure/trauma to the auditory pathways as well as a blast-induced direct impact to the brain.

Introduction

Tinnitus is a phantom auditory perception that occurs in the absence of external stimulation (Møller, 2006). If chronic, it can severely affect a person's daily life and produce anxiety, annoyance, irritability, disturbed sleep patterns, and depression (Dobie et al., 1993; Hoffman and Reed, 2004; Langguth et al., 2011; McKenna, 2000; Tyler, 1993). Tinnitus can be caused by various conditions however noise trauma is most commonly reported. Due to the increased use of explosive devices and weapons of excessive noise on the battlefield, the incidence of tinnitus is becoming a major health problem among war veterans (Henry et al., 2009; Taber et al., 2006). Blast waves can affect structures with air-fluid interfaces and therefore, the middle ear is susceptible to damage (Gondusky and Reiter, 2005; Walsh et al., 1995). A recent study evaluating soldiers in Iraq and Afghanistan found that 49% of combat personnel exposed to blast trauma developed tinnitus (Henderson, 2011). Often co-occurring with traumatic brain injury (TBI) and posttraumatic stress disorder (PTSD), tinnitus is currently the number one service-connected disability affecting military personnel, resulting in over one billion dollars in annual disability compensation (Fausti et al., 2009; Lew et al., 2007; Rauschecker et al., 2010). The underlying mechanisms of tinnitus are largely unknown which has contributed to the lack of reliable treatments. Given the health and economic impact surrounding tinnitus in veterans, it is increasingly important to investigate its pathophysiology so effective treatments can be developed.

Evidence suggests that tinnitus arises from centralized plastic changes initiated by damage to peripheral structures, such as hair cells or the auditory nerve (Eggermont and Roberts, 2004; Kaltenbach, 2011; Roberts et al., 2010). Such peripheral injury can result in deafferentation and lead to compensatory enhancement of neural activity in the central auditory system (Kaltenbach, 2011; Roberts et al., 2010). Following intense noise exposure, hyperactivity, bursting events, hypersynchrony, and tonotopic plasticity have been identified along the auditory axis including in the dorsal cochlear nucleus (DCN), inferior colliculus (IC) and auditory cortex (AC) (Bauer et al., 2008; Brozoski et al., 2002; Dong et al., 2010a; Eggermont, 2007; Eggermont and Komiya, 2000; Eggermont and Roberts, 2004; Finlayson and Kaltenbach, 2009; Gourevitch and Eggermont, 2010; Kaltenbach,

2011; Lanting et al., 2009; Ma et al., 2006; Muhlnickel et al., 1998; Mulders and Robertson, 2011; Norena and Eggermont, 2003; Roberts et al., 2010; Seki and Eggermont, 2002; Shore et al., 2008; Yang et al., 2011; Zhang et al., 2006), and recently in the ventral cochlear nucleus (VCN) (Kraus et al., 2011; Pienkowski and Eggermont, 2010). A better understanding of the brain regions and mechanisms involved in TBI-associated tinnitus would aid in the development of effective diagnostic and management strategies.

Imaging studies have produced significant advances in uncovering the location, degree, and magnitude of tinnitus-related neural activity. Tinnitus-related changes in central auditory structures have been demonstrated using positron-emission tomography (PET) (Arnold et al., 1996; Cacace et al., 1999; Giraud et al., 1999; Langguth et al., 2006; Lockwood et al., 1998; Mirz et al., 2000; Wang et al., 2001), functional magnetic resonance imaging (fMRI) (Lanting et al., 2008; Melcher et al., 2000; Smits et al., 2007), DTI (Crippa et al., 2010; Mao et al., 2011), voxel based morphometry (VBM) (Landgrebe et al., 2009; Muhlau et al., 2006), and manganese (Mn^{2+})-enhanced MRI (MEMRI) (Brozoski et al., 2007; Holt et al., 2010). MEMRI is a relatively new structural and functional imaging technique that has been used to detect changes in central neural activity. MEMRI uses Mn^{2+} as an activity-dependent paramagnetic contrast agent that accumulates in active neurons through voltage-gated calcium channels (Pautler, 2006; Silva et al., 2004). Since tinnitus is associated with abnormal neuronal activity in the central auditory system, MEMRI provides a feasible and valuable way to uncover the brain regions involved in tinnitus perception. In an ex-vivo MEMRI study, noise exposed (16 kHz, 115 dB SPL, 1 hr) rats with behavioral evidence of tinnitus showed increased activity in the ipsilateral paraflocculus, the ipsilateral posteroventral cochlear nucleus, and the contralateral IC and decreased activity in the contralateral AC, MGB, and AMG (Brozoski et al., 2007). An in-vivo MEMRI study found that noise exposed rats (10 kHz, 118 dB SPL, 4 hrs) with behavioral evidence of tinnitus and hearing loss had increased activity in the dorsal cortex of the IC (DCIC) (Holt et al., 2010). While imaging studies have shed light on the structures that may be involved in tinnitus pathology, there is a need to further explore the neural correlates of TBI-associated tinnitus. Our study is the first to use MEMRI to explore the effects of blast-induced tinnitus and its associated TBI on central auditory structures.

In this study, we characterized blast-induced tinnitus using the gap detection acoustic startle reflex paradigm and evaluated hearing thresholds using auditory brainstem responses (ABR). 35 days following unilateral blast exposure (10ms, 14 psi), we performed MEMRI scanning to study the neuroplastic effects of blast-induced tinnitus and its associated TBI on central auditory structures. We compared our results with published MEMRI studies looking at noise-induced tinnitus and with other imaging and electrophysiological studies. We hypothesized that animals with behavioral evidence of tinnitus would display increased activity in specific auditory structures compared to control animals. Overall, our results demonstrated that animals with tinnitus showed an increase in activity in the brainstem structures and both an increase and a decrease of activity in midbrain structures. Our data suggests that hypoactivity may also contribute to the etiology of tinnitus. The information gained will be helpful in implicating changes in central auditory structures to be responsible for the tinnitus percept.

Part 2: Materials and Methods

2.1 Animal subjects

In our study, we used 24 male Sprague Dawley rats (60-70 days old) from Harlan Laboratories (Indianapolis, IN). Four animals were screened out for demonstrating unstable baseline behavior data. We divided the remaining 20 animals into a control group (n=6) and an experimental group (n=14). One animal died following blast exposure, 1 animal in the control group developed behavioral evidence of tinnitus, and 2 animals failed to uptake Mn^{2+} and therefore they were excluded from the study. Of the remaining 16 animals, 4 were in the control group and 12 were in experimental group. All procedures were approved by the Institutional Animal Care and Use Committee at Wayne State University and were in accordance with the regulations of the Federal Animal Welfare Act.

2.2 Baseline GAP and PPI

As described previously (Zhang et al., 2011), gap-detection (GAP) and PPI were used to evaluate tinnitus and central hearing detection, respectively. Behavior testing was conducted inside a sound-attenuation booth with Kinder Scientific's acoustic startle reflex hardware and software (Kinder Scientific, Poway, CA). Each rat was placed in a custom-made animal holder that was secured to a platform inside an SM100 Startle Monitor cabinet. The bottom of each platform was connected to a piezoelectric transducer, which measured the startle force (Newtons). Startle Monitor cabinets were equipped with one ceiling speaker to present background sounds and prepulse stimuli, and a second ceiling speaker to present startle stimuli. Startle force and acoustic stimuli were calibrated using a Newton Impulse Calibrator (Kinder Scientific, Poway, CA) and a microphone (Model 4016, ACO Pacific).

In the GAP procedure, rats were presented with constant, 60 dB SPL 2 kHz bandpass background noise centered at 6-8, 10-12, 14-16, 18-20, 26-28 kHz, and broadband noise (BBN). During the background noise, rats were presented with a 50 ms, 115 dB startle stimulus alone (startle only) or the startle stimulus preceded by a silent gap embedded within the background noise (GAP condition). Silent gaps were 40 ms in duration with a lead interval of 90 ms to the startle stimulus. For each frequency band and BBN, there were a total of 16 trials, eight startle only and eight GAP conditions.

PPI parameters were the same as for the GAP procedure, except that no background noise was used. During PPI testing, rats were presented with either the startle stimulus alone (startle only) or the startle stimulus preceded by a 60 dB SPL, 50 ms narrow-band noise (PPI condition). Eight trials for both the startle only and PPI conditions were administered for each prepulse frequency and BBN prepulses.

When the rat is able to hear the GAP or pre-pulse, the startle force it exerts on the platform during the GAP or PPI condition will be significantly lower than the force exerted during the startle only trials ($p<0.05$). If the startle reflex during the GAP and PPI condition is not inhibited, the test is considered positive. A negative PPI test together with a positive gap test signifies behavioral evidence of tinnitus in the rat (Fitch et al., 2008; Turner et al., 2006). At the time of MEMRI scanning, rats that consistently exhibited a negative PPI test, positive GAP test, and significantly increased GAP ratio compared with pre-blast level ($p<0.05$), were diagnosed as tinnitus$^{(+)}$.

GAP and PPI were run sequentially with a 2 minute acclimatization period before each test. Two trials of the startle stimulus without background noise were presented after the acclimatization period to trigger and dispose of any initial, exaggerated startle reflexes. Startle-only and GAP or PPI conditions were arranged pseudorandomly to prevent order effects. The running time for both tests was approximately 1 hour and 40 minutes. GAP and PPI testing was conducted 2-3 times per week for 1 month in order to get baseline data. Only animals that exhibited stable startle behaviors were selected to proceed with further experimentation and blast exposure.

2.3 Baseline Auditory brainstem responses (ABRs)

ABR procedures to obtain hearing thresholds were conducted inside a sound-attenuation booth. Anesthesia was induced through inhalation of mixed air (0.6 L/min) and isoflurane (5%, v/v), and was reduced to 0.4 L/min and 2–3%, v/v for maintenance during testing. Each rat was arranged in prone position with its head fixed to a stereotaxic apparatus. Body temperature was regulated with a warming blanket connected to a homoeothermic control unit. ABR responses were elicited by click and tone-burst stimuli (10 ms duration, 0.1 ms rise/fall) delivered from a TDT (Tucker Davis Technologies, Alachua, FL) EC1 model electrostatic speaker using a tube that was inserted into the external auditory canal. Stimuli were generated by an RX6 multifunction processor and calibrated before experimentation with a microphone. Stimuli were presented from 100dB peak equivalent SPL down to 5 dB in 5 dB decrements.

Evoked potentials were recorded using subdermal platinum-coated tungsten needle electrodes. The positive recording electrode was placed at the vertex, the reference electrode was placed below the ear pinna ipsilateral to the speaker, and the ground electrode was placed below the contralateral ear pinna. Data were collected from both ears. ABR responses were amplified, bandpass-filtered at 300-3000 Hz, and notch-filtered at 60 Hz. Responses to click and tone-burst stimuli were averaged 300-400 times, respectively. The sampling rate for data

acquisition was 50 kHz. Experimental operation was controlled by SigGenRP® and BioSigRP® TDT software installed in an IBM terminal connected to a System 3 TDT workstation. For analysis, ABR threshold was considered the lowest intensity at which a distinct portion of the biological waveform remained.

2.4 Intense blast exposure to induce tinnitus and TBI

After stable baseline gap-detection and PPI data were collected, rats were subjected to a single blast exposure using a custom-designed shock tube located at the Wayne State University Bioengineering Center (Leonardi et al., 2011). Before the blast exposure, each rat was anesthetized using a mixture of ketamine and xylazine (100 mg/kg + 10 mg/kg IP). The right ear canal was then occluded with an earplug followed by application of mineral oil to seal additional open spaces. The rat was placed on supportive netting via a metal surround and secured on a pole with a locking device 44 inches up from the open end of the tube. The rat was placed in prone position with its head facing the oncoming shockwave. The 10 msec blast shock wave generated was similar to that of a free-field blast wave and was estimated to encompass a wide range of frequencies. The positive phase duration was 2 msec. After the exposure, each animal was carefully monitored until it regained consciousness.

Rats were unilaterally exposed to retain at least one viable ear for detecting background noise, gaps, prepulses and startle stimuli in the gap-detection and PPI tests. Rats in the control group underwent sham blast shock wave exposure. They were anesthetized and placed in the shock tube but no shock wave was generated or delivered.

2.5 Gap-detection, PPI, and ABR testing – After tone exposure

Following tone exposure, behavior testing and ABRs were conducted using the same parameters as before exposure. Rats were tested behaviorally within 4 hours after exposure and continued to be tested two times per week. ABR testing was administered 1 or 2 days before MEMRI scanning.

2.6 MEMRI

5 weeks after blast exposure, animals underwent MRI scanning with a 7T Siemens ClinScan MRI scanner (Siemens Medical Solutions USA, Inc., Malvern, PA). We choose to perform MEMRI scanning 5 weeks post-blast based on research indicating that 2–4 weeks after blast-induced injury the brain has begun its recovery process which includes improvements in structural integrity and other neuroplastic changes (Mao et al., 2011). Awake animals were injected intraperitoneally with MnCl2 (67 mg MnCl2·4H2O/kg, 0.1 M) and placed in a sound-proof chamber for 8 hours before scanning. Accumulation of manganese for 8 hours is adequate for functional imaging, and using anesthesia during scanning does not affect Mn^{2+} uptake (Bissig and Berkowitz, 2009; Lee et al., 2005). Prior to image acquisition, each rat was anesthetized in an induction chamber with a 4% isoflurane/air mixture. Anesthesia is maintained with a 2% isoflurane/air mixture using a commercially made MRI compatible nose cone. A whole body transmit-only coil and a 4-element Bruker mouse-brain receive-only surface coil placed dorsal to the animals head were used for scanning. Individual images are acquired with 2 sets of MPRAGE (TR: 2500 msec, TB: 3 msec) and PDGE (TR: 1000 msec, TE: 3 msec) sequences with flip angle of 3 and total scanning time of 23 min. The field of view is a 25X25 section of space (192 pixel X 192 pixel or 130 micron X 130 micron) and the thickness of each slice is 0.26 mm. At the end of the scan, the animal is monitored until awake on a heating pad.

The only drawback of using Mn^{2+} as a contrasting agent is its cellular toxicity. Chronic overexposure to Mn^{2+} can cause neurological symptoms similar to Parkinson's disease (Pan et al., 2011). To minimize the toxic effects, we used the lowest dosage possible while preserving detectability by MRI and carefully planned the timing of MEMRI injection to 8 hours before scanning.

2.7 GAP/PPI and ABR Data Analysis

Consistent with previous reports, ratio values were calculated and averaged by dividing gap-detection responses by their corresponding mean startle only responses at each frequency band (Turner et al., 2006; Zhang et al., 2011). Mean force values more than 2 standard deviations above the mean were considered anomalies and were deleted. Significantly smaller responses within the gap condition compared to startle only reflect that the rats could clearly hear the silent gap. If tinnitus developed, the silent gap would be filled by tinnitus and the animal could not hear the silent gap. Similarly, rats were considered positive for hearing impairment when the values of

post-blast PPI ratios were greater than pre-blast ratios. Positive hearing loss data were also considered when post-blast ABR thresholds were higher than pre-blast thresholds. To evaluate the effects of blast exposure on tinnitus and hearing loss, the gap-detection ratio values were compared before exposure, immediately after exposure, and 4-5 weeks after exposure. ANOVA with the Bonferroni post hoc tests for multiple comparisons were performed to examine the effects of blast exposure on tinnitus and hearing. Significant differences were judged by $p<0.05$.

2.8 MEMRI Imaging Analysis

For MRI imaging, we used Mn^{2+} as a contrasting agent to detect the changes in activity among central auditory system structures. For each scanning, 2 MPRAGE and PDGE image sets were created with Siemens software. Images were processed with R scripts developed by Mr. D. Bissig (v2.12.1, http://www.R-project.org). The addition of two sets of MPRAGE images was divided by the addition of PDGE images to mitigate the intensity field bias. The corrected images were used for further analysis. Two separate reviewers performed a double blind analysis of the 3D MRI images and used MRIcro to measure the degree of Mn^{2+} uptake in each region-of-interest (ROI). We examined the following auditory structures which are implicated to be related to the etiology of tinnitus; DCN, VCN, central nucleus of the IC (CIC), external cortex of the IC (ECIC), DCIC, AC, and medial geniculate body (MGB). The locations of the structures were identified based on a rat brain atlas (Paxinos and Watston, 1998). The ROI was manually drawn in the DCN and VCN and spanned 2 and 3 consecutive coronal slices, respectively. Spherical ROIs were used to characterize the IC structures, AC, and MGB. The ROIs are placed at the rostrocaudal center of each anatomical region and drawn to occupy the entire coronal profile of each region, excluding a buffer (≥1 voxel wide) at the borders with neighboring brain regions and tissues. ROI placement is confirmed using the sagittal and transverse views. For each structure, we compared the ROI divided by the ROI of the adjacent muscle in order to compare the accumulation of Mn^{2+}. Muscle normalization can compensate for potential inter-individual differences in peripheral $MnCl^2$ uptake (e.g. liver acquisition). Examples of ROIs can be seen in Figure 1.

One-way ANOVA, with *post-hoc* Bonferroni tests to adjust alpha values, were performed to examine the effects of blast exposure on activity in central auditory structures.

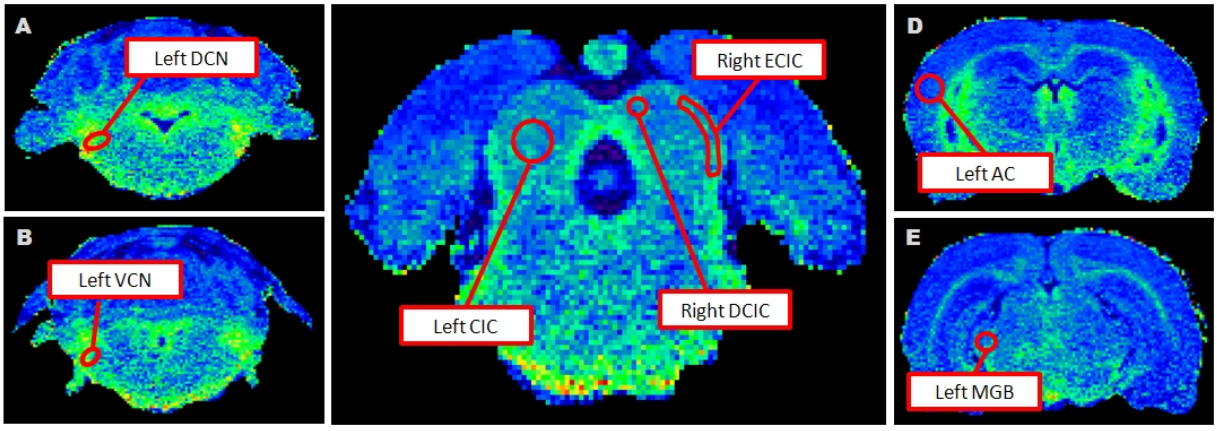

FIG. 1. Representative regions of interest (ROIs) for the (A) DCN, (B) VCN, (C) IC, (D) AC, and (E) MGB. Dorsal cochlear nucleus; DCN, ventral cochlear nucleus; VCN, central nucleus of the inferior colliculus (IC); CIC, external cortex of the IC; ECIC, dorsal cortex of the IC; DCIC, auditory cortex; AC, and medial geniculate body; MGB.

Part 3: RESULTS

3.1 GAP and PPI testing

The composite baseline group average was calculated using 3 out of the 4 behavior tests given right before the blast exposure. We choose the 3 out of 4 most consistent tests and screened out 4 animals that showed unstable

behavior data. The exclusion criteria were as follows: (1) startle forces were less than 1 N; (2) in the PPI test, the animal did not show inhibition in more than three frequencies, which indicate that the animal was nervous; and (3) in GAP procedure, no more than 5% (8 out of 152) trials yielded anomalies. At baseline, all animals showed inhibition at all frequencies in both GAP detection and PPI tests (GAP or PPI vs. Stl, $p<0.05$); moreover, all group average gap or PPI ratios were below 0.8, which further affirmed diagnosis of normal hearing for all groups. Among three groups, at 8K, the gap ratio of tinnitus$^{(-)}$ group was higher than that of tinnitus positive group ($p<0.05$); at 20 kHz, the PPI ratio of control group was higher than tinnitus positive group ($p<0.05$).

Based on previous studies using identically blast shock wave parameters, blast exposure at 14 psi (194 dB SPL) induced early onset of tinnitus and central hearing impairment at a broad frequency range (Mao et al., 2011). At 35 days post-exposure, the blasted animals were reorganized into tinnitus$^{(+)}$ (n=7) or tinnitus$^{(-)}$ (n=5) groups. To compose the group analysis, 3 out of the 4 tests right before the MEMRI scanning were selected using the same selection criteria as above. At all frequencies, all groups exhibited inhibition in PPI tests (PPI vs. Stl, $p<0.05$) and all group average PPI ratios were below 0.8, which indicates behavioral evidence of hearing. In gap-detection tests, the tinnitus$^{(-)}$ and control group showed inhibition at all frequencies (gap vs. Stl, $p<0.05$) and their group average gap ratios were below 0.8. However, in the tinnitus$^{(+)}$ group, the group average gap ratios were above 0.8 at 8, 16, 20, and 28 kHz. In addition, the tinnitus$^{(+)}$ group failed to exhibit inhibition at 28K (gap vs. Stl, $p>0.05$). Among the three groups, the tinnitus$^{(+)}$ gap ratios were higher at 8 through 28 kHz than that of control group and at 20 kHz and the tinnitus$^{(-)}$ group at 28 kHz ($p<0.05$). The tinnitus$^{(+)}$ PPI ratios were higher than that of the control group at 20 and 28 kHz and the tinnitus$^{(-)}$ group at 28 kHz ($p<0.05$).

3.2 ABR testing

Baseline ABR data revealed that all animals had normal hearing as evidenced by click and tone-burst ABR. At the baseline, thresholds of tone burst at 8 through 28 kHz were lower than 45 dB SPL for both ears in all groups, and there was no difference among groups and between the two ears ($p>0.05$). 5 weeks after exposure and immediately before MEMRI, hearing thresholds recovered to baseline levels in all experimental animals (n=12). For control group, the average tone burst threshold of the left ears at 8 kHz was lower than baseline ($p<0.05$). For the tinnitus$^{(-)}$ group, the average tone burst threshold of right ears at 20 kHz and average click threshold of left ears were lower than baseline ($p<0.05$). For the tinnitus$^{(+)}$ group, the average tone burst thresholds of left ears at 8 and 12 kHz of the right ears and at 8 through 28 kHz were lower than baseline ($p<0.05$). Among groups, the tone burst thresholds at 8 and 20 kHz in the left ears of the tinnitus$^{(-)}$ group were lower than that of control group ($p<0.05$).

Data for each frequency and post-blast time point are depicted in Figure 3.

3.2 MEMRI

MEMRI data collected 35 days post-blast demonstrated that left ear blast exposure induces significant activity changes in auditory structures. We chose to analyze the significance of our data in 3 ways; (1) lateralized effects of blast between groups (control, tinnitus$^{(-)}$, and tinnitus$^{(+)}$); (2) lateralized effect of blast within groups; and (3) bilateral effects of blast between groups. Looking at the lateralized effect of unilateral blast between groups may reveal differences in specific structures or pathways caused by the blast-induced TBI and/or tinnitus. By examining the bilateral effects of blast exposure between groups, we are taking into account the ability of the blast wave to affect the whole brain. In addition to affecting peripheral auditory structures, such as hair cells or the tympanic membrane, blast shock waves can also have sheering or stretching effects to the brainstem, directly causing brain damage (Taber et al., 2006). Lastly, the lateralized effects of blast within groups may reveal whether the unilateral blast caused any differences within blast exposed animals without tinnitus (tinnitus$^{(-)}$) and with tinnitus (tinnitus$^{(+)}$). Also, it is important to consider that while we attempted to induce left-sided tinnitus using unilateral, left-ear exposure, our current GAP detection behavior paradigm cannot differentiate between left-sided and right-sided tinnitus. Therefore, we cannot authenticate that the tinnitus is signal is only perceived unilaterally and in the exposed ear. This further implicates the importance of analyzing our MEMRI results using the three parameters outlined above.

3.2.1 Lateralized effect within groups

Left ear blast exposure significantly affected the neural activity in several auditory structures. Specifically, rats with chronic tinnitus demonstrated an increase in Mn^{2+} accumulation in the ipsilateral VCN compared to rats with transient tinnitus ($F_{(2,29)} = 4.004$, p = 0.035) (ANOVA and *post-hoc* Bonferroni tests; Fig. 4a). As shown in Fig. 4b, however, chronic tinnitus rats demonstrated a decrease in Mn^{2+} accumulation compared to control rats in the ipsilateral CIC ($F_{(2,29)} = 3.861$, p = 0.031), ECIC ($F_{(2,29)} = 5.677$, p = 0.006), and DCIC ($F_{(2,29)} = 4.845$, p = 0.013). Rats with transient tinnitus, on the other hand, showed a decrease in the right MGB compared to controls ($F_{(2,29)} = 3.794$, p = 0.044), as seen in Fig. 4c. These results show that…

3.2.2 Lateralized effect between groups

In addition to blast-induced changes between groups, there were also induced changes within a single group when comparing brain structures ipsilateral and contrateral to the blasted ear, respectively. Significant changes, however, were only observed in chronic tinnitus rats. Fig. 4a shows significant elevations in Mn^{2+} accumulation in the contralateral structures compared to the ipsilateral structures for the DCN (t [24] = 3.65, p = 0.001) and VCN (t [24] = 3.23, p = 0.004). Fig. 4b shows significant elevations in the contralateral ECIC compared to the ipsilateral ECIC (t [25] = 2.44, p = 0.022). This data indicates that…

3.2.3 Bilateral effect between groups

When pooling ipsilateral and contralateral data together and comparing between groups, there were statistically significant differences across almost all structures. Rats with chronic tinnitus exhibited higher Mn^{2+} accumulation in the VCN compared to rats with transient tinnitus ($F_{(2,61)} = 5.141$, p = 0.007) (ANOVA and *post-hoc* Bonferroni tests; Fig. 5a). Chronic tinnitus rats showed lower accumulation in the CIC ($F_{(2,61)} = 4.516$, p = 0.012) and DCIC ($F_{(2,61)} = 4.789$, p = 0.010) compared to controls, while transient tinnitus rats showed less accumulation in the ECIC ($F_{(2,61)} = 3.536$, p = 0.038) compared to controls (Fig. 5b). In the MGB, rats with transient tinnitus demonstrated lower accumulation compared to controls ($F_{(2,61)}$ 4.586, p = 0.023) as well as chronic tinnitus rats ($F_{(2,61)} = 4.586$, p = 0.047) (Fig. 5c). These findings suggest that…

DISCUSSION:

4.1 Summary of Results

Our results revealed that blast exposure (14 PSI) induced early-onset tinnitus and central hearing impairment at multiple frequencies. At the time of MEMRI scanning, hearing thresholds recovered in all blasted animals and in the tinnitus$^{(-)}$ group (n=5), tinnitus recovered, indicating a difference in susceptibility across individual animals. The MEMRI results indicated that the blast exposure resulted in compensatory plastic changes in the auditory brain structures, which correlate with the presence of tinnitus and/or TBI.

4.2 Same-side comparisons between groups

When comparing the effects of blast exposure on auditory structures, we found a decrease in Mn^{2+} accumulation in the ipsilateral CIC, ECIC and DCIC in tinnitus$^{(+)}$ rats compared to the controls.

The IC is a critical midbrain station for auditory processing that is believed to play a role in tinnitus generation (Ma et al., 2006; Manabe et al., 1997; Zhang et al., 2003). MEMRI and PET studies have indicated that the CIC experiences tinnitus-related plastic changes in the form of altered activity (Brozoski et al., 2007; Holt et al., 2010; Melcher et al., 2000; Smits et al., 2007). In our study, we observed a significant decrease in activity in the ipsilateral CIC in the tinnitus$^{(+)}$ animals compared to the controls. Our results differ from Brozoski, who observed an increase in Mn^{2+} accumulation in the contralateral CIC following noise exposure (Brozoski et al., 2007). The difference in results may be due to the timeline and/or tinnitus induction method Changes in tinnitus-related activity is highly dependent upon the time after noise exposure. In our study, MEMRI was performed 35 days post blast-exposure, whereas Brozoski performed MEMRI over a year after noise-exposure. Additionally, the extent and severity of cochlear damage is related to the spectral composition of the traumatizing sound (Bilak et al., 1997; Eldredge et al., 1981) and therefore, noise exposure may produce different changes in neural activity compared to our blast exposure model. In human studies, researchers also reported less fMRI activation in the left IC of patients with right-sided tinnitus, suggesting a more active left IC during the resting conditions (saturation model) (Melcher et al., 2000). Contrary to Melcher's results, Lanting reported increased responses to sound stimuli in the IC of tinnitus patients compared to the controls, which may suggest an overall decrease in

IC activity during rest conditions based on the saturation model (Lanting et al., 2008). In a recent DTI study using identical blast exposure parameters, significant damage and compensatory plastic changes were found in the CIC 2 and 4 week after bilateral blast exposure (Mao et al., 2011). It is possible that the TBI-associated effects of blast are responsible for the observed tinnitus-related hypoactivity in the ipsilateral CIC of the tinnitus$^{(+)}$ rats.

While the predominant ascending projections to the CIC originate in the contralateral cochear nucleus, the CIC receives bilateral input from numerous auditory structures, including the cochlear nuclei and the contralateral CIC through the commisure of the IC (Brunso-Bechtold et al., 1981; Moore et al., 1998). Based on this information, the ipsilateral CIC could be generating or receiving abnormal activity from the contralateral CIC or from both of the DCN. Although the loud noise caused by the blast would most likely affect the ipsilateral DCN and its main output structure, the contralateral IC, the contralateral DCN and ipsilateral CIC may be affected due to the ability of the blast waves to affect the whole brain, possible through bone conduction.

Few studies have examined changes in the ECIC and/or DCIC in the generation or processing of tinnitus. Within 5 hours following salicylate injection, a reliable tinnitus inducer, Chen found an increase of spontaneous activity and an abnormal pattern of discharges in the ECIC, which were believed to represent tinnitus-related neural activity (Chen and Jastreboff, 1995). In our study, we observed a decrease in activity in the ipsilateral ECIC in the tinnitus$^{(+)}$ animals compared to the controls. The ECIC and DCIC are the first stage of the extralemniscal pathways, where auditory and somatosensory information interact, and are believed to be involved in the tinnitus signal (Chen and Jastreboff, 1995; Holt et al., 2010; Moller et al., 1992). The ECIC receives input from CIC bilaterally and from multiple sensory modalities, and re-directs the auditory information to non-auditory areas of the brain, such as the amygdala (Moller and Rollins, 2002). As a multisensory structure, it is possible that the brain trauma caused by blast could affect various sensory inputs to the structure, which manifests as a decrease in activity in the ipsilateral ECIC.

~~Finally, in the contralateral ECIC, the tinnitus$^{(+)}$ rats had increased activity compared to the tinnitus$^{(-)}$ rats. The mean intensity for the tinnitus$^{(+)}$ group and the control is very similar however, there is an apparent decrease in activity in the tinnitus$^{(-)}$ animals. It is possible that the blunt force of the blast disrupted the balance of excitation and inhibition in the ECIC and caused an overall decrease in activity in blasted rats as reflected by data from the tinnitus$^{(-)}$ rats. However, in the tinnitus$^{(+)}$ group, the tinnitus associated hyperactivity masks the initial decrease in activity from the blast. If true, our results would suggest that hyperactivity in the contralateral ECIC may underlie blast-induced tinnitus. These results are supported by studies demonstrating that hyperactivity in the IC may be related to tinnitus and this hyperactivity normally occurs in the contralateral IC (Brozoski et al., 2007; Ma et al., 2006; Mulders and Robertson, 2009). Overall, the differences in activity between the contralateral and ipsilateral IC structures suggest that commissural pathways may be affected by the impact of blast.~~

4.3 Asymmetrical effects of blast on the left and right sides of the brain (Ipsilateral vs. Contralateral)

To further examine the effects of blast-induced tinnitus and its associated TBI, we looked at the lateralization of activity within groups. Using these parameters, we found that in the tinnitus$^{(+)}$ group, there was a lateralization of tinnitus-related activity in the DCN, VCN, and ECIC. Specifically, tinnitus$^{(+)}$ had increased activity in the right side of the brain compared to the left in the VCN, DCN, and ECIC.

Evidence suggests that the DCN is an important brain center involved in triggering and modulating tinnitus (Kaltenbach and Godfrey, 2008). While available MEMRI studies did not find any significant difference in rats with noise induced tinnitus compared to the controls bilaterally in the DCN (Holt et al., 2010) or asymmetrically between groups (Brozoski et al., 2007), we found an increase in activity in the contralateral DCN compared to the ipsilateral DCN. The differences between studies could be explained as an effect of blast exposure vs. noise exposure, given that the shearing and stretching forces from blast exposure can directly cause damage to the auditory brainstem (Fausti et al., 2009). In one VBM study, researchers found a tinnitus-related decrease in volume of the mesial heschl's gyrus, a DCN structure, in the hemisphere ipsilateral to the affected ear (Schneider et al., 2009). Our decrease in activity in the ipsilateral DCN compared to the contralateral DCN could be a compensatory mechanism resulting from the tinnitus-related decrease in gray matter. Several studies

have shown an increase in DCN spontaneous activity following noise exposure (Brozoski et al., 2002; Kaltenbach, 2011; Kaltenbach and McCaslin, 1996; Zhang and Kaltenbach, 1998) that develops 1-2 months following trauma (Kaltenbach, 2006; Kaltenbach et al., 1998; Kaltenbach and McCaslin, 1996). Noise-induced DCN hyperactivity has been noted across several species, including in the rat (Zhang and Kaltenbach, 1998), hamster (Kaltenbach and Afman, 2000), guinea pig (Shore et al., 2008), gerbil (Wallhausser-Franke et al., 2003) and chinchilla (Brozoski et al., 2002). The observed activity increase in the right DCN of tinnitus$^{(+)}$ animals may coincide with the hyperactivity observed in the DCN after noise exposure. The increased activity in the contralateral DCN could also be explained as a bilateral effect of blast exposure, since blast has the ability to affect the whole brain not just the auditory periphery. DCN hyperactivity following noise trauma is generally thought to arise from plasticity-induced alterations in the balance of excitatory and inhibitory inputs to the DCN and/or other auditory structures (Kaltenbach et al., 2000; Salvi et al., 2000). Such imbalance may ultimately give rise to tinnitus perception. Some studies suggest that tinnitus-related DCN hyperactivity is driven by a lack of glycinergic inhibition (Brozoski et al., 2002; Wang et al., 2009) and/or decreased GABAergic inhibition (Middleton et al., 2011) stemming from a trauma-induced loss of DCN afferent input. In our study, we found the activity increase to occur in the DCN contralateral to the exposed ear in the tinnitus$^{(+)}$ group. Although the DCN ipsilateral to the blast-exposed ear is expected to be most affected, downregulation of inhibition, or upregulation of excitation, occurs bilaterally in the brainstem following unilateral auditory insult (Brozoski et al., 2011). The major input to the DCN is the auditory nerve however, the DCN also receives input from the contralateral cochlear nucleus via commissural pathways (Adams and Warr, 1976; Alibardi, 2000; Arnott et al., 2004; Shore et al., 1992). Studies suggest that most commissural neurons are glycinergic and therefore, activation of the crossed pathway from one cochlear nucleus to the other has an inhibitory effect (Schofield and Cant, 1996). Based on this information, the contralateral DCN activation could be caused by diminished inhibition from the ipsilateral blasted ear and neural pathways.

In recent years, the VCN has received more attention for its role in tinnitus generation. Like the DCN, the VCN receives input from all primary afferent auditory nerve fibers and provides major direct and indirect pathways to higher auditory centers (Vogler et al., 2011). In our study, we found a significant elevation of activity in the contralateral VCN compared to the ipsilateral VCN. Studies have demonstrated hyperactivity in the VCN following acoustic trauma (Brozoski et al., 2007; Vogler et al., 2011; Zheng et al., 2006). In Brozoski's study, noise exposed rats with behavioral evidence of tinnitus had a significant increase in Mn^{2+} accumulation in the ipsilateral posterior VCN (Brozoski et al., 2007). As stated above, the differences in MEMRI results in the VCN could be attributed to the timeline or tinnitus induction method.

Because the DCN projects its output mainly to the contralateral IC (Adams, 1979; Brunso-Bechtold et al., 1981; Oliver, 1984; Osen, 1972; Ryugo et al., 1981), we had expected that the hyperactivity in the contralateral DCN would be passed on to the ipsilateral IC structures. However, our results show that there is a decrease in the ipsilateral ECIC compared to the contralateral within the tinnitus$^{(+)}$ group. While this increase is not large, it is significant. These results further implicate the complex relationships between the ECIC with auditory structures and non-auditory structures to be involved in the tinnitus signal. It is possible that the increase in the left ECIC compared to the right side is a result of the impaired commissural connections between the CIC structures as a result of the blast exposure.

4.4 Bilateral Effects of TBI on tinnitus

Unilateral blast exposure may affect the whole brain, not just the side of brain ipsilateral to the exposed ear. The high pressure associated with blast exposure can cause diffuse axonal injury, contusion, and subdural hemorrhage on both sides of the brain (Saatman et al., 2008; Taber et al., 2006). To explore the effect of TBI-associated tinnitus on the brain as a whole, we look at the bilateral effects of blast exposure on the brain. We found significant changes in activity the VCN, IC structures, and MGB. Specifically, tinnitus$^{(+)}$ rats had increased activity in the VCN compared to animals with tinnitus$^{(-)}$. In the IC structures, tinnitus$^{(-)}$ rats had decreased activity in the ECIC compared to controls, and tinnitus$^{(+)}$ rats had decreased activity in the DCIC and CIC compared to controls. Finally, in the MGB, tinnitus$^{(-)}$ rats had decreased activity compared to controls and the tinnitus$^{(+)}$ group.

Comparing the asymmetric effects of blast exposure within groups, we found hyperactivity in the ipsilateral VCN in tinnitus$^{(+)}$ rats compared to the tinnitus$^{(-)}$ group. While analyzing the bilateral effects of blast on tinnitus, we found that tinnitus$^{(+)}$ rats had increased activity compared to the tinnitus$^{(-)}$ group. Results from the bilateral VCN analysis further suggest that the tinnitus signal may be associated with hyperactivity within the VCN.

Within the IC structures, we found that the blast exposure induced widespread changes in activity. In the CIC and DCIC, rats with tinnitus$^{(+)}$ had decreased activity compared to controls. In the ECIC, rats with tinnitus$^{(-)}$ had decreased activity compared to controls. In Holt's MEMRI study, there was an increase in Mn^{2+} accumulation in the DCIC following unilateral noise exposure (10 kHz 118 dB). Additionally, Holt found an increase in the ECIC, CIC, and DCN after salicylate injection (Holt et al., 2010). Contrary to Holt's data, our blast model induced an overall decrease in activity in IC structures rather than an increase in animals with tinnitus. There are several plausible reasons for the differences in IC activity between our study and Holt's. As mentioned above, there may be different patterns of plastic changes in tinnitus-related activity depending on the amount of time after noise exposure. Imaging in Holt's study was done 55 hours after noise exposure, which may have been too early to observe the plasticity-induced changes in certain auditory structures following noise trauma. Additionally, the presence or absence of hearing loss and/or tinnitus may also result in different patterns of neural activity. At the time of imaging, noise exposed animals in Holt's study demonstrated behavioral evidence of tinnitus and hearing loss and therefore, it is unknown whether the activity changes can be attributed to the presence of hearing loss or tinnitus. Our blasted animals had normal hearing at the time of imaging and therefore, we were able to look at effects of tinnitus and its associated TBI without the effects of hearing loss. Lastly, research has shown that depending on the difference in tinnitus etiology, the anatomic pathologies and underlying mechanisms may be different (Møller, 2011). Holt had used noise exposure, whereas we used a blast exposure model.

In the CIC, ECIC, and DCIC, the tinnitus$^{(+)}$ and tinnitus$^{(-)}$ animals had similar mean intensities. However, the activity changes were significant between the tinnitus$^{(+)}$ group and controls in the DCIC and CIC, and between the tinnitus$^{(-)}$ group and controls in the ECIC. Because both blasted groups had similar levels of Mn^{2+} accumulation in the IC structures, we speculate the blast exposure may be causing the bilateral hypoactivity in these structures.

The overall changes in the ECIC, DCIC, and MGB further suggest the involvement of extralemniscal pathways in the generation and/or perception of tinnitus. In the MGB, the tinnitus$^{(-)}$ animals had significantly lower activity than controls and the tinnitus$^{(+)}$ animals. Additionally, the mean intensity value of the MGB in the tinnitus$^{(+)}$ animals was more similar to the control animals. Based on these results, it is possible that blast wave causes a TBI-related decrease in activity in the MGB, but in the tinnitus$^{(+)}$ animals, the tinnitus signal generated elsewhere in the auditory pathway caused activity in the MGB to increase. Studies using a lateral fluid percussion-induced TBI model found significant neuronal loss in the MGB (Blaha et al., 2000; Hicks et al., 1996; Sanderson et al., 1999). These observed changes in the MGB reflect damage and compensatory plastic changes in the MGB that result from blast exposure-induced direct contusion to the brain from skull fracture and/or the shearing and stretching of brain tissue. The damage may manifest as a decrease in neuronal activity, as observed in our tinnitus$^{(-)}$ group.

In the tinnitus$^{(+)}$ group, our results differ from Brozoski, who found a significant decrease in Mn^{2+} accumulation in the contralateral MGB following noise exposure. Again, the differences could be a result of the timeline and/or level of noise trauma. In a VBM study, Muhlau found an increase of gray matter in the MGB of tinnitus patients compared to healthy controls (Muhlau et al., 2006). This increase in gray matter could be a result of the reorganization of the MGB following the peripheral-damage induced deprivation of auditory input to the central nervous system. The increase in MGB activity in the tinnitus$^{(+)}$ group compared to the tinnitus$^{(-)}$ group could be a degenerative and/or compensatory mechanism caused by the combined brain injury and MGB reorganization in response to decreased auditory input. DTI studies looking at blast-induced tinnitus found significant changes in the MGB following bilateral blast exposure (Mao et al., 2011). Specifically, they found an increase in axial diffusivity and the apparent diffusion coefficient in the MGB reflecting damage and compensatory plastic changes to the MGB's axonal integrity and demyelination-related plasticity following blast exposure. Lastly, an

fMRI study found that in patients with unilateral tinnitus, fMRI activation was significantly decreased in the contralateral MGB (Smits et al., 2007). The decrease in fMRI activation signifies an increase of spontaneous activity during the rest condition (saturation model). This data is comparable to our findings and suggests that the tinnitus signal causes an increase in activity in the MGB.

4.4 Conclusion

The AC was the only structure with no significant change in activity in any of the analysis parameters. The lack of significant activity change in the AC could be explained by the fact that MEMRI is believed to be less sensitive in detecting neural activity in deeper brain regions (i.e. forebrain structures) in comparison to brainstem structures (Yu et al., 2005). Additionally, tinnitus-related changes in forebrain neural activity may involve a subpopulation of neurons whose activity is not resolved by MEMRI (Brozoski et al., 2007). While Brozoski found a decrease in the contralateral AC in rats with tinnitus, Holt did not find any significant changes in the AC following salicylate or noise exposure. In an fMRI study, no statistically significant tinnitus-related difference were observed in the AC (Lanting et al., 2008). One study found that in individuals with unilateral tinnitus, the ipsilateral AC had significantly smaller volumes than controls (Schneider et al., 2009). As speculated by a recent study (Groschel et al., 2011), hyperactivity could be masked in the experimental group during the MEMRI measurement because of the tinnitus-related volume reduction.

Overall, we demonstrated using MEMRI that blast exposure affects the brain through the auditory system and via direct impact to the brain. Our results revealed that blast exposure can induce a change in activity in a variety of auditory structures, which suggests that tinnitus may be a system-wide pathology. There is a great need to further investigate imaging techniques, including MEMRI, using different blast parameters, including duration, intensity, and number of exposures. Examining the immediate effects of blast exposure would be beneficial given that proper TBI detection and management, especially within 48 hours of the injury, can significantly alter the clinical course (Lee and Newberg, 2005). Additionally, a study comparing the effects of noise exposure versus blast exposure using a similar imaging and behavior study could help distinguish the differences and similarities between blast exposure and noise exposure, as well as tinnitus and/or TBI. It would also be beneficial to examine the state the tympanic membrane following blast exposure and its relationship, if any, to the tinnitus and/or aberrant neural activity as detected using MEMRI. The tympanic membrane is the structure injured most frequently by blasts and has been recommended as a marker of blast exposure (DePalma et al., 2005). Overall, the results of our study have a direct effect on future tinnitus research because it further establishes MEMRI as an objective indicator of tinnitus-related neural activity in auditory structures. Continued efforts to understand the etiology of tinnitus and to develop strategies for its treatment will benefit from studies using MEMRI.

Acknowledgements:

This work was supported by a grant from the Department of Defense (grant award #W81XWH-11-2-0031) to J.S. Zhang and a grant from AANA Foundation to J. Ouyang. The authors wish to thank Dr. Berkowitz for granting us access to 7T MRI scanner, to thank Dr. Bissig for assistance in using MEMRI.

References

Adams, J.C. (1979). Ascending projections to the inferior colliculus. Eur J Neurosci *183*, 519-538.

Adams, J.C., and Warr, W.B. (1976). Origins of axons in the cat's acoustic striae determined by injection of horseradish peroxidase into severed tracts. Eur J Neurosci *170*, 107-121.

Alibardi, L. (2000). Cytology, synaptology and immunocytochemistry of commissural neurons and their putative axonal terminals in the dorsal cochlear nucleus of the rat. AnnAnat *182*, 207-220.

Arnold, W., Bartenstein, P., Oestreicher, E., Romer, W., and Schwaiger, M. (1996). Focal metabolic activation in the predominant left auditory cortex in patients suffering from tinnitus: a PET study with [18F]deoxyglucose. ORL JOtorhinolaryngolRelat Spec *58*, 195-199.

Arnott, R.H., Wallace, M.N., Shackleton, T.M., and Palmer, A.R. (2004). Onset neurones in the anteroventral cochlear nucleus project to the dorsal cochlear nucleus. J AssocResOtolaryngol *5*, 153-170.

Bauer, C.A., Turner, J.G., Caspary, D.M., Myers, K.S., and Brozoski, T.J. (2008). Tinnitus and inferior colliculus activity in chinchillas related to three distinct patterns of cochlear trauma. J NeurosciRes.
Bilak, M., Kim, J., Potashner, S.J., Bohne, B.A., and Morest, D.K. (1997). New growth of axons in the cochlear nucleus of adult chinchillas after acoustic trauma. ExpNeurol *147*, 256-268.
Bissig, D., and Berkowitz, B.A. (2009). Manganese-enhanced MRI of layer-specific activity in the visual cortex from awake and free-moving rats. Neuroimage *44*, 627-635.
Blaha, G.R., Raghupathi, R., Saatman, K.E., and McIntosh, T.K. (2000). Brain-derived neurotrophic factor administration after traumatic brain injury in the rat does not protect against behavioral or histological deficits. Neuroscience *99*, 483-493.
Bouilleret, V., Cardamone, L., Liu, Y.R., Fang, K., Myers, D.E., and O'Brien, T.J. (2009). Progressive brain changes on serial manganese-enhanced MRI following traumatic brain injury in the rat. J Neurotrauma *26*, 1999-2013.
Brozoski, T.J., and Bauer, C.A. (2005). The effect of dorsal cochlear nucleus ablation on tinnitus in rats. Hearing Research *206*, 227-236.
Brozoski, T.J., Bauer, C.A., and Caspary, D.M. (2002). Elevated fusiform cell activity in the dorsal cochlear nucleus of chinchillas with psychophysical evidence of tinnitus. JNeurosci *22*, 2383-2390.
Brozoski, T.J., Ciobanu, L., and Bauer, C.A. (2007). Central neural activity in rats with tinnitus evaluated with manganese-enhanced magnetic resonance imaging (MEMRI). HearRes *228*, 168-179.
Brozoski, T.J., Wisner, K.W., Sybert, L.T., and Bauer, C.A. (2011). Bilateral Dorsal Cochlear Nucleus Lesions Prevent Acoustic-Trauma Induced Tinnitus in an Animal Model. J Assoc Res Otolaryngol.
Brunso-Bechtold, J.K., Thompson, G.C., and Masterton, R.B. (1981). HRP study of the organization of auditory afferents ascending to central nucleus of inferior colliculus in cat. Eur J Neurosci *197*, 705-722.
Cacace, A.T., Cousins, J.P., Parnes, S.M., McFarland, D.J., Semenoff, D., Holmes, T., Davenport, C., Stegbauer, K., and Lovely, T.J. (1999). Cutaneous-evoked tinnitus. II. Review Of neuroanatomical, physiological and functional imaging studies. AudiolNeurootol *4*, 258-268.
Cavazzini, M., Bliss, T., and Emptage, N. (2005). Ca2+ and synaptic plasticity. Cell Calcium *38*, 355-367.
Cernak, I., Vink, R., Zapple, D.N., Cruz, M.I., Ahmed, F., Chang, T., Fricke, S.T., and Faden, A.I. (2004). The pathobiology of moderate diffuse traumatic brain injury as identified using a new experimental model of injury in rats. Neurobiology of disease *17*, 29-43.
Chen, G.D., and Jastreboff, P.J. (1995). Salicylate-induced abnormal activity in the inferior colliculus of rats. HearRes *82*, 158-178.
Crippa, A., Lanting, C.P., van Dijk, P., and Roerdink, J.B. (2010). A diffusion tensor imaging study on the auditory system and tinnitus. Open Neuroimag J *4*, 16-25.
DePalma, R.G., Burris, D.G., Champion, H.R., and Hodgson, M.J. (2005). Blast injuries. The New England journal of medicine *352*, 1335-1342.
Dobie, R.A., Sakai, C.S., Sullivan, M.D., Katon, W.J., and Russo, J. (1993). Antidepressant treatment of tinnitus patients: report of a randomized clinical trial and clinical prediction of benefit. AmJOtol *14*, 18-23.
Dong, S., Mulders, W.H., Rodger, J., Woo, S., and Robertson, D. (2010a). Acoustic trauma evokes hyperactivity and changes in gene expression in guinea-pig auditory brainstem. EurJNeurosci *31*, 1616-1628.
Dong, S., Rodger, J., Mulders, W.H., and Robertson, D. (2010b). Tonotopic changes in GABA receptor expression in guinea pig inferior colliculus after partial unilateral hearing loss. Brain Res *1342*, 24-32.
Eggermont, J.J. (2007). Correlated neural activity as the driving force for functional changes in auditory cortex. HearRes *229*, 69-80.
Eggermont, J.J., and Komiya, H. (2000). Moderate noise trauma in juvenile cats results in profound cortical topographic map changes in adulthood. HearRes *142*, 89-101.
Eggermont, J.J., and Roberts, L.E. (2004). The neuroscience of tinnitus. Trends Neurosci *27*, 676-682.
Eldredge, D.H., Miller, J.D., and Bohne, B.A. (1981). A frequency-position map for the chinchilla cochlea. The Journal of the Acoustical Society of America *69*, 1091-1095.
Fausti, S.A., Wilmington, D.J., Gallun, F.J., Myers, P.J., and Henry, J.A. (2009). Auditory and vestibular dysfunction associated with blast-related traumatic brain injury. J Rehabil Res Dev *46*, 797-810.
Finlayson, P.G., and Kaltenbach, J.A. (2009). Alterations in the spontaneous discharge patterns of single units in the dorsal cochlear nucleus following intense sound exposure. HearRes *256*, 104-117.

Fitch, R.H., Threlkeld, S.W., McClure, M.M., and Peiffer, A.M. (2008). Use of a modified prepulse inhibition paradigm to assess complex auditory discrimination in rodents. Brain Res Bull *76*, 1-7.
Giraud, A.L., Chery-Croze, S., Fischer, G., Fischer, C., Vighetto, A., Gregoire, M.C., Lavenne, F., and Collet, L. (1999). A selective imaging of tinnitus. Neuroreport *10*, 1-5.
Gondusky, J.S., and Reiter, M.P. (2005). Protecting military convoys in Iraq: an examination of battle injuries sustained by a mechanized battalion during Operation Iraqi Freedom II. Military medicine *170*, 546-549.
Gourevitch, B., and Eggermont, J.J. (2010). Maximum decoding abilities of temporal patterns and synchronized firings: application to auditory neurons responding to click trains and amplitude modulated white noise. J Comput Neurosci *29*, 253-277.
Groschel, M., Muller, S., Gotze, R., Ernst, A., and Basta, D. (2011). The possible impact of noise-induced Ca(2+)-dependent activity in the central auditory pathway: A manganese-enhanced MRI study. Neuroimage.
Henderson, D., Bielefeld, E.C, Lobarinas, E., and Tanaka, C. (2011). Noise-Induced Hearing Loss: Implication for Tinnitus. In Textbook of tinnitus, A.G. Møller, Langguth, B., De Ridder, D., Kleinjung, T., ed. (New York, Springer), pp. 511-516.
Henry, J.A., James, K.E., Owens, K., Zaugg, T., Porsov, E., and Silaski, G. (2009). Auditory test result characteristics of subjects with and without tinnitus. Journal of Rehabilitation Research and Development *46*, 619-632.
Hicks, R., Soares, H., Smith, D., and McIntosh, T. (1996). Temporal and spatial characterization of neuronal injury following lateral fluid-percussion brain injury in the rat. Acta neuropathologica *91*, 236-246.
Hoffman, H.J., and Reed, G.W. (2004). Epidemiology of tinnitus. In Tinnitus: Theory and Management Hamilton, J.B. Snow, ed. (Ontario, BC Decker, Inc), pp. 16-41.
Holt, A.G., Bissig, D., Mirza, N., Rajah, G., and Berkowitz, B. (2010). Evidence of key tinnitus-related brain regions documented by a unique combination of manganese-enhanced MRI and acoustic startle reflex testing. PLoS One *5*, e14260.
Kaltenbach, J.A. (2006). The dorsal cochlear nucleus as a participant in the auditory, attentional and emotional components of tinnitus. Hearing Research *216–217*, 224-234.
Kaltenbach, J.A. (2011). Tinnitus: Models and mechanisms. Hear Res *276*, 52-60.
Kaltenbach, J.A., and Afman, C.E. (2000). Hyperactivity in the dorsal cochlear nucleus after intense sound exposure and its resemblance to tone-evoked activity: a physiological model for tinnitus. HearRes *140*, 165-172.
Kaltenbach, J.A., and Godfrey, D.A. (2008). Dorsal cochlear nucleus hyperactivity and tinnitus: are they related? Am J Audiol *17*, S148-S161.
Kaltenbach, J.A., Godfrey, D.A., Neumann, J.B., McCaslin, D.L., Afman, C.E., and Zhang, J. (1998). Changes in spontaneous neural activity in the dorsal cochlear nucleus following exposure to intense sound: relation to threshold shift. HearRes *124*, 78-84.
Kaltenbach, J.A., and McCaslin, D.L. (1996). Increases in spontaneous activity in the dorsal cochlear nucleus following exposure to high intensity sound: A possible neural correlate of tinnitus. Audit Neurosci *3*, 57-78.
Kaltenbach, J.A., Zhang, J., and Afman, C.E. (2000). Plasticity of spontaneous neural activity in the dorsal cochlear nucleus after intense sound exposure. HearRes *147*, 282-292.
Kaltenbach, J.A., Zhang, J., and Finlayson, P. (2005). Tinnitus as a plastic phenomenon and its possible neural underpinnings in the dorsal cochlear nucleus. HearRes *206*, 200-226.
Kerr, A.G. (1980). Trauma and the temporal bone. The effects of blast on the ear. The Journal of laryngology and otology *94*, 107-110.
Kerr, A.G., and Byrne, J.E. (1975). Concussive effects of bomb blast on the ear. The Journal of laryngology and otology *89*, 131-143.
Kraus, K.S., Ding, D., Jiang, H., Lobarinas, E., Sun, W., and Salvi, R.J. (2011). Relationship between noise-induced hearing-loss, persistent tinnitus and growth-associated protein-43 expression in the rat cochlear nucleus: does synaptic plasticity in ventral cochlear nucleus suppress tinnitus? Neuroscience *194*, 309-325.
Landgrebe, M., Langguth, B., Rosengarth, K., Braun, S., Koch, A., Kleinjung, T., May, A., De, R.D., and Hajak, G. (2009). Structural brain changes in tinnitus: grey matter decrease in auditory and non-auditory brain areas. Neuroimage *46*, 213-218.
Langguth, B., Eichhammer, P., Kreutzer, A., Maenner, P., Marienhagen, J., Kleinjung, T., Sand, P., and Hajak, G. (2006). The impact of auditory cortex activity on characterizing and treating patients with chronic tinnitus--first results from a PET study. Acta OtolaryngolSuppl, 84-88.

Langguth, B., Landgrebe, M., Kleinjung, T., Sand, G.P., and Hajak, G. (2011). Tinnitus and depression. World J Biol Psychiatry *12*, 489-500.
Lanting, C.P., de, K.E., and van, D.P. (2009). Neural activity underlying tinnitus generation: results from PET and fMRI. HearRes *255*, 1-13.
Lanting, C.P., De Kleine, E., Bartels, H., and Van Dijk, P. (2008). Functional imaging of unilateral tinnitus using fMRI. Acta Otolaryngol *128*, 415-421.
Lauritzen, M. (2005). Reading vascular changes in brain imaging: is dendritic calcium the key? Nat Rev Neurosci *6*, 77-85.
Leaver, A.M., Renier, L., Chevillet, M.A., Morgan, S., Kim, H.J., and Rauschecker, J.P. (2011). Dysregulation of limbic and auditory networks in tinnitus. Neuron *69*, 33-43.
Lee, B., and Newberg, A. (2005). Neuroimaging in Traumatic Brain Imaging. NeuroRX *2*, 372-383.
Lee, J.H., Silva, A.C., Merkle, H., and Koretsky, A.P. (2005). Manganese-enhanced magnetic resonance imaging of mouse brain after systemic administration of MnCl2: dose-dependent and temporal evolution of T1 contrast. Magn Reson Med *53*, 640-648.
Leonardi, A.D., Bir, C.A., Ritzel, D.V., and VandeVord, P.J. (2011). Intracranial pressure increases during exposure to a shock wave. Journal of neurotrauma *28*, 85-94.
Lew, H.L., Jerger, J.F., Guillory, S.B., and Henry, J.A. (2007). Auditory dysfunction in traumatic brain injury. J Rehabil Res Dev *44*, 921-928.
Lockwood, A.H., Salvi, R.J., Coad, M.L., Towsley, M.L., Wack, D.S., and Murphy, B.W. (1998). The functional neuroanatomy of tinnitus: evidence for limbic system links and neural plasticity. Neurology *50*, 114-120.
Ma, W.L., Hidaka, H., and May, B.J. (2006). Spontaneous activity in the inferior colliculus of CBA/J mice after manipulations that induce tinnitus. HearRes *212*, 9-21.
Manabe, Y., Yoshida, S., Saito, H., and Oka, H. (1997). Effects of lidocaine on salicylate-induced discharge of neurons in the inferior colliculus of the guinea pig. HearRes *103*, 192-198.
Mao, J.C., Pace, E., Pierozynski, P., Kou, Z., Shen, Y., Vandevord, P., Haacke, E.M., Zhang, X., and Zhang, J. (2011). Blast-Induced Tinnitus and Hearing Loss in Rats: Behavioral and Imaging Assays. J Neurotrauma.
Mattson, M.P. (2007). Mitochondrial regulation of neuronal plasticity. Neurochemical research *32*, 707-715.
McKenna, L. (2000). Tinnitus and insomnia. In Tinnitus Handbook, R.S. Tyler, ed. (San Diego, Singular), pp. 59-84.
Melcher, J.R., Sigalovsky, I.S., Guinan, J.J., Jr., and Levine, R.A. (2000). Lateralized tinnitus studied with functional magnetic resonance imaging: abnormal inferior colliculus activation. JNeurophysiol *83*, 1058-1072.
Middleton, J.W., Kiritani, T., Pedersen, C., Turner, J.G., Shepherd, G.M., and Tzounopoulos, T. (2011). Mice with behavioral evidence of tinnitus exhibit dorsal cochlear nucleus hyperactivity because of decreased GABAergic inhibition. Proceedings of the National Academy of Sciences of the United States of America *108*, 7601-7606.
Mirz, F., Gjedde, A., Ishizu, K., and Pedersen, C.B. (2000). Cortical networks subserving the perception of tinnitus--a PET study. Acta OtolaryngolSuppl *543*, 241-243.
Møller, A.R. (2006). Neural plasticity in tinnitus. ProgBrain Res *157*, 365-372.
Møller, A.R. (2011). Pathology of the Auditory System that Can Cause Tinnitus. In Textbook of Tinnitus, A.R. Møller, B. Langguth, D. Ridder, and T. Kleinjung, eds. (Springer New York), pp. 77-93.
Moller, A.R., Moller, M.B., and Yokota, M. (1992). Some forms of tinnitus may involve the extralemniscal auditory pathway. Laryngoscope *102*, 1165-1171.
Moller, A.R., and Rollins, P.R. (2002). The non-classical auditory pathways are involved in hearing in children but not in adults. NeurosciLett *319*, 41-44.
Moore, D.R., Kotak, V.C., and Sanes, D.H. (1998). Commissural and lemniscal synaptic input to the gerbil inferior colliculus. JNeurophysiol *80*, 2229-2236.
Muhlau, M., Rauschecker, J.P., Oestreicher, E., Gaser, C., Rottinger, M., Wohlschlager, A.M., Simon, F., Etgen, T., Conrad, B., and Sander, D. (2006). Structural brain changes in tinnitus. Cereb Cortex *16*, 1283-1288.
Muhlnickel, W., Elbert, T., Taub, E., and Flor, H. (1998). Reorganization of auditory cortex in tinnitus. ProcNatlAcadSciUSA *95*, 10340-10343.
Mulders, W.H., Ding, D., Salvi, R., and Robertson, D. (2011). Relationship between auditory thresholds, central spontaneous activity, and hair cell loss after acoustic trauma. J Comp Neurol *519*, 2637-2647.

Mulders, W.H., and Robertson, D. (2009). Hyperactivity in the auditory midbrain after acoustic trauma: dependence on cochlear activity. Neuroscience *164*, 733-746.
Mulders, W.H.A.M., and Robertson, D. (2011). Progressive centralization of midbrain hyperactivity after acoustic trauma. Neuroscience *192*, 753-760.
Norena, A.J., and Eggermont, J.J. (2003). Changes in spontaneous neural activity immediately after an acoustic trauma: implications for neural correlates of tinnitus. HearRes *183*, 137-153.
Oliver, D.L. (1984). Dorsal cochlear nucleus projections to the inferior colliculus in the cat: a light and electron microscopic study. The Journal of comparative neurology *224*, 155-172.
Osen, K.K. (1972). Projection of the cochlear nuclei on the inferior colliculus in the cat. The Journal of comparative neurology *144*, 355-372.
Pautler, R.G. (2006). Biological applications of manganese-enhanced magnetic resonance imaging. Methods Mol Med *124*, 365-386.
Paxinos, G., and Watston, C. (1998). The Rat Brain in Stereotaxic Coordinates, Vol 4th (San Diego, USA, Academic Press).
Pienkowski, M., and Eggermont, J.J. (2010). Nonlinear cross-frequency interactions in primary auditory cortex spectrotemporal receptive fields: a Wiener-Volterra analysis. J Comput Neurosci *28*, 285-303.
Rauschecker, J.P., Leaver, A.M., and Muhlau, M. (2010). Tuning out the noise: limbic-auditory interactions in tinnitus. Neuron *66*, 819-826.
Roberts, L.E., Eggermont, J.J., Caspary, D.M., Shore, S.E., Melcher, J.R., and Kaltenbach, J.A. (2010). Ringing Ears: The Neuroscience of Tinnitus. Journal of Neuroscience *30*, 14972-14979.
Ryugo, D.K., Willard, F.H., and Fekete, D.M. (1981). Differential afferent projections to the inferior colliculus from the cochlear nucleus in the albino mouse. Brain Res *210*, 342-349.
Saatman, K.E., Duhaime, A.C., Bullock, R., Maas, A.I., Valadka, A., and Manley, G.T. (2008). Classification of traumatic brain injury for targeted therapies. Journal of neurotrauma *25*, 719-738.
Salinska, E., Danysz, W., and Lazarewicz, J.W. (2005). The role of excitotoxicity in neurodegeneration. Folia Neuropathol *43*, 322-339.
Salvi, R.J., Wang, J., and Ding, D. (2000). Auditory plasticity and hyperactivity following cochlear damage. HearRes *147*, 261-274.
Sanderson, K.L., Raghupathi, R., Saatman, K.E., Martin, D., Miller, G., and McIntosh, T.K. (1999). Interleukin-1 receptor antagonist attenuates regional neuronal cell death and cognitive dysfunction after experimental brain injury. Journal of cerebral blood flow and metabolism : official journal of the International Society of Cerebral Blood Flow and Metabolism *19*, 1118-1125.
Schneider, P., Andermann, M., Wengenroth, M., Goebel, R., Flor, H., Rupp, A., and Diesch, E. (2009). Reduced volume of Heschl's gyrus in tinnitus. Neuroimage *45*, 927-939.
Schofield, B.R., and Cant, N.B. (1996). Origins and targets of commissural connections between the cochlear nuclei in guinea pigs. Eur J Neurosci *375*, 128-146.
Seki, S., and Eggermont, J.J. (2002). Changes in cat primary auditory cortex after minor-to-moderate pure-tone induced hearing loss. HearRes *173*, 172-186.
Shore, S.E., Godfrey, D.A., Helfert, R.H., Altschuler, R.A., and Bledsoe, S.C., Jr. (1992). Connections between the cochlear nuclei in guinea pig. Hearing Research *62*, 16-26.
Shore, S.E., Koehler, S., Oldakowski, M., Hughes, L.F., and Syed, S. (2008). Dorsal cochlear nucleus responses to somatosensory stimulation are enhanced after noise-induced hearing loss. EurJNeurosci *27*, 155-168.
Silva, A.C., and Bock, N.A. (2008). Manganese-enhanced MRI: An exceptional tool in translational neuroimaging. Schizophrenia Bull *34*, 595-604.
Silva, A.C., Lee, J.H., Aoki, I., and Koretsky, A.P. (2004). Manganese-enhanced magnetic resonance imaging (MEMRI): methodological and practical considerations. NMR Biomed *17*, 532-543.
Smits, M., Kovacs, S., De Ridder, D., Peeters, R.R., van Hecke, P., and Sunaert, S. (2007). Lateralization of functional magnetic resonance imaging (fMRI) activation in the auditory pathway of patients with lateralized tinnitus. Neuroradiology *49*, 669-679.
Taber, K.H., Warden, D.L., and Hurley, R.A. (2006). Blast-related traumatic brain injury: what is known? J Neuropsychiatry Clin Neurosci *18*, 141-145.

Tang, H.L., Sun, H.P., Wu, X., Sha, H.Y., Feng, X.Y., and Zhu, J.H. (2011). Detection of neural stem cells function in rats with traumatic brain injury by manganese-enhanced magnetic resonance imaging. Chin Med J (Engl) *124*, 1848-1853.
Turner, J.G., Brozoski, T.J., Bauer, C.A., Parrish, J.L., Myers, K., Hughes, L.F., and Caspary, D.M. (2006). Gap detection deficits in rats with tinnitus: a potential novel screening tool. BehavNeurosci *120*, 188-195.
Tyler, R.S. (1993). Tinnitus disability and handicap questionnaires, pp. 377-383.
Vogler, D.P., Robertson, D., and Mulders, W.H. (2011). Hyperactivity in the ventral cochlear nucleus after cochlear trauma. J Neurosci *31*, 6639-6645.
Voglis, G., and Tavernarakis, N. (2006). The role of synaptic ion channels in synaptic plasticity. EMBO Rep *7*, 1104-1110.
Wallhausser-Franke, E., Mahlke, C., Oliva, R., Braun, S., Wenz, G., and Langner, G. (2003). Expression of c-fos in auditory and non-auditory brain regions of the gerbil after manipulations that induce tinnitus. ExpBrain Res *153*, 649-654.
Walsh, R.M., Pracy, J.P., Huggon, A.M., and Gleeson, M.J. (1995). Bomb blast injuries to the ear: the London Bridge incident series. JAccidEmergMed *12*, 194-198.
Wang, H., Brozoski, T.J., Turner, J.G., Ling, L., Parrish, J.L., Hughes, L.F., and Caspary, D.M. (2009). Plasticity at glycinergic synapses in dorsal cochlear nucleus of rats with behavioral evidence of tinnitus. Neuroscience *164*, 747-759.
Wang, H., Tian, J., Yin, D., Jiang, S., Yang, W., Han, D., Yao, S., and Shao, M. (2001). Regional glucose metabolic increases in left auditory cortex in tinnitus patients: a preliminary study with positron emission tomography. Chin MedJ(Engl) *114*, 848-851.
Yang, S., Weiner, B.D., Zhang, L.S., Cho, S.J., and Bao, S. (2011). Homeostatic plasticity drives tinnitus perception in an animal model. Proc Natl Acad Sci U S A *108*, 14974-14979.
Yu, S.P., Canzoniero, L.M., and Choi, D.W. (2001). Ion homeostasis and apoptosis. Curr Opin Cell Biol *13*, 405-411.
Yu, X., Wadghiri, Y.Z., Sanes, D.H., and Turnbull, D.H. (2005). In vivo auditory brain mapping in mice with Mn-enhanced MRI. NatNeurosci *8*, 961-968.
Zhang, J., Zhang, Y., and Zhang, X. (2011). Auditory cortex electrical stimulation suppresses tinnitus in rats. J Assoc Res Otolaryngol *12*, 185-201.
Zhang, J.S., and Kaltenbach, J.A. (1998). Increases in spontaneous activity in the dorsal cochlear nucleus of the rat following exposure to high-intensity sound. NeurosciLett *250*, 197-200.
Zhang, J.S., Kaltenbach, J.A., Godfrey, D.A., and Wang, J. (2006). Origin of hyperactivity in the hamster dorsal cochlear nucleus following intense sound exposure. J NeurosciRes *84*, 819-831.
Zhang, J.S., Kaltenbach, J.A., Wang, J., and Kim, S.A. (2003). Fos-like immunoreactivity in auditory and nonauditory brain structures of hamsters previously exposed to intense sound. ExpBrain Res *153*, 655-660.
Zheng, Y., Seung, L.H., Smith, P.F., and Darlington, C.L. (2006). Neuronal nitric oxide synthase expression in the cochlear nucleus in a salicylate model of tinnitus. Brain Res *1123*, 201-206.

Blast overpressure induces long lasting astroglial up-regulation and diffuse axonal injury

S Kallakuri, H Lu, L Hao, E Pace, X Zhang, JM Cavanaugh and J Zhang

Address for correspondence:
Jinsheng Zhang, Ph.D.
Professor & Research Director
Otolaryngology-Head and Neck Surgery
Communication Sciences & Disorders
Wayne State University
Room 268, Lande Medical Building
550 East Canfield, Detroit, MI 48201
Jinzhang@med.wayne.edu
Tel:313-577-0066 (Office)
Tel:313-577-0190 (Lab)
Fax:313-577-6318

Acknowledgements: This research was supported by a grant from Congressionally Directed Medical Research. We thank Mrs. Brandy Broadbent for her valuable help with image analysis.

ABSTRACT

The role of central auditory structures such as the dorsal cochlear nucleus (DCN), inferior colliculus (IC), and auditory cortex (AC) in the pathophysiology of tinnitus is well established. While blast induced tiunnitus has become one of the co-morbidities in the spectrum of blast induced neurotrauma, studies related to glial reactivity and axonal degenerative changes in these central auditory structures and their implication following blast are limited. Adult male Sprague Dawley rats were subjected to a single insult of blast overpressure of 22 psi by a custom built shock tube and were allowed to survive for either 1day, 1 month or 3 months. Following conclusion of neurophysiological recording from auditory centers, brains were harvested and processed astrocytic reactivity and axonal degenerative changes. Astrocytes were identified by glial fibrillary acidic protein immunoreactivity and axonal injury was detected by silver impregnation technique. Blast exposure resulted in loss of consciousness as shown by significantly prolonged duration to surface right. Blast exposed rats also showed significantly high astrocytes compared to sham with their number reaching significantly high at 1 month after blast. Astrocytic proliferation in DCN was elevated at all time points. However, in IC, astrogliosis was maximal at 1 month after blast. AC showed a temporal increase in astrocytic proliferation with significant levels at 1 month after blast. Axonal degenerative changes were observed in sections from all three regions with axonal injury being observed as late as 3 months after blast. Taken together, these findings suggest a single blast exposure results in sustained astrogliosis and axonal injury changes that may contribute to or extend reactive changes in auditory centers.

INTRODUCTION

Blast induced neurotrauma (BINT) is the signature wound of the conflicts in Iraq and Afghanistan. In fact, a recent analysis of association between military deployment experience and health outcome in a sample population of service members (deployed and non-deployed) has shown an association between blast exposure and hearing loss and tinnitus (Vanderploeg et al., 2012). Furthermore, a significant increase in the number of servicemen suffering from noise induced hearing injury and blast related co-morbidities such as tinnitus and others were also reported in US service personnel (Lew et al., 2007, Helfer et al., 2011). With blast related traumatic brain injury producing greater rates of tinnitus and hearing loss compared with non blast related traumatic brain injury (Lew et al., 2007), auditory dysfunction has become the most common service related disability with annual compensations reaching around 1 billion dollars (Fausti et al., 2009).

The role of central auditory structures such as the dorsal cochlear nucleus (DCN), inferior colliculus (IC) and the auditory cortex (AC) in the pathobiology of tinnitus has been well established. For example, it was previously shown that acoustic trauma may lead to changes in the physiology and pharmacology of dorsal cochlear nucleus neurons which may underlie the pathophysiology of tinnitus (Chang et al., 2002). Additionally, it was also shown that the modulation of DCN through somatosensory electrical stimulation may modulate acoustic induced neural activity (a neural correlate of certain forms of tinnitus) in DCN neurons (Zhang and Guan, 2007). Also shown was that electrical stimulation of DCN results in tonotopic organization in the areas of inferior colliculus suggesting a direct relay along the ascending auditory pathways (Hoa et al., 2008).

On the other hand, we previously showed that blast overpressure (14 psi or 194 dB) results in early onset of tinnitus and central hearing impairment at broad frequency ranges. Also shown were injury and compensatory changes in inferior colliculus and medial geniculate body (Mao et al., 2012). In fact, neuroanatomical studies on the effects of blast overpressure have recently gained prominence considering the wide ranging associated co-morbidities of which tinnitus is very prominent. Previous studies have shown that blast over-pressure leads to accumulation of neurofilaments (Saljo et al., 2000), formation of perineural spaces and vacuoles (Cernak et al., 2001) suggesting ongoing alterations in axonal transport machinery and other pathological change. Subsequently, others have shown that blast overpressure induces axonal injury (Long et al., 2009), cytoskeletal proteolysis even at low levels of exposure (Park et al., 2011) and even signs of impaired axoplasmic transport (Koliatsos et al., 2011). Axonal injury during the initial 2 week period was supported by silver staining studies in rats subjected to a single blast overpressure of 35 psi (Garman et al., 2011). However, descriptions related to the extent of axonal injury in brain regions encompassing the central auditory structures is limited

(Garman et al., 2011) to nonexistent especially after prolonged survival periods following a single exposure to blast.

Besides axonal injury, blast overpressure induced glial responses may also underlie the associated pathophsyiological changes. These glial reactivity changes were reported from periods ranging a month to a day. One of the earliest studies supporting glial reactivity changes following blast overpressure revealed microglial hypertrophy that subsided by 21 days after injury (Kaur et al., 1995). Recently Svetlov et al (2010) reported persistent glial fibrillary acidic protein (GFAP) accumulation 30 days after exposure (258 kPa) in hippocampus (Svetlov et al., 2010). This was further supported by Cernak et al (2011) in a mouse model of blast neurotrauma as evidenced by elevated GFAP gene response in preparations of hippocampus and brainstem 30 days after injury (Cernak et al., 2011). However, whether the elevated GFAP levels correspond to quantified reactive astrocytosis seen histologically needs validation especially in auditory centers such as DCN, IC and AC. Histological evidence of GFAP reactive astrocytes and elevated serum GFAP levels extending to 7 days after blast overpressure were reported (Svetlov et al., 2012) and suggested enhanced neuro-glial and systemic mechanisms in the ensuing pathological response. Where as, a more recent investigation reported significant hippocampal GFAP expression extending to 24 hours after exposure to 22 psi blast overpressure (Sajja et al., 2012).

Taken together, these studies offer support for neuronal and glial reactivity changes in brain following blast overpressure. We hypothesize that blast overpressure induced auditory changes may in part be related to axonal injury changes and sustained chemical (e.g. pro/anti inflammatory and excitatory amino acid) imbalances that are influenced by reactive astrocytosis. However, studies aimed at understanding the extent of astrocytic proliferation and associated axonal injuries in auditory centers have never been undertaken. Accordingly, this study attempted to assess the extent of astrocyte proliferation and axonal injury at 1 day, 1month and 3 months after exposure to a single insult of blast overpressure in the range of 22 psi.

MATERIALS AND METHODS

Anesthesia and animal preparation:

All procedures were approved by the Institutional Animal Care and Use Committee (IACUC). Adult male Sprague Dawley rats (381±15.8 grams, Harlan Laboratories, Indianapolis, IN) were anesthetized by a mixture of isoflurane (3%) and 0.6 L/min of oxygen for a total duration of 6 minutes. While still maintaining anesthesia, they were harnessed and placed on a sled to reduce dynamic pressure load and prevent translation of the entire body. With only the head and ears exposed, they were positioned 1.09 m from the open end of shock tube with a rostral cephalic orientation facing the oncoming shockwave. The right ear was plugged by an ear plug and was secured in place by a tape ensuring that only left ear was exposed to the blast overpressure

Blast overpressure induction: All rats without chest protection were exposed to a single blast overpressure in the range of 22 psi. The shock front and dynamic overpressure were generated by a custom-built shock tube (12'' diameter, 6 m shock-producing tube attached to 1 m exposure chamber, ORA Inc. Fredericksburg, VA) (Figure 1). Peak static overpressure in the range of 22 psi (figure 1B) was produced with compressed helium and calibrated Mylar sheets (GE Richards Graphics Supplies Inc., Landsville, PA) to induce a free field blast wave (Leonardi et al., 2011). Exposure pressures were measured by 3 sensors placed with in the tube and one sensor placed on the rat holding platform. Pressure measurements were collected at 250 kHz using a Dash 8HF data acquisition system (Astro-Med, Inc, West Warwick, RI) and shock wave profiles were verified to maintain consistent exposure pressures between subjects. This blast overpressure generator has been employed as part of our ongoing neurophysiological studies related to tinnitus (Mao et al., 2012) a major co-morbidity among post deployment service members (Helfer et al., 2011). Sham rats were subjected to identical procedures including plugging the right ear but were not subjected to blast overpressure exposure. Immediately after sham or blast overpressure exposure, they were monitored for duration to surface right, an indirect marker of loss of consciousness (Solt et al., 2011) that has been correlated with the severity of brain injury (Li et al., 2011a, Li et al., 2011b).

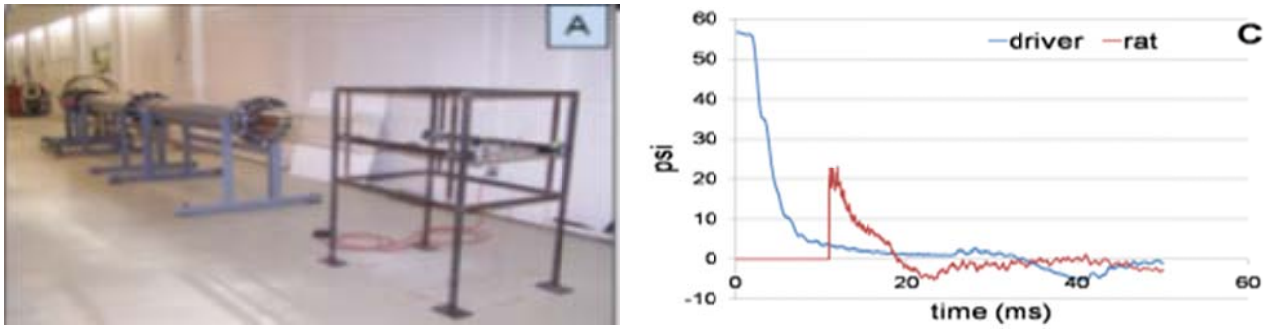

Figure1 shows custom built shock tube and pressure and time history profile. Figure A shows the shock tube that was used as part of this research. Figure B shows the pressure profile generated following rupture of membranes by compressed helium. Pressure profile in blue indicates peak pressure generated at the site of driver. Profile in red indicates the pressure sustained by the rat. Pressure and time profiles were similar in all overpressure exposed rats.

Termination and fixation

Following sham (n=6) or blast exposure they were allowed to survive for a predetermined survival period of 1 day (n=5), 1 month (n=7) or 3 months (n=9). At the end of their respective survival period and the conclusion of neurophysiological recordings, each rat was euthanized by lethal dose of isoflurane (5% v/v)) and perfused transcardially first with 100 ml saline followed by 300 ml 4% paraformaldehyde in 0.1M PB (pH 7.4). The brain was then removed and post-fixed for over 72 hours and subsequently cryoprotected by immersion in 30% sucrose in 0.1M PB (pH 7.4) (Luo et al., 2012). Then, 50 μm thick frozen (−22 C) serial coronal sections encompassing DCN, IC and AC were cut and collected in 1X PBS filled multi-well plates. DCN sections were collected between bregma -10.68 and -11.76. IC sections between -7.80 and -9.24 from bregma and for AC, sections between -4.08 and -6.84 from bregma were collected (Paxinos and Watson, 2007). These sections were further processed for astrocytic reactivity and axonal injury.

Glial fibrillary acidic protein immunocytochemistry for astrocytosis

For quantitative analysis of reactive astrocytosis in DCN, IC and AC regions, 5 representative sections from each region were subjected to antigen retrieval by incubation in a citrate buffer (pH6.0) at 90^{o}C for 1 hour followed by immersion in hydrogen peroxide (0.3%) to quench endogenous peroxidase activity. The sections were then incubated overnight in mouse anti GFAP antibody (NE1015, EMD chemicals, Gibbstown, NJ) diluted in 2% normal goat serum

(Vector Laboratories, Burlingame, CA) in 1% bovine serum albumin (BSA). Sham sections were also incubated in anti GFAP antibody. The sections were then incubated in biotinylated anti-mouse IgG (Vector Laboratories, Burlingame, CA) followed by exposing to Vectastain Elite ABC reagent and chromogen development by diaminobenzidine. In control incubations, normal goat serum was substituted for primary antibody. All sections were observed under a light microscope (Leica DMLB, Leica Microsystems Ltd, Heerburg, Switzerland) to visualize GFAP reactive astrocytes.

Quantitative analysis of reactive astrocytosis:

To quantify the extent of reactive astrocytosis, 10 representative digital images (x20 magnification) from each section encompassing bilateral regions of DCN, IC or AC were obtained (Table 1). The total number of identifiable astrocytes was counted using the cell counter function in ImageJ (http://rsb.info.nih.gov/ij/) by a blinded observer. The average number of astrocytes per group and region were calculated and statistically compared for group-wise differences using one-way analysis of variance or t-test using SPSS (IBM).

	stained sections and total images			total sections and images per group
Group (# of animals)	DCN	IC	AC	
Sham n=6	30/300	30/300	30/300	90/900
1 day (n=5)	25/250	25/250	25/250	75/750
30 days (n=7)	35/350	35/350	35/350	105/1050
90 days (n=9)	45/450	45/450	45/450	135/1350

Silver staining for degenerating axons

For qualitative analysis of the extent of blast overpressure induced axonal injury in sections encompassing DCN, IC and AC, 5 representative additional sections from each region per rat were subjected to a silver impregnation staining technique described previously (Gallyas et al., 1980) and used to demonstrate diffuse axonal injury (Kallakuri et al., 2003, Kallakuri et al., 2008). The sections were immersed for 3 min in pretreatment solution prepared with a mixture of equal volumes of 9% sodium hydroxide and 15% hydroxylamine. The sections were then

thoroughly washed in 0.5% acetic acid (3x3 min) or until the sections turned opaque. The sections were then incubated in an impregnation solution (5 mg/ml ferric nitrate and 100 mg/ml silver nitrate) for 30 min. Sections turn reddish yellow following incubation in the impregnation solution. They were then washed in 1% citric acid (4x2 min) followed by a wash in 0.5% acetic acid for 5 min. The sections were then placed in a developer solution previously (Gallyas et al., 1980) until the sections became pale gray. After sufficient development they were removed and washed thoroughly in 0.5% acetic acid (3x10 min), rinsed in distilled water, mounted on a slide and cover-slipped. The mounted sections were examined under light microscope (Leica DMLB, Leica Microsystems Ltd, Heerburg, Switzerland) for degenerating axons.

RESULTS

Surface Righting Duration: Following blast exposure, animals showed no gross abnormalities except for a small number of animals that developed mild respiratory depression that required no special intervention. However, animals subjected to blast overpressure demonstrated significantly prolonged duration to surface right compared to sham animals (figure 2). Sham animals were subjected to the same duration of anesthesia but not subjected to blast overpressure exposure.

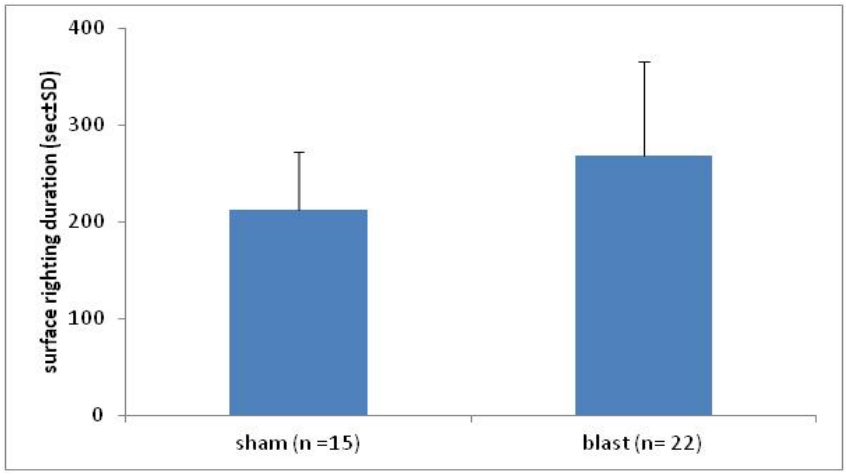

Figure 2: Chart showing surface righting duration in blast overpressure and sham exposed rats. Blast overpressure exposed rats demonstrated significantly high surface righting duration compared to sham animals ($p<0.05$). Prolonged surface righting duration and brief apnea are attributed to the effects of blast overpressure.

Reactive astrocytosis:

Observation of sections from sham, 1day, 1 month and 3 month post blast revealed the presence of astrocytes in all the brain regions. However, quantification on the extent astrocyte presence was limited to DCN (figure 3), IC (figure 4) and AC (figure 5) considering their predominant involvement in auditory functions.

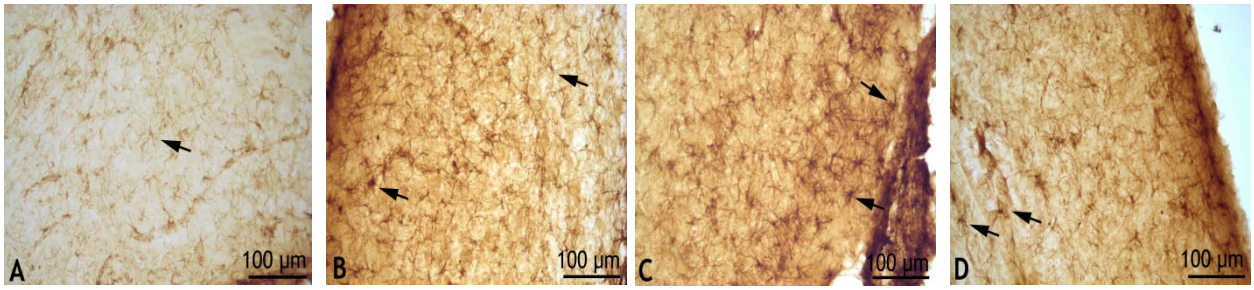

Figure 3 showing astrocytic reaction in brain section encompassing DCN. Figure 3A shows GFAP reactive astrocytes in sham sections. Figure 3B shows astrocytic reaction 1day after blast overpressure exposure. Figure 3C shows astrocytes in DCN 1 month after exposure. Figure 3D shows GFAP reactivity in region of AC after 3 months

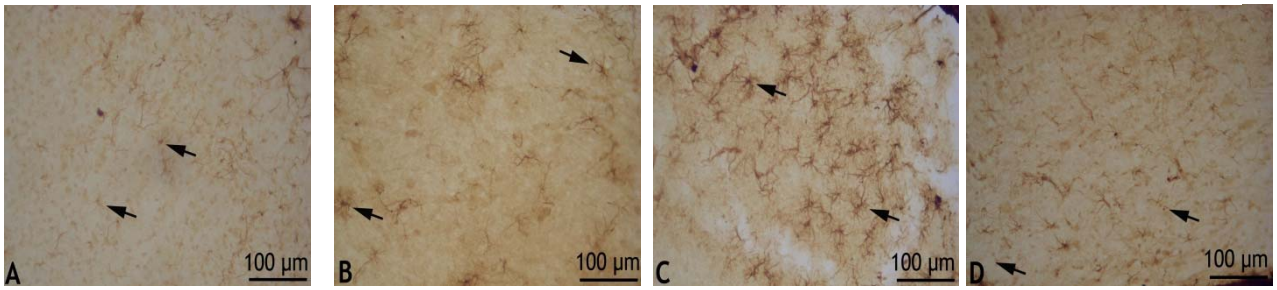

Figure 4 showing astrocytic reaction in brain section encompassing IC. Figure 4A shows GFAP reactive astrocytes in sham sections. Figure 4B shows astrocytic reaction 1day after blast overpressure exposure. Figure 4C shows astrocytes in IC 1 month after exposure. Figure 4D shows GFAP reactivity in region of AC after 3 months

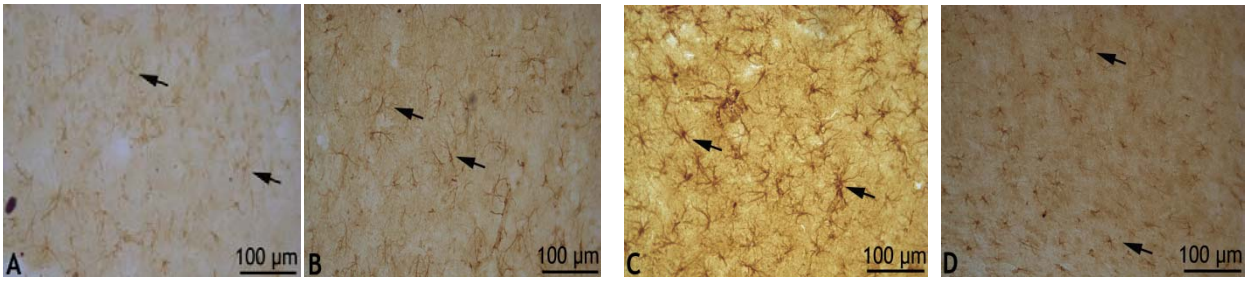

Figure 5 showing astrocytic reaction in brain section encompassing AC. Figure 5A shows GFAP reactive astrocytes in sham sections. Figure 5B shows astrocytic reaction 1day after blast overpressure exposure. Figure 5C shows astrocytes in AC 1 month after exposure. Figure 5D shows GFAP reactivity in the region of AC after 3 months

Quantification of the extent of reactive astrocytosis revealed that sections from blast overpressure exposure expressed a significantly high number of astrocytes (*p=<0.05)* compared to sections from sham exposure (figure 6). Furthermore, the extent of astrocytosis was significantly high in blast exposure sections harvested after 1 month compared to sham (*p =0.027482)*. The number of astrocytes although were high at 1 day and 3 months after exposure they were not significantly different from sham and no other changes were observed (figure 7).

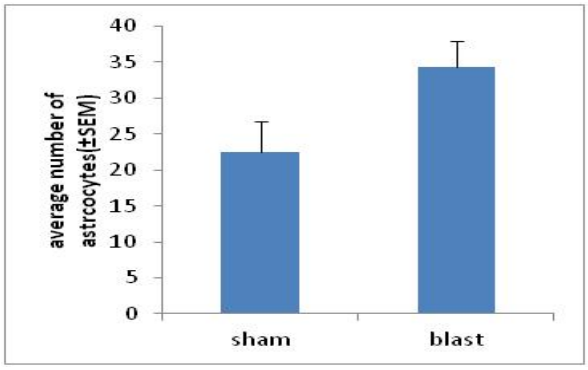

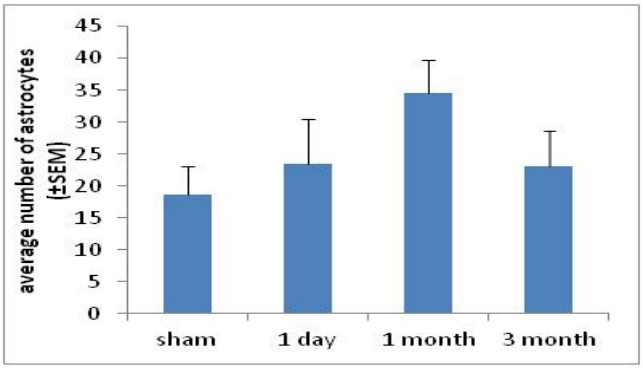

Figure 6 **Figure 7**

Figure 6 shows the extent of astrocytic proliferation in blast and sham exposed rats. Sections from blast exposed animals demonstrated significantly high astrocytic proliferation (p< 0.5) compared to sections from sham animals. Figure 7 shows the extent of astrocytic proliferation at 1 day, 1 month and 3 months after overpressure exposure. Astrocytic proliferation was significantly high 1 month after overpressure exposure.

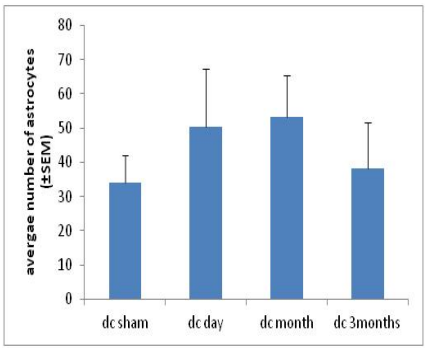

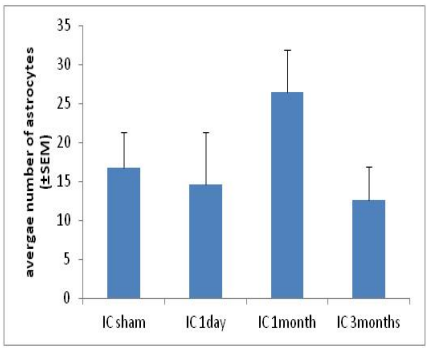

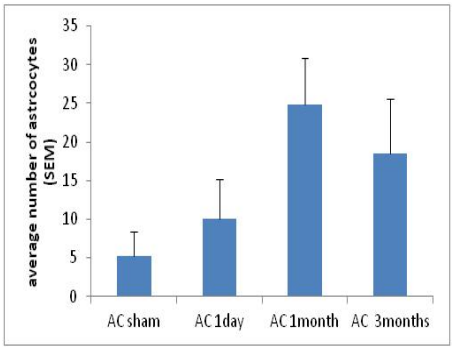

Figure 8A **Figure 8B** **Figure 8C**

Figure 8 shows the extent of astrocytic proliferation in brain sections encompassing regions of DCN, IC and AC. In DCN, although considerably high astrocytic proliferation was observed at 1 day, 1 month and 3 months post blast, it was not significant compared to levels in sham (Figure 8A). In IC, the extent of astrocytic proliferation was markedly high at 1 month period after exposure (Figure 8B). In AC, the extent of astrocytic proliferation was significantly high at 1 month period after exposure that stayed elevated even 3months after exposure (Figure 8C).

A further analysis of astrocyte count in DCN alone shows a dramatic increase in the number of astrocytes by 1 day after blast that stayed elevated up to 1 month blast overpressure exposure with their number by 3 months post blast reaching slightly higher levels than sham (figure 8A). However, in the case of IC, the most pronounced increase in the number of astrocytes was observed at 1 month after blast overpressure exposure (figure 8B). This increase was just was just shy of significance when compared the number of astrocytes observed at 3 months after blast overpressure (this may suggest a heterogeneous response of the brain regions following blast overpressure). A further analysis of representative AC regions revealed a temporal elevation in the number of astrocytes (figure 8C) There was a marked increase in the number of astrocytes by 1 day with a significant increase by 1 month ($p=<0.05$) compared to sham. By 3 months after blast overpressure exposure, the number of astrocytes was still elevated compared to sham but this elevation was not significant. In brainstem regions incorporating DCN and IC, a high number of astrocytes were observed in blast exposed sections (31.398 ±4.61 SEM) compared to those in sham tem region (25.410 ±5.09 SEM)

Qualitative analysis of axonal injury

Representative sections of brain regions encompassing DCN, IC and AC from sham and those exposed to a single insult of blast overpressure were investigated for degenerating axons. These sections were observed for the presence degenerating axons in white and gray matter areas at 1 day, 1 month and 3 months. Observation of sham sections revealed long tracts of axons with uniform caliber in sections of brainstem encompassing DCN, IC and AC. In all the sham sections, axons could be seen coursing through long distances uninterrupted in various white matter tracts (figure 9A). In the case of blast overpressure exposed sections, axons at various stages of degeneration could be found in region trapezoid, spinal trigeminal tract, pyramids, ventral spinocerebellar tract, medial longitudinal fasciculus, transverse fibers of pons, pons, tracts of lateral lemniscus, commissure of inferior colliculus and occasionally in the most posterior aspects of corpus callosum. In sections of DCN degenerating axons could be found at 1 day, 1 month and even at 3 months after exposure in various tracts such as trapezoid, spinal trigeminal tract, pyramids, ventral spinocerebellar tract and medial longitudinal fasciculus (figure 9B). In sections after 1 day after exposure, axons could be found with signs of increased inter-axonal spacing, swellings could be found in tracts such as spinocerebellar tract and axons in cochlear nucleus. In DCN sections from 1 month, degenerating axons could be found swellings and beads with dark stained axons associated with axonal debris and axons with vacuolations could be found. In DCN sections from 3 months after exposure, the incidence of axonal degeneration appears to be more preponderant as indicated by higher incidence of axonal swellings, axons with uneven caliber, and even retraction balls. Furthermore, the extent of uneven caliber axons appears to be more intense as revealed by a high number of wrinkled axons. By 3 months after exposure, degenerating axons could be found in long tracts such as medial longitudinal fasciculus.

In the case of sections encompassing IC, the brainstem regions involved are white matter tracts such as transverse fibers of pons, pons, lateral lemniscus and commissure of inferior colliculus (Figure 9C). In sections 1 day after the exposure, degenerating axons could be observed in the form of axons with beads, swellings and vacuoles. The vacuolated axons could be observed in trapezoid and other white matter tracts such as lateral lemniscus. Furthermore, in these sections, large caliber axons could found to be prominently injured appearing as swollen axons. Sections at 3 month survival appear to have preponderance of degenerating axons than

sections from 1 m after exposure. In 3 month sections degenerating axons appear to be similar to those in 1 day after exposure with the number of wrinkled axons appearing more prominently. In sections of AC, degenerating axons at various stages could be observed in regions of corpus callosum, fimbria of hippocampus, optic radiations, and areas of thalamus (Figure 9D). These degenerative changes were predominantly found in sections at 1 day and at 3 months after exposure as debris of degenerating axons and as wrinkled axons.

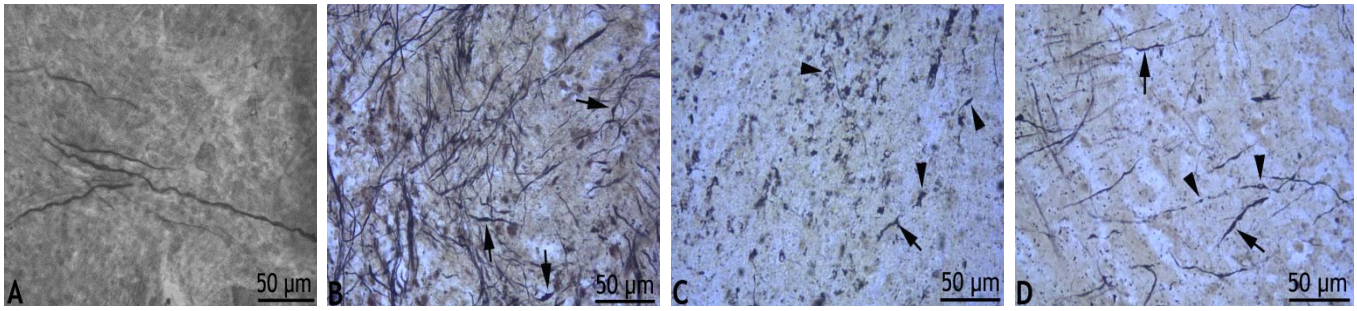

Figure 9 images showing the extent of degenerating axons. In sham sections axons with uniform caliber could be seen coursing through region could be observed (Figure 9A). In DCN, degenerating axons could be seen in various regions of the section stained. In this image from a 1 day survival section shows axonal swellings (arrows) in a region between DCN and ganglion of the spinal nerve 5 (Figure 9B). In this section of IC 1 month after exposure (Figure 9C) shows degenerating axons in the form swellings (arrow) and retraction balls and debris (arrow heads Figure 9C). In this section encompassing AC, swollen axons (arrows) and axons with vacuoles and retraction balls (arrow heads) could be observed in thalamic region besides others (Figure 9D).

DISCUSSION

This study for the first time documents blast overpressure induced behavioral changes as indicated by significantly prolonged surface righting duration an indirect indicator of loss consciousness as consequence of blast exposure. A prolonged surface righting duration was also reported in other animal models of traumatic brain injury (Li et al., 2011a, Li et al., 2011b). Potential other effects of blast exposure in these animals include apnea as indicated by a brief and mild form of respiratory suppression. In fact other investigators have reported mortality following blast exposure.

However, the primary purpose of this study was to assess the extent of reactive astrocytosis and axonal degeneration in brain regions encompassing the auditory system at 1 day,

1 month and 3 months after blast overpressure exposure in rats. Thus far, there are several investigations that assessed reactive astrocytosis (Svetlov et al., 2010, Cernak et al., 2011, Garman et al., 2011, Sajja et al., 2012, Svetlov et al., 2012) and axonal degeneration (Saljo et al., 2000, Cernak et al., 2001, Long et al., 2009, Svetlov et al., 2010, Garman et al., 2011, Koliatsos et al., 2011, Wang et al., 2011, Svetlov et al., 2012) following blast overpressure exposure. However, quantitative studies related to the extent of astrocytosis in brain regions encompassing auditory structures extending to 3 months after a single blast overpressure exposure of 22 psi are non-existent. Similarly, the same may be applicable to investigation of axonal degenerative changes. Consistent with previous studies, results from our study support reactive astrocytosis following blast exposure with sustained levels extending up to 1 month after exposure in the areas of DCN, IC and AC. In the case of AC, the elevations persisted up to 3 months after exposure. These results are significant considering that previous studies on astrocytosis following blast overpressure exposure are either limited to histological signs of astrogliosis and elevations in serum GFAP at 7 days after exposure (Svetlov et al., 2012) or GFAP accumulations at 30 days in hippocampus (358 kPa) (Svetlov et al., 2010). Cernak et al (2011) showed sustained elevations in the gene expression of GFAP up to 30 days following moderate blast overpressure exposure in mice (driver pressure ranging from 25-45 psi) in hippocampus and brainstem preparations. Elevated GFAP expression in the current study at 1 month after exposure is similar to the elevated GFAP gene expression in brainstem preparations (Cernak et al., 2011) On the other hand, Garman et al (2011) reported no prominent increase in GFAP in deep cerebellar white matter regions (same regions that showed axonal injury evidenced by amino cupric staining) even in sections studied at 2 weeks after blast exposure (35 psi). This is different from the current study that showed prominent GFAP expression by 1 day after exposure that reached significant levels by 1 month which stayed elevated in certain regions such as auditory cortex for up to 3 months after exposure. Although the present study focused on the extent of GFAP reactivity in brain regions related to auditory system alone, GFAP reactive astrocytes were also found prominently in all the other areas of sections studied including various associated white matter tracts. Therefore, the influence of astrocytosis may not be limited to the structures quantified but may encompass the other brain regions and systems. Findings from the current study that support sustained astrogliosis extending to chronic time periods involving diverse brain regions necessitates the potential need to address the ensuing glial mediated

inflammatory and other biochemical changes that may have critical implications in the performance and maintenance of various neural circuits such as those in the auditory system.

Besides astrogliosis, the presence of axonal degenerative changes albeit limited at all time points studied suggests blast overpressure induced axonal injury. Some of the earliest findings on axonal injury following blast overpressure were reported by Saljo et al that showed phosphorylated neurofilament accumulation in various cortical regions potentially due to a disturbed axonal transport (Saljo et al., 2000). Subsequently, Cernak et al (2001) expanded perineural spaces, increased numbers of cytoplasmic vacuoles, and laminal body formation were reported 24 hours after blast exposure (Cernak et al., 2001). Subsequently several other studies reported silver stained degenerating axons (Long et al., 2009, Svetlov et al., 2010, Koliatsos et al., 2011, Wang et al., 2011)

The findings of degenerating axons in various white matter tracts in our study are similar to those previously reported by others at 7 and 14 days after exposure in mice (Koliatsos et al., 2011). However, our findings extend the presence of degenerating axons event at 3 months after exposure and suggest the possibility of degenerative processes at long periods after the exposure. In fact Koliatsos degenerating axons were reported in optic tract, LL, forceps major of CC, cerebral and cerebellar peduncles and other brainstem regions by silver staining at 7 and 14 days (Koliatsos et al., 2011). The most prominent findings on axonal injury were reported by Garman et al in rats at extending to 2 weeks after exposure with the most prominent staining deep cerebellar and brainstem regions (Garman et al., 2011). However, our study extends these findings to a time point of 3 months which has never been reported before. This may also suggest that traumatic axonal injury changes may evolve over prolonged periods of time beyond the initial period of insult and may also explain for lack of or limited axonal degeneration findings by others (Svetlov et al., 2012). Furthermore, the presence of highly wrinkled axons as reported in our study is also similar to the findings of axons with irregular contours as reported by others (Garman et al., 2011).

Sustained or ongoing axonal degenerative changes may contribute to sustained reactive injury changes. The process of proliferation and activation of astrocytes known as reactive astrogliosis (Allaman et al., 2011) and such reactive astrogliosis trigged following a traumatic insult such as blast overpressure and maintained as an independent injury consequence of the initial traumatic insult or sustained in response to ongoing degenerative process such as axonal

degeneration may exacerbate a cascade of injury processes leading to imbalance in neural circuits and tinnitus may very well be a consequence of such alteration. An increasing and accumulating body of evidence supports the role of astrocytes in various neurological diseases (McGann et al., 2012). Reactive astrocytes can release a wide array of pro and anti-inflammatory chemical mediators which can potentially tilt the balance between neurotoxicity and protection (Liberto et al., 2004, Farina et al., 2007, Sofroniew and Vinters, 2010). Furthermore, a functional consequence of astroglial activation can be very complex. For example astrocytic glutamate transporters (GLT-1) are involved in the uptake of glutamate toward a balanced extracellular glutamate concentration (Ren and Dubner, 2008). However, this balance may not be possible despite activation of astrocytes due to reduced GLT-1 as in models of neuropathic pain (Sung et al., 2003, Liaw et al., 2005, Weng et al., 2006) and thus a reduction in GLT-1 expression may lead to enhanced glutamate concentration in the synaptic cleft leading to neuronal hyper-excitability (Ren and Dubner, 2008). Glutamate uptake by astrocytes is an energetically expensive process (Pellerin et al., 1998, Hertz et al., 1999). However, a blast overpressure exposure may lead to potential alterations or impairment in energy metabolism or related pathways leading to astrocytic impairment resulting in elevated glutamate levels. Furthermore, long lasting or delayed micro alterations in cerebral blood flow may also contribute to glucose imbalances and may influence the astrocytic function and contribute to a disturbed glutamate uptake.

The presence of long lasting axonal injury changes may also contribute to the sustenance of the reactive astrogliosis which in turn may lead to release of various chemical mediators including proinflammatory cytokines such as such as interleukin 1beta (IL-1β) which may be coupled to increased activity of neuronal N-methyl-D-aspartate receptors and subsequent changes (Ren and Dubner, 2008). In fact, elevated expression of IL-1β following blast exposure was also reported (Svetlov et al., 2012).

CONCLUSIONS:

Results from the current study support astrocytic proliferation and axonal degenerative changes in various brain regions following a single exposure to blast overpressure. Our findings also suggest that these degenerative changes taking place up to 3 months after the initial exposure.

Combination of astrocytic proliferation and axonal injury in brain regions encompassing auditory circuits may play a role in the initiation and maintenance of impaired auditory percept.

Acknowledgements:

This work was supported by a grant from the Department of Defense (grant award #W81XWH-11-2-0031)

REFERENCES

Allaman I, Belanger M, Magistretti PJ (2011) Astrocyte-neuron metabolic relationships: for better and for worse. Trends in neurosciences 34:76-87.

Cernak I, Merkle AC, Koliatsos VE, Bilik JM, Luong QT, Mahota TM, Xu L, Slack N, Windle D, Ahmed FA (2011) The pathobiology of blast injuries and blast-induced neurotrauma as identified using a new experimental model of injury in mice. Neurobiol Dis 41:538-551.

Cernak I, Wang Z, Jiang J, Bian X, Savic J (2001) Ultrastructural and functional characteristics of blast injury-induced neurotrauma. J Trauma 50:695-706.

Chang H, Chen K, Kaltenbach JA, Zhang J, Godfrey DA (2002) Effects of acoustic trauma on dorsal cochlear nucleus neuron activity in slices. Hear Res 164:59-68.

Farina C, Aloisi F, Meinl E (2007) Astrocytes are active players in cerebral innate immunity. Trends Immunol 28:138-145.

Fausti SA, Wilmington DJ, Gallun FJ, Myers PJ, Henry JA (2009) Auditory and vestibular dysfunction associated with blast-related traumatic brain injury. J Rehabil Res Dev 46:797-810.

Gallyas F, Wolff JR, Bottcher H, Zaborszky L (1980) A reliable method for demonstrating axonal degeneration shortly after axotomy. Stain Technol 55:291-297.

Garman RH, Jenkins LW, Switzer Iii RC, Bauman RA, Tong LC, Swauger PV, Parks S, Ritzel DV, Dixon CE, Clark R, Bayir H, Kagan V, Jackson E, Kochanek PM (2011) Blast exposure in rats with body shielding is characterized by diffuse axonal injury. Journal of neurotrauma.

Helfer TM, Jordan NN, Lee RB, Pietrusiak P, Cave K, Schairer K (2011) Noise-induced hearing injury and comorbidities among postdeployment U.S. Army soldiers: April 2003-June 2009. Am J Audiol 20:33-41.

Hertz L, Dringen R, Schousboe A, Robinson SR (1999) Astrocytes: glutamate producers for neurons. J Neurosci Res 57:417-428.

Hoa M, Guan Z, Auner G, Zhang J (2008) Tonotopic responses in the inferior colliculus following electrical stimulation of the dorsal cochlear nucleus of guinea pigs. Otolaryngol Head Neck Surg 139:152-155.

Kallakuri S, Cavanaugh JM, Ozaktay AC, Takebayashi T (2003) The effect of varying impact energy on diffuse axonal injury in the rat brain: a preliminary study. Exp Brain Res 148:419-424.

Kallakuri S, Singh A, Lu Y, Chen C, Patwardhan A, Cavanaugh JM (2008) Tensile stretching of cervical facet joint capsule and related axonal changes. Eur Spine J 17:556-563.

Kaur C, Singh J, Lim MK, Ng BL, Yap EP, Ling EA (1995) The response of neurons and microglia to blast injury in the rat brain. Neuropathol Appl Neurobiol 21:369-377.

Koliatsos VE, Cernak I, Xu L, Song Y, Savonenko A, Crain BJ, Eberhart CG, Frangakis CE, Melnikova T, Kim H, Lee D (2011) A mouse model of blast injury to brain: initial pathological, neuropathological, and behavioral characterization. Journal of neuropathology and experimental neurology 70:399-416.

Leonardi AD, Bir CA, Ritzel DV, VandeVord PJ (2011) Intracranial pressure increases during exposure to a shock wave. J Neurotrauma 28:85-94.

Lew HL, Jerger JF, Guillory SB, Henry JA (2007) Auditory dysfunction in traumatic brain injury. J Rehabil Res Dev 44:921-928.

Li Y, Zhang L, Kallakuri S, Zhou B, Cavanaugh JM (2011a) Injury Predictors for Traumatic Axonal Injury in a Rodent Head Impact Acceleration Model. Stapp Car Crash J 55:25-47.

Li Y, Zhang L, Kallakuri S, Zhou R, Cavanaugh JM (2011b) Quantitative relationship between axonal injury and mechanical response in a rodent head impact acceleration model. Journal of Neurotrauma 28:1767-1782.

Liaw WJ, Stephens RL, Jr., Binns BC, Chu Y, Sepkuty JP, Johns RA, Rothstein JD, Tao YX (2005) Spinal glutamate uptake is critical for maintaining normal sensory transmission in rat spinal cord. Pain 115:60-70.

Liberto CM, Albrecht PJ, Herx LM, Yong VW, Levison SW (2004) Pro-regenerative properties of cytokine-activated astrocytes. Journal of neurochemistry 89:1092-1100.

Long JB, Bentley TL, Wessner KA, Cerone C, Sweeney S, Bauman RA (2009) Blast overpressure in rats: recreating a battlefield injury in the laboratory. J Neurotrauma 26:827-840.

Luo H, Zhang X, Nation J, Pace E, Lepczyk L, Zhang J (2012) Tinnitus suppression by electrical stimulation of the rat dorsal cochlear nucleus. Neuroscience letters 522:16-20.

Mao JC, Pace E, Pierozynski P, Kou Z, Shen Y, VandeVord P, Haacke EM, Zhang X, Zhang J (2012) Blast-induced tinnitus and hearing loss in rats: behavioral and imaging assays. Journal of Neurotrauma 29:430-444.

McGann JC, Lioy DT, Mandel G (2012) Astrocytes conspire with neurons during progression of neurological disease. Curr Opin Neurobiol 22:850-858.

Park E, Gottlieb JJ, Cheung B, Shek PN, Baker AJ (2011) A model of low-level primary blast brain trauma results in cytoskeletal proteolysis and chronic functional impairment in the absence of lung barotrauma. Journal of Neurotrauma 28:343-357.

Paxinos G, Watson C (2007) The rat brain in stereotaxic coordinates. New York: Academic Press.

Pellerin L, Pellegri G, Bittar PG, Charnay Y, Bouras C, Martin JL, Stella N, Magistretti PJ (1998) Evidence supporting the existence of an activity-dependent astrocyte-neuron lactate shuttle. Dev Neurosci 20:291-299.

Ren K, Dubner R (2008) Neuron-glia crosstalk gets serious: role in pain hypersensitivity. Current opinion in anaesthesiology 21:570-579.

Sajja VS, Galloway MP, Ghoddoussi F, Thiruthalinathan D, Kepsel A, Hay K, Bir CA, Vandevord PJ (2012) Blast-induced neurotrauma leads to neurochemical changes and neuronal degeneration in the rat hippocampus. NMR Biomed 25:1331-1339.

Saljo A, Bao F, Haglid KG, Hansson HA (2000) Blast exposure causes redistribution of phosphorylated neurofilament subunits in neurons of the adult rat brain. J Neurotrauma 17:719-726.

Sofroniew MV, Vinters HV (2010) Astrocytes: biology and pathology. Acta neuropathologica 119:7-35.

Solt K, Cotten JF, Cimenser A, Wong KF, Chemali JJ, Brown EN (2011) Methylphenidate actively induces emergence from general anesthesia. Anesthesiology 115:791-803.

Sung B, Lim G, Mao J (2003) Altered expression and uptake activity of spinal glutamate transporters after nerve injury contribute to the pathogenesis of neuropathic pain in rats. The Journal of neuroscience : the official journal of the Society for Neuroscience 23:2899-2910.

Svetlov SI, Prima V, Glushakova O, Svetlov A, Kirk DR, Gutierrez H, Serebruany VL, Curley KC, Wang KK, Hayes RL (2012) Neuro-glial and systemic mechanisms of pathological

responses in rat models of primary blast overpressure compared to "composite" blast. Front Neurol 3:15.

Svetlov SI, Prima V, Kirk DR, Gutierrez H, Curley KC, Hayes RL, Wang KK (2010) Morphologic and biochemical characterization of brain injury in a model of controlled blast overpressure exposure. The Journal of trauma 69:795-804.

Vanderploeg RD, Belanger HG, Horner RD, Spehar AM, Powell-Cope G, Luther SL, Scott SG (2012) Health Outcomes Associated With Military Deployment: Mild Traumatic Brain Injury, Blast, Trauma, and Combat Associations in the Florida National Guard. Archives of physical medicine and rehabilitation 93:1887-1895.

Wang Y, Wei Y, Oguntayo S, Wilkins W, Arun P, Valiyaveettil M, Song J, Long JB, Nambiar MP (2011) Tightly coupled repetitive blast-induced traumatic brain injury: development and characterization in mice. Journal of Neurotrauma 28:2171-2183.

Weng HR, Chen JH, Cata JP (2006) Inhibition of glutamate uptake in the spinal cord induces hyperalgesia and increased responses of spinal dorsal horn neurons to peripheral afferent stimulation. Neuroscience 138:1351-1360.

Zhang J, Guan Z (2007) Pathways involved in somatosensory electrical modulation of dorsal cochlear nucleus activity. Brain research 1184:121-131.

American Journal of Speech-Language Pathology

Reliability of broadband middle-ear power-reflectance in younger and older adults: Application of Generalizability Theory

Journal:	*The American Journal of Audiology*
Manuscript ID:	AJA-12-0063
Manuscript Type:	Research Article
Date Submitted by the Author:	06-Nov-2012
Complete List of Authors:	Mahoney, Marty; Wayne State University, Communication Sciences and Disorders McFarland, Dennis; Wadsworth Labs, New York State Health Department Carpenter, MiChelle; Wayne State University, Department of Communication Sciences and Disorders Rizvi, Sabahet; Wayne State University, Communcation Sciences and Disorders Cacace, Anthony; Wayne State University, Communication Sciences and Disorders;
Keywords:	Adults, Audiology, Hearing

Reliability of broadband middle-ear power-reflectance in younger and older adults: Application of Generalizability Theory

Marty J. Mahoney[1], Dennis J. McFarland[2],

MiChelle S. Carpenter[1], Sabahet Rizvi[1], Anthony T. Cacace[1]

[1]Department of Communication Sciences & Disorders
Wayne State University
Detroit, MI

and

[2]The Wadsworth Center,
NYS Department of Health
Albany, NY

Correspondence to: Anthony T. Cacace, Ph.D.
Department of Communication Sciences & Disorders
Wayne State University
207 Rackham, 60 Farnsworth
Detroit, MI 48202
Phone: 313-577-6753
Fax: 313-577-8885
E-mail: cacacea@wayne.edu

Abstract

Purpose: To assess the reliability of broadband middle ear power reflectance (BMEPR) and transmittance profiles for chirps and tones using Generalizability Theory (GT).

Methods: In 56 adults without a history of middle-ear disease, we assessed the reliability of BMEPR using a multivariate approach based on an analysis-of-variance model. We also assessed Pearson's Product Moment Correlation Coefficients to allow for comparisons with other published studies in the literature.

Results: Based on chirp stimuli, BMEPR measures had good reliability; however, the reliability of individual profiles across frequencies and ears was less than optimal. Lower Generalizability coefficients were found when transmittance was evaluated. Using Pearson's *r*, test re-test reliability was better for right *vs*. left ears and mid-frequencies were generally more reliable than those at either extreme of the frequency range. In contrast, tonal stimuli had both higher Generalizibility coefficients and Pearson's *r* values than chirps for all frequencies tested.

Conclusions: We extend the use of GT as a method to evaluate the reliability of BMEPR. While "unidimensional" pair-wise correlations of individual data points provides useful information regarding the reliability of specific frequencies or bands of frequencies, the "multivariate" approach of GT allows for a more comprehensive evaluation.

Introduction

Measurement of broadband middle ear power reflectance (BMEPR) represents an emerging technology for evaluating electroacoustic characteristics of human middle-ear function *in vivo* (Allen, Jeng, & Levitt, 2005; Jeng, Allen, Lapsey-Miller, & Levitt, 2008). With this method, high resolution frequency-reflectance profiles offer bio-inspired assessment opportunities for evaluating the middle ear under normal and pathological conditions (e.g., Feeney, Grant, & Marryott, 2003; Feeney, Grant, & Mills, 2009; Hunter, Tubaugh, Jackson, & Propes, 2008; Keefe & Simmons, 2003; Shahnaz, Bork, Polka, Longridge, Bell, & Westerberg, 2009). As BMEPR measures transition from the laboratory to the clinic, the need for establishing the reliability of these measures is an important factor for test evaluation and clinical decision making.

Given the broadband characteristics of this metric, methodological and design considerations should take into account whether to base reliability on: **1)** individual data points (frequencies) (Hunter et al. 2008), **2)** select bands of frequencies (e.g., Shahanaz et al., 2009; Vander Werff, Prieve, & Georgantas, 2007; Beers, Shahnaz, Westerberg, & Kozak, 2010), or **3)** the shape of the entire frequency-reflectance profile (Mahoney et al., present study). Moreover, special consideration should be given whether to compute reliability metrics based on: **1)** absolute difference measures of central tendency and dispersion (means and standard deviations), **2)** Pearson's Product Moment Correlation Coefficients (Pearson's *r*), or **3)** Generalizability Theory (GT).

While different approaches have been used to assess test re-test reliability, some methods are on more secure scientific ground than others. For example, absolute differences of BMEPR have been used as indices of test re-test reliability when values are

measured over two or more points-in-time (e.g., Shahnaz et al., 2009; Vander Werff et al,. 2007; Beers et al., 2010; Werner, Levi, & Keefe, 2010; Rosowski, Nakajima, Hamade, Mahfoud, Merchant, Halpin, & Merchant, 2012). On face value, this approach makes intuitive sense, since a reliable test is one that produces similar results on two different occasions. However, with the absolute difference method, the interpretation of good or poor reliability is unduly subjective. This is due to the fact that this method does *not* take variability into account and its meaning depends upon the scale-of-measurement applied. In contrast, the more conventional Pearson's Product Moment Correlation Coefficient (Pearson's *r*) provides a "standardized" metric for reliability calculations since it is based on the proportion-of-variance that is repeatable. Because Pearson's *r* represents a "normalized difference metric" that is signed, it allows for direct comparisons to be made with other studies since it is independent of the unit of measurement (e.g., Hunter et al., 2008; Werner et al., 2010; Mahoney et al., present investigation). While the advantages of using Pearson's *r* over the absolute difference method are apparent, this approach is limited to pair-wise comparisons and therefore, the univariate nature of this metric is not well suited for complex data sets. In comparison to these later two measures, GT is a multivariate approach to reliability based on an analysis-of-variance (ANOVA) model, where more than two time points and where multiple independent variables can be jointly considered in the computations. Furthermore, GT is unique when compared to the typical ANOVA model. Whereas the ANOVA model typically considers subjects as the source-of-error and trends over time as the effect-of-interest, in GT, the variance associated with subjects is the effect-of-interest and the variance over time is the source-of-error. With this strategy, the resultant

Generalizability coefficient becomes a measure of the effect size (i.e., the size of the main effect for subjects) which represents the proportion-of-variance that is due to consistent individual differences. Thus, GT provides a framework for assessing multiple time points, including main effects and interactions between multiple independent variables. Of particular relevance to the current area-of-interest is the interaction between subjects and stimulus frequency, since this relationship allows for the reliability of individual frequency-reflectance profiles to be assessed.

Lastly, the choice and rationale of whether to base reliability estimates on individual data points, on select bands of frequencies, or on profiles, should depend on how these measurements are actually used to diagnose middle-ear disorders. For example, if a diagnosis is based on a single point or on a single band, independent of the overall shape of the profile, then the reliability of individual data points or bands would be the appropriate index. However, as noted by Keefe and Simmons (2003), "There is no evidence to suggest that the use of a single frequency, as in clinical tympanometry, is optimal for assessing middle-ear function at all frequencies important in auditory communication systems, no more than would a single frequency suffice for assessing cochlear, behavioral, or neural function. Wideband measurements of middle-ear functioning appear to have promise as a clinical diagnostic test." Herein, we extend this logic to include the fact that if clinicians base their diagnosis on the shape of the entire profile, then the reliability of the “profile” would be the most appropriate feature to evaluate. This paper focuses on the use of GT for establishing test re-test reliability of BMEPR data, where the effects of multiple variables are to be considered (e.g., Cronbach, Nageswari, & Gleser, 1963; Crocker & Algina 1986; Laenen, Vangeneugden,

Geys, & Mohenberghs, 2006).

Lastly, because GT has not been used extensively in the audiological/hearing science literature, we provide a concise overview to acquaint the readership with this topic (Appendix A).

Materials and Methods

Fifty-six adults categorized into two age groups (Group 1: 18-25 years, n = 28; Group 2: ≥50 and ≤ 66 years, n = 28) were studied. Each age group was stratified by gender (14 males; 14 females per group) and ear (56 left and 56 right) and provided a balanced design between age group, gender, ear, and frequency. Because participants were recruited by word-of-mouth from friends, relatives, and students, the data obtained was considered a convenience sample. Inclusion criteria were a negative history of middle-ear disease, no air-bone gaps exceeding 10 dB for any frequency, and ear canals free of obstruction or debris, based on a screening otoscopic exam. The Human Investigation Committee at Wayne State University approved this study and signed informed consent was obtained from each individual prior to data collection.

Audiometric testing was conducted in a commercial sound booth (Acoustic Systems, Austin, Texas; Model RE-144) using a clinical audiometer (Grason-Stradler, model 61) with standard earphones (Telephonics, TDH-50P) enclosed in supra-aural ear cushions (MX-41/AR). Pure-tone air-conduction audiometry was performed at octave frequencies from 250 through 8000 Hz and at one half-octave frequency (3000 Hz) bilaterally. Bone conduction testing used a standard oscillator (Radioear B-71) and a standard headband. Bone-conduction thresholds were assessed at octave frequencies from 250 through 4000 Hz.

Broadband middle ear power reflectance was measured using commercially available hardware and software (Mimosa Acoustics, MEPA3 Clinical Reflectance System) and a high quality probe assembly (Etymotics, model ER10C) to transduce acoustic stimuli and record acoustic responses from the ear canal. Prior to each recording session, the MEPA system was successfully calibrated in a four-chamber coupler (model: CC4-V) in accordance with guidelines provided by the manufacturer. Particular care was taken to ensure that the foam ear tip of the probe was properly seated and stable in the ear canal. There were no crimps in the foam and this coupling device was fully expanded in the ear canal before testing was initiated. After measurements from chirp and tonal stimuli were obtained from each ear, the probe was removed and re-inserted into the same ear canal and a second set of chirp and tonal measures was acquired. Then, the second ear was tested using the same approach. For the present investigation, both sets of within-session data were used in this analysis. The sound pressure level (SPL) of the chirp stimulus was set to 60 dB (re: 20 uPa) and data were collected over a 1 s time epoch at ambient ear canal air pressure. This allowed for 24 individual chirps (~5 ms in total duration) to be collected and averaged. The SPL of the tonal stimuli was also set to 60 dB (re: 20 uPa) and 9 individual pure tones (ranging from 257 Hz to 6000 Hz) were analyzed. Individual tonal stimuli were 300 ms in total duration, presented sequentially from low-to-high frequency and separated by a 150 ms silent inter-stimulus interval. Selection of the initial ear of measurement was randomized by a physical coin toss (heads = left ear; tails = right ear) to avoid potential order effects that might confound data interpretation (e.g., Thornton, Marotta, & Kennedy, 2003). The same medium size foam ear tips (14A) were used during instrument calibration and data collection. With respect

to chirp stimuli, out of a possible 248 frequencies measured, we selectively sampled a subset of 16 frequencies (258, 307, 398, 492, 633, 750, 796, 1008, 1270, 1500, 1590, 1992, 2530, 3000, 4060, 5040 Hz) for this investigation. With respect to tonal stimuli, we used default values and sampled 9 separate frequencies (258, 492, 750, 1007, 1500, 1992, 3000, 4007, 6000 Hz). Power reflectance values associated with both chirp and tonal stimuli were extracted from separate stored output files which were available from each participant.

To allow for reliability to be evaluated from a multivariate perspective, an ANOVA was used to compute Generalizability coefficients. Additionally, to allow for comparisons other published studies in the literature, Pearson's *r* were also used to evaluate test re-test reliability for individual frequencies.

Results

Figure 1 shows grand averaged frequency-reflectance profiles for chirp and tonal stimuli collapsed across age group, gender, and ear. Except for the highest frequency studied, average power reflectance values corresponding to each stimulus type (chirp and tone) were virtually identical. In Figure 2, individual scatter plots are shown for 16 frequencies and all test re-test conditions using chirp stimuli. The general trends observed in these plots show that within-session variability increases from low-to-high frequencies. Figure 3 shows individual scatter plots for 9 frequencies and for all test re-test conditions for the tonal stimuli. While a similar trend for increased within-session variability with increases of stimulus frequency was also observed, tonal stimuli showed less within-session variability than chirps.

For comparison with previous studies, Table 1 (left side) provides Pearson's *r*

values for the test re-test reliability of 16 individual frequencies for chirp stimuli, separately for each ear. Trends in these data reveal higher reliabilities for right *vs*. left ears with mid-frequency reliabilities generally higher than those at either extreme. Table 1 (right side) provides test re-test reliability of Pearson's *r* values for the 9 individual frequencies separately for each ear obtained for tonal stimuli. These data show higher test re-test correlation values in comparison to chirps at corresponding frequencies; right ears also showed higher test re-test correlations than left ears.

Next, both chirp and tonal data sets were analyzed with an ANOVA in two ways. First, the effect of subjects was used in the error terms to evaluate the consistency of age, gender, ear, and test effects across subjects (i.e., traditional null-hypothesis significance testing). The second set of analyses used tests in the error terms to evaluate the proportion-of-variance due to subject effects that was consistent across tests (i.e., generalizability or test re-test reliability). Results were calculated for both power reflectance and transmittance. The transmittance metric was analyzed since it was thought that this transformation might reduce variability and thus potentially improve the Generalizability coefficients (Allen et al., 2005). Keep in mind that while this assertion has been suggested by Allen and colleagues, it has never been proven by empirical assessment.

Generalizability Theory:

Chirps

Using a 6-way ANOVA, effects of age and gender were used as between-subject variables; ear, frequency, and time were used as within-subject variables. Using subject effects as the error term, the ANOVA showed a significant main effect for frequency (F =

350.31, p<0.0001) resulting from the lower power reflectance in mid-frequencies, as seen in Figure 1. There were also gender x ear (F = 4.22, p<0.045), gender x frequency (F = 2.38, <0.002), and age x gender x ear interactions (F = 4.60, p<0.037). The gender x frequency interaction was due in part to greater reflectance in males at the highest frequencies. The three-way interaction was associated with greater reflectance in the right ear of older females and the left ear of older males with less difference in younger females and males.

The results of the ANOVA using test effects as the error term resulted in the Generalizability coefficients shown in Table 2 (left side). Also shown in Table 2 (right side) are Generalizability coefficients for the transmittance values, computed as:

$$T = 10 \times \log_{10}[1-(|R|^2)] \ (dB) \qquad \text{Equation 1)}$$

where: T is the transmittance and $|R|^2$ is the power reflectance expressed as a proportion in decibels (dB).

These data show that the Generalizability coefficient associated with the main effect of subjects is 0.82. This score represents the average for each subject collapsed over frequency and ear. The reliability associated with the interaction between subjects and frequency is 0.56. This effect corresponds to the profile for individual subjects across frequencies averaged over both ears. The reliability of the subjects x ear x frequency interaction is 0.35. This corresponds to the shape of the profile for individual subjects across frequencies for individual ears and probably represents the feature of greatest interest to the clinician. Generalizability coefficients for transmittance are somewhat

lower, particularly for the three-way interaction.

Tonal Stimuli

Generalizability coefficients for middle ear power reflectance using tonal stimuli are shown in Table 3 (left side). The Generalizability coefficient associated with the main effects of subjects is 0.86. The reliability associated with the subjects x frequency interaction is 0.72. The reliability associated with subjects x ear is 0.75 and that for the subjects x ear x frequency interaction is 0.63. These values are considerably higher than those for chirps. Values for the transmittance data for tonal stimuli (Table 3, right side) are similar to the power-reflectance data.

Discussion

Generalizability Theory was initially introduced into the educational psychology literature by Cronbach and colleagues (1963; 1972) to evaluate the reliability of profiles of standardized test scores in school-aged children. Because of its unique capabilities of assessing reliability from a multivariate perspective, GT has garnering increased interest in other fields-of-inquiry including speech, hearing, vestibular, and the physical sciences, where a wide range of topics (physiology, electroacoustics, perception, responses to questionnaires, etc.), have already been investigated. Relevant examples include the reliability of distortion product otoacoustic emissions over a 24-hour time period (Cacace, McClelland, Weiner, & McFarland, 1996), postural control in the evaluation of concussion (Broglio, Zhu, Sopiarz, & Oark, 2009), speech-reading abilities (Demorest & Bernstein 1992), perceptual scaling (O'Brian, Packman, Onslow, & O'Brian, 2003), analysis of observational data (Scarsellone, 1998; O'Brian, O'Brian, Packman, & Onslow, 2003), videographic representation of tooth and lip position in smiling and

speech following orthodontic and dentofacial surgery (van de Geld et al., 2007) and in force measurements used in physical therapy and rehabilitation (Roebroeck, Hariaar, & Lankhors, & 1993). Use of GT to assess reliability of BMEPR profiles expands this list of testing domains to include another form of auditory based electroacoustic analysis where profiles involving multiple frequencies evaluated at two or more points-in-time, and numerous independent variables (age, gender, and ear) are under consideration.

We chose to analyze power-reflectance profiles of individual frequencies as our primary metric, since this is the relevant feature derived from commercially available instrumentation and the one that clinicians would actually use to make inferences about normal or pathological states of the middle ear. Moreover, advanced text books on research design and statistics consider GT as the most comprehensive technique available for estimating test measurement reliability (Schiavetti & Metz, 2006, p. 123) and they do not even recognize the absolute difference method (described herein) as a metric of reliability (Maxwell & Satake, 2006).

Established diagnostic exemplars of this methodology include categories of tympanometric types (i.e., profiles of immittance shape as a function of positive and negative air pressures) (e.g., JergerJerger, & Mauldin, 1972) or on more quantitative immittance typologies based on the theoretical model of Vanhuyse (see Margolis, Van Camp, Wilson, & Creten, 1985; Van Camp, Margolis, Wilson, Creten, & Shanks, 1986; Vanhuyse, Creten, & Van Camp, 1975). The potential for BMEPR measures to identify and delineate different pathological conditions of the middle ear provides the rationale and support for instituting a profile analysis, since diagnostic interpretations are already being made using this approach (e.g., Feeney et al., 2003, Feeney, Grant, & Mills, 2009;

Keefe & Simmons, 2003; Allen et al., 2005; Shahnaz, Longridge, & Bell, 2009).

Based on GT using chirps, the reliability for the overall effect (i.e., the power reflectance averaged across all frequencies) was 0.82; this is acceptable by standard convention (Cicchetti, 1994). The reliability of the frequency-reflectance profile (the shape of the profile independent of height) is 0.56, which would be considered fair. Repeating the test and averaging the results gives a profile reliability of 0.72, which is considered good. However, profiles involving ears and ear x frequency interactions are at levels conventionally considered to be poor (0.35). For tonal stimuli, the reliability of the overall effect was 0.86. The reliability of the frequency reflectance profile was 0.72. Repeating the test and averaging the results gives a profile reliability of 0.75 and profiles involving ears and ear x frequency interactions are at .63. Thus, in comparison to chirps, the reliability for tones was better.

Using chirps, within session test re-test reliability measures were made using Pearson's *r* for 16 individual frequencies ranging from 258 Hz to 5040 Hz. These data, which were collapsed across gender and age group, ranged from 0.30 to 0.85 for the right ear and 0.18 to 0.57 for the left ear. These values agreed favorably with the adult data of Werner et al. (2010), which assessed 15 frequencies across a similar bandwidth (281 Hz to 7336 Hz). Their correlation values from adults, where data were collapsed across gender and were presented for right ears only, ranged from 0.28 to 0.95. Additionally, Hunter and colleagues (2008) provided test re-test correlation coefficients for 9 frequencies ranging from 258 Hz to 6000 Hz, with data collapsed across age, gender, and ear and focused on children ranging in age from 3 days to 47 months. Their correlation values ranged from 0.68 to 0.97 and were higher than those reported in adults. Test re-test

correlation values for tonal stimuli from the present study ranged from 0.52 to 0.92.

Werner and colleagues (2010) used a hybrid approach to assess reliability of power reflectance in infants and adults using three different metrics: absolute difference measures, test re-test correlations of 15 individual frequency bands using Pearson's *r*, and the cross-correlation method to examine reliability of the entire profile for the same ear and for left and right ears on two occasions. In their study, test re-test correlations for individual frequency bands were predominantly positive and were statistically significant. Highest correlation values were generally observed in the lower frequency range; lowest correlations were observed in the higher frequency range. When test re-test correlations were averaged across frequency for the individual age groups (our computations based on Table 1 of Werner, et al., 2010), they were rank ordered: being lowest for 5 to 9 month olds (mean: 0.274, SD: 0.158, range: -0.05 to 0.44), intermediate for 2 to 3 month olds (mean: 0.401, SD: 0.139, range: 0.16 to 0.57), and highest for adults (mean: 0.551, SD: 0.196, range: 0.30 to 0.95). Focusing on adults, the cross-correlation method which was used to assess reliability of the shape of the profile and collapsed across age group produced a value of 0.85; the average between ear cross-correlation was 0.84. However, it is noteworthy that the cross-correlation statistic is typically performed by comparing two time series, using a "lag term" to shift one function against the other as a way to determine the maximum correlation. Werner and colleagues indicate that "frequency was the lag variable (p. 7)," but they do not elaborate on the non-conventional use of this statistic. Applying the cross-correlation in this way results in profiles being aligned at different frequencies; a practice which contrasts with typical usage and one that has a questionable theoretical rationale since direct comparisons across frequency is not

possible. Nevertheless, it is our contention that the overall shape of the profile (e.g., power-reflectance values across frequencies) within individual ears is the primary feature-of-interest to the clinician to use for diagnostic purposes.

As noted above, we found that the reliability estimates of BMEPR and transmittance values were better for tones than for chirps. While the precise reason for this disparity remains to be determined, there are several factors that can be investigated in future studies. Consider that a broadband chirp is a continuously changing dynamic waveform in the time domain that is spectrally complex in the frequency domain. Even though the input waveform has a short duration (~5 ms), it is evaluated over a longer time epoch (1 s), such that acoustic reflections from the eardrum can be captured by the probe microphone allowing for computations to be made on the metric-of-interest. With this in mind, single cycles of individual frequencies may be susceptible to interference and/or perturbations from physiologic variables present in a closed ear canal, such as respirations, blood-flow pulsations from surface vessels, spontaneous or evoked otoacoustic emissions, subject movement, cord noise, etc. Either alone or in combination, we speculate that these factors can lead to increased variability in measurement. On the other hand, individual tonal stimuli are repetitive steady-state oscillations and perhaps are less affected by physiologic (state) and subject (trait) variables. Nevertheless, direct comparisons between these two different stimuli may not be possible because of different input characteristics during testing. With tonal stimuli, consider that the number of individual cycles-per-frequency *differ* when stimulus duration is kept constant (300 ms), as is currently performed by this device. In this context, cycles-per-frequency range from 76.92 (258 Hz) to 1818 (6007 Hz) (Figure 4). Also note that variability in the tonal data

shows a tendency to increase with frequencies ≥1992 Hz (Figure 3). We speculate that keeping cycles-per-frequency constant *vs*. keeping duration constant could represent a better strategy for improving reliability. With the present data, a 600 cycle-per-frequency cut-off value would be within the realm of possibilities for consideration.

Ear-specific "profiles" of measurements across frequencies are common place in the field of diagnostic audiology; obvious examples include: audiograms, iso-level/frequency profiles of DPOAEs (aka, DPGrams), tympanograms, and BMEPR profiles. Thus, the problem of assessing reliability is ubiquitous in this field and GT provides a robust solution to this problem. As noted above, we have already applied GT to DPGrams and evaluated the influences of time-of-day, stimulus frequency, stimulus SPL, and gender in adults with normal hearing (Cacace et al., 1996). We found that DPGrams were reliable measures within-subjects over a contiguous 24 hour time period. Significant and reliable differences and interactions across frequency, SPL, and gender were also observed.

Another issue that requires further study concerns which characteristics of a profile might be meaningful clinically and how clinicians/researchers could potentially use this information to improve reliability estimates. As an example, Feeney et al. (2003) and Shahnaz et al. (2009) describe trends associated with middle-ear pathology as alterations in broadband features (e.g., increased low frequency power reflectance associated with otosclerosis). Since broadband changes as in otosclerosis involve lower-order trends, we speculate that it might be useful to fit these profiles with simple functions that capture these trends and smooth over measurement noise. Therefore, trend analysis might be a useful way to model these effects and thereby improve reliability.

However, it remains to be seen if all clinically relevant information would be captured in lower-order trends; we suspect that this would *not* be the case. One alternative is to consider the possibility that "variability" of a profile, made multiple times in the same individual, might represent a pathologic feature. In this context, it would be of interest to determine if high variance in the residual after removing lower-order trends would be associated with clinically useful information. Pathological states of the middle ear that might show such effects include: tympanic membrane perforations, monomeric tympanic membranes secondary to healed perforations, and ossicular discontinuities. Thus, further work in this area will be necessary to assess this hypothesis.

Based on the arguments presented herein and with respect to current clinical usage, profile analysis of BMEPR values appears to be the most relevant metric for evaluating and diagnosing middle-ear disorders. In contrast to tympanometry, which typically uses only one (226 Hz) or perhaps only a few specific probe-tone frequencies (e.g., 226 Hz, 660 Hz, 1200 Hz) to estimate characteristics of middle-ear function, power-reflectance techniques can rapidly measure hundreds of points over a much broader bandwidth and in a considerably shorter period of time(seconds) . This is noteworthy because it allows for a more comprehensive account of energy transfer characteristics of the middle ear than is currently available from other methods. Combined with computer-controlled hardware and based on rapidity of measurement, BMEPR has many desirable attributes consistent with a viable clinical tool. Therefore, improving reliability of measurement is an essential requisite in the evolution of this method if it is to transition effectively from the laboratory to the clinic.

In conclusion, reliability of BMEPR measurements is an important consideration

in establishing this method for clinical decision making. The application of GT allows for a more comprehensive evaluation of these types of data in comparison to other approaches and we advocate for the strategic use of this metric in future investigations.

Acknowledgments

Data were collected by MJM and MSC as part of a capstone research project for satisfying the Doctor of Audiology degree; SR analyzed the tonal data, as part of a separate research project. Portions of this work were presented as a poster at the annual meeting of the American Auditory Society, March 5, 2010, Scottsdale, Az and at the annual Michigan-Toledo P30 Post-ARO Podium and Poster Meeting, sponsored by the Kresge Hearing Research Laboratory, University of Michigan, March 30, 2010. We also thank Dr. Robert H. Margolis for constructive comments and suggestions.

There are no conflicts of interest associated with this paper.

References

Allen, J. B., Jeng, P. S., & Levitt, H. (2005). Evaluation of human middle ear function via an acoustic power assessment. Journal of Rehabilitation Research and Development 42, 63-78.

Beers, A. N., Shahnaz, N., Westerberg, B. D., & Kozak, F. K. (2010). Wideband reflectance in normal Caucasian and Chinese school-aged children and in children with otitis media with effusion. Ear and Hearing 31, 221-233.

Broglio, A. T. C., Zhu, W., Sopiarz, K., & Oark, Y. (2009). Generalizability theory analysis of balance error scoring system reliability in healthy young adults. Journal of Athletic Training 44, 497-502.

Cacace, A. T., McClelland, W. A., Weiner, J., & McFarland, D. J. (1996). Individual differences and the reliability of 2F1-F2 distortion-product otoacoustic emissions: Effects of time-of-day, stimulus variables, and gender. Journal of Speech and Hearing Research 39, 1138-1148.

Cicchetti, D. V. (1994). Guidelines, criteria, and rules of thumb for evaluating normed and standardized assessment instruments in psychology. Psychological Assessessment 6, 284-290.

Crocker, L., & Algina, J. (1986). Introduction to Classical and Modern Test Theory. New York: Harcourt Brace.

Cronbach, L. J., Gleser, G. C., Nanda, H., & Rajaratnam, N. (1972). The Dependability of Behavioral Measurements: Theory of Generalizability for Scores and Profiles. New York: John Wiley.

Cronbach, L. J., Nageswari, R., & Gleser, G. C. (1963). Theory of generalizability: A

liberation of reliability theory. British Journal of Statistical Psychology 16, 137-163.

Demorest, M. E., & Bernstein, L. E. (1992). Sources of variability in speechreading sentences: a generalizability analysis. Journal of Speech and Hearing Research, 35, 876-891.

Di Nocera, F., Ferlazzo, F., & Borghi, V. (2001). G theory and the reliability of psychophysiological measures: A tutorial. Psychophysiology 38, 796-806.

Feeney, M. P., Grant, I. L., & Marryott, L. P. (2003). Wideband energy reflectance measurements in adults with middle-ear disorders. Journal of Speech, Language, and Hearing Research 46, 901-911.

Feeney, M. P., Grant, I. L., & Mills, D. M. (2009). Wideband energy reflectance measurements of ossicular chain discontinuity and repair in human temporal bone. Ear and Hearing 30, 391-400.

Hunter, L. L., Tubaugh, L., Jackson, A., & Propes, S. (2008). Wideband middle ear power measurement in infants and children. Journal of the American Academy of Audiology 19, 309-324.

Jeng, P. S., Allen, J. B., Lapsey-Miller, J. A., & Levitt, H. (2008). Wideband power reflectance and power transmittance as tools of assessing middle-ear function. Perspectives on Hearing and Hearing Disorders in children, 44-57.

Jerger, J., Jerger, S., & Mauldin, L. (1972). Studies in impedance audiometry. Normal and sensorineural ears. Archive of Otolaryngology 96, 513-523.

Keefe, D. H., & Simmons, J. L. (2003). Energy transmittance predicts conductive hearing loss in older children and adults. Journal of the Acoustical Society of America

114, 3217-3238.

Laenen, A., Vangenneugden, T., Geys, H., & Molenberghs, G. (2006). Generalized reliability estimation using repeated measures. British Journal of Mathematical and Statistical Psychology, 59, 113-131.

Margolis, R. H., Van Camp, K. J., Wilson, R. H., & Creten, W. L. (1985). Multifrequency tympanometry in normal ears. Audiology 24, 44-53.

Maxwell, D. L., & Satake, E. (2006). Research and Statistical Methods in Communication Sciences & Disorders. Canada: Thomson Delmar Learning.

Mushquash, C., & O'Connor, B. (2006). SPSS and SAS programs for Generalizability theory analysis. Behavioral Research Methods 38, 542-547.

O'Brian, N., O'Brian, S., Packman, A., & Onslow, M. (2003). Generalizability Theory I: Assessing reliability of observational data in the communication sciences. Journal of Speech, Language, and Hearing Research 46, 711-717.

O'Brian, S., Packman, A., Onslow, & O'Brian, N. (2003). Generalizability Theory II: Application to perceptual scaling of speech naturalness in adults who stutter. Journal of Speech, Language, and Hearing Research 46, 718-723.

Roebroeck, M. E., Hariaar, J., & Lankhors, G. J. (1993). The application of generalizability theory to reliability assessment: An illustration using isometric force measurements. Physical Therapy 73, 386-395.

Rosowski, J. J, Nakajima, H. H., Hamade, M. A., Mahfoud, L., Merchant, G. R., Halpin, C. F., & Merchant, S. N. (2012). Ear-canal reflectance, umbo velocity, and tympanometry in normal-hearing adults. Ear and Hearing 33, 19-34.

Scarsellone, J. M. (1998). Analysis of observational data in speech and language research

using generalizability theory. Journal of Speech, Language, and Hearing Research 41, 1341-1347.

Schiavetti, N., & Metz, D. E. (2006). Evaluating Research in Communicative Disorders, Fifth Edition. Boston: Pearson Education, Inc.

Shahnaz, N., Bork, K., Polka, L., Longridge, N., Bell., & Westerberg, B. D. (2009). Energy reflectance and tympanometry in normal and otosclerotic ears. Ear and Hearing 30, 219-233.

Shahnaz, N., Longridge, N., & Bell, D. (2009). Wideband energy reflectance patterns in preoperative and post-operative otosclerotic ears. International Journal of Audiology 48, 240-247.

Thornton, A. R. D., Marotta, N., & Kennedy, C. (2003). The order of testing effect in otoacoustic emissions and its consequences for sex and ear differences in neonates. Hearing Research 184, 123-130.

Van Camp K. J., Margolis, R. H., Wilson, R. H., Creten, W. L., & Shanks, J. E. (1986). Principles of Tympanometry. American Speech and Hearing Association Monograph 24, 1-88.

Van de Geld, P. A., Oosterveld, P., van Waas, M. A., Kuijpers-Jaqtman, A. M. (2007). Digital videographic measurement of tooth display and lip position in smiling and speech: reliability and clinical application. American Journal of Orthodontics and Dentofacial Orthopedics 131, e1-8.

Vander Werff, K., Prieve, B., & Georgantas, L. (2007). Test-retest reliability of wideband reflectance measures in infants under screening and diagnostic test conditions. Ear and Hearing 28, 669-681.

Vanhuyse, V. J., Creten, W. L., & Van Camp, K. J. (1975). On the W-notching of tympanograms. Scandinavian Audiology 4, 45-50.

Werner, L. A., Levi, E. C., & Keefe, D. H. (2010). Ear-canal wideband transfer functions of adults and two- to nine-month-old infants. Ear and Hearing 31, 1-12.

Figure legends.

Figure 1. Grand averaged frequency-reflectance profiles for chirps and tonal stimuli. Data were collapsed across age, gender, and ear. Note: that for the last point on the graph, frequencies were different for chirp and tonal stimuli (chirp = 5039 Hz; tone = 6000 Hz) but were aligned for comparison purposes only.

Figure 2. Composite scatter plots for 16 frequencies for different variables studied. Data collected from Test 1 is plotted on the y-axis and data collected from Test 2 is plotted on the x-axis. If the within-session data from Test 1 and Test 2 were identical for each of the different frequencies, then data points would fall directly on the solid-diagonal line in each of the plots. Based on the scatter of data points observed, the degree of within-session variability appears rank ordered from low, mid, to higher frequencies. The figure legend along the side of the graph identifies all relevant variables by different symbols.

Figure 3. Composite scatter plots for 9 frequencies for different variables studied. Data collected from Test 1 is plotted on the y-axis and data collected from Test 2 is plotted on the x-axis. The figure legend along the side of the graph identifies all relevant variables by different symbols.

Figure 4. Plot of cycles per duration (y-axis) of individual tonal frequencies (x-axis, log base 10) where stimulus duration is kept constant at 300 ms. Based on the period of the individual frequency oscillations used to measure BMEPR, the cycles per duration increase substantially from 258 Hz to 6000 Hz.

Figure 5. Examples of tests with differing generalizability coefficients. In both plots each of three subjects' scores on four test sessions is represented by a line. The main effect of subjects represents the variance in the average difference between subjects. This is large

when the profiles are parallel. The interaction between subjects and sessions represents the extent to which the ordering of subjects varies across sessions. This is large when the profiles are non-parallel. In A, the three subjects perform relatively consistently across the four test sessions. As a result the main effect of subjects is large relative to the interaction between subjects and test sessions. In B, the three subjects perform inconsistently across the four test sessions. As a result, the main effect of subjects is small relative to the interaction between subjects and test sessions.

Table captions.

Table 1. Summary of example "thought experiment" of power reflectance at 1500 Hz in the right ear for 56 subjects tested on two occasions. Columns represent measures obtained from a standard ANOVA summary table; column 1 = source, 2 = degrees of freedom (df), 3 = sums of squares (SS), 4 = mean square, (MS), 5 = estimated mean square (EMS), 6 = subjects pooled, 7 = subject single test.

Table 2. Summary of test-retest Pearson's Product Moment Correlation Coefficients by frequency and ear for chirps and tones. Levels of significant correlations are represented by an asterisk, where: * = $p \leq 0.05$; ** = $p \leq 0.01$.

Table 3. Summary of generalizability coefficients for power reflectance and transmittance for chirps: where: ρ^2 values represent the proportion-of-the-variance in subject effects that was consistent across tests.

Table 4. Summary of generalizability coefficients for power reflectance and transmittance for tones: where: ρ^2 values represent the proportion-of-the-variance in subject effects that was consistent across tests.

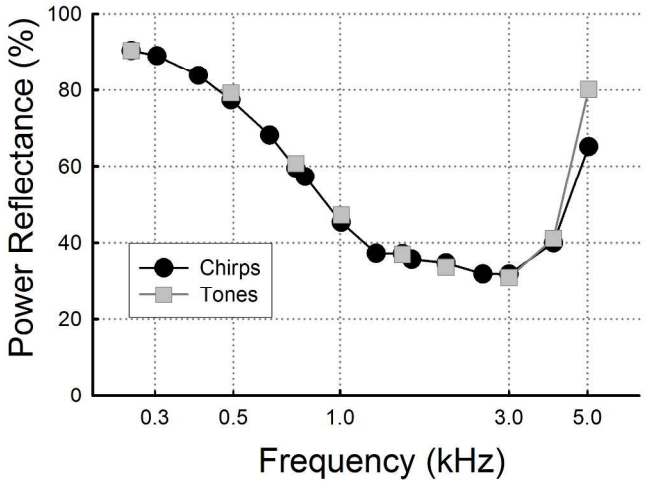

215x278mm (300 x 300 DPI)

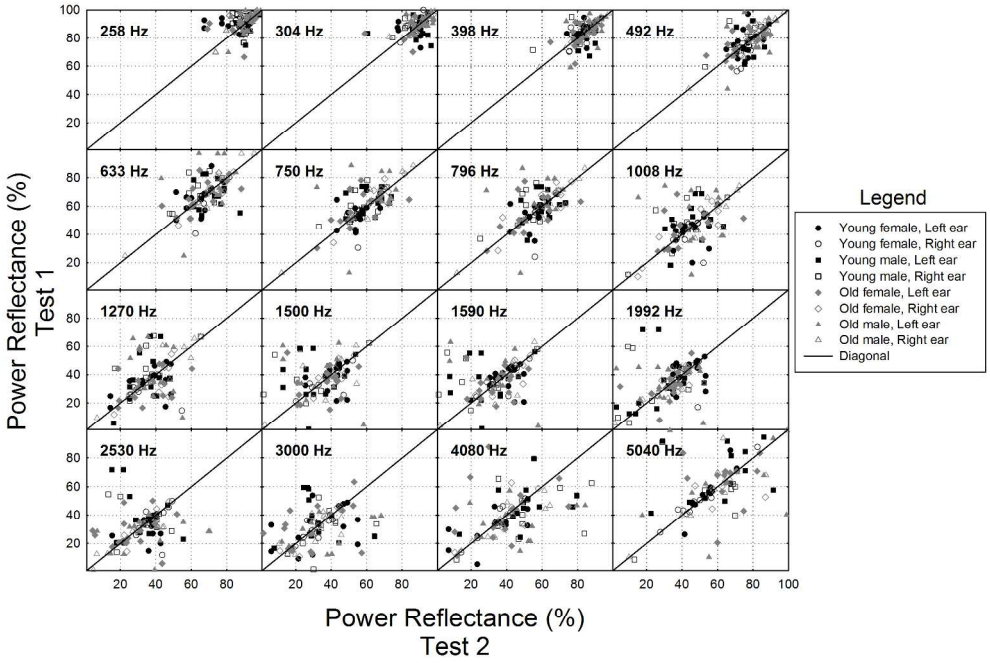

279x215mm (300 x 300 DPI)

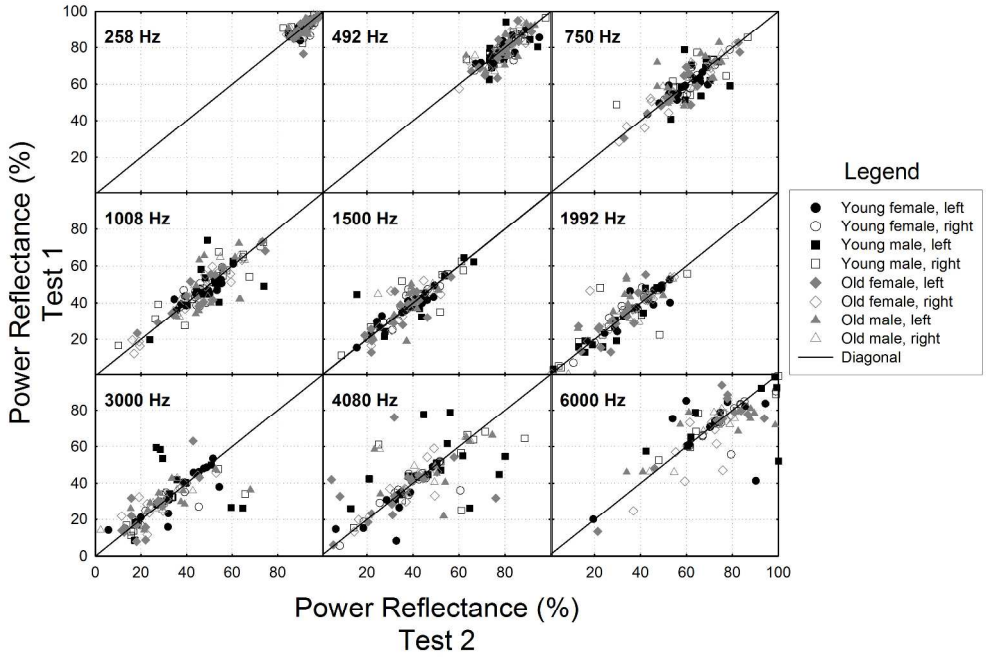

279x215mm (300 x 300 DPI)

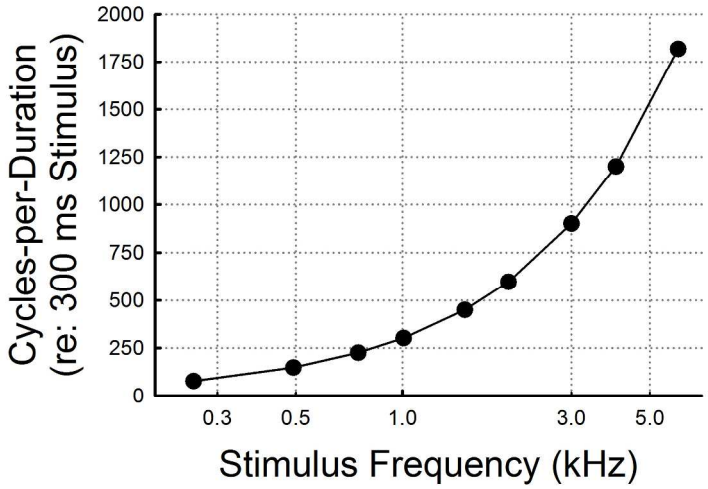

215x278mm (300 x 300 DPI)

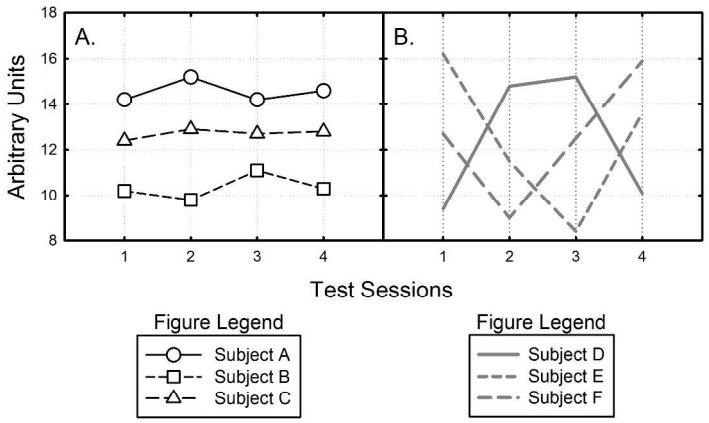

279x215mm (300 x 300 DPI)

Table 1.

1) Source	2) df	3) SS	4) MS	5) EMS	6) Subjects pooled	7) Subjects single test
a) Time	1	13.99	13.99			
b) Subjects	55	14794.53	268.99	$\sigma^2_{err} + k\sigma^2_{subj}$	0.917	0.847
c) Time x Subjects	55	1224.78	22.27	σ^2_{err}		

Table 2

Pearson's r Correlations for Chirps and Tones

Chirps			**Tones**	
Frequency (Hz)	**Left ear**	**Right ear**	**Left ear**	**Right ear**
257	0.24	0.50**	0.75**	0.66**
304	0.17	0.70**		
398	0.44**	0.83**		
492	0.52**	0.83**	0.78**	0.83**
632	0.50**	0.85**		
750	0.60**	0.85**	0.82**	0.87**
796	0.57**	0.82**		
1007	0.53**	0.81**	0.82**	0.92**
1265	0.44**	0.69**		
1500	0.30*	0.60**	0.52**	0.85**
1593	0.34**	0.64**		
1992	0.55**	0.61**	0.58**	0.87**
2531	0.31*	0.63**		
3000	0.38**	0.73**	0.67**	0.84**
4007	0.51**	0.66**	0.64**	0.78**
5039	0.26	0.72**	0.79	0.89**

Table 3.

Chirp Generalizability for Reflectance and Transmittance

		Reflectance			Transmittance	
Effect/Error	**MS**	**ρ^2**	**Std Err**	**MS**	**ρ^2**	**Std Err**
Subjects	2360.880	0.8196	0.0241	55.95144	0.7788	0.0296
Subjects x Time	260.713			6.95624		
Subjects x Frequency	291.408	.5621	0.0585	18.49421	0.4771	0.0699
Subjects x Frequency x Time	81.681			6.54339		
Subjects x Ear	609.427	.3877	0.0818	11.19549	0.2581	0.0991
Subjects x Ear x Time	268.925			6.60240		
Subjects x Ear x Frequency	108.633	.3484	0.0871	6.98064	0.0133	0.1319
Subjects x Ear x Frequency x Time	52.494			6.79778		

Table 4.

Tone Generalizability for Reflectance and Transmittance

		Reflectance			Transmittance	
Effect/Error	**MS**	**ρ^2**	**Std Err**	**MS**	**ρ^2**	**Std Err**
Subjects	988.5041	0.8546	0.0194	10.39252	0.8505	0.0200
Subjects x Time	77.5189			0.83962		
Subjects x Frequency	258.4342	0.7218	0.0372	3.06893	0.7888	0.0282
Subjects x Frequency x Time	41.7633			0.36238		
Subjects x Ear	321.4741	0.7541	0.0315	4.30111	0.7114	0.0386
Subjects x Ear x Time	42.9896			0.72534		
Subjects x Ear x Frequency	100.8526	0.6296	0.0495	0.83801	0.5346	0.0622
Subjects x Ear x Frequency x Time	22.9267			0.25412		

Appendix A.

The conceptual basis of GT requires a detailed understanding of repeated measures ANOVA; tutorial and computational methods are available to assist the clinician or researcher in this regard (see Di Nocera, Ferlazzo, & Borghi, 2001; Mushquash & O'Connor, 2006). However, we caution that there is no simple "cookbook" approach to data analysis with GT. This is due in part to the many designs features that are possible within a given experimental framework. Thus, as would be the case for any experimental design using ANOVA, it will depend on the complexity of the experiment and the statistical model being utilized.

In Figure 5, two hypothetical cases involving four test sessions in three subjects are shown in diagrammatic form. The figure illustrates a case where the relative ranking of each subjects' test scores is consistent across test sessions (Panel A). In this case, the main effect of subjects is large relative to the interaction between subjects and test sessions. In a second case, the ranking of the subjects' test scores varies considerably across test sessions (Panel B). This results in a large interaction between subjects and test sessions relative to the main effect of subjects. The generalizability coefficient is a ratio of the main effect of subjects to the sum of that main effect and the interaction between subjects and test sessions. Thus, this ratio would be much larger in the first case than in the second.

The metric used in GT is expressed as the proportion of the total variance due to subjects that is common to the testing occasions of interest. For a single measure determined on two testing occasions, this can be computed as Pearson's *r*; for *k* testing occasions, it is computed as:

$$\rho^2 = \sigma^2_{subj} / (\sigma^2_{subj} + \sigma^2_{err}) \quad \text{Equation 1)}$$

where: σ^2_{subj} is the variance due to the main effects of subjects and σ^2_{err} is the variance due to error (i.e., the non-additive or inconsistency effect of subjects across testing occasions).

As a relevant example, we present a "thought experiment" whereby the reliability of middle ear power reflectance is assessed at 1500 Hz for the right ear on two occasions. Here, our sample consists of 56 adults without a history of middle-ear disease. Results from the ANOVA are depicted in Table 4. The values shown in Columns 1 through 4 can be obtained from many statistical programs that are commercially available in the marketplace (e.g., Statistical Analysis System, SAS; Statistical Package for the Social Sciences, SPSS; Statistica, etc.). Statistical programs such as these report F-values and probability estimates (p-values) associated with the effects of time of testing and their significance. The F-value is simply the ratio of the mean square values from Rows A and C in Column 4. In this example, the p-value is not significant ($p>0.05$; result not shown).

The expected mean square (EMS) for the effects of subjects is:

$$EMS_{subj} = k\sigma^2_p + \sigma^2_{err} \quad \text{Equation 2)}$$

after Crocker and Algina (1986). The mean square for subject's represents the variance summed over all testing occasions and associated error. The EMS for the error is $MS_{time \times subj}$ and represents the non-additive effect of subjects over time (i.e., the effect of test

sessions); often computed as the residual in this design, see below:

$$\sigma^2_{subj} = (MS_{subj} - MS_{err})/k \quad \text{Equation 3)}$$

A pooled estimate of the proportion of the variance in subject scores that is consistent across time (additive) can be obtained by the equation:

$$\rho^2_{pooled} = (MS_{subj} - MS_{err}) / (MS_{subj} - MS_{err}) + MS_{err} \quad \text{Equation 4)}$$

This represents the reliability of a composite of the test scores summed across time and is reported in Column 6, Row B of Table 4. Since we are usually interested in the reliability of single tests, this is computed as:

$$\rho^2 = ((MS_{subj} - MS_{err}) / k) / ((MS_{subj} - MS_{err})/k + MS_{err}) \quad \text{Equation 5)}$$

and takes into account the estimate of single test variance from Equation 3 and is reported in Column 7, Row B.

More complex models that include additional facets that interact with participants can also be constructed. For example, if separate measurements were taken for each ear on several occasions, then an interaction of ear x subjects could be computed. In this case, the model would be:

$$\rho^2 = ((MS_{ear\ x\ subj} - MS_{err}) / ek) / ((MS_{ear\ x\ subj} - MS_{err})/ek + MS_{err}) \quad \text{Equation 6)}$$

where: *e* represents the number of ears and *k* represents the number of test sessions. The MS_{err} is now the value of $MS_{time\ x\ ear\ x\ subj}$. Thus, interactions between subjects and various measures repeated across subjects can be generated by substituting these interaction terms for the main-effect terms in Equation 5. Conceptually, in a model including subjects, ears, and occasions, the Generalizability coefficient associated with the main effects of subjects (MS_{subj}) represents the reliability of a score averaged across ears, while the Generalizability coefficient associated with the ear x subjects interaction, represents the reliability of a score as the difference between the ears. In fact, a wide variety of models can be generated following the logic of the General Linear Model (see Laenen et al., 2006).

Although statistical packages such as SAS, SPSS, or Statistica do not offer explicit tools for computing Generalizability coefficients, the individual MS values are provided in the standard ANOVA summary table for a model including time as a repeated measure (i.e., in within-subject designs). Thus, Generalizability coefficients can be readily computed with just a few simple operations. To aid in these computations, Mushquash and O'Connor (2006) provide a guide for users of SAS, SPSS, or MatLab.

Elsevier Editorial System(tm) for Hearing Research

Manuscript Draft

Manuscript Number:

Title: Left hemisphere fractional anisotropy increase in noise-induced tinnitus: A diffusion tensor imaging (DTI) study of white matter tracts in the brain

Article Type: Research paper

Keywords: Tinnitus
Diffusion tensor imaging
MRI
Noise induced hearing loss

Corresponding Author: Dr. Anthony Thomas Cacace, PhD

Corresponding Author's Institution: Wayne State University

First Author: Anthony Thomas Cacace, PhD

Order of Authors: Anthony Thomas Cacace, PhD; Randall R Benson, M.D.; Ramtilak Gattu, M.S.

Abstract: Diffusion tensor imaging (DTI) is a contemporary neuroimaging modality used to study connectivity patterns and microstructure of white matter tracts in the brain. The use of DTI in the study of tinnitus is a relatively unexplored methodology with no studies focusing specifically on tinnitus induced by noise exposure. In this investigation, participants were two groups of adults matched for etiology, age, and degree of peripheral hearing loss but differed by the presence or absence of tinnitus. It is assumed that matching individuals on the basis of peripheral hearing loss, with and without tinnitus, allows for differentiating changes in white matter microstructural changes associated with hearing loss from other potential changes due to the effects of chronic tinnitus. Alterations in white matter tracts using the fractional anisotropy (FA) metric were quantified using tract based spatial statistics (TBSS). Based on the diffusion properties of water, increased FA was observed in individuals with moderate-to-severe noise-induced tinnitus in 9 out of the 10 voxel clusters which differentiated the two groups. These findings were asymmetric, with 7 of 9 voxel-cluster regions showing higher FA values in thalamic, frontal, and parietal white matter of the left hemisphere of the tinnitus group. These foci were localized to the anterior thalamic nuclei and the inferior and superior longitudinal fasciculi. Two right-sided regions with increase FA values were localized to the inferior fronto-occipital fasciculus and superior longitudinal fasciculus. The only decrease in FA in the tinnitus-positive group was found within one voxel cluster in white matter of the superior longitudinal fasciculus in the left parietal lobe.

December 2, 2012

Barbara Conlon, Ph.D.
Editor-in-Chief
Hearing Research

Dear Dr. Conlon,

We wish to submit the paper, "Left hemisphere fractional anisotropy increase in noise-induced tinnitus: A diffusion tensor imaging (DTI) study of white matter tracts in the brain," for consideration of publication in Hearing Research.

The paper represents original work and has not been submitted elsewhere. There are no conflicts of interest.

Thank you for your consideration and we look forward to hearing from you.

Sincerely,

Anthony T. Cacace, Ph.D.
Professor

***Suggested Reviewers**

Reviewers

Pim Vandijk

Fatima Hussain

Jennifer Melcher

Highlights

- Diffusion tensor imaging was used to study white matter tracts in the brain
- Increased fractional anisotropy (FA) was observed 9 out of the 10 voxel clusters
- Increased FA values were found in thalamic, frontal, and parietal white matter
- Only one *decrease* in FA was found in left parietal superior longitudinal fasciculus

Left hemisphere fractional anisotropy increase in noise-induced tinnitus: A diffusion tensor imaging (DTI) study of white matter tracts in the brain

Randall R. Benson[1], Ramtilak Gattu[2], Anthony T. Cacace[3]

[1]Center for Neurological Studies
Novi, MI

[2]Department of Radiology
Wayne State University School of Medicine
Detroit, MI

[3]Department of Communication Sciences & Disorders
Wayne State University
Detroit, MI

Correspondence to: Anthony T. Cacace, Ph.D.
Department of Communication Sciences & Disorders
Wayne State University
207 Rackham, 60 Farnsworth
Detroit, MI 48202
Phone: 313-577-6753
Fax: 313-577-8885
e-mail: cacacea@wayne.edu

Abstract

Diffusion tensor imaging (DTI) is a contemporary neuroimaging modality used to study connectivity patterns and microstructure of white matter tracts in the brain. The use of DTI in the study of tinnitus is a relatively unexplored methodology with no studies focusing specifically on tinnitus induced by noise exposure. In this investigation, participants were two groups of adults matched for etiology, age, and degree of peripheral hearing loss but differed by the presence or absence of tinnitus. It is assumed that matching individuals on the basis of peripheral hearing loss, with and without tinnitus, allows for differentiating changes in white matter microstructural changes associated with hearing loss from other potential changes due to the effects of chronic tinnitus. Alterations in white matter tracts using the fractional anisotropy (FA) metric were quantified using tract based spatial statistics (TBSS). Based on the diffusion properties of water, *increased* FA was observed in individuals with moderate-to-severe noise-induced tinnitus in 9 out of the 10 voxel clusters which differentiated the two groups. These findings were asymmetric, with 7 of 9 voxel-cluster regions showing *higher* FA values in thalamic, frontal, and parietal white matter of the left hemisphere of the tinnitus group. These foci were localized to the anterior thalamic nuclei and the inferior and superior longitudinal fasciculi. Two right-sided regions with increase FA values were localized to the inferior fronto-occipital fasciculus and superior longitudinal fasciculus. The only *decrease* in FA in the tinnitus-positive group was found within one voxel cluster in white matter of the superior longitudinal fasciculus in the left parietal lobe.

Key words: Noise-induced tinnitus, magnetic resonance imaging, diffusion tensor imaging, fractional anisotropy, tract based spatial statistics

Abbreviations

ADHD: attention deficit hyperactivity disorder

CANS: central auditory nervous system

DTI: diffusion tensor imaging

FA: fractional anisotropy

FOF: frontal occipital fasciculus

GABA: gamma-aminobutyric acid

ILF: inferior longitudinal fasciculus

IRTK: image registration tool kit

MNI: Montreal Neurological Institute

MRI: magnetic resonance imaging

MRS: magnetic resonance spectroscopy

mTBI: mild traumatic brain injury

NIHL: noise induced hearing loss

ROI: region-of-interest

SLF: superior longitudinal fasciculus

T: Tesla

TBSS: tract based spatial statistics

THI: tinnitus handicap inventory

1. Introduction

Noise induced hearing loss (NIHL) is a ubiquitous phenomenon observed in modern society (Clark and Bohne, 1999). It is also a prominent concern for individuals serving in the military (Humes et al., 2006) and represents a known risk factor for developing tinnitus (e.g., Dong et al., 2010; Henderson et al., 2011; Yankaskus, 2012). Epidemiological studies indicate that as hearing thresholds exceed the mild range of severity in the better ear at 4.0 kHz, the odds ratio for expressing moderate to severely annoying tinnitus increases from 5 to 27 (Coles, 2000). Other studies confirm this observation by documenting that over 83% of individuals with NIHL have tinnitus (Mazurek et al., 2010). While mechanisms involved in tinnitus expression are not completely known, available evidence suggests that temporary or permanent damage to sensory cells in the inner ear is a known trigger of this phenomenon resulting in temporary or permanent elevations in auditory thresholds, physiological changes in auditory nerve discharge properties (e.g., Liberman and Kiang, 1978; Henderson et al., 2011; Kajawa & Liberman, 2009) and secondary anatomical and physiological effects in the central auditory nervous system (CANS) (e.g., Morest et al., 1998; Salvi et al., 2000; Syka, 2002; Schreiner and Cheung, 2004). These aforementioned effects suggest that reduced afferent drive from the periphery leads to an imbalance between inhibitory and excitatory inputs to auditory neurons at various levels in central auditory pathways (e.g., Middleton et al., 2010; Wang, Brozoski, and Caspary, 2011; Brozoski et al., 2012; Browne et al., 2012; Godfrey et al., 2012). This alteration in neurobiochemical equilibrium is thought to destabilize circuits in the brainstem and cortex resulting in plastic readjustments attempting to compensate for this disparity (e.g., Eggermont and Roberts, 2004; Roberts et al., 2010). Either alone or in combination, neuronal hyperactivity, bursting discharges, and increased cortical or brainstem/diencephalic neural synchrony are

thought to be electrophysiological counterparts that result in the perception of tinnitus (e.g., Dong et al., 2010; Henderson et al., 2011; Kaltenbach 2011; Brozoski et al., 2012). Interestingly, while excessive noise exposures can produce anatomical, physiological, and biochemical changes in peripheral and central auditory pathways, not all individuals with NIHL or other otopathologies develop tinnitus (e.g., Lockwood et al., 2002). Indeed, the precise reasons for this discrepancy remain unknown.

To better understand the neurobiology of noise-induced tinnitus and evaluate its relationship to white matter changes in the brain, diffusion-tensor imaging (DTI) was used as a platform for discovery. Diffusion-tensor imaging represents a neuroimaging modality that can provide insight into plastic/reactive changes in white matter microstructure and connectivity associated with tinnitus that cannot be detected by conventional magnetic resonance imaging (MRI). Specifically, this imaging modality measures the displacement of water molecules (diffusion) along white matter tracts, providing information on the microstructure of cerebral white matter and thus serves as a surrogate biomarker of tissue integrity (e.g., Ling et al., 2012). For each voxel under consideration, DTI estimates diffusion in terms of the axes (eigenvectors) of an ellipsoid, separated into one major and two minor axes, each being orthogonal to the primary eigenvector. The most prominent metric to quantify these effects is fractional anisotropy (FA); a normalized scalar that represents the fraction of the tensor that can be assigned to anisotropic diffusion. Herein, we focus on FA, because it provides information about the degree of fiber organization and integrity; yielding values between 0 and 1, where: 0 represents unrestricted or “isotropic” diffusion, such as is found in the CSF, and 1 represents “anisotropic” or restricted diffusion due to barriers, such as is found in organized white matter fibers.

To date, use of DTI in tinnitus research is limited to a small number of studies with mixed results (e.g., Yoo et al., 2006; Lee et al., 2007; Crippa et al., 2010; Husain et al., 2010; Aldhafeeri et al., 2012). Therefore, to enhance understanding in this area, improve the specificity of results and to help distinguish white matter changes due to pathologic plasticity associated with noise-induced tinnitus, two groups of individuals *with* and *without* tinnitus were studied.

2. Methods

Two groups of adults with a common history of occupational, recreational, or military noise exposure, *with* and *without* tinnitus, matched for degree/severity of hearing loss and age were evaluated. Participants were recruited from newspaper ads, referrals from medical and/or allied health professionals in the greater Detroit metropolitan area (i.e., otolaryngologists, neurologists, audiologists) and from word-of-mouth. Group 1 consisted of adults with NIHL *without* tinnitus (n =13, mean age 58 years, range 22 to 88 years); Group 2 consisted of adults with NIHL *with* tinnitus (n =13, mean age 54 years, range 28 to 80 years). Our selection criteria was based on the assumption that homogeneous groups of individuals with similar etiologies will improve biomarker specificity and that matching groups with respect to as many relevant factors as possible, will be beneficial to enhance understanding of this condition.

Inclusion criteria: All participants with tinnitus were required to have chronic/constant tinnitus over at least the prior 6-month period and score in the moderate or higher range of severity on the Tinnitus Handicap Inventory (THI score; $\geq$35) (Newman et al., 1996; also see Newman and Sandridge, 2004 for severity score criteria).

Exclusion criteria: Documented history of blast exposure, retro-cochlear or neurologic disease (e.g., auditory nerve and/or skull-base tumors, brain tumors, strokes, demyelinating

disease, etc.), active use of GABAergic agonist medications, and/or other pharmaceutical compounds used to treat depressive illness.

This study was approved by the Human Investigation Committee of Wayne State University and signed informed consent was obtained from each individual prior to data collection.

2.1 Procedures

Audiologic testing

Audiometric testing was conducted in a commercial sound booth (Acoustic Systems, Austin, Texas; Model RE-144) using a clinical audiometer (Grason-Stradler, model 61) with standard earphones (Telephonics, TDH-50P) enclosed in supra-aural ear cushions (MX-41/AR). Pure-tone air-conduction audiometry was performed at octave frequencies from 0.25 through 8.0 kHz and also at one half-octave frequency (3.0 kHz) bilaterally. Bone conduction testing used a standard oscillator (Radioear B-71) and headband; bone-conduction thresholds were assessed at octave frequencies from 0.25 through 4.0 kHz. Additionally, if any of the participants had audiological testing performed within 3 months of enrollment in the study by an ASHA certified, state licensed, or Veterans Administration audiologist, then, this type of testing was not repeated.

2.2 DTI image acquisition

Magnetic resonance imaging data were collected at the MR Research Facility of Wayne State University located at Harper Hospital of the Detroit Medical Center. For data acquisition, a 3 Tesla (T) Siemens MAGNETOM Verio scanner employing a 32-channel head coil with diffusion-sensitizing gradients applied in 20 non-collinear directions was utilized. Diffusion tensor imaging data was acquired with a diffusion-weighted single shot spin-echo EPI sequence,

where: TR = 7400 ms, TE = 106 s, flip angle = 90^{o}, in-plane resolution = 2 x 2 mm^2, slice thickness = 3 mm and NEX = 2.

2.3 DTI image processing

DTI Studio (Jiang et al., 2006) (https://www.dtistudio.org/) was used. All individual images were visually inspected to discard slices with motion artifacts, after which the remaining images were added for each slice. The pixel intensities of the multiple diffusion-weighted images were then fitted to obtain the six elements of the symmetric diffusion tensor. The diffusion tensors at each pixel were diagonalized to obtain pixel eigenvalues and eigenvectors. Fractional anisotropy maps of the diffusion tensor were obtained for additional analyses.

2.4 Voxel-based analysis using tract-based spatial statistics.

For whole brain voxel-wise analysis of FA, tract-based spatial statistics (TBSS) (Smith et al., 2006) was used. This is part of the Oxford Center for Functional Magnetic Imaging of the Brain (FMRIB) Software Library (FSL), which is a compendium of computer programs containing image analysis and statistical procedures for evaluating functional, structural, and diffusion MRI data of the brain (Smith et al., 2004; also see (http://www.fmrib.ox.ac.uk/fsl/). Fractional anisotropy maps from each individual were co-registered using the nonlinear image registration tool kit (IRTK) (Rueckert et al., 1999) (www.doc.ic.ac.uk/~dr/software) to a single subject. After image registration, FA maps were averaged to produce a group mean FA image. A skeletonization algorithm was applied to the group mean FA image to define a group template of the lines of maximum FA, thought to correspond to centers of white matter tracts. Fractional anisotropy values for each participant were then projected onto the group skeleton template by searching along perpendiculars from the skeleton to find local maxima. Voxel-wise analyses of FA across the group of subjects were performed only on data projected onto the skeleton

template (which is recruited from the nearest tract center in each subject's image). Comparison of white matter microstructural differences between the two groups which differed by presence of tinnitus used a voxel-wise permutation-inference analysis (5,000 permutations); this is part of TBSS. Other parameters included an FA minimum threshold of 0.3 to avoid partial volume effects with gray matter and a voxel-wise lower threshold of $t = 3$ for cluster analysis to detect regional group differences.

3. Results

3.2 Audiograms

Figure 1 shows audiograms of the tinnitus and non-tinnitus groups, matched for degree of hearing loss. On average, pure tone hearing sensitivity was in the normal range from 0.25 to 2.0 kHz and increased in severity from 3.0 to 8.0 kHz. Loss of pure tone hearing sensitivity was bilateral, generally symmetric, and ranged from mild to severe. In all cases, hearing loss was sensorineural in nature. Top panels (A and B) show pure-tone audiograms for individuals with NIHL *without* tinnitus; bottom panels (C and D) show pure-tone audiograms for individuals *with* NIHL with tinnitus. The degree and configuration of hearing loss did not differentiate those with and without tinnitus. To reiterate, we assumed that by controlling for degree of hearing loss, differences in white matter FA between groups would be attributed to tinnitus-related effects.

3.3 Imaging

While global white matter FA did not differ significantly between groups ($t = 2.06$, $p>0.05$), there were 9 regions which showed significantly increased FA for the tinnitus positive (+) group ($p<0.0001$) (see Figure 2A; Table 1, red). The majority (7 of 9) were left-sided, including five regions localized to left anterior thalamic radiations, one in the superior longitudinal fasciculus (SLF), and one in the inferior (ILF). The two right-sided regions were

localized to the inferior fronto-occipital fasciculus (FOF) and SLF. In contrast, only a single region in the SLF in the left parietal lobe (Figure 2B; Table, blue) showed *reduced* FA [MNI_{xyz} = 125, 90, 96].

4. Discussion

The major findings in this study were the presence of foci of *increased* anisotropic diffusion in the white matter in a group of individuals with moderate-to-severe noise-induced tinnitus compared with a similar group of individuals without tinnitus. These white matter foci were asymmetric and localized predominantly to the left anterior thalamic radiations and the superior and inferior longitudinal fasciculi of the left hemisphere. Decreased FA was observed in only a single region localized to the superior longitudinal fasciculus of the left parietal lobe. These neuroanatomical findings and their connectivity patterns suggest a specific role of the anterior thalamic radiations, the superior and inferior longitudinal fasciculi in noise-induced tinnitus. Anterior thalamic radiations project to the frontal lobe (anterior cingulate cortex) and primary auditory cortex; the superior longitudinal fasciculi project from the occipital area to fronto-temporal and fronto-parietal regions in a bidirectional manner, and the inferior longitudinal fasciculi interconnect occipital with ipsilateral temporal lobes (e.g., Catani et al., 2002; Makris et al., 2005). While these specific white-matter tracts can be considered default pathways when viewed in the context of cortical connectivity of the normal brain, the pathological changes observed in FA may be consistent with a fronto-parietal-cingulate network of brain activations observed in highly distressed people with tinnitus (Golm et al., 2012) and/or as part of a more generalized fear/anxiety/emotion network (Etkin et al., 2011).

Recent neurobiochemical data in rats with behavioral evidence of tinnitus induced by noise exposure is illuminating with respect to understanding our results. Using high-field proton

(^{1}H) magnetic resonance spectroscopy (MRS), Brozoski et al. (2012) showed a down-regulation of the neurotransmitter gamma-aminobutyric acid (GABA) at the level of the thalamus and an up-regulation of glutamate in the dorsal cochlear nucleus and in primary auditory cortex. Accordingly, these "bidirectional" alterations in glutamate and GABA may reflect large-scale changes in excitatory and inhibitory neurotransmission, respectively, that may underlie the generation and then maintenance of noise-induced tinnitus (Brozoski et al., 2012; also see Kaltenbach, 2011 for a review). The increased FA in the thalamic radiations found in our study is likely the downstream consequence of these local changes in synaptic activity which over time lead to increases or decreases in connectivity (neuroplasticity) in response to acoustic trauma (e.g., Mulders and Robertson, 2011; Mulders et al., 2011).

While the axonal morphological changes underlying increased FA in noise-induced tinnitus remain unknown, increases in FA have been related to increased myelination, decreased axonal diameter, decreased axonal branching and increased packing density of white matter fibers (Beaulieu, 2002). In addition to results found in the current study, increased and decreased FA values have been reported in other disorders of the brain, including: Williams (aka, Williams-Beuren) syndrome (Hoeft et al., 2007; Arlinghaus et al., 2011; Haas and Reiss, 2012), juvenile myoclonic epilepsy (Keller et al., 2011), cryptogenic temporal-lobe epilepsy (Rugg-Gunn et al., 2001), recurrent psychomotor seizures (Gerdes et al., 2012), Huntington's disease (Klöppel et al., 2008; Doudaud et al., 2009), pantothenate kinase-associated neurodegeneration formerly known as Hallervorden-Spatz disease (Awasthi et al., 2010), brain tumors (e.g., gliomas) associated with hemorrhage (Harris et al., 2006), attention deficit hyperactivity disorder (ADHD) (Li et al., 2010), developmental and adult-onset stuttering (Chang et al., 2010), bipolar disorder (Versace et al., 2008), and mild traumatic brain injury (mTBI) (Gattu et al., 2012; Ling et al., 2012). The

plethora of neurologic and behavioral disorders associated with FA abnormalities suggests that FA is likely a local marker of aberrant neural connectivity. Whether causally related to the functional abnormalities or the secondary effect of synaptic alterations may vary by the specific disorder. In the case of noise-induced tinnitus, it is likely that CNS alterations in FA reflect a new steady state of functional and anatomical connectivity induced by peripheral end organ induced damage/deafferentation.

What makes Williams syndrome unique in this regard is the fact that auditory abnormalities are a prominent feature in conjunction with other medical issues[1]. In addition to increased FA values in white matter tracks in Williams syndrome reported by Hoeft et al. (2007), well described auditory anomalies such as hyperacusis (Levitin et al., 2005; Attias et al., 2008; Matsumoto et al., 2011; Elsabbagh et al., 2011), auditory allodynia (Levitin and Bellugi, 1998; Levitan et al., 2003; Levitan et al., 2005; Miani et al., 2001; Nigam and Samuel, 1994), dysfunction of the olivocochlear efferent system (Attias et al., 2008) and structural anomalies of auditory cortical structures have been reported. These cortical anomalies include reduced volume and altered sulcal morphology of the Sylvian fissure, atypical cytoarchitecture in Heschl's gyrus, and increased volume of the superior temporal gyrus (Eckert et al., 2006; Holinger et al., 2005; Reiss et al., 2004). Interestingly, the auditory system anomalies are similar to those observed in individuals with tinnitus.

In Williams syndrome, increased FA has been observed in the superior and inferior longitudinal fasciculi of the right hemisphere (Hoeft et al., 2007). While the mechanism(s) for

[1] Williams-Beuren syndrome is a multisystem neurodevelopmental genetic disorder with clinical features that include: ear, nose, and throat, cardiovascular, endocrine, dental, gastrointestinal/weight related, genitourinary, and other miscellaneous features (see Pober, 2010 for a medical systems overview). Neuropsychological/cognitive features often show deficits in visual-spatial processing, processing of human faces, lack of fear of strangers, inappropriate friendliness, preserved language abilities, interest and potential aptitude in musical abilities.

increased FA is uncertain, there is indirect linkage to increased packing density in other brain areas associated with this syndrome, such as a laminar-specific area of visual cortex (IVcß). This observation was also associated with an increased expression of small caliber "parvocellular" neurons in this and other sub-layers of the visual cortex, including: IVA, IVcα, IVcß, V, and VI (e.g., Galaburda et al., 2002). In addition to increased expression of parvocellular neurons and increased packing density in laminar-specific areas of visual cortex, individuals with Williams syndrome also have smaller than normal brains. Thus, when viewed together, these findings may help to explain abnormalities in white-matter microstructure and connectivity patterns noted above (e.g., Schmitt et al., 2001; Jernigan and Bellugi, 1990; Reiss et al., 2000).

A related perspective in this regard is the recent functional magnetic resonance imaging (*f*MRI) study of Gu et al. (2011) in individuals with tinnitus. Gu and colleagues found that *f*MRI activations were better correlated with presence of hyperacusis than with tinnitus per se. Therefore, one must consider the possibility that hyperacusis, which is commonly associated with tinnitus (e.g., Baguley, 2003; Baguley and Anderson, 2007), could be related to the altered FA in individuals with noise-induced tinnitus. While hyperacusis was not studied specifically in the current investigation, further scrutiny in this area is warranted.

In epilepsy/seizure-related disorders, Huntington's disease, and hemorrhagic brain lesions secondary to tumors, increased FA values has been linked to alterations in local iron concentration (e.g., Ikeda, 2001; Gerdes et al., 2012; Douaud et al., 2009; Kloppel et al., 2008) particularly within the putamen (Dexter et al., 1991, 1992; Pfefferbaum et al., 2010) where cell atrophy also occurs (Ruocco et al., 2006). Furthermore, in pantothenate kinase associated neurodegeneration, where increases in FA have also been reported, excessive iron accumulation in basal ganglia nuclei (substantia nigra and globus pallidus) but not the putamen is manifest

(Awasthi et al., 2010). Thus, available evidence suggests that local iron deposition influences DTI metrics (Pfeifferbaum et al., 2010; Pal et al., 2011) and could play a role by introducing local field gradients that appear to increase intravoxel anisotropy (Xia et al., 2000). Another explanation is that cellular degeneration may be associated with iron accumulation and with axonal thinning or decreased branching with the latter morphological changes accounting for the FA change.

Using TBSS in adults with bipolar disorder versus controls, Versace and colleagues (2008) found a left/right asymmetry in FA values in the orbital medial prefrontal cortex; where increased FA was observed in the left hemisphere and reduced FA was found in the right hemisphere. The uncinate fasciculus, a white matter track which interconnects the inferofrontal and anterotemporal cortices and regions in the orbital medial prefrontal cortex is directly involved and is thought to be important for mood regulation.

In ADHD, Li et al. (2010) found increased FA in the right frontal lobe which correlated positively with tests of executive function (Stroop test). The authors speculate that hyperplasia of white matter myelin and a lower degree of branching may contribute to increased FA and also to the cognitive deficits found in this disorder. Increases in FA have also been observed in mild traumatic brain injury (mTBI) (Ling et al., 2012). Increased FA has been shown to be time-dependent; Ling et al. (2012) found increased FA for mTBI compared with controls in the semi-acute stage following injury which localized to the genu of the corpus callosum. Gattu et al., (2012) have shown a distinct evolution pattern of FA over three days from increased to decreased in a rodent model where DTI was compared with histopathologic markers of axonal injury. Increased FA in an acute TBI rat Marmarau model was followed by decreased FA during the subacute stage. Lastly, in a DTI study idiopathic developmental stuttering and adult-onset

stuttering, using a region-of-interest (ROI) analysis, Chang et al. (2010) found increased FA in the developmental stuttering group localized to the rolandic operculum of the right hemisphere with a similar trend found in the adult cases. The authors state that the increased FA may result from "compensatory neuroplasticity in response to impairments in the left hemisphere, p. 8."

4.1 DTI and Tinnitus-related Studies

Diffusion tensor imaging studies in adults with tinnitus are few in number and vary by methodology, design, and scope (e.g., Yoo et al., 2006; Lee et al., 2007; Crippa et al., 2010; Husain et al., 2011; Aldhafeeri et al., 2012). Yoo et al. (2006) used DTI to study 10 adults with tinnitus (7 males, 3 women) ranging in age from 27 to 57 years. While preliminary in nature, no details were provided regarding etiologic, medical, audiometric, and/or severity-related details of tinnitus, or whether a control group was used. The authors report only average white matter volume and variability on their DTI images (913.3 $\pm$158.9 cm^3). While a metric for estimating white matter volume could be valuable in evaluating the aging process (Madden et al., 2009), without additional details, it remains uncertain how these findings contribute to understanding mechanisms of tinnitus. Lee et al. (2007) used DTI to study adults with mild-to-severe hearing loss and tinnitus (n = 28; 11 female, 17 males; age range 22 to 70 years) and compared results to a group of "normal hearing" younger controls (n = 12; 6 males, 6 females; age range 22 to 34 years). While they indicated that 12 had left-sided tinnitus for a duration of 1 to 8 years (mean duration 3 years), details regarding etiology were not provided. In comparison to the control group, Lee et al. (2007) found significant *reductions* in FA in the left frontal and right parietal arcuate fasciculus. However, because the control group was not matched for hearing loss or age, it would be difficult to differentiate white matter changes due to tinnitus from changes due to

hearing loss or age effects. Thus, these findings are indeterminate with respect to tinnitus-related dysfunction.

Crippa and colleagues (2010) used ROI analysis and probabilistic tractography as methods to study DTI changes in tinnitus. In theory, this latter method is of interest because it might allow investigators to resolve dominant and non-dominant (crossed) fiber tracts in their ROI analysis scheme and thus help to isolate white matter fiber connections in classical (inferior colliculus to auditory cortex) and non-classical (auditory cortex to amygdala) auditory pathways. Their approach was partially successful in that a subpopulation of participants showed a right lateralization of increased FA values in the tinnitus group which they describe as "an increased patency of the white matter tracts between the auditory cortex and the amygdala in tinnitus patients as compared to healthy controls, p. 16."

Husain and colleagues (2011) were unable to detect differences in FA in adults with tinnitus (n = 8) in comparison to age and hearing loss-matched controls without tinnitus (n = 7). Possible reasons for their negative results include: a small sample size, heterogeneity of etiology of hearing loss and/or tinnitus, and the fact that the average severity rating of tinnitus in their sample was in the "mild" range.

Aldafeeri et al. (2012) studied cortical and white matter FA and diffusivity in volunteers with normal hearing (n = 14; 9 males, 5 females; age range 30 to 60 years, mean age 46.5 years) and participants with tinnitus and hearing loss, described as no worse than 40 dB HL at 2.0 kHz and 60 dB HL at 4.0 kHz (n = 14, 8 males, 6 females, 30 to 60 years of age, mean age 49.5 years. Whereas cortical thickness was found to negatively correlate with hearing thresholds; in comparison to controls, *reduced* white matter FA values were found in the right prefrontal cortex, right auditory cortex, and corpus callosum. However, this study was also limited by the

fact that comparisons of FA were made between a tinnitus positive group *with* hearing loss to a control group *without* hearing loss.

In summary, out of 5 studies using DTI to study tinnitus, one had negative results (Hussain et al), one lacked a control group (Yoo et al., 2006), two had inadequate control groups (Lee et al., 2007; Aldafferi et al., 2012) and one showed positive results (Crippa et al., 2010) but their quantification methodology, while novel, requires further development in order to be successfully applied to all participants. Nevertheless, both whole brain (voxel-wise) and ROI DTI analyses have proven successful in identifying brainstem and cortical pathway anomalies in tinnitus positive groups. While there are both strengths and weaknesses to each type of analysis methodology (e.g., Snook et al., 2007), combining both procedures may be the most comprehensive approach to be applied in future endeavors in this area.

4.2 Issues regarding the Control Condition

Issues related to the control condition are relevant to the interpretation of these data. As we indicated in the Introduction and Method sections, in order to examine the effects of tinnitus in those individuals with noise-induced hearing loss, we matched participants as closely as possible for degree of hearing loss and compared groups with and without tinnitus. However, in the limited number of studies evaluating the effects of sensorineural hearing loss on brainstem and cortical white matter tracts, investigators have used a control group with "normal" hearing sensitivity. In this context, Lin et al. (2008) found the FA values were *reduced* in comparison to controls (no hearing loss group) at the level of the lateral lemniscus and inferior colliculus (N = 37 sensorineural hearing loss (mean age 32.4years; $\pm$11.9 years) 10 age-matched controls (mean age 31.1 years; $\pm$11.6 years). In an alternative analysis, Chang et al. (2004) found that FA was *reduced* in one of five regions studied (superior olivary nucleus, inferior colliculus, trapezoid

393 body, lateral lemniscus and auditory radiations) in sensorineural hearing loss (8/10 being
394 binaural). In this sample, the inferior colliculus was most vulnerable to FA anomalies.

395 In subjects with unilateral cochlear nerve deficiency (aplasia and hypoplasia), Wu et al.
396 (2009b) found significantly *decreased* FA on both ipsilateral and contralateral lateral lemnisci
397 and inferior colliculus which could be attributed to transynaptic axonal atrophy of these
398 brainstem auditory structures. In long-term unilateral sensorineural hearing loss and using a ROI
399 analysis (lateral lemniscus and inferior colliculus), Wu et al. (2009a) found *decreased* FA on the
400 side contralateral to hearing loss and attributed these effects to "axonal loss and/or
401 demyelination."

402 Interpretive issues could potentially arise if areas of decreased FA in the group of noise-
403 induced hearing loss without tinnitus were similar in location to those sites where increases in
404 FA were observed. Clearly, this was not the case in our study but it could potentially become an
405 issue in other investigations.

406 **5. Conclusions**

407 This is the first report demonstrating increased FA in individuals with noise-induced
408 tinnitus using well-matched controls. The foci observed were asymmetric and lateralized
409 predominantly to left anterior thalamic radiations and the superior and inferior longitudinal
410 fasciculi of the left hemisphere. Only a single focus of *reduced* FA was observed. Increased FA
411 could be attributed to a number of factors, including: increased myelinization, decreased axonal
412 diameter, increased packing density, and decreased branching. We emphasize that by limiting the
413 inclusion criteria to individuals with tinnitus severity in the moderate-to-severe range and to a
414 specific etiology, heterogeneity of results is minimized and the ability to interpret results is
415 enhanced. It is also noteworthy that the pathological changes observed for FA in the current

study is consistent with a distributed fronto-parietal-cingulate network of tinnitus "distress" that has been reported by others.

6. Acknowledgements

We thank Paula Morton, R.N., for performing safety questionnaire review prior to imaging and to Mr. Yang Xuan, for excellent technical MR scanning skills.

7. References

Aldhafeeri, F. M., Mackenzie, I., Kay, T., Alghamdi, J., Sluming, V., 2012. Neuroanatomical correlates of tinnitus revealed by cortical thickness analysis and diffusion tensor imaging. Neuroradiol., e-pub ahead of print.

Attias, J., Raveh, E., Farber Ben-Naftali, N., Zarchi, O., Gothelf, D., 2008. Hyperactive auditory efferent system and lack of acoustic reflexes in Williams syndrome. J. Basic Clin. Physiol. Pharmacol., 19, 193-207.

Arlinghaus, L. R., Thornton-Wells, T. A., Dykens, E. M., Anderson, A. W., 2011. Alterations in diffusion properties of white matter in Williams syndrome. Mag. Res. Imag., 29, 1165-1174.

Awasthi, R., Gupta, R. K., Trivedi, R., Singh, J. K., Paliwal, V. K., Rathore, R. K. S., 2010. Diffusion tensor MRI imaging in children with pantothenate kinase-associated neurodegeneration with brain iron accumulation and their siblings. Am. J. Neuroradiol., 31, 442-447.

Baguley, D. M., 2003. Hyperacusis. J. Royal Soc. Med., 96, 582-585.

Baguley, D. M., Andersson, G., 2007. Hyperacusis. San Diego: Plural Publishing, Inc.

Basser, P. J., 1995. Inferring microstructural features and the physiological state of tissues from diffusion weighted images. NMR in Biomed., 8, 333–344.

Beaulieu, C., 2002. The basis of anisotropic water diffusion in the nervous system - a technical review. NMR in Biomed., 15, 435-455.

Browne, C. J., Morley, J. W., Parsons, C. H., 2012. Tracking the expression of excitatory and inhibitory neurotransmission-related proteins and neuroplasticity markers after noise induced hearing loss. PLoS ONE, 7, e33272.

448 Catani, M., Howard, R., J., Pajevic, S., Jones, D.K., 2002. Virtual in vivo interactive dissection
449 of white matter fasciculi in the human brain. NeuroImage, 17, 77-94.
450 Chang, Y., Lee, S-H, Lee, Y-J., Hwang, M-J, Bae, S-J., Kin, M-N., Lee, J., Woo, S., Lee, H.,
451 Kang, D-S., 2004. Auditory neural pathway evaluation on sensorineural hearing loss
452 using diffusion tensor imaging. NeuroReport, 15, 1699-1703.
453 Chang, S-E., Synnestvedt, A., Ostuni, J., Ludlow, C. L. 2010. Similarities in speech and white
454 matter characteristics in idiopathic developmental stuttering and adult-onset stuttering. J.
455 Neurolinguistics, 23, 455-469.
456 Clark, W. W., Bohne, B. A., 1999. Effects of noise on hearing. J. Am. Med. Assoc., 281, 1658-
457 1659.
458 Coles, R., 2000. Medicolegal issues, in Tinnitus Handbook, R Tyler, (Editor). San Diego:
459 Singular Publishing Co., 399-417.
460 Crippa, A., Lanting, C. P., van Dijk, P., Roerdink, J. B., 2010. A diffusion tensor imaging study
461 on the auditory system and tinnitus. The Open Neuroimag. J., 4, 16-25.
462 Dong, S., Mulders, W. H., Rodger, J., Woo, S., Robertson, D., 2010. Acoustic trauma evoked
463 hyperactivity and changes in gene expression in guinea-pig auditory brainstem. Eur. J.
464 Neurosci., 31, 1616-1628.
465 Douaud, G., Behrens, T. E., Poupon, C., Cointepas, Y, Jbabdi, S., Gaura, V., Golestani,
466 N., Krystkowiak, P. et al., 2009. In vivo evidence for the selective subcortical
467 degeneration in Huntington's disease. NeuroImage, 46, 958-966.
468 Eckert, M. A., Galaburda, A. M., Karchemskiy, A., Liang, A., Paul Thompson, P., Dutton, R. A.,
469 Lee, A. D., Bellugi, U., Korenberg, J. R., Mills, D., Rose, F. E., Reiss, A. L., 2006.
470 Anomalous Sylvian fissure morphology in Williams syndrome. NeuroImage, 33, 39-45.

Etkin, A., Egner, T., Kalisch, R., 2011. Emotional processing in anterior cingulate and medial prefrontal cortex. Trends Cog. Sci., 15, 85-93.

Eggermont, J. J., Roberts, L. E., 2004. The neuroscience of tinnitus. Trends Neurosci., 27, 676-682.

Elsabbagh, M., Cohen, H., Cohen, M., Rosen, S., Karmiloff-Smith, A., 2011. Severity of hyperacusis predicts individual differences in speech perception in Williams syndrome. J. Intellect. Dis. Res., 55, 563-571.

Gattu, R., Benson, R. R., Kou, Z., Zakaria, N., Kallakuri, S., Shen, Y., Cavanaugh, J. M., Haacke, E. M., 2012. Increased FA in acute TBI rat Marmarau model followed by decreased FA during subacute stage: A TBSS study. Proc. Int. Soc. Mag. Reson. Med., May 5-11, Melbourne, Australia.

Gerdes, J. S., Keller, S. S., Schwindt, W., Evers, S., Mohammadi, S., Deppe, M., 2012. Progression of microstructural alterations in a case of symptomatic recurrent seizures using diffusion tensor imaging. Seizure, e-pub ahead of print.

Godfrey, D. A., Kaltenbach, J. A., Chen, K., Ilyas, O., Liu, X., Licari, F., Sacks, J., McKnight, D., 2012. Amino acid concentrations in the hamster central auditory system and long-term effects of intense tone exposure. J. Neurosci. Res. e-pub ahead of print.

Golm, D., Schmidt-Samoa, C., Dechent, P., Kröner-Herwig, B., 2012. Neural correlates of tinnitus related distress: An fMRI-study. Hear. Res., epub ahead of print.

Harris, M., Gupta, R. K., Hussain, N., Hasan, K. M., Husain, M., Narayana, P. A., 2006. Measurement of DTI metrics in hemmorhagic brain lesions: possible implication in MRI interpretation. J. Mag. Reson. Imag., 24, 1259-1268.

Haas, B. W., Hoeft, F., Barnea-Goraly, N., Golaria, G., Bellugi, U., Reiss, A. L., (2012).

494 Preliminary evidence of abnormal white matter related to the fusiform gyrus in Williams
495 syndrome: a diffusion tensor imaging tractography study. Genes, Brain, Behav., 11, 62-
496 68.
497 Haas, B. W., Reiss, A. L. 2012. Social brain development in Williams syndrome: the current
498 status and directions for future research. Front. Psychol., 3, 1-13.
499 Henderson, D., Bielefeld, E. C., Lobarinas, E., Tanaka, C., 2011. Noise-Induced Hearing Loss:
500 Implication for Tinnitus. In: Møller, A. R., Langguth, B., De Ridder, D., Kleinjung, T.,
501 (Eds.) Textbook of Tinnitus. New York: Springer, pp. 301-309.
502 Hoeft, F., Barnea-Goraly, N., Haas, B. W., Golarai, G., Ng, D., Mills, D., Korenberg, J., Bellugi,
503 U., Galaburda, A., Reiss, A. L., 2007. More is not always better: Increased fractional
504 anisotropy of superior longitudinal fasciculus associated with poor visual spatial abilities
505 in Williams syndrome. J. Neurosci. 27, 11960-11965.
506 Holinger, D. P., Bellugi, U., Mills, D. L., Korenberg, J. R., Reiss, A. L., Sherman, G. F.,
507 Galaburda, A. M., 2005. Relative sparing of primary auditory cortex in Williams
508 Syndrome. Brain Res., 1037, 39-45.
509 Houenou, J., Wessa, M., Douaud, G., Leboyer, M., Chanraud, S., Perrin, M., Poupon, C.,
510 Martinot, J. L., Paillere-Martinot, M. L. 2007. Increased white matter connectivity in
511 euthymic bipolar patients: diffusion tensor tractography between the subgenual
512 cingulate and the amygdalo-hippocampal complex. Mol. Psychiatry, 12, 1001-1010.
513 Humes, L. E., Joellenbeck, L. M., Durch, J. S., 2006. Noise and Military Service: Implications
514 for Hearing Loss and Tinnitus. Washington, D.C.: Institute of Medicine of the National
515 Academies, The National Academies Press.
516 Husain, F. T., Medina, R. E., Davis, C. W., Szymko-Bennett, Y., Simonyan, K., Pajor, N. M.,

517 Horwitz, B., 2010. Neuroanatomical changes due to hearing loss and chronic tinnitus: A
518 combined VBM and DTI study. Brain Res., 1369, 74-88.
519 Jernigan, T., Bellugi, U., 1990. Anomalous brain morphology on magnetic resonance images in
520 Williams syndrome and Down syndrome. Arch. Neurol., 47, 529-533.
521 Jiang , H., van Zijl, P. C., Kim, J., Pearlson, G.D., Mori, S., 2006. DtiStudio: resource program
522 for diffusion tensor computation and fiber bundle tracking. Comp. Meth. Progr. Biomed.,
523 81, 106-116.
524 Kaltenbach, J. A., 2011. Tinnitus: Models and mechanisms. Hear. Res., 276, 52-60.
525 Keller, S. S., Ahrens, T., Mohammadi, S., Moddel, G., Kugel, H., Ringelstein, E. B., Deppe, M.,
526 2011. Microstructural and columeric abnormalities of the putamen in juvenile myoclonic
527 epilepsy. Epilepsia, 52, 1715-1724.
528 Keller, S. S., Ahrens, T., Mohammadi, S., Gerdes, J. S., Kellinghaus, C., Kugel, H., Weber, B.,
529 Ringelstein, E. B., Deppe, M., 2011. Voxel-based statistical analysis of fractional
530 anisotropy and mean diffusivity in patients with unilateral temporal lobe epilepsy of
531 unknown cause. J. Neuroimage. e-pub ahead of print.
532 Klöppel, S., Draganski, B., Golding, C. V., Chu, C., Nagy, Z., Cook, P. A., Hicks, S. L.,
533 Kennard, C., Alexander, D. C., Parker, G. J., Tabrizi, S. J., Frackowiak, R. S., 2008.
534 White matter connections reflect changes in voluntary-guided saccades in pre-
535 symtomatic Huntington's disease. Brain, 131, 196-204.
536 Lee, Y-J., Bae, S. J., Lee, S. H., Lee, J. J., Lee, K. Y., Kim, M. N., Kim, Y. S., Baik, S. K., Woo,
537 S., Chang, Y., 2007. Evaluation of white matter structures in patients with tinnitus using
538 diffusion tensor imaging. J. Clin. Neurosci., 14, 515-519.
539 Levitan, D. J., Bellugi, U., 1998. Musical abilities in individuals with Williams syndrome.

musical Percept., 15, 357-389.

Levitin, D. J., Menon, V., Schmitt, J. E., Eliez, S., White, C. D., Glover, G. H., Kadis, J., Korenberg, J. R., Bellugi, U., Reiss, A. L., 2003. Neural correlates of auditory perception in Williams Syndrome: An fMRI study. NeuroImage, 18, 74-82.

Levitin, D., Cole, K., Lincoln, A., Bellugi, U., 2005. Aversion, awareness, and attraction: investigating claims of hyperacusis in the Williams syndrome phenotype. J. Child Psychol. Psychiatry, 46, 514-523.

Li, Q., Sun, J., Guo, L., Zang, Y., Feng, Z., Huang, X., Yang, H., Lv, Y., Huang, M., Gong, Q., 2010. Increased fractional anisotropy in white matter of the right frontal region in children with attention-deficit/hyperactivity disorder: A diffusion tensor imaging study. Neuro-Endocrinol. Lett., 31, 747-753.

Liberman, M. C., Kiang, N, Y-S., 1978. Acoustic trauma in cats. Cochlear pathology and auditory-nerve activity. Acta Otolaryngol. (Suppl.), 358, 1-63.

Ling, J. M., Pena, A., Yeo, R. A., Merideth, F. L., Klimaj, S., Gasparovic, C., Mayer, R., 2012. Biomarkers of increased diffusion anisotropy in semi-acute mild traumatic brain injury: a longitudinal perspective. Brain, 135, 1281-1292.

Lockwood, A. H., Salvi, R. J., Burkard, R. F. 2002. Tinnitus. N. Engl. J. Med., 347, 904-910.

Madden, D. J., Bennett, I. J., Song, A. W., 2009. Cerebral white matter integrity and cognitive aging: Contributions from diffusion tensor imaging. Neuropsychol. Rev., 19, 415-435.

Makris, N., Kennedy, D. N., McInerney, S., Sorensen, A. G., Wang, R., Caviness, V. S., J., Oandya, D. N., ,(2005,). Segmentation of subcomponents within the superior longitudinal facicle in humans: A quantitative, in vivo, DT-MRI study. Cerebral Cortex, 15, 854-869.

Matsumoto, N., Kitani, R., Kalinec, F., 2011. Linking LIMK1 deficiency to hyperacusis and

563 progressive hearing loss in individuals with Williams syndrome. Commun. Integr. Biol.,
564 4, 208-210.
565 Mazurek, B., Olze, H., Haupt, H., Szczepek, A. J., 2010. The more the worse: the grade of noise-
566 induced hearing loss associates with the severity of tinnitus. Int. J. f Environ. Res. Public
567 Health, 7, 3071-3079.
568 Miani, C., Passon, P., Bracale, A. M., Barotti, A., Panzolli, N., 2001. Treatment of hyperacusis
569 in Williams syndrome with bilateral conductive hearing loss. Eur. Arch.
570 Otorhinolaryngol., 258, 341-344.
571 Middleton, J.W., Kiritani, T., Pedersen, C., Turner, J.G., Shepherd, G.M., Tzounopoulos, T.,
572 2011. Mice with behavioral evidence of tinnitus exhibit dorsal cochlear nucleus
573 hyperactivity because of decreased GABAergic inhibition. Proc. Natl. Acad. Sci. USA,
574 108, 7601-7606.
575 Morest, D. K., Kim, J., Potashner, S. J., Bohne, B. A., 1998. Long-term degeneration in the
576 cochlear nerve and cochlear nucleus of the adult chinchilla following acoustic
577 overstimulation. Microscopic Res. Technol., 41, 205-216.
578 Mulders, W. H. A. M., Robertson, D., 2011. Progressive centralization of midbrain hyperactivity
579 after acoustic trauma. Neurosci., 192, 753-760.
580 Mulders, W. H. A. M., Ding, D., Salvi, R., Robertson, D., 2011. Relationship between auditory
581 thresholds, central spontaneous activity, and hair cell loss after acoustic trauma. J. Comp.
582 Neurol. 519, 2637-2647.
583 Newman, C. W., Sandridge, S. A., 2004.Tinnitus questionnaires. In: J. B. Snow Jr., (Ed.).
584 Tinnitus: Theory and management. Hamilton: B. C. Decker, Inc., pp.237-254.
585 Newman, C. W., Jacobson, G. P., Spitzer, J. B., 1996. Development of the tinnitus handicap

586 inventory. Arch. Otolaryngol. Head Neck Surg., 122, 143-148.
587 Nigam, A., Samuel, P. R., 1994. Hyperacusis in Williams syndrome. J. Laryng. Otol., 08, 494-
588 496.
589 Pfefferbaum, A., Adalsteinsson, E., E., Rohlfing, T., Sullivan, E.V., 2010. Diffusion tensor
590 imaging of deep gray matter brain structures: effects of age and iron concentration.
591 Neurobiol. Aging, 31, 482-493.
592 Pal, D., Trivedi, R., Saksena, S., Yadav, A., Kumar, M., Pandey, C. M., Rathore, R. K., Gupta,
593 R. K., 2011. Quantification of age- and gender-related changes in diffusion tensor
594 imaging indices in deep grey matter of the normal human brain. J. Clin. Neurosci., 18,
595 193-196.
596 Pober, B. R., 2010. Williams-Beuren Syndrome. N. Eng. J. Med., 62, 239-252.
597 Reiss, A., Eckert, M. A., Rose, F. E., Karchemskiy, A., Kesler, S., Chang, M., Reynolds, M. F.,
598 Kwon, H., Galaburda, A., 2004. An experiment of nature: brain anatomy parallels
599 cognition and behavior in Williams syndrome. J. Neurosci., 24, 5009-5015.
600 Reiss, A., Eliez, S., Schmitt, J.E., Straus, E., Lai, Z., Jones, W., Bellugi, U., 2000. IV.
601 Neuroanatomy of Williams syndrome: a high-resolution MRI study. J. Cog. Neurosci.,
602 (Suppl. 1)12, 65-73.
603 Roberts, L. E., Eggermont, J. J., Caspary, D. M., Shore, S. E., Melcher, J.R., Kaltenbach, J.A.,
604 2010. Ringing Ears: The Neuroscience of Tinnitus. J. Neurosci., 30, 14972-14979.
605 Rueckert, D., Sonoda, L. I., Hayes, C., Hill, D. L., Leach, M. O., Hawkes, D. J., 1999. Nonrigid
606 registration using free form deformations: application to breast MR images. IEEE Trans.
607 Med. Imaging, 18, 712-721.
608 Rugg-Gunn, FJ, Eriksson, S. H., Symms, M. R. Barker, G. J., Duncan, J. S., 2001. Diffusion

609 tensor imaging of cryptogenic and acquired partial epilepsies. Brain, 124, 627-636.
610 Ruocco, H. H., Lopes-Cendes, I, Li, L. M., Santos-Silva, M., Cendes, F., 2006. Striatal and
611 extrastriatal atrophy in Huntington's disease and its relationship with length of the CAG
612 repeat. Braz. J. Med. Biol. Res., 39, 1129-1136.
613 Salvi, R. J., Wang, J., Ding, D., 2000. Auditory plasticity and hyperactivity following cochlear
614 damage. Hear. Res., 147, 261-274.
615 Schmahmann, J. D., Pandya, D. N., 2006. Fiber Pathways of the Brain. New York: Oxford
616 University Press.
617 Schmitt, J. E., Eliez, S., Bellugi, U., Reiss, A. L., 2001. Analysis of cerebral shape in Williams
618 syndrome. Arch. Neurol., 58, 283-287.
619 Schreiner, C. E., Cheung, S. W., 2004. Cortical plasticity and tinnitus. In: J. B. Snow (ed.).
620 Tinnitus: Theory and Management. Hamilton: B. C. Decker, pp. 189-202.
621 Smith, S. M., Jenkinson, M., Woolrich, M. W., Beckmann, C. F., Behrens, T.E.J., Johansen-
622 Berg, H., 2004. Advances in functional and structural MR image analysis and
623 implementation as FSL. NeuroImage, 23, 208-219, 2004.
624 Smith, S. M., Jenkinson, M., Johansen-Berg, H., Rueckert, D., Nichols, T. E., Mackay, C.
625 E., Watkins, K. E., Ciccarelli, O., Cader, M. Z., Matthews, P. M., Behrens, T. E., 2006.
626 Track-based spatial statistics: voxelwise analysis of multi-subject diffusion data.
627 NeuroImage, 31, 1487- 1505.
628 Snook, L., Plewes, C., Beaulieu, C., 2007. Voxel based versus region of interest analysis in
629 diffusion tensor imaging of neurodevelopment. NeuroImage, 34, 243-252.
630 Syka, J., 2002. Plastic changes in the central auditory system after hearing loss, restoration of
631 function, and during learning. Physiol. Rev., 82, 601-636.

632 Versace, A., Almeida, J. R. C., Hassel, S., Walsh, N. D., Novelli, M., Klein, C. R., Kupfer, D. J.,
633 Phillips, M. L. 2008. Elevated left and reduced right orbitomedial prefrontal fractional
634 anisotropy in adults with bipolar disorder revealed by tract-based spatial statistics. Arch.
635 Gen. Psychiatry, 65, 1041-1052.
636 Wang, H., Brozoski, T. J., Caspary, D. M., 2011. Inhibitory neurotransmission in animal models
637 of tinnitus: Maladaptive plasticity. Hear. Res., 279, 111-117.
638 Wu, C. M., Ng, S. H., Liu, T. C., 2009a. Diffusion tensor imaging of the subcortical auditory
639 tract in subjects with long-term unilateral sensorineural hearing loss. Audiol. Neuro-otol.,
640 14, 248-253.
641 Wu, C. M., Ng, S. H., Wang, J. J., Liu, T. C., 2009b. Diffusion tensor imaging of the subcortical
642 auditory tact in subjects with congenital cochlear nerve deficiency. Am. J. Neuroradiol.,
643 30, 1773-1776.
644 Xia, Z., Nguyen, B. D., La Mar, G. N., 2000. The use of chemical shift temperature gradients to
645 establish the paramagnetic susceptibility tensor orientation: implication for structure
646 determination/refinement in paramagnetic metalloproteins. J. Biomol. Nucl. Mag. Reson.
647 Imaging, 17, 167-174.
648 Yankaskas, K., 2012. Prelude: Noise-induced tinnitus and hearing loss in the military. Hear.
649 Res., epub ahead of print.
650 Yoo, D-S, Choi, W. Y., Lee, S. Y.,Jeong, J-w, Lee, J. W., Kim, S., Chang, Y., 2006. Quantitative
651 analysis of white matter in DTI images of patients with tinnitus: Preliminary report. Proc.
652 28th IEEE EMBS Ann. Int. Conf., New York City, 1870-1872.
653

8. Figure legends

Figure 1. Top panels represent audiograms (mean ±1SD) for left (unfilled squares) and right ears (filled circles) for individuals without tinnitus; bottom panels represent audiograms (mean ±1SD) for left (unfilled squares) and right ears (filled circles) for individuals with tinnitus.

Figure 2. **A.** One of 9 foci with significantly higher FA for tinnitus (+) group compared with tinnitus (-) group (see cluster index 1 in table); **B.** A single focus of significantly reduced FA for tinnitus (+) vs. tinnitus (-) groups (see cluster index 10 in table).

9. Table legend

Table 1. Results of TBSS analysis of tinnitus (+) vs. tinnitus (-) groups. Clusters 1-9 have increased FA for tinnitus (+) group. Cluster 10 had reduced FA for tinnitus (+) group. *x, y, z* = millimeters in MNI coordinate space; L = left, R = right; ** $p < 0.0001$.

Figure(s)

Click here to download high resolution image

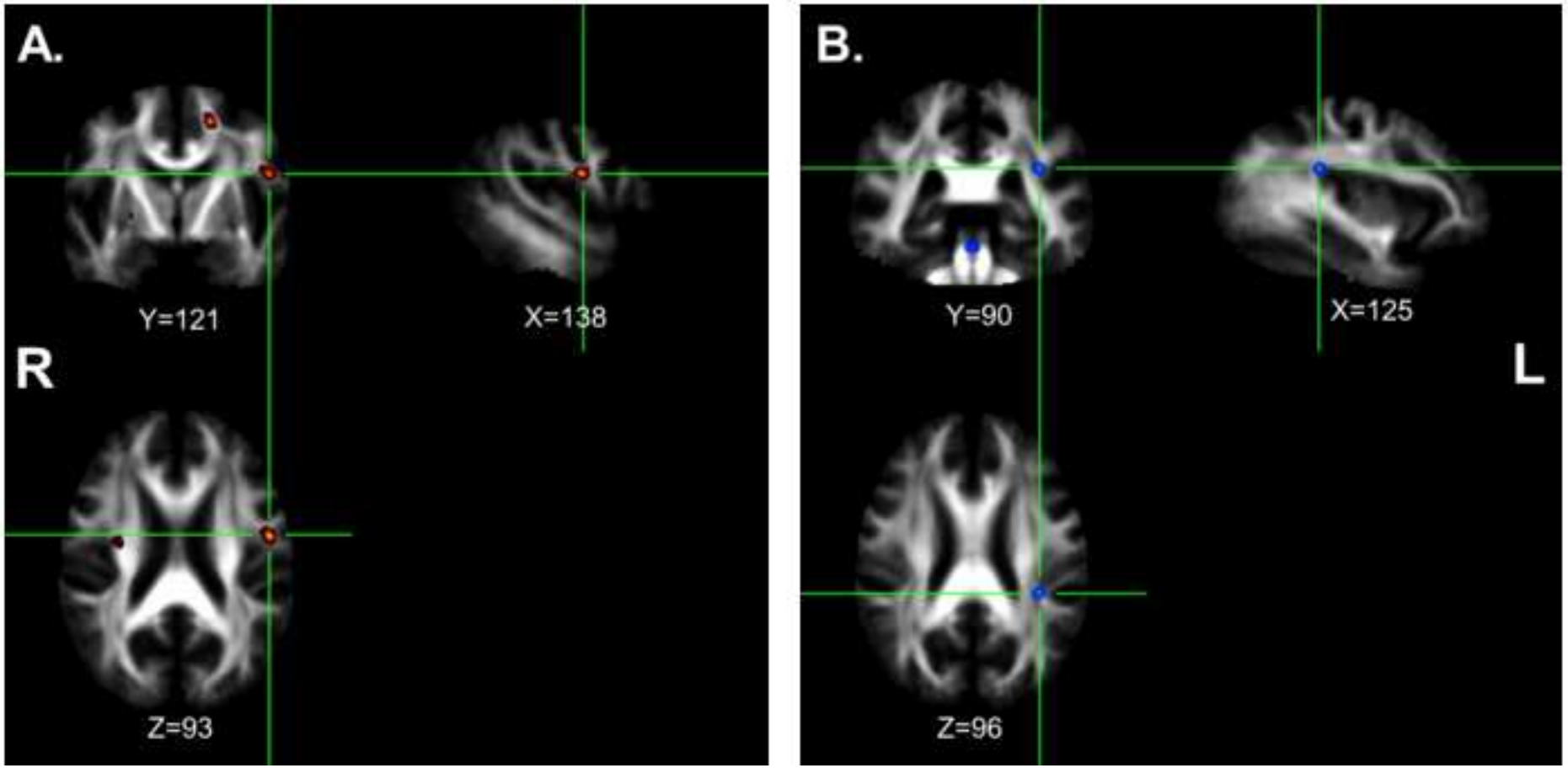

Figure(s)

Click here to download high resolution image

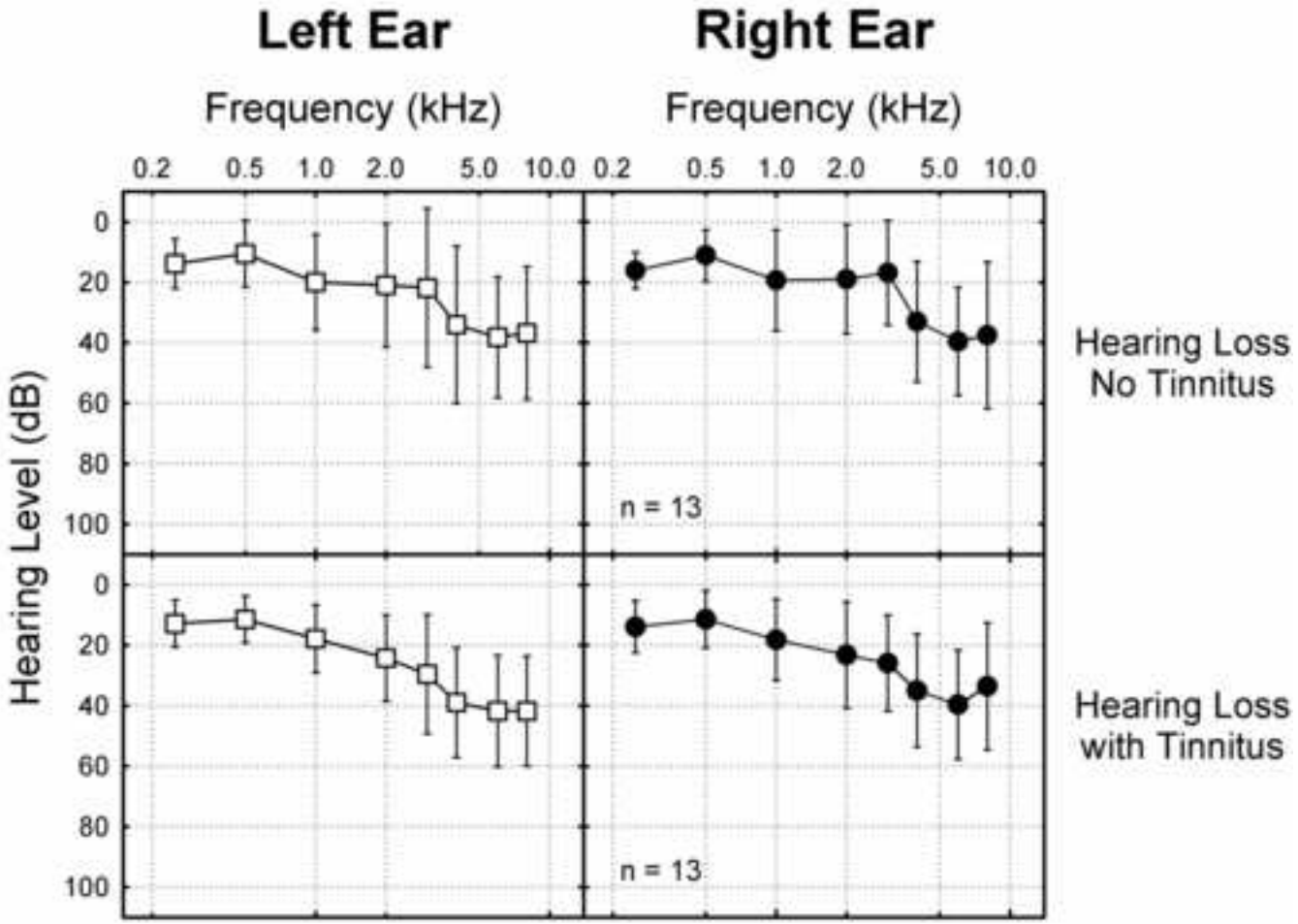

Table(s)

Cluster	*t*-value (Local Maximum)	Cluster Size (Voxels)	X	Y	Z	Anatomical	Side	White Matter Label
1	5.54**	21	138	121	93	Frontal	L	Superior Longitudinal Fasciculus
2	4.33**	10	121	169	81	Frontal	L	Anterior Thalamic Radiation
3	4.75**	18	107	123	122	Frontal	L	Anterior Thalamic Radiation
4	4.62**	23	110	64	107	Parietal	L	Inferior Longitudinal Fasciculus
5	4.35**	13	67	68	106	Parietal	R	Inferior Fronto-Occipital Fasciculus
6	4.20**	12	112	136	89	Caudate	L	Anterior Thalamic Radiation
7	3.50**	11	106	128	82	Caudate	L	Anterior Thalamic Radiation
8	3.88**	13	56	117	96	Unclassified	R	Superior Longitudinal Fasciculus
9	3.79**	15	105	132	81	Caudate	L	Anterior Thalamic Radiation
10	3.38**	4	125	50	96	Parietal	L	Superior Longitudinal Fasciculus